UNITED STATES DEPARTMENT OF COMMERCE
HARRY L. HOPKINS, Secretary
NATIONAL BUREAU OF STANDARDS
Lyman J. Briggs, Director

✦

Journal of Research

of the

National Bureau of Standards

✦

Volume 22, Number 1
January 1939

[Published with approval of the Director of the Budget]

UNITED STATES
GOVERNMENT PRINTING OFFICE
WASHINGTON : 1939

For sale by the Superintendent of Documents, Washington, D. C. - - - - - - Price 30 cents
$3.50 per year on subscription

The prices of the separate Research Papers appearing in this JOURNAL are given on the front cover page. If 100 or more copies of any separate are ordered, a discount of 25 percent is allowed. Those who desire copies of separate Research Papers should send their orders and remittances without delay to the Superintendent of Documents, U. S. Government Printing Office, Washington, D. C. This will aid him to determine the number of copies to be printed for sale. Research Papers are not printed from electrotypes, and usually no more reprints can be had when the first and only printing is exhausted.

U. S. DEPARTMENT OF COMMERCE NATIONAL BUREAU OF STANDARDS

RESEARCH PAPER RP1163

Part of Journal of Research of the National Bureau of Standards, Volume 22, January 1939

HETEROSTATIC LOADING AND CRITICAL ASTATIC LOADS

A Generalization of Southwell's Method for the Analysis of Experimental Observations in Problems of Elastic Instability

By L. B. Tuckerman

ABSTRACT

Southwell has shown how, in some cases, it is possible to compute the critical astatic load, that is, the elastic buckling load, of a structure from measurements of its heterostatic deflections at lower loads. The history of the theory of heterostatic loading and Southwell's method is briefly reviewed. Westergaard's general theory is then applied to the problem. It is shown that Southwell's method and Lundquist's modification of it are theoretically accurate for results of measurements which are proportional to the value of any one astatic parameter. These measurements need not be deflection measurements but may be strain measurements or, theoretically, measurements of any effect linearly dependent upon the deformation. Further, the parameter need not be the parameter corresponding to the lowest critical load but, theoretically, may correspond to any higher critical load.

Southwell's method is thus useful in cases where measurements within the elastic range can be made to depend primarily upon the change of a single astatic parameter. The theory is valid only for cases in which the buckling loads are lower than the load at which appreciable plastic deformation of the material or appreciable deviation from Hooke's law would occur. If, even within the elastic range, the measurements are affected appreciably by changes in other parameters, the critical elastic load computed by Southwell's method or Lundquist's modification may still be considerably in error. A combined numerical and graphical method of computation is outlined which by successive approximations, gives more accurate results in such cases. Finally, experimental results are given in which the second and third critical loads of a "round-end" Euler column are computed from strain-gage measurements taken at loads below the first critical load.

CONTENTS

	Page
I. Introduction	2
1. Ideal cases of elastic instability	2
2. Practical cases of mixed actions	2
3. Westergaard's general theory and nomenclature	3
4. Southwell's method of analysis	3
5. Difficulties in application	4
6. Methods previously suggested for overcoming these difficulties	4
7. Limitations of previous work	5
II. Application of Westergaard's general theory	5
1. Summary statement of the theory	5
2. Mathematical transformations used	8
3. Application to a single astatic parameter	9
4. Comparison with Southwell's and Lundquist's equations	9
5. Application to the general case	10
6. Approximation by expansion in a power series	11
7. Use of this approximation in computation	11
8. Possible accuracy attainable	12
9. Discussion of limitations of the method	13
III. Experimental data verifying the theory	13
1. Determination of lowest critical load	13
2. Theoretical possibility of determining higher critical loads	14
3. Experimental arrangement for second critical load	14
4. Experimental results for second critical load	15
5. Experimental arrangement for third critical load	15
6. Experimental results for third critical load	16
7. Agreement with Euler column theory	17
IV. Summary	17

I. INTRODUCTION

1. IDEAL CASES OF ELASTIC INSTABILITY

In theoretically ideal cases of elastic instability, structures are considered whose individual elements obey Hooke's law and which, under the action of a system of two or more proportional loads in equilibrium, called, as a system, the "load P," initially deform in a mode determined by the distribution of the individual components of P and are in stable equilibrium up to a certain critical load, Q, or, more generally, a discrete series of critical loads, Q_1, Q_2, . . . Q_h, . . .; $Q_{h+1}>Q_h$. Under the action of any one of these critical loads, the equilibrium, although remaining stable with respect to further deformation in the initial mode, becomes neutral with respect to some different (buckling) mode of deformation.

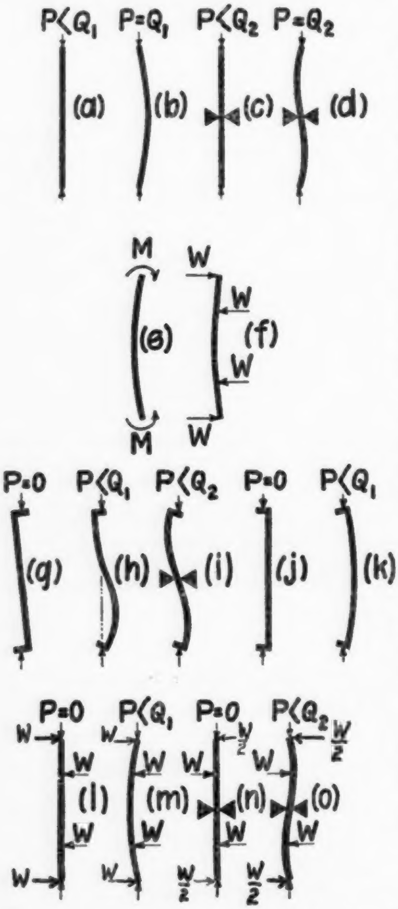

FIGURE 1.—*Examples of astatic loading, a, b, c, d; orthostatic loading, e, f; and heterostatic loading, g, h, i, j, k, l, m, n, o.*

The classical example of this type of behavior is the ideal straight "round-end" Euler[1] column. See figure 1. Under an exactly axial load its initial mode of deformation is pure axial compression proportional to the load, but under any one of a series of critical loads it is in neutral equilibrium in another mode of deformation, a lateral deflection in the shape of a single or multiple-lobed sine wave.

A comprehensive summary of the theory of these ideal cases with important additions was given by Southwell.[2]

2. PRACTICAL CASES OF MIXED ACTIONS

In actual structures these ideal cases are never attained, but, in general, buckling deformations in modes corresponding to the different Q_h are present even under small loads. They increase at first slowly under increasing load, but the mode corresponding to Q_1 increases with greatly increasing rapidity as Q_1 is approached. If the mode of buckling deformation corresponding to this load is prevented by outside constraints (fig. 1), the mode corresponding to Q_2 will increase more and more rapidly as that

[1] Leonhard Euler, Methodus inveniendi Lineas Curvas Maximi Minimive proprietate gaudentes, Bousquet, Lausanne (1744).
[2] R. V. Southwell, *On the general theory of elastic stability*, Phil. Trans. Roy. Soc. (London), **213** [A], 187–244 (1913).

load is approached, etc. The theory of these mixed actions of structures has been studied in much detail by many writers in special cases, more especially in the case of columns of inhomogeneous material, initially deformed, eccentrically loaded, and/or subjected to combined transverse and axial loads. These theoretical developments, even in this case, are practically all confined to purely elastic action and are not valid for loads at which appreciable plastic deformation occurs.

3. WESTERGAARD'S GENERAL THEORY AND NOMENCLATURE

Finally, Westergaard [3] gave a very general theory of buckling which covers all cases in which, although Hooke's law applies to the individual elements of the structure and the deformations are small enough so that second-order terms may be neglected, the deformations and stresses are, in general, not proportional to the load. These assumptions cover the elastic behavior of practically all the usual cases of structural instability, but they also are not valid for loads at which plastic deformation occurs.

Westergaard introduced a convenient nomenclature. He defined as "orthostatic" (fig. 1), quantities and actions which are proportional to the applied load, such as occur in a beam bent under transverse loads; as "astatic" (fig. 1), quantities and actions in the theoretically ideal cases of elastic instability, such as the ideal Euler column; and as "heterostatic" (fig. 1), combinations of astatic and orthostatic quantities and actions.

4. SOUTHWELL'S METHOD OF ANALYSIS

Unavoidable heterostatic action under practical test conditions has been one of the major difficulties in the experiments on elastic instability. In an interesting paper, Ayrton and Perry [4] in 1886 showed how it was theoretically possible to calculate the Euler load approximately from the lateral deflections under lower loads, of an initially bent inhomogeneous and/or eccentrically loaded column, and gave a graphic method for determining it. Ayrton and Perry were primarily interested in verifying their theory of bent or eccentrically loaded columns and only incidentally noted this possibility.

In 1932 Southwell [5] noted that within the elastic range before plastic deformation occurred the load, P, deflection, δ, curve of an initially bent or eccentrically loaded column approximated a rectangular hyperbola passing through the origin and asymptotic to the line $P=Q_1$. If this were rigorously so, plotting δ, the lateral deflection, measured from the position of zero load as ordinate and δ/P as abscissa would give a straight line whose slope was equal to Q_1. Examination of the data published by Von Kármán [6] and the unpublished data of A. Robertson showed that the slopes of lines so plotted were, in a number of the tests, in excellent agreement with the measured critical load.

Southwell gave a detailed discussion of the theory of this method of plotting in the case of the initially bent centrally loaded round-end column.

---

[3] H. M. Westergaard, *Buckling of elastic structures*, Trans. Am. Soc. Civil Engrs. **85**, 576–654 (1922). This contains a comprehensive bibliography.

[4] W. E. Ayrton and John Perry, *On struts*, Engineer **62**, 464–465, 513–515 (1886).

[5] R. V. Southwell, *On the analysis of experimental observations in problems of elastic stability*, Proc. Roy. Soc. (London) **135** [A] 601–616 (1932).

[6] Th. von Kármán, Untersuchungen über Knickfestigkeit, Forsch. Gebiete Ingenieurw. Heft 81 (1910).

Gough and Cox [7] applied this method of plotting to the shear buckling of thin strip, finding good agreement between theory and experiment.

Fisher [8] extended Southwell's reasoning to the case of a spar under combined axial and transverse loading, finding agreement between theory and experiment.

Recently, Ramberg, McPherson, and Levy [9] have applied the method with some success to the study of sheet-stringer combinations.

Donnell [10] has recently presented a variation of Southwell's method by plotting the load against the load divided by the deflection. The critical load then appears as the intercept on the P-axis. He also discusses the special cases of elastically supported struts, plates supported on three or four sides, cylinders under axial compression, and struts in the plastic range, finding that Southwell's method can be applied to all these cases in which the buckling does not introduce appreciable second-order stresses.

Hill [11] has applied the method to measurements of the lateral deflection of aluminum-alloy columns tested with "flat ends" and to the buckling of the stems of T-sections similarly tested. He found good agreement with the theory up to loads at which plastic yielding becomes appreciable.

5. DIFFICULTIES IN APPLICATION

In the application of this method it has been found that the lower portion of the (δ), (δ/P) graph was frequently curved and irregular, even when the upper portion was reasonably straight, and further, that straighter graphs could frequently be obtained by plotting $(\delta-\delta_0)$ as ordinate and $(\delta-\delta_0)/P$ as abscissa, where δ_0 represented a zero-point "correction" so chosen as to make the upper portion of the graph approximate most closely to a straight line. Unavoidable irregularities of deflection and strain readings under low loads is a well known difficulty in structural testing, ascribable partly to the practical impossibility of securely seating sensitive measuring instruments until they have been "worked in," and partly to inelastic settling of the structure itself, such as by slipping of rivets, under low loads.

Southwell [12] pointed out that the zero-point correction in an initially bent column would necessarily be present unless the initial bend was exactly a sine wave corresponding to the lateral deflection under the first Euler load, and generalized the statement to apply to other types of instability for which analogous equations applied.

6. METHODS PREVIOUSLY SUGGESTED FOR OVERCOMING THESE DIFFICULTIES

Various methods have been used to determine the zero-point correction and free the method from the uncertainties arising from initial irregularities. Southwell [13] suggested making a series of plots with

[7] H. J. Gough and H. L. Cox, *Some tests on the stability of thin strip material under shearing forces in the plane of the strip*, Proc. Roy. Soc. (London) **137** [A] 145–157 (1932).

[8] H. R. Fisher, *An extension of Southwell's method of analysing experimental observations in problems of elastic stability*, Proc. Roy. Soc. (London) **144** [A] 609–630 (1934).

[9] W. Ramberg, A. E. McPherson, and S. Levy, Experimental Study of Deformation and Effective Width in Axially Loaded Sheet-Stringer Panels, NACA Tech. Note 684, (January 1939.)

[10] L. H. Donnell, On the Application of Southwell's Method for the Analysis of Buckling Tests, Contributions to the Mechanics of Solids—Stephen Timoshenko 60th Anniversary Volume, p. 27–38 (Macmillan Co., New York, N. Y., 1938).

[11] H. N. Hill, Note on the Analytical Treatment of Lateral Deflection Measurements from Tests Involving Stability Problems (Aluminum Company of America) P. T. Report 38–71.

[12] R. V. Southwell, *On the analysis of experimental observations in problems of elastic stability*, Proc. Roy. Soc. (London) **135** [A] 601–616 (1932).

[13] See footnote 12.

different zero-point corrections and choosing the one which gave the straightest line in its upper portion. Gough and Cox [14] used the method of least squares and Fisher [15] a graphic method based on Pascal's hexagram theorem.

A simpler method of eliminating the effect of irregularities under low load has been given by Lundquist.[16] This consists in plotting $(\delta-\delta')$ as ordinate and $(\delta-\delta'),(P-P')$ as abscissa, where δ' is the deflection under some definite initial load P'/which is chosen somewhere in the middle of the observations where the P, δ curve is smooth.

None of these methods can be expected to give straight-line graphs for high loads at which plastic yielding has become appreciable, and for which the theory is no longer applicable.

7. LIMITATIONS OF PREVIOUS WORK

In all of this work following Southwell's 1932 paper,[17] except the very recent paper by Donnell, the detailed theoretical development has been limited to the theory of columns. The extension to other types of instability is only indicated by Southwell [18] by the statement: "In all ordinary examples of elastic instability, an equation of the same form as (7)[19] governs the deflection as controlled by its initial value, provided that both are small. Corresponding with Euler's theory of the initially straight strut we have a series of 'critical loadings', each associated with a particular 'normal' type of displacement, and by expressing both the initial and final displacement in a series of normal components, we can show that the relation (11)[20] will hold between the original and final amplitudes of the n'th normal component." Donnell, as noted above, extends the theory of the method to other special cases.

In none of the papers we have seen has it been noted that the theory of this type of plotting, and the range and limitation of its applicability, can simply and readily be deduced in very general form from Westergaard's[21] general theory.

II. APPLICATION OF WESTERGAARD'S GENERAL THEORY

1. SUMMARY STATEMENT OF THE THEORY

Westergaard shows that if Hooke's law applies to the elements of a structure under a certain type of astatic loading, P, whose critical values are $Q_1, Q_2, \ldots, Q_h, \ldots ; Q_{h+1}>Q_h$, then there can be defined a corresponding series of astatic parameters, u_{hj}, that is $u_{11}, u_{12}, \ldots u_{1j}, \ldots u_{1n_1}$, corresponding to Q_1; $u_{21}, u_{22}, \ldots u_{2j}, \ldots u_{2n_2}$, corresponding to Q_2, etc., an orthostatic parameter, v, and independent parameters, $t_1, t_2, \ldots t_k, \ldots t_m$.

---

[14] H. J. Gough and H. L. Cox, *Some tests on the stability of thin strip material under shearing forces in the plane of the strip*, Proc. Roy. Soc. (London) **137** [A] 145–157 (1932).

[15] H. R. Fisher, *An extension of Southwell's method of analysing experimental observations in problems of elastic stability*, Proc. Roy. Soc. (London) **144** [A], 609–630 (1934).

[16] Eugene E. Lundquist, Generalized Analysis of Experimental Observations in Problems of Elastic Stability, NACA Note 658 (July 1938).

[17] R. V. Southwell, *On the analysis of experimental observations in problems of elastic stability*, Proc. Roy. Soc. (London) **135** [A] 601–616 (1932).

[18] See footnote 17.

[19] $EI(y''-y''_0)+Py=0$.

[20] $\frac{w_n}{w_n'}=\frac{1.}{1-\frac{P}{P_n}}$

[21] H. M. Westergaard, *Buckling of elastic structures*, Trans. Am. Soc. Civil Engrs. **85**, 576–654 (1922).

These parameters are "generalized coordinates" in the Lagrangian sense, which define the displacements of the structure. In an axially symmetric Euler column, for example, the u_{11} and u_{12} might be chosen as the two components obtained by resolving the deflection at the midpoint in two mutually perpendicular directions, when the column is bent in a single-lobed sine wave, the type of deflection which corresponds to the lowest critical load. u_{21} and u_{22} might be chosen as the components of the deflection at the quarter points when the column is bent in a two-lobed sine wave, the type of deflection which corresponds to the second critical load, etc. In general, the u_{h1} and u_{h2} might be chosen as the coefficients of the Fourier series expansion of the lateral deflection in two orthogonal planes, the v as the axial shortening of the column and the t_k as coordinates determining inter-

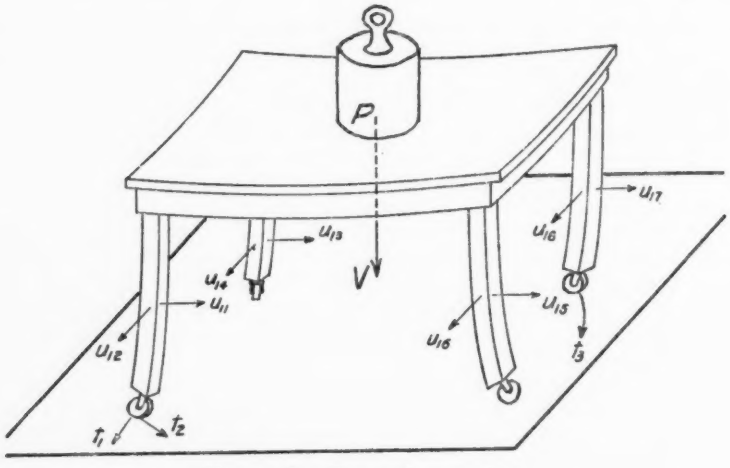

FIGURE 2.—*Types of parameters.*

Eight astatic parameters, u_{hj}, correspond to each critical load, Q_h; one orthostatic parameter, v, corresponds to deflection of the top of the table; and three independent parameters, t_k, correspond to motion of the table as a body.

nal strains or motions of the column as a whole, which involve no deformation.

It is only exceptionally that more than one astatic parameter corresponds to any one critical astatic load. If the Euler column were not axially symmetric and the two principal moments of inertia bore an irrational ratio to each other, there would be two series of critical loads, of which no two could be equal and each would have only a single corresponding astatic parameter. However, it is easy to devise structures in which many astatic parameters would be necessary. For instance, a table (fig. 2) with equal axially symmetric legs centrally loaded would require eight astatic parameters to define the possible magnitudes and directions of the sine-wave components of the deflection of its four legs corresponding to each of its critical loads.

When these parameters are sufficient to define all the significant small displacements and deformations of the structure under some type of heterostatic loading composed of the astatic loading, P, and

an orthostatic loading, W, Westergaard proves that the value of each of these parameters is given by

$$\bar{u}_{hj}=u_{hj}+\frac{P}{Q_h-P}u_{hj}=\frac{Q_h}{Q_h-P}u_{hj}, \tag{1}$$

where $\bar{u}_{hj}$ is the value of the parameter under heterostatic loading and u_{hj} is its value under the orthostatic loading, W, acting alone. This is of the same form as Ayrton and Perry's [22] eq 15 and Southwell's [23] eq 11, but refers to the astatic parameters instead of the deflections, and is proved to be applicable under much more general conditions.

Westergaard further shows that any effect, F, such as a stress, strain, deflection, curvature, etc., depending upon the deformation of the structure under these conditions, which under orthostatic loading, can be expressed in the form

$$F=F_0(t_1, \ldots t_k \ldots t_m)+\sum_{h=1}^{h=\infty}\sum_{j=1}^{j=n_h}f_{hj}u_{hj}, \tag{2}$$

under heterostatic loading is subject to an equation of the form

$$\overline{F}=F_0+f_p pP+\sum_{h=1}^{h=\infty}\frac{Q_h}{Q_h-P}\sum_{j=1}^{j=n_h}f_{hj}u_{hj}, \tag{3}$$

where $\overline{F}$ is the value of the effect under the heterostatic loading and F_0 is its value under the action of the independent parameters alone. The f_{hj}, f_p, and p are constants independent of both the orthostatic loading, W, and the astatic loading, P, but, in general, are functions of the location in the structure, determined by the nature of the effect, the geometry of the structure, and the type of astatic loading, P. The constant, p, is so chosen that the orthostatic parameter $v=pP$.

If F, for example, represented the strain on one side at the quarter point of an Euler column, the parameter, u_{11}, corresponding to the single-lobed sine-wave deflection characteristic of the lowest critical load would enter the summation with a coefficient whose relative value $f_{11}=\sin 45°=1/\sqrt{2}$, while the parameter u_{21} corresponding to the double-lobed deflection characteristic of the second critical load would enter the summation with a coefficient whose relative value $f_{21}=\sin 90°=1$. If the deflections were measured at the sixth points the corresponding coefficients would have the relative values, $f_{11}=\sin 30°=1/2$ and $f_{21}=\sin 60°=\sqrt{3}/2$, etc., f_p would determine the average axial strain under the load, P, and be inversely proportional to its length, while F_0 would represent any internal strains present in the column under no load.

Southwell's eq 9[24] is a special case of this general expression.

[22] W. E. Ayrton and John Perry, *On struts*, Engineer **62**, 464-465, 513-515 (1886).
[23] R. V. Southwell, *On the analysis of experimental observations in problems of elastic stability*, Proc. Roy. Soc. (London), **135** [A], 601-616 (1932).
[24] R. V. South well, *On the analysis of experimental observations in problems of elastic stability*, Proc. Roy. Soc. (London), **135** [A] 601-616 (1932).

$$y=\sum_{n=1}^{\infty}\left[w_n \sin\frac{n\pi x}{2}\right]$$

For these equations to hold, all of the components of the astatic loading, P, must change proportionally to each other, but the orthostatic loading, W, may have components which are independent. These equations could be applied to any case of loading of the structure, but their practical value lies largely in cases in which the orthostatic loading consists of a constant component and a component proportional to the astatic loading, P. That would be the case, for example, in a girder under a combination of a constant transverse load and an eccentrically applied axial load, as in Fisher's [25] experiments. The u_{hj} are linear functions of the linearly independent components of W. In the ideal case in which the loading, P, is exactly astatic, the u_{hj} vanish with W, but in the practical case, there will be initial eccentricities of shape and loading, which may be treated as constant additive terms in the u_{hj}.

It is desirable to emphasize the implications of the assumptions upon which these equations are based.

The equations are strictly applicable only to materials which obey Hooke's law. Experience has shown, however, that they can be usefully applied to materials such as some alloy steels or high-strength aluminum alloys whose stress-strain graphs depart appreciably from a straight line, but they cannot be expected to give more than rough approximations if the stresses are so high that plastic yielding of the material becomes comparable to the elastic deformation.

The equations are limited to small deflections. If the deflections should become too large, an effect, F, might cease to be even an approximately linear function of the parameters, and eq 3 would no longer be adequate to represent it. Further, the equations are valid only if the astatic parameters selected are sufficient to define all the significant small displacements and deformations of the structure under the type of heterostatic loading considered. For example, the coefficients of the Fourier series expansion of the lateral deflections give astatic parameters adequate to describe the significant deformations of a sturdy column. They are, however, inadequate to describe the significant deformations of a column which may fail by twisting or by local buckling of its web or outstanding flanges. For such columns, additional astatic parameters are needed to define all the significant small deformations.

2. MATHEMATICAL TRANSFORMATIONS USED

In the further development, repeated use will be made of certain transformations which are a generalization of those used by Southwell and Lundquist. If

$$z=\frac{Q(a+bP)}{Q-P}-f(P)=\frac{Q(a+bQ)}{Q-P}-bQ-f(P), \tag{4}$$

where z and P are variables, $f(P)$ is any arbitrary function of P alone, and Q, a, and b are constants, let

$$w=z+bQ+f(P). \tag{5}$$

Then

$$w=\frac{Q(a+bQ)}{Q-P}. \tag{6}$$

[25] H. R. Fisher, An *extension of Southwell's method of analysing experimental observations in problems of lastic stability*, Proc. Roy. Soc. (London) 144 [A] 609-630 (1934).

Designating by primes quantities corresponding to a particular constant value of P, P';

$$w'=\frac{Q(a+bQ)}{Q-P'} \tag{7}$$

from which,

$$\frac{w}{Q-P'}=\frac{w'}{Q-P}=\frac{w-w'}{P-P'} \tag{8}$$

or,

$$(w-w')=(Q-P')\frac{w-w'}{P-P'}-w'. \tag{9}$$

By substituting values from eq 5 for w and w',

$$(z-z')+f(P)-f(P')=(Q-P')\frac{z-z'+f(P)-f(P')}{P-P'}-w' \tag{10}$$

3. APPLICATION TO A SINGLE ASTATIC PARAMETER

Under the condition of an orthostatic loading consisting of a constant component and a component proportional to the astatic loading, P, arising from initial eccentricity either of shape or elastic inhomogeneity of the material in a structure, eq 1 will become

$$\bar{u}_{hj}=\frac{Q_h}{Q_h-P}(u_{hj}+p_{hj}P), \tag{11}$$

where u_{hj} is the value of the astatic parameter under the constant component of the orthostatic loading acting alone and p_{hj} is a constant determining the contribution of the orthostatic component of P to the value of the corresponding astatic parameter. This is of the same form as eq 4 with $f(P)=0$ and may be written

$$\bar{u}_{hj}+p_{hj}Q_h=\frac{Q_h}{Q_h-P}(u_{hj}+p_{hj}Q_h) \tag{12}$$

This is in the same form as eq 1, except for the displacement of the zero of the u_{hj} by a constant amount $p_{hj}Q_h$. Equation 10 then gives

$$\bar{u}_{hj}-\bar{u}'_{hj}=(Q_h-P')\frac{\bar{u}_{hj}-\bar{u}'_{hj}}{P-P'}-(\bar{u}'_{hj}+p_{hj}Q_{hj}). \tag{13}$$

If then, under these general conditions, any measurement or measurements can be taken on the structure which will determine a quantity proportional to any one of the astatic parameters, $\bar{u}_{hj}$, for varying astatic loads, P, and if the differences $\bar{u}_{hj}-\bar{u}'_{hj}$ between its value for the varying loads and its value $\bar{u}'_{hj}$ for a fixed load P', be plotted as ordinates with the ratios $(\bar{u}_{hj}-\bar{u}'_{hj})/(P-P')$ as abscissas, the resulting plot should be a straight line whose slope is (Q_h-P').

4. COMPARISON WITH SOUTHWELL'S AND LUNDQUIST'S EQUATIONS

Equation 13 is of the same form as Lundquist's [26] eq 15, and with P' chosen as zero, it is of the same form as Southwell's [27] eq 17.

[26] Eugene E. Lundquist, Generalized Analysis of Experimental Observations in Problems of Elastic Stability, NACA Tech. Note 658 (July 1938).

[27] R. V. Southwell, *On the analysis of experimental observations in problems of elastic stability*, Proc. Roy. Soc. (London) **135** [*A*], 601–616 (1932).

Plotting deflection against deflection divided by load gives curves which approximate straight lines because, as Southwell pointed out, when the load approaches the first critical load, Q_1, the modes of buckling corresponding to that load and represented by the u_{1j}, are large in comparison with the modes of buckling corresponding to higher loads. Accordingly, the deflections become approximately proportional to the u_{1j}.

5. APPLICATION TO THE GENERAL CASE

In practical testing it is impossible to so locate deflection-and/or strain-measuring apparatus that quantities proportional to any one astatic parameter can be determined from their readings. Only such quantities would necessarily be subject to an equation of the form of eq 13. The measurements can only determine some more general heterostatic effect, $\overline{F}$, subject to an equation of the form of eq 3, in which each of the u_{hj} is replaced by a linear function of P, as in eq 11. Each of the terms of the double summation can be transformed, as in eq 12. Equation 3 will then have the form

$$\overline{F}=r+sP+\sum_{h=1}^{h=\infty}\frac{q_h}{Q_h-P}, \tag{14}$$

where r, s, and the q_h are constants. Their exact value, which could be determined from eq 3, 11, and 12, is of no significance in this connection. Practical interest in this equation is largely confined to cases in which one term of the summation is large in comparison with the others. This may occur in two ways. It may be possible to arrange the measurements so that one of the coefficients, q_h, is large in comparison with any of the others. More frequently one of the critical loads, Q_1, is much lower than any of the others. In such cases when the load approaches Q_1, even though q_1 is not large in comparison with the other q_h, the term$q_1/(Q_1-P)$ may become large in comparison with any other $q_h/(Q_h-P)$. That, however, is not necessarily the case, as may be illustrated by the observations of Gough and Cox. Only when their deflection measurements were taken accurately on the crest of the buckle were they able to get satisfactory results with Southwell's method. In either of these cases the largest variable term on the right-hand side of eq 3 containing the factor $q_h/(Q_h-P)$ corresponding to the critical load, Q_h (usually Q_1), may be selected for special consideration and all the other terms treated as a single function of P, $f(P)$. Equation 14 will then be of the same form as eq 4 with $\overline{F}$ substituted for z, so that an equation in $\overline{F}$ of the same form as eq 10 may immediately be written down. In this case

$$-f(P)=r+sP+\sum_{k\neq h}\frac{q_k}{Q_k-P} \tag{15}$$

and

$$f(P)-f(P')=-s(P-P')-\sum_{k\neq h}\frac{q_k}{Q_k-P'}\cdot\frac{P-P'}{Q_k-P}, \tag{16}$$

so that eq 10 gives

$$\overline{F}-\overline{F}'+[w'+Q_hs]-sP+\sum_{k\neq h}\frac{q_k}{Q_k-P'}\cdot\frac{Q_h-P}{Q_k-P}=(Q_h-P')\frac{\overline{F}-\overline{F}'}{P-P'}. \tag{17}$$

6. APPROXIMATION BY EXPANSION IN A POWER SERIES

If all the (Q_k-P') are greater in absolute magnitude than $(P-P')$, the summation can be expanded in a convergent power series in $(P-P')$ with positive integral exponents,
so that

$$\overline{F}-\overline{F}'-\sum_{k=0}^{k=\infty}c_k(P-P')^k=(Q_h-P')\frac{\overline{F}-\overline{F}'}{P-P'}, \tag{18}$$

where the c_k are constants. Their exact value which could be determined from eq 17 is of no significance in this connection. This equation will be practically useful in the analysis of experimental data only in the case where the series is very rapidly convergent.

7. USE OF THIS APPROXIMATION IN COMPUTATION

Computations based upon Euler's column indicate that in some experimental cases it may be worth-while to take into account second-order terms in P in eq 18. To avoid cumbersome notation it is convenient to change the notation, and to write

$$\begin{aligned} z&=\overline{F}-\overline{F}' \\ Q&=Q_h-P' \end{aligned} \tag{19}$$

and to replace $P-P'$ by P. Equation 18 then becomes

$$z+c_0-Q\frac{z}{P}-c_1P-c_2P^2=0, \tag{20}$$

where z represents the difference of the measured value of some effect such as a displacement, a strain, or some linear combination of displacements and/or strains produced by the change in load, P, from the arbitrary fixed load, P', and Q represents the difference between the particular critical load, Q_h, selected for special treatment and the same fixed load, P'. z/P should be calculated to *two significant figures beyond* [28] the number of significant figures observed in z. When c_1 and c_2 are small, plotting z as ordinate and z/P as abscissa will give a curve which approximates a straight line. The slope of the curve for highest values of the load within the range for which Hooke's law is approximately valid should be fairly close to Q. To determine Q more closely, draw a straight line, $\bar{z}=\overline{A}+\overline{B}(z/P)$, approximating closely the upper portion of the z, (z/P) curve, choosing the nearest convenient round numbers for $\overline{A}$ and $\overline{B}$. For each observed value of z/P calculate the value of $\bar{z}$ to *two significant figures beyond* the observed significant figures in z. Plot the difference $z-\bar{z}$ as ordinates to a scale so large that the estimated error of a single reading is at least 1 mm, with z/P as abscissas. This will make it easier to estimate changes in curvature and to distinguish between average trend and accidental errors. Choose some convenient round number as a trial value of c_1, and plot $z-\bar{z}-c_1P$ as ordinates with z/P as abscissas. Compare the resulting curve with the $z-\bar{z}$, (z/P) curve. The resulting—curve may be:

1. More curved.
2. Curved in the opposite direction.

[28] Carrying the intermediate computations to *two significant figures beyond* the determinate significant figures is important. If it is not done there may be a cumulation of computational error which will materially affect the accuracy of the results.

3. Less curved in the same direction.
4. Have an inflection.
5. Practically straight for lower values of P and curved for larger values.
6. Straight within the limits of experimental error.

In case 1 change the sign of c_1 and proceed as in 2, 3, 4, or 5.

In case 2 repeat with smaller trial values of c_1, until case 3, 4, or 5 is observed.

In cases 3 and 4 repeat with larger trial values of c_1 until the portion of the curve corresponding to the lower values of P is straight within the limits of experimental error. The last trial value should then be a good approximation to the actual value of c_1. This gives either case 5 or case 6. If it gives case 6, it shows that the term c_2P^2 is negligible and the computation is completed.

In case 5 choose some convenient round number as a trial value of c_2 and plot $z\text{-}\bar{z}\text{-}c_1P\text{-}c_2P^2$ as ordinates with z/P as abscissas, and compare with the $z\text{-}\bar{z}\text{-}c_1P$, (z/P) curve. The resulting curve may be:

1. More curved.
2. Curved in the opposite direction.
3. Less curved in the same direction.
4. Have an inflection.
5. Practically straight within the experimental error.

In case 1, change the sign of c_2 and proceed as in 2, 3, 4, or 5.

In case 2 repeat with smaller trial values of c_2 until case 3, 4, or 5 is observed.

In case 3 repeat with larger trial values of c_2 until case 4 or 5 is observed.

In case 4 start again the sequence of corrections of the first order leading to a new approximation to c_1, and then repeat the sequence of corrections of the second order leading to better approximation to c_2.

In case 5 the computation is completed.

These successive approximations, although complicated in their expression, can, provided data are consistent with eq 20, be made easily and quickly once the method is learned.

8. POSSIBLE ACCURACY ATTAINABLE

To gain some idea of the computational error involved in this type of approximation from data involving appreciable amounts of more than one term of the form $q_k/(Q_k-P)$ of eq15, strains corresponding to different assumed combinations of different types of eccentricity and lack of straightness of an Euler column were computed. The combinations were so chosen that, at the highest loads assumed the contributions other than the major term amounted to 10 percent of the total computed strain. To these theoretically computed strains "accidental errors" taken at random from Shewhart's [29] "drawings from a normal universe," and of the magnitude found in good strain-gage readings were added.

From these synthetic "load-strain" data the critical load was computed by the method outlined. In all cases the critical load so computed agreed with the assumed critical load within less than 2 percent.

[29] Walter A. Shewhart, Economic Control of Quality, p. 442-445 (D. Van Nostrand Co., Inc., 250 Fourth Avenue, New York, N. Y. (1931)).

9. DISCUSSION OF LIMITATIONS OF THE METHOD

As Southwell [30] has pointed out, it is, at present, impossible in most practical experiments to predict in advance how closely critical astatic loads can be determined from measurements of heterostatic action under lower loads. Only in cases where one term $q_h/(Q_h-P)$ of eq 14 is or becomes large in comparison with the other terms of the summation for loads below those at which the material shows appreciable plastic yielding will the $(\bar{F}-\bar{F}')$, $(\bar{F}-\bar{F}')/(P-P')$, graph be found to be reasonably straight for any considerable range. Only in such cases can any accuracy at all be expected.

The relative magnitude of the different terms of the form $q_h/(Q_h-P)$ will, in general, depend upon small irregularities of shape and material of the structure and small inaccuracies of loading which, in many cases, are difficult, if not impossible, to control. In practically all cases of simple deflection or strain measurements the term corresponding to the lowest critical load will predominate as that load is approached, but this may not occur before plastic yielding has become appreciable.

However, a single term will not necessarily ever become predominant, and, in particular, it is not likely to do so in a structure in which the two lowest critical loads corresponding to two different modes of instability are nearly equal. This may have been the case in one of the experiments reported by Ramberg, McPherson, and Levy.[31] Whether another type of analysis might be successful in such cases has not been investigated. In some relatively simple cases, however, it is possible to alter the conditions of loading and/or the type of measurement so as to ensure that even a term corresponding to a higher critical load will predominate below loads at which plastic yielding becomes appreciable.

Even if the measurements are such that one term predominates sufficiently to enable a close determination of the corresponding theoretical critical astatic load, the stresses corresponding to that load may exceed and even far exceed the stresses at which the material yields plastically as is the case in short and medium length sturdy columns.

In such cases the calculated critical loads will only give an upper limit to the strength of the structure. In spite of these limitations the method can be expected in many cases to give valuable information concerning the stability of structures, but the determination whether it will give valuable information in the case of any given structure under a given type of loading can, for the present at least, only be determined by trial.

III. EXPERIMENTAL DATA VERIFYING THE THEORY

1. DETERMINATION OF LOWEST CRITICAL LOAD

Experimental data sufficient to show the value of this method of analysis in determining the lowest critical astatic load of some structures, have, as noted above, been presented by Southwell; Gough and Cox; Fisher; Ramberg, McPherson, and Levy; and Lundquist. Fur-

[30] R. V. Southwell, *On the analysis of experimental observations in problems of elastic stability*, Proc. Roy. Soc. (London) **135** [A] 601–616 (1932).

[31] W. Ramberg, A. E. McPherson, and S. Levy, Experimental Study of Deformation and of Effective Width in Axially Loaded Sheet Stringer Panels, NACA Tech. Note. 684. (Jan. 1939.)

ther data of the same kind will be of interest only in cases where the critical loads of the structures themselves are of interest.

2. THEORETICAL POSSIBILITY OF DETERMINING HIGHER CRITICAL LOADS

The general theory here presented, however, indicates that the method is not necessarily limited to the determination of the lowest critical load, but may, in suitable cases, be used to determine higher critical loads.[32] It was thought worth-while to check this experimentally. To do this it is necessary to arrange the loading conditions and measurements of a structure, so that an effect $\overline{F}$ of the loading may be determined in which the q_k, $k<h$ of eq14 will be very small and q_h relatively large.

3. EXPERIMENTAL ARRANGEMENT FOR SECOND CRITICAL LOAD

Two arrangements of this kind were set up. In the first a commercial straight piece of cold-rolled steel, ¼ by ½ by 13.5 inches (see fig. 3), was loaded as a "round end" column with approximately equal and opposite eccentricities at either end secured by bevelling the ends to form eccentric knife-edges. This introduced relatively large orthostatic components of the load corresponding to all the critical loads of even order but principally of the second order. Three pairs of 2-inch Tuckerman optical strain gages were placed on opposite sides of the specimen, one pair at the midpoint and one at each of the quarter points (see fig. 3). The difference between the readings of each pair of gages is proportional to the average bending strain over the gage length. It is easy to see that changes in the astatic parameters of even order will contribute but little to the bending strain at the midpoint and also to the sum of the bending strains at the quarter points. These will, provided the corresponding term of $\overline{F}$ is sufficiently predominant, depend chiefly upon the variation of the astatic parameter corresponding to the lowest critical load. Application of the analysis to either of these should therefore be expected to determine the first critical load. Further, changes in the astatic parameters of odd order will contribute but little to the difference of the bending strains at the quarter points. This difference will depend chiefly upon the astatic parameter corresponding to the second critical

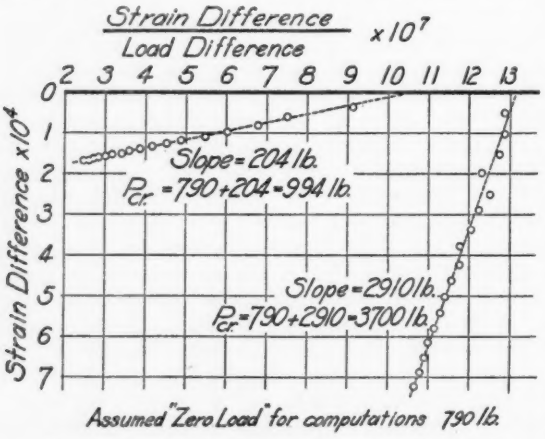
Strain Difference / Load Difference x10⁷
2 3 4 5 6 7 8 9 10 11 12 13
0 1 2 3 4 5 6 7
Strain Difference x10⁴
Slope=204 lb.
Pcr.=790+204=994 lb.
Slope=2910 lb.
Pcr.=790+2910=3700 lb.
Assumed "Zero Load" for computations 790 lb.

FIGURE 4.—*Southwell analysis of eccentrically loaded column*

[32] Donnell's recent paper also notes this possibility in the case of columns. (See ref. 10.)

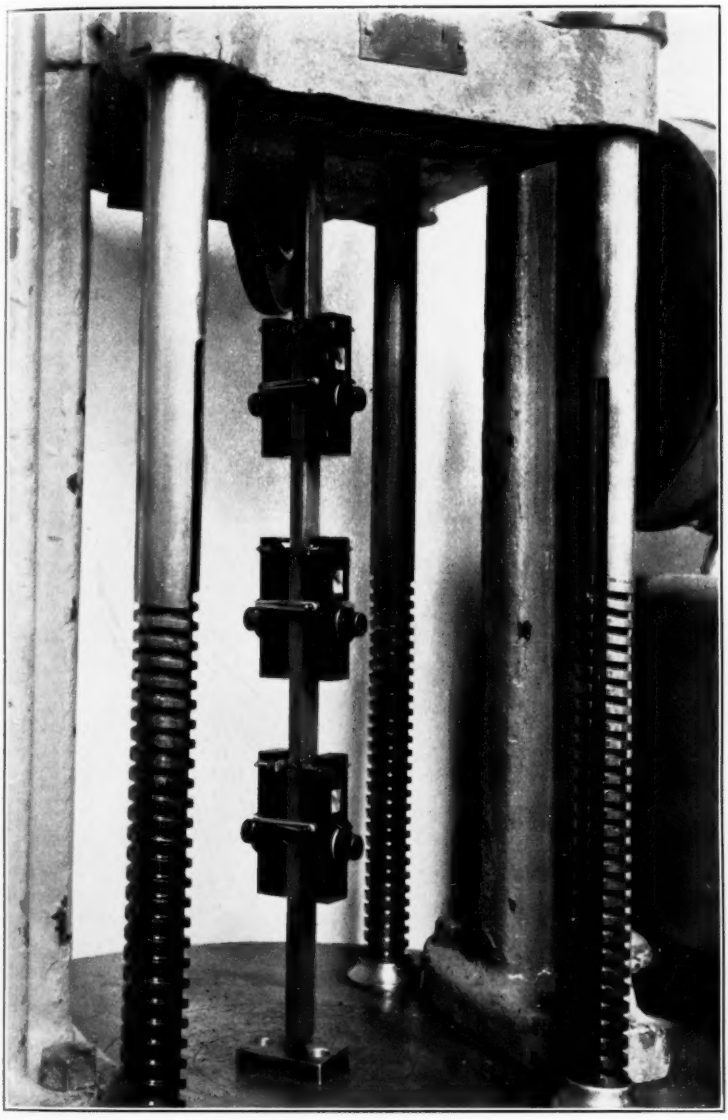

FIGURE 3.—*Straight column with equal and opposite eccentricities with gages at the quarter points and center to determine the first and second critical loads.*

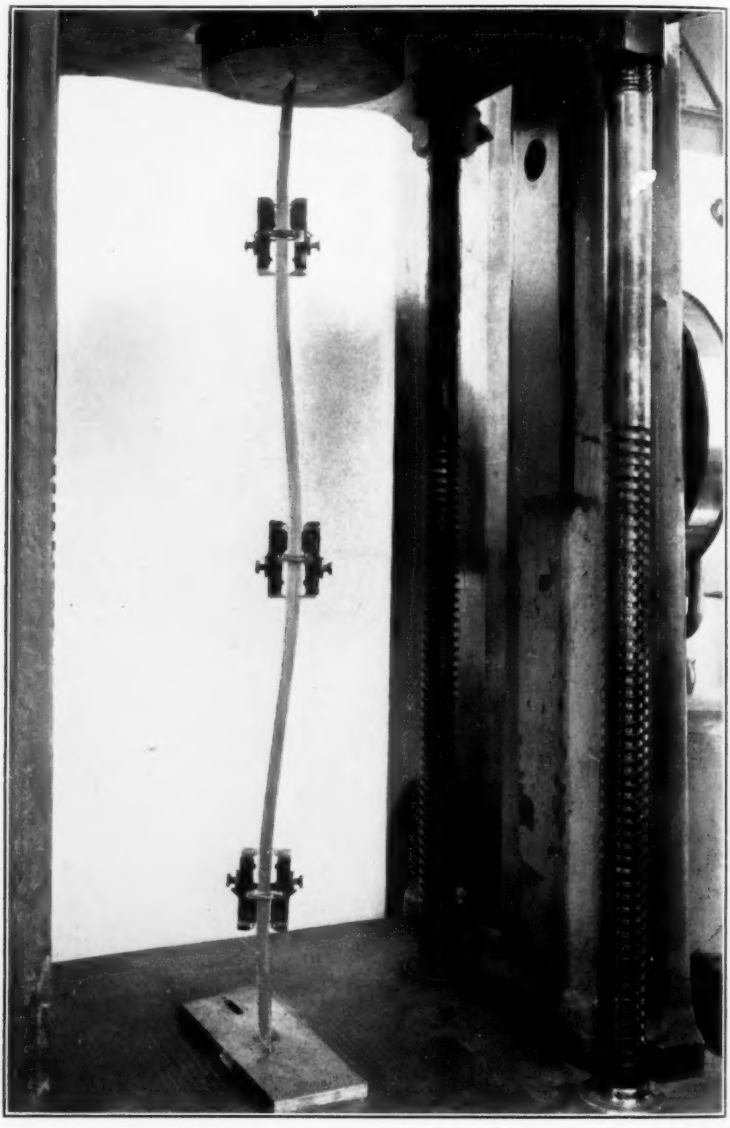

FIGURE 5.—*Eccentrically loaded bent column with gages at the sixth points and center to determine the first and third critical loads.*

load, which is theoretically four times the first critical load. Application of the analysis to this difference should therefore be expected to determine this second critical load, provided the corresponding term of $\overline{F}$ is sufficiently predominant.

4. EXPERIMENTAL RESULTS FOR SECOND CRITICAL LOAD

The experimental data are given in table 1 and the final curves are plotted in figure 4.

In table 2 the theoretical critical loads calculated from Euler's theory are compared with the critical loads computed from the strain-gage readings. The values agree within 0 and 3 percent for the first critical load and 11 percent for the second.

TABLE 1.—*Critical load of 13.5-by-¼ by ½-inch cold-rolled steel column with equal and opposite eccentricities at the ends*

Load	[a]Δ_T	[a]Δ_M	[a]Δ_B	P_1	$\frac{1}{2}d_1$[b]$=\left(\frac{\Delta_M}{2}\right)$	$\frac{\frac{1}{2}d_1}{P_1}$[b]	d_2[b]$=\left(\frac{\Delta_T-\Delta_B}{2}\right)$	$\frac{d_2}{P_1}$[b]
lb	10^{-4}	10^{-4}	10^{-4}	*lb*	10^{-4}	$\frac{10^{-4}}{lb}$	10^{-4}	$\frac{10^{-4}}{lb}$
790	0	0	0	0	0		0	
750	−1.02	−0.73	+0.01	−40	−0.37	+0.00912	−0.51	0.01288
710	−1.93	−1.20	+.13	−80	−.60	.00750	−1.03	.01288
670	−2.73	−1.63	+.33	−120	−.81	.00679	−1.53	.01275
630	−3.40	−1.93	.54	−160	−.96	.00602	−1.97	.01231
590	−4.10	−2.19	.91	−200	−1.09	.00548	−2.50	.01252
550	−4.67	−2.34	1.21	−240	−1.17	.00488	−2.94	.01225
510	−5.23	−2.53	1.52	−280	−1.26	.00452	−3.38	.01205
470	−5.73	−2.66	1.82	−320	−1.33	.00416	−3.78	.01179
430	−6.29	−2.78	2.19	−360	−1.39	.00386	−4.24	.01178
390	−6.74	−2.87	2.52	−400	−1.44	.00359	−4.63	.01158
350	−7.22	−3.01	2.83	−440	−1.50	.00342	−5.02	.01142
310	−7.69	−3.05	3.14	−480	−1.52	.00318	−5.42	.01130
270	−8.14	−3.13	3.47	−520	−1.56	.00301	−5.80	.01115
230	−8.53	−3.19	3.79	−560	−1.60	.00285	−6.16	.01100
190	−9.01	−3.26	4.08	−600	−1.63	.00272	−6.55	.01090
150	−9.40	−3.35	4.40	−640	−1.68	.00262	−6.90	.01080
110	−9.78	−3.36	4.71	−680	−1.68	.00247	−7.24	.01065

[a] Δ is the difference in strain on opposite sides of the specimen (bending strain) arranged to be zero at the arbitrary "zero load" for computations of 790 lb.

[b] d_1 and d_2 are the bending strains corresponding to the first and second critical loads, respectively.

TABLE 2.—*Critical load of 13.5- by ¼- by-½-inch cold-rolled steel column with equal and opposite eccentricities at the ends*

	Pounds
FIRST CRITICAL LOAD	
From strain at middle	994
From strain at quarter points	1,015
Theoretical $\left(\frac{\pi^2 EI}{l^2}\right)$	1,020
(Assumed $E=29\times10^6$ lb/in.^{2})	
SECOND CRITICAL LOAD	
From strain at quarter points	3,700
Theoretical $\left(\frac{4\pi^2 EI}{l^2}\right)$	4,100
(Assumed $E=29\times10^6$ lb/in.^{2})	

5. EXPERIMENTAL ARRANGEMENT FOR THIRD CRITICAL LOAD

The fair success obtained in the calculation of the second critical load from heterostatic strains below the first critical load made it seem worth-while to see if still higher critical loads could be similarly

determined. A piece of cold-rolled steel, ⅜ by ¾ by 27.7 inches, was chosen so as to allow strain gages to be placed one-sixth of its length from each end without coming too close to the ends. To ensure that the term of the summation in eq 14 corresponding to the third critical load should be fairly large, it was loaded as a "round-end" column with approximately equal like eccentricities at either end. This automatically ensured that terms corresponding to the second critical load would be small. To keep the terms corresponding to the first critical load small, the bar was slightly bent symmetrically at the middle in a direction toward the line of application of the eccentric load. It is readily seen that difference between the sum of the bending strains (difference in strain on opposite gages) at the two-sixth points and the bending strain at the middle will depend chiefly upon the variation of the astatic parameter corresponding to the third critical load, while their sum plus twice the bending strain at the middle will depend chiefly upon the astatic parameter corresponding to the first critical load. Two tests were made, one in which the bending strains corresponding to the first critical load were predominant and, a second, after bending to the shape shown in figure 5, in which the bending strains corresponding to the third critical load were predominant.

6. EXPERIMENTAL RESULTS FOR THIRD CRITICAL LOAD

The data are given in table 3 and the final curves are plotted in figure 6.

In table 4 the theoretical critical loads calculated by Euler's theory are compared with the critical loads computed from the strain-gage readings. The values agree within 1 percent for the first critical load and 12 percent for the third critical load.

TABLE 3.—*Critical load of 27.7-by ⅜-by ¼-inch cold-rolled steel column with equal eccentricities at the ends*

P	[a]Δ_T	[a]Δ_M	[a]Δ_B	d_3[b]$=\left(\frac{2\Delta_M+\Delta_B+\Delta_T}{3}\right)$	P_3[a]	a_1[b]	[a]Δ_T	[a]Δ_M	[a]Δ_B	d_1[b]$=\left(\frac{\Delta_M-\Delta_T-\Delta_B}{3}\right)$	P_1[a]	$\frac{d_1}{P_1}$[b]
lb	10^{-4}	10^{-4}	10^{-4}	10^{-4}	*lb*	$\frac{10^{-4}}{lb}$	10^{-4}	10^{-4}	10^{-4}	10^{-4}	*lb*	$\frac{10^{-4}}{lb}$
100	1.81	−6.03	1.16	−3.03	−900	0.00337	0	0		0	0	
200	1.53	−5.60	0.96	−2.90	−800	.00363	−1.10	+1.32	−1.59	+1.34	100	0.01337
300	1.22	−5.24	.74	−2.84	−700	.00406	−2.55	+2.57	−3.07	2.73	200	.01365
400	0.92	−4.81	.51	−2.73	−600	.00455	−3.81	+3.96	−4.60	4.12	300	.01373
500	.66	−4.31	+.31	−2.55	−500	.00510	−5.13	+5.34	−6.21	5.56	400	.01390
600	.41	−3.78	+.10	−2.35	−400	.00587	−6.44	+6.75	−7.80	7.00	500	.01399
700	.17	−3.20	−.06	−2.10	−300	.00699	−7.87	+8.23	−9.55	8.55	600	.01425
800	+.01	−2.40	−.17	−1.65	−200	.00960	−9.26	+9.77	−11.25	10.09	700	.01442
900	−.11	−1.49	−.20	−1.10	−100	.01097	−10.70	+11.35	−13.01	11.69	800	.01461
1,000	0	0	0	0	0		−12.09	+12.79	−14.75	13.21	900	.01469

[a] Δ is the difference in strain on opposite sides of the specimen (bending strain) arranged to be zero at the arbitrary "zero load" for computations of 1,000 lb.

[b] d_1 and d_3 are the bending strains corresponding to the first and third critical loads, respectively.

[a] For these readings the column was bent as shown in figure 5 to emphasize the third harmonic. For these the arbitrary "zero load" for computations is 100 lb.

TABLE 4.—*Critical load of a 27.7- by ⅛- by ¾-inch cold-rolled steel column*

	Pounds
FIRST CRITICAL LOAD	
From strain gages	1,251
Theoretical $\left(\frac{\pi^2 EI}{l^2}\right)$	1,240
(Assumed, E=29x10⁶ lb/in.²)	
THIRD CRITICAL LOAD	
From strain gages	9,825
Theoretical $\left(\frac{9\pi^2 EI}{l^2}\right)$	11,100
(Assumed, E=29x10⁶ lb/in.²)	

7. AGREEMENT WITH EULER COLUMN THEORY

The agreement in the case of the first critical load (in all cases within 3 percent) is materially better than in the case of the second and third critical loads, (within 11 percent and 12 percent, respectively). This was to be expected since in spite of the fact that the experimental conditions were adjusted to make q_1 as small as possible, the denominator, (Q_1-P), decreased rapidly with increasing P, so that $q_1/(Q_1-P)$, may have been appreciable in comparison with $q_2/(Q_2-P)$, and $q_3/(Q_3-P)$. Further, it was impossible in the experimental arrangement to eliminate wholly terms corresponding to still higher loads. In spite of careful work the experimental errors were so great that it was not feasible to secure better values by means of the successive approximations outlined in section II, 7. The calculation of these higher critical loads is in effect an extrapolation of loads over a range of nearly *5 to 1* in the case of the second critical load and of nearly *10 to 1* in the case of the third critical load. In view of the experimental difficulties involved, the errors are less than might have been expected for extrapolations over such great ranges.

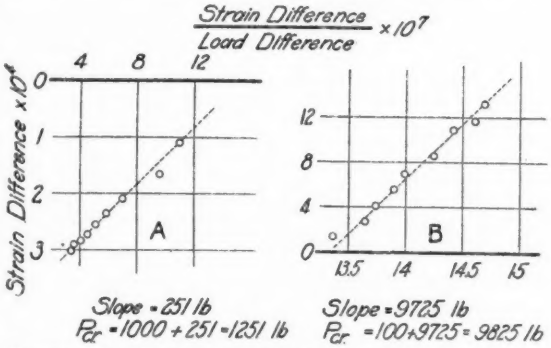

FIGURE 6.—*Southwell analysis of eccentrically loaded column.*

Curve *A*, column bent to accentuate fundamental mode. Curve *B*, same column bent to accentuate third harmonic mode. Assumed "zero load" for computations *A*, 1,000 pounds; *B*, 100 pounds.

IV. SUMMARY

1. The history of Southwell's method for the analysis of experimental observations in problems of elastic instability is reviewed.
2. Westergaard's general theory is applied to the problem.
3. It is shown that Southwell's method and Lundquist's modification of it are theoretically accurate for results of measurements which are proportional to the value of any one astatic parameter.

4. If the measurements are affected appreciably by changes in other parameters, the critical load computed by Southwell's method or Lundquist's modification may be considerably in error. A combined numerical and graphical method of computation is outlined which by successive approximations gives more accurate results in some such cases.

5. Finally, experimental results are given in which the second and third critical loads of a "round-end" Euler column are computed from strain-gage measurements taken at loads below the first critical load.

The author is much indebted to A. E. McPherson and S. Levy for making the experimental measurements reported and for valuable suggestions and assistance in preparing the manuscript.

WASHINGTON, October 15, 1938.

U. S. DEPARTMENT OF COMMERCE NATIONAL BUREAU OF STANDARDS

RESEARCH PAPER RP1164

Part of Journal of Research of the National Bureau of Standards, Volume 22, January 1939

SECOND SPECTRUM OF XENON [1]

By Curtis J. Humphreys

ABSTRACT

The description of the various xenon spectra excited in condensed Geissler-tube discharges has been improved and extended to include about 2,600 lines ranging from 2200 to 10200 A in wave length. The use of the method employed in the investigation of analogous spectra, that is, of noting intensity changes accompanying variations of inductance in the electrical circuit, has led to the selection of the lines belonging to the second spectrum of xenon (Xe II) characteristic of once-ionized xenon atoms (Xe^+). This description of Xe II includes estimates of relative intensities, wave-length measurements, and wave numbers for 1,200 lines, the list being abridged somewhat by the omission of very faint lines. 633 lines are classified as transitions between 103 energy levels, 75 of which have been more or less definitely identified with quantum numbers and electron configurations. Revisions and extensions of an earlier preliminary analysis are incorporated into the paper.

The $5s^2\ 5p^5$ electron configuration of the Xe^+ ion in its normal state is represented by a previously known doublet P term with a level separation of 10537.3 cm^{-1}. The excited states, described by doublet and quartet terms, are built upon the ^3P, ^1D, and ^1S states of Xe III by the addition of *ns*, *np*, *nd*, or *nf* electrons to the $5s^2\ 5p^4$ group constituting the outer structure of the doubly charged atom (Xe^{++}). Nearly all levels of excited states with lowest *n* values are accounted for. Quantum designations are given for most of the higher even levels. The use of extensive extreme-ultraviolet data, furnished by J. C. Boyce, which contain the combinations of even terms with the low doublet, has aided greatly in the location and confirmation of these levels. Limitations on the meaning of the quantum symbols imposed as a result of configuration interactions and approximate realization of *jj* coupling are discussed.

CONTENTS

	Page
I. Introduction	19
II. Observations and wave-length measurements	21
1. Sources	21
2. Spectrographs	21
3. Separation of Xe II from other xenon spectra	21
4. Description of Xe II	22
5. Precision of wave-length measurements	47
6. Spectra of xenon in the extreme ultraviolet	47
III. Analysis of Xe II	48
1. Theoretical terms	48
2. Table of terms	49
3. Low levels of Xe II	51
4. High levels of Xe II	52
5. Absolute values of terms	53
IV. References	53

I. INTRODUCTION

The spectra of the noble gases of the atmosphere have been the subject of an extensive series of investigations by members of the Spectroscopy Section of the National Bureau of Standards. These

[1] A report on this investigation was presented at the Washington meeting of the American Physical Society, April 1938. Phys. Rev. **53**, 940 (1938).

investigations, which have dealt principally with krypton and xenon, have included observations of the spectra of various stages of excitation throughout the wave-length range accessible to photography in air, preparation of descriptions of these spectra, comprising wave lengths in air, wave numbers in vacuum, estimated intensities and notes on the character of the lines, and, finally, the classification of the lines of the various spectra as transitions among the energy levels characteristic of the respective atoms. Spectra originating in neutral atoms, and in singly ionized and doubly ionized atoms have been studied. The investigation here reported is the last needed to complete the set of descriptions and analyses of the following spectra: Kr I, Kr II, and Kr III, and Xe I, Xe II, and Xe III. The title of this paper refers specifically to Xe II, the spectrum of singly ionized xenon, as distinguished from the composite spectrum of successive stages excited when the discharge circuit contains a spark gap and condensers. In old papers the word "second spectrum" is frequently used in the latter sense.

An account of earlier work on xenon spectra is given in a paper on the first spectrum by Meggers, deBruin, and the author, published in 1929 [1].[2] Subsequent to the preparation of a description of xenon spectra excited in Geissler-tube discharges with condensers and spark gap in the circuit, the same authors published in 1931 [2] a brief paper on Xe II. The low doublet, $s^2p^5\ ^2P$, having a separation of 10537.3 cm^{-1} and 30 higher levels, together with quantum-number assignments, were reported. Revision of this work has resulted in the retention of 20 of these levels with some changes of assignment. The present paper incorporates these revisions and contains a description consisting of wave lengths, wave numbers, and intensity estimates of 1,200 lines. Classifications are given for 633 of these lines as transitions among 103 levels. In the interim since the appearance of the preliminary publication, the wave-length data have been improved by additional observations with instruments of higher resolving power than those previously used and have been extended to beyond 10000 A in the infrared by use of new photographic materials.

It was intended originally by those who had collaborated previously in the program of investigations of noble-gas spectra that the analysis of Xe II should be brought to a state of completion comparable with that of Kr II reported by deBruin, Humphreys, and Meggers in 1933 [3]. This expectation has been substantially realized. The number of observed and measured lines is somewhat greater for Xe II, a feature attributable in part to extensive observations with recently discovered sensitizing agents for extending the range of photographically recorded spectra in the infrared, but mainly because of inherently greater complexity in the spectra of heavier atoms. The number of discovered energy levels whose reality seems beyond question and the number of lines classified as transitions between such levels is slightly less for Xe II, the relative number being about 80 percent for both levels and classified lines.

A Zeeman-effect analysis was included in the Kr II paper. The assignment of quantum numbers to the levels of Xe II was made without the aid of Zeeman effects. After completion of the analysis in essentially its present form, about 70 Zeeman-effect patterns were made available through the kindness of T. L. deBruin, who made the

[2] Numbers in brackets indicate the literature references at the end of this paper.

observations at the laboratory "Physica" in Amsterdam. A study of these patterns, which made possible the computation of g values for many of the low terms, did not indicate any important changes of assignment. In only one instance was a correction made. It was decided, therefore, to publish the analysis without Zeeman effects.

II. OBSERVATIONS AND WAVE-LENGTH MEASUREMENTS

1. SOURCES

Geissler tubes operated by alternating-current transformers have been used exclusively as sources for the production of xenon spectra in this investigation. Tubes manufactured by Robert Gotze in Leipzig were used for all the recent observations. In some cases these had been refilled after they had become inoperative because of the occlusion of xenon resulting from sputtering of the electrodes. These tubes are so constructed as to permit end-on exposure, and, when operated with condensers and spark gap in the circuit, thus producing the spectra of ionized xenon, give a very brilliant discharge. Exposures of only a few minutes, using 21-foot grating mountings, were sufficient to record the spectrum in the regions of strongest emission for Xe II, the strongest lines of which, barring the extreme ultraviolet lines involving the normal state, are within the range of visible radiation.

2. SPECTROGRAPHS

The compilation of wave lengths of all observed lines in the composite xenon spectrum from condensed park discharges contains about 2600 entries, beginning at 2230 A in the ultraviolet and extending to 10220 A in the infrared. The ultraviolet region was observed, using quartz tubes along with a Hilger E_1 spectograph. It was found possible to extend grating observations down to 2575 A with the extremely thin-walled Gotze glass tubes. Consequently, all wave lengths greater than 2575 A are based on grating observations.

Most of the observations were made with the 21-foot radius, 20,000 lines-per-inch Rowland grating. For wave lengths greater than 8000 A the 7,500 lines-per-inch Anderson grating was used. These infrared observations have been extended whenever new sensitizing agents became available. Eastman Z-type plates being used in the most recent exposures. During the past year the Bureau obtained a new 30,000 lines-per-inch grating. A series of observations in the visible region was made with this instrument in order to improve the wave lengths.

3. SEPARATION OF Xe II FROM OTHER XENON SPECTRA

The method of separating higher spark spectra from the spectrum of the singly ionized atom by noting the intensity changes accompanying the introduction of inductance into the discharge circuit has been discussed in previous publications, particularly in the paper on Xe III [4]. The effect of inductance is to weaken or suppress the higher spark lines or, in general, those requiring greater excitation energy. The behavior of an electrodeless discharge source may also be used to differentiate between stages of excitation. Here the essential criteria are the effect of pressure and applied voltage on relative line intensities and the spatial distribution of ions in the tube, as indi-

cated by the length of the lines when end-on illumination of a long slit is utilized. Lines of the first spark spectrum appear as short lines originating in the center of the tube; whereas, lines of the second or higher spark spectra are long lines whose emitters have greater population near the walls. Bloch, Bloch, and Déjardin [5] observed about 1,000 xenon spark lines, using the electrodeless discharge and noted the spectrum to which each line was assigned. The essential agreement of what we may call the roman-numeral classification made from the Bureau's data with the separation made by Bloch, Bloch, and Déjardin has been noted [4]. As determined by the final term analysis, it is more satisfactory for Xe II than for Xe III. It was estimated in the publication on Xe III [4] that three-fourths of the observed spark lines belonged to Xe II. Following the intensive examination of the wave-length list required in making the term analysis of Xe II, any revision of this estimate would be downward, although Xe II lines are clearly more abundant than those of all higher spectra taken together. The estimate is made difficult by the several hundred faint unclassified lines of uncertain origin. Furthermore, it was not feasible to test the effect of inductance on infrared lines beyond 8000 A because of the length of exposures required.

4. DESCRIPTION OF Xe II

The list of lines selected for publication is assembled in table 1, which gives estimated intensity, wave length in air, wave number in vacuum, and the levels involved in the transition for each classified line. The intensity estimates are given in two columns, the first being the intensity indicated with inductance; the second, without inductance. The intensities are comparable only over short ranges. Lines marked 1- are so faint as to be just barely measurable. The intensity estimates are in some cases accompanied by symbols which are explained as follows: *h* indicates that the line is hazy or diffuse; *H* very hazy; *l*, unsymmetrical and shaded towards longer wave lengths; *s*, unsymmetrical and shaded toward shorter wave lengths; *w*, wide; and *d*, double. Combinations of these symbols of obvious meaning are used, such as *hw* or *hl*. The table contains 1,200 entries, including all well-observed lines for which there is any reasonable probability of origin in Xe II ions. A small number of lines are included which show behavior with inductance contrary to that expected for Xe II. These are marked by an asterisk (*) and are, in all cases, lines attributed to Xe II by Bloch, Bloch, and Déjardin [5]. Because of the very poor agreement of the wave lengths of these observers with ours, the same line may not be under consideration in every instance. The list of Xe III lines published [4] included only those which could be classified as transitions between known levels. Following the publication of the list contained in table 1, there remain in our description about 1,100 lines, of which at least 450 originate in Xe III or higher spectra, the balance being very faint lines of uncertain origin. The latter group for the most part are observed only once and the wave lengths cannot be measured precisely.

TABLE 1.—*List of* Xe II *lines*

Intensity		Wave length (air)	Wave number (vac)	Transition
1*h*		2230. 79	44813. 2	$(^3P)\ 5d\ ^4D_{2\frac{1}{2}} - (^1S)\ 6p\ ^2P_{1\frac{1}{2}}$
2*h*		2241. 86	44591. 9	$(^3P)\ 5d\ ^4D_{3\frac{1}{2}} - 15_{2\frac{1}{2}}$
4		2249. 86	44433. 4	$(^3P)\ 6s\ ^4P_{1\frac{1}{2}} - 9_{1\frac{1}{2}}$
1*h*		2256. 56	44301. 5	$(^3P)\ 5d\ ^4D_{1\frac{1}{2}} - 19_{1\frac{1}{2}}$
1*h*		2259. 22	44249. 1	$(^3P)\ 5d\ ^4D_{2\frac{1}{2}} - 11_{2\frac{1}{2}}$
2		2262. 95	44176. 4	$(^3P)\ 5d\ ^4D_{1\frac{1}{2}} - (^1S)\ 6p\ ^2P_{1\frac{1}{2}}$
2		2264. 20	44152. 0	$(^3P)\ 5d\ ^4D_{1\frac{1}{2}} - 17_{0\frac{1}{2}}$
3*h*		2265. 62	44124. 4	$(^3P)\ 6s\ ^2P_{0\frac{1}{2}} - 31_{1\frac{1}{2}}$
2*h*		2265. 94	44118. 1	$(^3P)\ 6s\ ^4P_{1\frac{1}{2}} - 7_{1\frac{1}{2}}$
3*h*		2266. 80	44101. 4	$(^3P)\ 5d\ ^4D_{2\frac{1}{2}} - 9_{1\frac{1}{2}}$
1*h*		2268. 72	44064. 1	$(^3P)\ 6s\ ^4P_{1\frac{1}{2}} - 5_{1\frac{1}{2}}$
2*h*		2285. 24	43746. 6	
8	2	2285. 94	43732. 2	$(^3P)\ 5d\ ^4D_{2\frac{1}{2}} - 5_{1\frac{1}{2}}$
2*h*		2290. 84	43638. 6	$(^3P)\ 5d\ ^2P_{1\frac{1}{2}} - 33_{1\frac{1}{2}}$
20	7	2292. 40	43608. 9	$(^3P)\ 5d\ ^4D_{2\frac{1}{2}} - 3_{3\frac{1}{2}}$
15	5	2294. 57	43567. 7	$(^3P)\ 5d\ ^4D_{3\frac{1}{2}} - 3_{3\frac{1}{2}}$
30	8	2296. 52	43530. 7	
2*h*		2299. 36	43476. 9	$(^3P)\ 5d\ ^4D_{0\frac{1}{2}} - 19_{1\frac{1}{2}}$
6	2	2299. 98	43465. 2	$(^3P)\ 5d\ ^4D_{1\frac{1}{2}} - 9_{1\frac{1}{2}}$
1*h*		2304. 60	43378. 1	$(^1D)\ 6s\ ^2D_{1\frac{1}{2}} - 39_{1\frac{1}{2}}$
3	1	2307. 28	43327. 7	$(^3P)\ 5d\ ^4D_{0\frac{1}{2}} - 17_{0\frac{1}{2}}$
5	1	2313. 70	43207. 5	$(^3P)\ 5d\ ^4P_{2\frac{1}{2}} - 37_{2\frac{1}{2}}$
10	3	2316. 80	43149. 7	$(^3P)\ 5d\ ^4D_{1\frac{1}{2}} - 7_{1\frac{1}{2}}$
7	2	2319. 70	43095. 8	$(^3P)\ 5d\ ^4D_{1\frac{1}{2}} - 5_{1\frac{1}{2}}$
2*h*		2335. 42	42805. 7	$(^3P)\ 5d\ ^4P_{2\frac{1}{2}} - 35_{2\frac{1}{2}}$
3*h*		2342. 18	42682. 2	
12	4	2344. 47	42640. 5	$(^3P)\ 5d\ ^4D_{0\frac{1}{2}} - 9_{1\frac{1}{2}}$
4*h*		2351. 18	42518. 8	
4*h*		2351. 56	42493. 9	
1*h*		2353. 52	42476. 5	$(^3P)\ 5d\ ^4P_{2\frac{1}{2}} - 33_{1\frac{1}{2}}$
1*h*		2353. 89	42469. 9	
1*h*		2356. 25	42427. 3	$(^3P)\ 5d\ ^4P_{0\frac{1}{2}} - 31_{1\frac{1}{2}}$
4*h*	1	2356. 72	42418. 9	
1*h*		2360. 42	42352. 4	
1*h*		2362. 60	42313. 3	$(^3P)\ 6s\ ^4P_{0\frac{1}{2}} - 23_{1\frac{1}{2}}$
5	1	2368. 68	42204. 7	$(^3P)\ 6s\ ^4P_{1\frac{1}{2}} - 1_{1\frac{1}{2}}$
4*h*	1	2369. 62	42188. 0	
1*h*		2378. 04	42038. 6	
1		2385. 85	41901. 0	$(^3P)\ 5d\ ^4P_{2\frac{1}{2}} - 31_{1\frac{1}{2}}$
2*h*		2386. 14	41895. 9	
4	1	2387. 75	41867. 6	$sp^6\ ^2S_{0\frac{1}{2}} - (^1D)\ 6p\ ^2P_{0\frac{1}{2}}$
2*h*		2392. 15	41790. 5	
2*h*		2392. 33	41787. 5	
4		2398. 76	41675. 5	$(^3P)\ 5d\ ^2D_{2\frac{1}{2}} - 37_{2\frac{1}{2}}$
2*h*		2401. 79	41622. 9	$(^3P)\ 5d\ ^4P_{0\frac{1}{2}} - 29_{1\frac{1}{2}}$
3*h*		2405. 92	41551. 5	$(^1D)\ 5d\ ^2F_{2\frac{1}{2}} - 39_{1\frac{1}{2}}$
40	2	2409. 74	41485. 6	
7	1	2410. 72	41468. 8	$(^3P)\ 5d\ ^2P_{0\frac{1}{2}} - 31_{1\frac{1}{2}}$
20*h*	1	2421. 27	41288. 1	
2		2422. 12	41273. 6	$(^3P)\ 5d\ ^2D_{2\frac{1}{2}} - 35_{2\frac{1}{2}}$

TABLE 1.—*List of* Xe II *lines*—Continued

Intensity		Wave length (air)	Wave number (vac)	Transition
10	1	2422. 94	41259. 6	
40*h*	4	2425. 05	41223. 6	
12	2	2432. 72	41093. 8	(^{3}P) $5d\ ^4P_{2½}-29\dot{1}_{1½}$
1	2	2435. 12	41053. 3	
6	1	2435. 47	41047. 4	(^{3}P) $5d\ ^2D_{1½}-33\dot{1}_{1½}$
1-		2438. 76	40992. 0	(^{3}P) $5d\ ^4P_{1½}-31\dot{1}_{1½}$
2*h*		2441. 60	40944. 3	(^{3}P) $5d\ ^2D_{2½}-33\dot{1}_{1½}$
1H		2442. 78	40924. 5	
2*h*		2444. 40	40897. 4	
1-		2464. 72	40560. 3	
2*h*		2466. 60	40529. 4	
5	1	2468. 43	40499. 3	
5	1	2469. 46	40482. 4	
5	1	2470. 18	40470. 5	(^{3}P) $5d\ ^2D_{1½}-31\dot{1}_{1½}$
100	12	2475. 89	40377. 0	
4		2478. 82	40329. 6	
50	5	2489. 11	40162. 9	(^{3}P) $5d\ ^4P_{1½}-27\dot{3}_{2½}$
20	4	2490. 76	40136. 3	(^{3}P) $5d\ ^4P_{1½}-25\dot{1}_{1½}$
5	1-	2491. 78	40119. 9	(^{1}D) $6s\ ^2D_{2½}-37\dot{2}_{1½}$
8	8	2506. 86	39878. 5	
5	6	2514. 29	39760. 7	
12	12	2516. 12	39731. 8	
6	6	2519. 17	39683. 7	
3		2524. 46	39600. 5	(^{3}P) $5d\ ^4F_{4½}-3\dot{3}_{3½}$
12	5	2526. 79	39564. 0	
12	5	2526. 98	39561. 0	(^{3}P) $5d\ ^2D_{2½}-29\dot{1}_{1½}$
6	6	2528. 49	39537. 4	(^{3}P) $5d\ ^2D_{2½}-27\dot{2}_{1½}$
2		2530. 18	39512. 0	(^{3}P) $5d\ ^2D_{2½}-25\dot{1}_{1½}$
3H		2531. 36	39492. 6	
3*h*		2538. 02	39389. 0	(^{1}D) $6s\ ^2D_{2½}-33\dot{1}_{1½}$
3*h*		2546. 37	39259. 8	
1-		2548. 90	39221. 8	
3	1-	2551. 70	39177. 8	(^{3}P) $6s\ ^4P_{0½}-19\dot{1}_{1½}$
1-		2554. 20	39139. 5	(^{3}P) $6s\ ^4P_{2½}-$(^{1}D) $6p\ ^2D\dot{2}_{1½}$
3		2560. 89	39037. 2	
2		2561. 48	39028. 2	(^{3}P) $6s\ ^4P_{0½}-17\dot{6}_{1½}$
15	4	2576. 97	38793. 6	$sp^6\ ^2S_{0½}-$(^{1}D) $6p\ ^2P\dot{1}_{1½}$
1		2584. 88	38675. 0	(^{3}P) $5d\ ^4F_{2½}-$(^{1}S) $6p\ ^2P\dot{1}_{1½}$
1		2585. 30	38668. 7	
1		2594. 64	38529. 5	
	5	2596. 86	38496. 5	
4	4	2597. 01	38494. 3	(^{3}P) $5d\ ^4F_{2½}-15\dot{3}_{3½}$
2	1	2598. 42	38473. 4	
50	10	2605. 54	38368. 3	
5	1	2606. 93	38347. 8	
1		2607. 52	38339. 2	(^{3}P) $6s\ ^4P_{0½}-9\dot{1}_{1½}$
2*h*		2621. 39	38136. 3	
1*h*	1*h*	2621. 74	38131. 2	
5*h*	1	2629. 54	38018. 1	
6*h*	2	2630. 40	38005. 7	(^{1}D) $6s\ ^2D_{2½}-29\dot{1}_{1½}$

TABLE 1.—*List of* Xe II *lines*—Continued

Intensity		Wave length (air)	Wave number (vac)	Transition
2[1]	2	2631. 25	37993. 4	$sp^6\ ^2S_{0\frac{1}{2}}-(^1D)\ 6p\ ^2F^\circ_{2\frac{1}{2}}$
2		2633. 88	37955. 5	$(^1D)\ 6s\ ^2D_{2\frac{1}{2}}-25i_{3\frac{1}{2}}$
2		2634. 20	37950. 9	
2*h*	1	2655. 39	37648. 1	
5*h*	1	2657. 00	37625. 2	$(^1D)\ 5d\ ^2D_{1\frac{1}{2}}-33i_{3\frac{1}{2}}$
1*h*		2659. 28	37593. 0	$(^3P)\ 5d\ ^4F_{2\frac{1}{2}}-5i_{3\frac{1}{2}}$
3	2	2663. 29	37536. 4	$(^3P)\ 6s\ ^2P_{1\frac{1}{2}}-19i_{3\frac{1}{2}}$
5	1	2668. 02	37469. 8	$(^3P)\ 5d\ ^4F_{2\frac{1}{2}}-3i_{3\frac{1}{2}}$
1	1	2670. 68	37432. 5	
4	1	2672. 22	37411. 0	$(^3P)\ 6s\ ^2P_{1\frac{1}{2}}-(^1S)\ 6p\ ^2P^\circ_{1\frac{1}{2}}$
1*h*	1*h*	2673. 80	37388. 9	
50*h*	50	2677. 18	37341. 7	
1*h*	1*h*	2681. 14	37286. 5	
1*h*	1*h*	2682. 75	37264. 1	
1*h*	1*h*	2682. 96	37261. 2	
3*h*		2686. 14	37217. 1	$(^1S)\ 5d\ ^2D_{2\frac{1}{2}}-39i_{3\frac{1}{2}}$
5	2	2687. 03	37204. 8	
1	1*h*	2689. 70	37167. 8	
1		2691. 40	37144. 4	$(^3P)\ 6s\ ^4P_{1\frac{1}{2}}-(^1D)\ 6p\ ^2D^\circ_{2\frac{1}{2}}$
	1	2691. 53	37142. 6	
1H	2H	2695. 24	37091. 4	
1*h*	3*h*	2699. 16	37037. 6	
2*h*		2701. 60	37004. 1	
2	1	2702. 22	36995. 6	$(^3P)\ 6s\ ^4P_{2\frac{1}{2}}-(^1D)\ 6p\ ^2F^\circ_{3\frac{1}{2}}$
2		2702. 34	36994. 0	$(^3P)\ 5d\ ^4P_{2\frac{1}{2}}-23i_{3\frac{1}{2}}$
10	15	2703. 44	36979. 0	$(^1D)\ 5d\ ^2D_{2\frac{1}{2}}-37i_{3\frac{1}{2}}$
1H	2H	2707. 39	36925. 0	
1*h*		2709. 52	36896. 0	
	1*h*	2709. 61	36894. 8	
1*h*		2709. 89	36890. 9	
1*h*	1*h*	2711. 02	36875. 6	
	2*h*	2711. 65	36867. 0	
1*h*		2711. 88	36863. 9	
1*h*		2713. 40	36843. 2	
	1*h*	2713. 64	36840. 0	
3	3	2715. 76	36811. 2	$(^3P)\ 5d\ ^4D_{2\frac{1}{2}}-(^1D)\ 6p\ ^2D^\circ_{2\frac{1}{2}}$
30	15	2717. 35	36789. 7	
1—		2718. 79	36770. 2	$(^3P)\ 5d\ ^4D_{3\frac{1}{2}}-(^1D)\ 6p\ ^2D^\circ_{2\frac{1}{2}}$
	1—	2721. 28	36736. 5	$(^3P)\ 6s\ ^2P_{0\frac{1}{2}}-21i_{1\frac{1}{2}}$
	1	2723. 40	36708. 0	$(^3P)\ 5d\ ^4D_{1\frac{1}{2}}-(^1D)\ 6p\ ^2P^\circ_{0\frac{1}{2}}$
1—	1—	2725. 66	36677. 5	
1—		2731. 46	36599. 6	$(^3P)\ 6s\ ^4P_{2\frac{1}{2}}-(^1D)\ 6p\ ^2P^\circ_{1\frac{1}{2}}$
25*hs*	25*hs*	2733. 15	36577. 0	$(^1D)\ 5d\ ^2D_{2\frac{1}{2}}-35i_{3\frac{1}{2}}$
50	50	2734. 14	36563. 8	$(^3P)\ 5d\ ^2P_{0\frac{1}{2}}-23i_{1\frac{1}{2}}$
1—	1	2739. 77	36488. 6	
2H	2*h*	2743. 16	36443. 5	
2	1	2744. 04	36431. 9	
1—	1*h*	2746. 77	36395. 6	
	1	2747. 68	36383. 6	
1*h*	1	2748. 79	36368. 9	

[1] This is probably a fortuitous combination since the selection rule for inner quantum numbers is violated.

TABLE 1.—*List of* Xe II *lines*—Continued

Intensity		Wave length (air)	Wave number (vac)	Transition
1—	1	2756. 48	36267. 4	
40*h*	40*h*	2757. 86	36249. 3	(^{1}D) 5*d* ^{2}D$_{2½}$—33$\mathring{i}_{1½}$
1—		2758. 36	36242. 7	(^{1}D) 5*d* ^{2}D$_{1½}$—29$\mathring{i}_{1½}$
2		2762. 77	36184. 9	(^{3}P) 6*p* ^{4}D$_{2½}$—(^{1}D) 6*d* ^{2}D$_{2½}$
1	2	2763. 56	36174. 5	(^{3}P) 5*d* ^{4}D$_{1½}$—(^{1}D) 6*p* ^{2}D$_{2½}$
1	2*h*	2767. 00	36129. 6	(^{3}P) 6*p* ^{4}P$_{0½}$—(^{1}D) 7*s* ^{2}D$_{1½}$
2*h*	3	2770. 41	36085. 1	(^{3}P) 6*s* ^{2}P$_{0½}$—19$\mathring{i}_{1½}$
5*h*	1	2773. 55	36044. 3	
15*h*	20	2774. 86	36027. 2	(^{1}D) 6*s* ^{2}D$_{1½}$—33$\mathring{i}_{1½}$
2*h*	2H	2782. 73	35925. 4	
	1*h*	2783. 80	35911. 5	
1	1*h*	2784. 98	35896. 3	
3	4	2785. 42	35890. 7	(^{3}P) 5*d* ^{4}D$_{1½}$—(^{1}D) 6*p* ^{2}D$\mathring{i}_{1½}$
2	1*h*	2789. 52	35837. 9	
1—		2792. 52	35799. 4	(^{3}P) 6*s* ^{4}P$_{2½}$—(^{1}D) 6*p* ^{2}F$\mathring{i}_{3½}$
	1	2794. 68	35771. 8	
2*h*	6*hl*	2796. 49	35748. 6	
	30*h*	2797. 65	35733. 8	(^{3}P) 5*d* ^{4}F$_{2½}$—1$\mathring{i}_{1½}$
	1*h*	2799. 69	35707. 7	
1*h*	2*h*	2802. 50	35671. 9	(^{1}D) 5*d* ^{2}D$_{2½}$—31$\mathring{i}_{1½}$
5	1*h*	2803. 02	35665. 3	
2H	10H*l*	2807. 55	35607. 8	
4*h*	1	2808. 56	35595. 0	
1H	2H	2819. 02	35462. 9	(^{3}P) 5*d* ^{2}D$_{2½}$—23$\mathring{i}_{1½}$
4*h*	10*h*	2820. 06	35449. 8	(^{1}D) 6*s* ^{2}D$_{1½}$—31$\mathring{i}_{1½}$
1	1	2824. 63	35392. 5	
1*h*	2*h*	2825. 34	35383. 6	
5H	20H*l*	2826. 94	35363. 5	
2*h*	8*h*	2827. 90	35351. 5	
1*h*	2*h*	2828. 69	35341. 7	
1*h*		2829. 04	35337. 3	
1*h*	1*h*	2830. 24	35322. 3	
1H	2*hl*	2830. 89	35314. 2	
2*h*	2*h*	2832. 00	35300. 4	
2	3*h*	2832. 46	35293. 6	
1*h*	2	2836. 16	35248. 6	(^{3}P) 6*s* ^{2}P$_{0½}$—9$\mathring{i}_{1½}$
3	1	2838. 85	35215. 2	
2	1	2839. 57	35206. 3	
1*hs*	3*hs*	2841. 81	35178. 5	
5	1	2844. 45	35145. 9	
8	1—	2845. 92	35127. 7	
3H	15*h*	2846. 48	35120. 8	
8	1	2849. 66	35081. 6	
3	5	2850. 95	35065. 8	(^{3}P) 5*d* ^{4}D$_{0½}$—(^{1}D) 6*p* ^{2}D$\mathring{i}_{1½}$
3*h*	4*h*	2852. 39	35048. 0	
1	2*h*	2853. 11	35039. 2	(^{3}P) 5*d* ^{4}P$_{0½}$—21$\mathring{i}_{1½}$
60	60	2854. 53	35021. 8	(^{3}P) 5*d* ^{2}P$_{1½}$—19$\mathring{i}_{1½}$
2	1*h*	2856. 65	34995. 8	
1*h*	2*h*	2857. 32	34987. 6	
1—	1	2859. 02	34966. 8	

TABLE 1.—*List of* Xe II *lines*—Continued

Intensity		Wave length (air)	Wave number (vac)	Transition
1	1—	2859. 54	34960. 4	
20*h*	20	2861. 90	34931. 6	(^{1}D) 5*d* ^{2}F$_{2½}$—37$\tilde{g}_{3½}$
150	200	2864. 73	34897. 1	(^{3}P) 5*d* ^{2}P$_{1½}$—(^{1}S) 6*p* ^{2}P$\tilde{}_{1½}$
5*h*	6	2866. 76	34872. 4	(^{3}P) 5*d* ^{2}P$_{1½}$—17$\tilde{g}_{2½}$
2*h*	2	2867. 36	34865. 1	(^{1}D) 5*d* ^{2}D$_{2½}$—29$\tilde{i}_{1½}$
1	1—	2869. 56	34834. 4	
50*hs*	10*hs*	2871. 24	34818. 0	
1H	2H	2877. 00	34748. 3	
1H	3H*l*	2878. 48	34730. 4	
	1—	2881. 14	34698. 3	(^{3}P) 5*d* ^{2}P$_{1½}$—13$\tilde{g}_{2½}$
12	14	2883. 71	34667. 4	(^{3}P) 5*d* ^{4}D$_{2½}$—(^{1}D) 6*p* ^{2}F$\tilde{}_{3½}$
10	15	2887. 12	34626. 5	(^{3}P) 5*d* ^{4}D$_{3½}$—(^{1}D) 6*p* ^{2}F$\tilde{}_{3½}$
10	15	2889. 07	34603. 1	(^{3}P) 6*s* ^{4}P$_{1½}$—(^{1}D) 6*p* ^{2}P$\tilde{}_{1½}$
150*h*	150*h*	2895. 22	34529. 6	(^{1}D) 5*d* ^{2}F$_{2½}$—35$\tilde{g}_{3½}$
3	5	2902. 68	34440. 9	
1	1—	2903. 66	34429. 2	
3	1	2904. 18	34423. 1	
2*h*	3*h*	2905. 10	34412. 2	(^{3}P) 6*p* ^{4}P$\tilde{}_{0½}$—(^{1}D) 6*d* ^{2}D$_{1½}$
80*h*	80	2907. 18	34387. 5	(^{3}P) 5*d* ^{4}P$_{0½}$—19$\tilde{i}_{1½}$
3H	4H	2910. 27	34351. 0	
1*h*	2	2910. 64	34346. 7	(^{3}P) 6*p* ^{4}P$\tilde{}_{2½}$—(^{1}D) 7*s* ^{2}D$_{2½}$
1—	1	2917. 01	34271. 7	
40	50	2919. 87	34238. 1	(^{3}P) 5*d* ^{4}P$_{0½}$—17$\tilde{g}_{1½}$
	1—	2923. 03	34201. 1	(^{1}D) 5*d* ^{2}F$_{2½}$—33$\tilde{i}_{1½}$
6	2	2923. 95	34190. 3	
2	5	2924. 38	34185. 3	(^{3}P) 5*d* ^{2}P$_{1½}$—9$\tilde{i}_{1½}$
2	3*h*	2927. 58	34147. 9	(^{3}P) 6*p* ^{4}P$\tilde{}_{1½}$—(^{3}P) 6*d* ^{2}D$_{1½}$
1H	3H	2929. 66	34123. 7	
1*h*	2*h*	2933. 34	34080. 9	(^{3}P) 5*d* ^{2}P$_{0½}$—21$\tilde{i}_{1½}$
2*h*	3*h*	2934. 80	34063. 9	(^{3}P) 5*d* ^{4}P$_{0½}$—13$_{0½}$
60*h*	50*h*	2935. 86	34051. 6	
5	2	2939. 72	34006. 9	
8	3	2941. 38	33987. 7	
20*h*	15	2942. 10	33979. 4	
4	1	2943. 41	33964. 3	
4*h*	1—	2944. 61	33950. 5	
4*h*	8*h*	2949. 77	33891. 1	
1*h*	2*h*	2950. 69	33880. 5	
2	2	2951. 58	33870. 3	(^{3}P) 5*d* ^{2}P$_{1½}$—7$\tilde{i}_{1½}$
2	3	2952. 48	33860. 0	(^{3}P) 5*d* ^{4}P$_{2½}$—19$\tilde{i}_{1½}$
2*d*	4H	2954. 78	33833. 6	
2	1*h*	2955. 84	33821. 5	
50	60	2963. 41	33735. 1	(^{3}P) 5*d* ^{4}P$_{2½}$—(^{1}S) 6*p* ^{2}P$\tilde{}_{1½}$
12*	1	2964. 19	33726. 2	
	2	2966. 74	33697. 2	*sp*^{6} ^{2}S$_{0½}$—(^{3}P) 6*p* ^{2}P$\tilde{}_{0½}$
	1	2968. 95	33672. 1	
3	1—	2969. 23	33669. 0	
12	4	2969. 80	33662. 5	
8	10	2972. 31	33634. 1	(^{3}P) 5*d* ^{4}D$_{1½}$—(^{1}D) 6*p* ^{2}P$\tilde{}_{1½}$
1	2	2972. 78	33628. 8	

TABLE 1.—*List of* Xe II *lines*—Continued

Intensity		Wave length (air)	Wave number (vac)	Transition
20H*l*	40H*l*	2974. 86	33605. 2	$(^3P)\ 5d\ ^4P_{1\frac{1}{2}}-21i_{1\frac{1}{2}}$
8	4	2976. 39	33588. 0	
	10H	2977. 90	33570. 9	
300	400	2979. 32	33554. 9	$(^3P)\ 5d\ ^4P_{2\frac{1}{2}}-15g_{2\frac{1}{2}}$
2	2	2982. 23	33522. 2	
10*	1	2986. 18	33477. 9	
8	15	2986. 82	33470. 7	$(^3P)\ 5d\ ^4D_{2\frac{1}{2}}-(^1D)\ 6p\ ^2F^0_{2\frac{1}{2}}$
1—	1	2988. 28	33454. 3	
12	15	2990. 54	33429. 0	$(^3P)\ 5d\ ^2P_{0\frac{1}{2}}-19i_{1\frac{1}{2}}$
3	5	2991. 73	33415. 8	$sp^6\ ^2S_{0\frac{1}{2}}-(^3P)\ 6p\ ^2D^0_{1\frac{1}{2}}$; $(^3P)\ 6p\ ^4D^0_{2\frac{1}{2}}-14_{2\frac{1}{2}}$
15H	15H	2999. 21	33332. 4	
1*h*	2*h*	3003. 10	33289. 2	
40	40	3003. 98	33279. 5	$(^3P)\ 5d\ ^2P_{0\frac{1}{2}}-17g_{0\frac{1}{2}}$
1—	1	3005. 97	33257. 5	
2	2	3006. 97	33246. 4	
1		3012. 88	33181. 2	$(^3P)\ 5d\ ^4P_{0\frac{1}{2}}-5i_{1\frac{1}{2}}$
	2*h*	3013. 82	33170. 8	$(^3P)\ 5d\ ^4P_{2\frac{1}{2}}-11i_{2\frac{1}{2}}$
20*h*	15*h*	3015. 52	33152. 2	$(^1S)\ 6s\ ^2S_{0\frac{1}{2}}-41i_{1\frac{1}{2}}$
100*h*	100*h*	3017. 43	33131. 2	
2*h*	3	3019. 78	33105. 4	$(^3P)\ 5d\ ^2P_{0\frac{1}{2}}-13g_{0\frac{1}{2}}$
2	1	3020. 29	33099. 8	
2H	5H	3022. 10	33080. 0	
1—	2*h*	3024. 24	33056. 6	
3	5	3027. 27	33023. 5	$(^3P)\ 5d\ ^4P_{2\frac{1}{2}}-9i_{1\frac{1}{2}}$
2*h*	3*h*	3027. 63	33019. 5	$(^3P)\ 6p\ ^2P_{0\frac{1}{2}}-1i_{1\frac{1}{2}}$; $(^3P)\ 6p\ ^4D_{1\frac{1}{2}}-(^1D)\ 7s\ ^2D_{1\frac{1}{2}}$
6*		3033. 11	32959. 9	
10	15	3033. 71	32953. 4	$(^3P)\ 5d\ ^4P_{1\frac{1}{2}}-19i_{1\frac{1}{2}}$
30*h*	30*h*	3036. 80	32919. 8	$(^1S)\ 5d\ ^2D_{1\frac{1}{2}}-41i_{1\frac{1}{2}}$
6*h*	8	3037. 35	32913. 9	$(^3P)\ 6p\ ^4D^0_{1\frac{1}{2}}-(^1D)\ 6d\ ^2D_{2\frac{1}{2}}$
	1	3041. 72	32866. 6	
12*h*	2*h*	3042. 12	32862. 3	
10	12	3044. 75	32833. 9	$(^3P)\ 5d\ ^4D_{1\frac{1}{2}}-(^1D)\ 6p\ ^4F^0_{2\frac{1}{2}}$
30	40	3045. 25	32828. 5	$(^3P)\ 5d\ ^4P_{1\frac{1}{2}}-(^1S)\ 6p\ ^2P^0_{1\frac{1}{2}}$
25	25	3046. 27	32817. 5	$(^1D)\ 5d\ ^2F_{2\frac{1}{2}}-29i_{1\frac{1}{2}}$
8H	12*h*	3047. 76	32801. 5	
5	1*h*	3048. 17	32797. 1	
	3*h*	3048. 50	32793. 5	$(^1D)\ 5d\ ^2F_{2\frac{1}{2}}-27g_{2\frac{1}{2}}$
3*h*		3048. 92	32789. 0	
3	4	3050. 98	32766. 8	$(^1D)\ 5d\ ^2F_{2\frac{1}{2}}-25i_{1\frac{1}{2}}$
20	25	3056. 49	32707. 8	$(^3P)\ 5d\ ^4P_{2\frac{1}{2}}-7i_{1\frac{1}{2}}$
12	15	3061. 54	32653. 8	$(^3P)\ 5d\ ^4P_{2\frac{1}{2}}-5i_{1\frac{1}{2}}$
1*h*	2*h*	3066. 60	32600. 0	$(^3P)\ 6p\ ^4D^0_{3\frac{1}{2}}-(^1D)\ 7s\ ^2D_{2\frac{1}{2}}$
30	40	3067. 30	32592. 5	$(^3P)\ 5d\ ^2P_{0\frac{1}{2}}-9i_{1\frac{1}{2}}$
6*h*	1*h*	3071. 39	32549. 1	
2*h*	3	3073. 17	32530. 3	$(^3P)\ 5d\ ^4P_{2\frac{1}{2}}-3g_{1\frac{1}{2}}$
20	25	3082. 62	32430. 5	$(^3P)\ 5d\ ^2D_{1\frac{1}{2}}-19i_{1\frac{1}{2}}$
2		3082. 87	32427. 9	$(^3P)\ 6p\ ^4D^0_{2\frac{1}{2}}-(^3P)\ 6d\ ^2D_{1\frac{1}{2}}$
1—	1*h*	3085. 12	32404. 3	
1—	1—	3087. 34	32381. 0	$sp^6\ ^2S_{0\frac{1}{2}}-(^3P)\ 6p\ ^2P^0_{1\frac{1}{2}}$
3	1	3088. 92	32364. 4	

TABLE 1.—*List of* Xe II *lines*—Continued

Intensity		Wave length (air)	Wave number (vac)	Transition
1	1	3090. 47	32348. 2	$(^3P)\ 6p\ {}^4P^\circ_{1½} - (^3P)\ 6d\ {}^4P_{1½}$
15	20	3092. 41	32327. 9	$(^3P)\ 5d\ {}^2D_{2½} - 19i_{1½}$
30*h*	25*h*	3094. 53	32305. 7	$(^3P)\ 5d\ {}^2D_{1½} - (^1S)\ 6p\ {}^2P^\circ_{1½}$
2	1—	3096. 42	32286. 0	
8	10	3096. 90	32281. 0	$(^3P)\ 5d\ {}^2D_{1½} - 17i_{0½}$
2	2	3098. 21	32267. 4	$(^3P)\ 6p\ {}^4P^\circ_{0½} - (^3P)\ 6d\ {}^2D_{1½}$
1	2	3098. 50	32264. 4	$(^3P)\ 5d\ {}^4P_{1½} - 11i_{2½}$
	1*h*	3099. 16	32257. 5	
50*h*	60*h*	3101. 51	32233. 0	$(^1S)\ 6s\ {}^2S_{0½} - 39i_{1½}$
3	1	3102. 73	32220. 4	
70*h*	80*h*	3104. 40	32203. 0	$(^3P)\ 5d\ {}^2D_{2½} - (^1S)\ 6p\ {}^2P^\circ_{1½}$
20H*l*	30H*l*	3107. 82	32167. 6	
20	25	3112. 74	32116. 8	$(^3P)\ 5d\ {}^4P_{1½} - 9i_{1½}$
	1*h*—	3115. 78	32085. 4	
2*h*	4	3116. 78	32075. 1	
250	300	3121. 87	32022. 8	$(^3P\ 5d\ {}^2D_{2½} - 15i_{2½}$
12*h*	15*h*	3124. 02	32000. 8	$(^1S)\ 5d\ {}^2D_{1½} - 39i_{1½}$
1H	2*h*	3128. 40	31956. 0	$(^3P)\ 5d\ {}^2P_{1½} - 1i_{1½}$
3H	4*h*	3130. 40	31935. 6	
6	10	3143. 62	31801. 3	$(^3P)\ 5d\ {}^4P_{1½} - 7i_{1½}$
4*h*	8	3145. 02	31787. 1	
	1*h*	3148. 07	31756. 3	
5	8	3148. 99	31747. 0	$(^3P)\ 5d\ {}^4P_{1½} - 5i_{1½}$
4*h*	8*h*	3159. 75	31638. 9	$(^3P)\ 5d\ {}^2D_{2½} - 11i_{2½}$
25	25	3162. 93	31607. 14	$(^3P)\ 6p\ {}^4P^\circ_{1½} - (^3P)\ 6d\ {}^4P_{2½}$
6	8	3164. 23	31594. 15	$(^3P)\ 5d\ {}^2D_{1½} - 9i_{1½}$
4*		3164. 44	31592. 05	
6	8	3165. 27	31583. 77	$(^3P)\ 6s\ {}^4P_{0½} - (^1D)\ 6p\ {}^2P^\circ_{0½}$
3*h*	4*h*	3168. 67	31549. 88	$(^3P)\ 6p\ {}^4P^\circ_{0½} - (^3P)\ 6d\ {}^2P_{0½}$
1	2	3174. 59	31491. 05	$(^3P)\ 5d\ {}^2D_{2½} - 9i_{1½}$
6*		3175. 25	31484. 50	
80	80	3175. 64	31480. 64	
3*h*	6*h*	3181. 39	31423. 74	$(^1D)\ 6s\ {}^2D_{2½} - 21i_{1½}$
1*h*	1	3193. 75	31302. 14	$(^3P)\ 6p\ {}^4D^\circ_{1½} - (^1D)\ 6d\ {}^2D_{1½}$
25	10	3196. 22	31277. 95	
	1	3198. 82	31252. 52	
1—	1—	3200. 72	31233. 97	
3*h*	6*h*	3201. 68	31224. 61	$(^3P)\ 5d\ {}^2D_{1½} - 5i_{0½}$
10	15	3202. 04	31221. 10	$(^3P)\ 6s\ {}^4P_{2½} - (^3P)\ 6p\ {}^2D^\circ_{1½}$
1	1	3205. 26	31189. 73	
	1—	3206. 72	31175. 54	$(^3P)\ 5d\ {}^2D_{2½} - 7i_{1½}$
1H	3H	3211. 59	31128. 26	
5*h*	6*h*	3212. 29	31121. 48	$(^3P)\ 5d\ {}^2D_{2½} - 5i_{1½}$
15	20	3225. 08	30998. 06	$(^3P)\ 5d\ {}^2D_{2½} - 3i_{1½}$
	1	3228. 29	30967. 24	
4*h*	6*h*	3229. 03	30960. 15	
1	1—	3233. 23	30919. 93	$(^3P)\ 6p\ {}^2D^\circ_{2½} - (^1D)\ 6d\ {}^2F_{2½}$
6H*l*	8H*l*	3247. 74	30781. 79	
	1—	3249. 35	30766. 54	$(^1D)\ 5d\ {}^2D_{2½} - 23i_{1½}$
2*h*	2	3250. 04	30760. 01	$(^3P)\ 6s\ {}^4P^\circ_{0½} - (^1D)\ 6p\ {}^2D^\circ_{1½}$

TABLE 1.—*List of* Xe II lines—Continued

Intensity		Wave length (air)	Wave number (vac)	Transition
25	30	3250. 56	30755. 09	$sp^6\ ^2S_{0\frac{1}{2}} - (^3P)\ 6p\ ^4S^\circ_{1\frac{1}{2}}$
12	10	3259. 36	30672. 05	$(^3P)\ 5d\ ^4F_{2\frac{1}{2}} - (^1D)\ 6p\ ^2D^\circ_{2\frac{1}{2}}$
2	2	3260. 73	30659. 17	$(^3P)\ 5d\ ^4F_{4\frac{1}{2}} - (^1D)\ 6p\ ^2F^\circ_{3\frac{1}{2}}$
4*h*	6*h*	3262. 02	30647. 05	$(^1D)\ 6s\ ^2D_{2\frac{1}{2}} - (^1S)\ 6p\ ^2P^\circ_{1\frac{1}{2}}$
	8*hw*	3266. 08	30608. 95	
6*		3267. 05	30699. 86	
3*h*	8	3267. 34	30597. 14	$(^1S)\ 5d\ ^2D_{2\frac{1}{2}} - 37^\circ_{2\frac{1}{2}}$
	1*h*	3268. 08	30590. 22	$(^3P)\ 6p\ ^4P^\circ_{1\frac{1}{2}} - (^3P)\ 7s\ ^2P_{1\frac{1}{2}}$
1	1—	3272. 24	30551. 33	
60	60	3272. 91	30545. 08	$(^1D)\ 6s\ ^2D_{1\frac{1}{2}} - 23^\circ_{1\frac{1}{2}}$
	2H	3274. 80	30527. 45	
4H		3274. 94	30526. 14	
8*	1	3280. 48	30474. 59	
12*h*	15*h*	3281. 26	30467. 35	$(^3P)\ 6p\ ^4P^\circ_{0\frac{1}{2}} - (^3P)\ 6d\ ^4P_{1\frac{1}{2}}$
1*h*	2*h*	3296. 20	30329. 26	
6	8	3298. 72	30306. 09	$sp^6\ ^2S_{0\frac{1}{2}} - (^3P)\ 6p\ ^2S^\circ_{0\frac{1}{2}}$
1	2	3302. 50	30271. 40	
2*h*	3*h*	3309. 39	30208. 38	
3*		3310. 38	30199. 35	
1*h*	1*h*	3310. 85	30195. 06	$(^1S)\ 5d\ ^2D_{2\frac{1}{2}} - 35^\circ_{2\frac{1}{2}}$
2	4	3311. 80	30186. 40	$(^3P)\ 6s\ ^4P_{2\frac{1}{2}} - (^3P)\ 6p\ ^2P^\circ_{1\frac{1}{2}}$
2*h*	3*h*	3313. 48	30171. 10	
6*h*	10*h*	3316. 39	30144. 62	$(^3P)\ 6p\ ^4D^\circ_{1\frac{1}{2}} - 14_{2\frac{1}{2}}$
1*h*	2*h*	3320. 57	30106. 68	
1—	1—	3324. 14	30074. 35	
15	15	3327. 46	30044. 34	$(^3P)\ 6s\ ^4P_{2\frac{1}{2}} - (^3P)\ 6p\ ^2D^\circ_{2\frac{1}{2}}$
1—	1	3330. 78	30014. 40	
4*h*	10	3338. 80	29942. 30	$(^3P)\ 6s\ ^2P_{1\frac{1}{2}} - (^1D)\ 6p\ ^2P^\circ_{0\frac{1}{2}}$
4*h*		3344. 97	29887. 07	$(^3P)\ 6p\ ^4D^\circ_{2\frac{1}{2}} - (^3P)\ 6d\ ^4P_{2\frac{1}{2}}$
3H	6H	3347. 27	29866. 54	$(^1S)\ 5d\ ^2D_{2\frac{1}{2}} - 33^\circ_{1\frac{1}{2}}$
6H	8H*l*	3350. 44	29838. 28	
	2H	3351. 24	29831. 16	
	1*h*	3353. 44	29811. 59	
2	1*h*	3363. 50	29722. 43	
300*h*	200*h*	3366. 72	29694. 00	$(^3P)\ 6p\ ^4D^\circ_{3\frac{1}{2}} - (^3P)\ 6d\ ^4P_{2\frac{1}{2}}$
2*h*	4*h*	3373. 92	29630. 63	
3*h*	5*h*	3375. 16	29619. 74	$(^1D)\ 6s\ ^2D_{2\frac{1}{2}} - 7^\circ_{1\frac{1}{2}}$
	1*h*	3381. 34	29565. 62	$(^1D)\ 6s\ ^2D_{2\frac{1}{2}} - 5^\circ_{1\frac{1}{2}}$
40*h*	30	3384. 13	29541. 24	$sp^6\ ^2S_{0\frac{1}{2}} - (^3P)\ 6p\ ^4D^\circ_{0\frac{1}{2}}$
2*h*	3*h*	3386. 30	29522. 31	$(^3P)\ 6p\ ^4D^\circ_{1\frac{1}{2}} - (^1D)\ 7s\ ^2D_{2\frac{1}{2}}$
2	3	3388. 05	29507. 06	$(^3P)\ 6s\ ^4P_{1\frac{1}{2}} - (^3P)\ 6p\ ^2P^\circ_{0\frac{1}{2}}$
3	4	3395. 50	29442. 32	$(^1D)\ 6s\ ^2D_{2\frac{1}{2}} - 3^\circ_{2\frac{1}{2}}$
1	1	3399. 37	29408. 80	$(^3P)\ 6s\ ^2P_{1\frac{1}{2}} - (^1D)\ 6p\ ^2D^\circ_{2\frac{1}{2}}$
8H	10H*l*	3409. 49	29321. 52	
1H—	1H	3412. 58	29294. 97	
6H	8H	3413. 20	29289. 65	$(^1S)\ 5d\ ^2D_{2\frac{1}{2}} - 31^\circ_{1\frac{1}{2}}$
1—	1—	3417. 04	29256. 73	$(^3P)\ 6p\ ^4P^\circ_{0\frac{1}{2}} - (^3P)\ 7s\ ^2P_{0\frac{1}{2}}$
1H	1H	3419. 20	29238. 25	
40	50	3420. 73	29225. 17	$(^3P)\ 6s\ ^4P_{1\frac{1}{2}} - (^3P)\ 6p\ ^2D^\circ_{1\frac{1}{2}}$
1	2	3432. 49	29125. 05	$(^3P)\ 6s\ ^2P_{1\frac{1}{2}} - (^1D)\ 6p\ ^2D^\circ_{1\frac{1}{2}}$

TABLE 1.—*List of* Xe II *lines*—Continued

Intensity		Wave length (air)	Wave number (vac)	Transition
	1*h*	3434. 35	29109. 28	
1—	1—	3436. 48	29091. 23	$(^3P)\ 6p\ {}^4P^\circ_{1\frac{1}{2}} - (^3P)\ 6d\ {}^4P_{0\frac{1}{2}}$
3H	1H*w*	3437. 73	29080. 66	
4*h*	5*h*	3440. 75	29055. 13	
25*h*	25	3446. 34	29008. 01	$(^1D)\ 5d\ {}^2D_{1\frac{1}{2}} - 19^\circ_{1\frac{1}{2}}$
	1*h*	3450. 08	28976. 56	
	1H	3452. 22	28958. 60	
1—	1—	3456. 69	28921. 15	
8	10	3460. 08	28892. 82	$(^3P)\ 5d\ {}^4D_{2\frac{1}{2}} - (^3P)\ 6p\ {}^2D^\circ_{1\frac{1}{2}}$
100*h*	100*h*	3461. 26	28882. 97	$(^1D)\ 5d\ {}^2D_{1\frac{1}{2}} - (^1S)\ 6p\ {}^2P^\circ_{1\frac{1}{2}}$
1—	1—	3462. 81	28870. 04	$(^3P)\ 6p\ {}^4D^\circ_{2\frac{1}{2}} - (^3P)\ 7s\ {}^2P_{1\frac{1}{2}}$
1—	1—	3463. 53	28864. 04	
1*h*	3*h*	3464. 17	28858. 71	$(^1D)\ 5d\ {}^2D_{1\frac{1}{2}} - 17^\circ_{0\frac{1}{2}}$
1—	1	3467. 68	28829. 50	
20*h*	25	3474. 23	28775. 15	$(^1D)\ 5d\ {}^2P_{1\frac{1}{2}} - 39^\circ_{1\frac{1}{2}}$
2*h*	2*h*	3482. 21	28709. 21	$(^3P)\ 6p\ {}^4P^\circ_{0\frac{1}{2}} - (^3P)\ 7s\ {}^2P_{1\frac{1}{2}}$
1*h*	2*h*	3485. 23	28684. 33	$(^1D)\ 5d\ {}^2D_{1\frac{1}{2}} - 13^\circ_{0\frac{1}{2}}$
30	20	3500. 36	28560. 35	$(^3P)\ 6s\ {}^4P_{2\frac{1}{2}} - (^3P)\ 6p\ {}^4S^\circ_{1\frac{1}{2}}$
20*h**	1*h*	3501. 77	28548. 85	
15	10	3503. 15	28537. 60	$(^3P)\ 5d\ {}^4D_{1\frac{1}{2}} - (^3P)\ 6p\ {}^2P^\circ_{0\frac{1}{2}}$
1	1	3504. 25	28528. 65	$(^3P)\ 5d\ {}^4F_{2\frac{1}{2}} - (^1D)\ 6p\ {}^2F^\circ_{3\frac{1}{2}}$
15	10	3506. 56	28509. 85	$(^3P)\ 6s\ {}^4P_{0\frac{1}{2}} - (^1D)\ 6p\ {}^2P^\circ_{1\frac{1}{2}}$
20	15	3508. 88	28491. 00	$(^3P)\ 6s\ {}^2P_{0\frac{1}{2}} - (^1D)\ 6p\ {}^2P^\circ_{0\frac{1}{2}}$
8H		3514. 58	28444. 80	
	1H*w*	3514. 91	28442. 13	
3H	6*h*	3530. 21	28318. 86	$(^1D)\ 5d\ {}^2D_{1\frac{1}{2}} - 11^\circ_{2\frac{1}{2}}$
	1*h*	3534. 61	28283. 61	$(^1D)\ 5d\ {}^2D_{2\frac{1}{2}} - 21^\circ_{1\frac{1}{2}}$
2		3537. 40	28261. 30	
2	4	3538. 08	28255. 87	$(^3P)\ 5d\ {}^4D_{1\frac{1}{2}} - (^3P)\ 6p\ {}^2D^\circ_{1\frac{1}{2}}$
1*h*	2	3546. 29	28190. 46	$(^3P)\ 6s\ {}^4P_{1\frac{1}{2}} - (^3P)\ 6p\ {}^2P^\circ_{1\frac{1}{2}}$
2*h*		3548. 69	28171. 39	$(^1D)\ 5d\ {}^2D_{1\frac{1}{2}} - 9^\circ_{1\frac{1}{2}}$
	1—	3561. 75	28068. 10	$(^3P)\ 6p\ {}^4S^\circ_{1\frac{1}{2}} - (^1D)\ 6d\ {}^2D_{2\frac{1}{2}}$
	1—	3562. 50	28062. 19	$(^1D)\ 6s\ {}^2D_{1\frac{1}{2}} - 21^\circ_{1\frac{1}{2}}$
20	20	3564. 30	28048. 02	$(^3P)\ 6s\ {}^4P_{1\frac{1}{2}} - (^3P)\ 6p\ {}^2D^\circ_{2\frac{1}{2}}$
1H	2H	3574. 18	27970. 49	
2	1	3578. 58	27936. 10	
6*h*	3	3588. 62	27857. 94	$(^3P)\ 5d\ {}^4D_{2\frac{1}{2}} - (^3P)\ 6p\ {}^2P^\circ_{1\frac{1}{2}}$
1H	2*h*	3589. 88	27848. 16	$(^3P)\ 6p\ {}^4P^\circ_{1\frac{1}{2}} - (^3P)\ 6d\ {}^4F_{1\frac{1}{2}}$
3*h*	4*h*	3604. 83	27732. 68	
8	10	3607. 41	27712. 84	$(^3P)\ 5d\ {}^4D_{0\frac{1}{2}} - (^3P)\ 6p\ {}^2P^\circ_{0\frac{1}{2}}$
1*h*	1*h*	3611. 52	27681. 31	$(^3P)\ 6p\ {}^4P^\circ_{2\frac{1}{2}} - (^3P)\ 6d\ {}^4F_{1\frac{1}{2}}$
20	10	3612. 37	27674. 79	$(^3P)\ 5d\ {}^4D_{3\frac{1}{2}} - (^3P)\ 6p\ {}^2D^\circ_{2\frac{1}{2}}$
3*h*	4*h*	3621. 98	27601. 37	$(^3P)\ 6p\ {}^4D^\circ_{1\frac{1}{2}} - (^3P)\ 6d\ {}^2D_{2\frac{1}{2}}$
1—	1	3634. 48	27506. 44	$(^1D)\ 5d\ {}^2D_{2\frac{1}{2}} - (^1S)\ 6p\ {}^2P^\circ_{1\frac{1}{2}}$
5	5	3644. 43	27431. 34	$(^3P)\ 5d\ {}^4D_{0\frac{1}{2}} - (^3P)\ 6p\ {}^2D^\circ_{0\frac{1}{2}}$
5	5	3644. 91	27427. 75	$(^3P)\ 5d\ {}^2P_{1\frac{1}{2}} - (^1D)\ 6p\ {}^2P^\circ_{0\frac{1}{2}}$
1	5	3650. 12	27388. 58	
5	5	3657. 74	27331. 53	$(^3P)\ 5d\ {}^4F_{2\frac{1}{2}} - (^1D)\ 6p\ {}^2F^\circ_{2\frac{1}{2}}$
6*h*	6	3658. 44	27326. 30	$(^1D)\ 5d\ {}^2D_{2\frac{1}{2}} - 15^\circ_{2\frac{1}{2}}$
20H	20H*l*	3661. 70	27301. 97	$(^3P)\ 6p\ {}^4P^\circ_{1\frac{1}{2}} - (^3P)\ 6d\ {}^4F_{2\frac{1}{2}}$

TABLE 1.—*List of* Xe II *lines*—Continued

Intensity		Wave length (air)	Wave number (vac)	Transition
5*h*	5	3663. 93	27285. 35	$(^1D)\ 6s\ ^2D_{1½} - (^1S)\ 6p\ ^2P^{\circ}_{1½}$
20	20	3672. 57	27221. 16	$(^3P)\ 5d\ ^4D_{1½} - (^3P)\ 6p\ ^2P^{\circ}_{1½}$
1—	1—	3674. 04	27210. 28	$(^3P)\ 6p\ ^4P^{\circ}_{0½} - (^3P)\ 6d\ ^4P_{½}$
2H*w*	1—	3680. 48	27162. 66	
1	1	3690. 74	27087. 15	$(^1D)\ 6s\ ^2D_{1½} - 13^{\circ}_{0½}$
1*h*	2	3691. 84	27079. 09	$(^3P)\ 5d\ ^4D_{1½} - (^3P)\ 6p\ ^2D^{\circ}_{2½}$
1H	1H	3695. 60	27051. 53	
1*h*	2*h*	3698. 49	27030. 40	
20H	30H*l*	3711. 64	26934. 63	$(^3P)\ 6p\ ^4P^{\circ}_{1½} - (^3P)\ 6d\ ^4D_{0½}$
2H	3H	3715. 69	26905. 28	$(^3P)\ 6p\ ^2S^{\circ}_{½} - (^1D)\ 6d\ ^2D_{1½}$
20	20	3717. 20	26894. 35	$(^3P)\ 5d\ ^2P_{1½} - (^1D)\ 6p\ ^2D^{\circ}_{2½}$
2	1—	3718. 06	26888. 12	
40	30	3720. 80	26868. 33	$(^3P)\ 6s\ ^2P_{1½} - (^1D)\ 6p\ ^2P^{\circ}_{1½}$
2*h*	1*h*	3727. 35	26821. 11	
2	1	3730. 22	26800. 48	
20	20	3731. 18	26793. 58	$(^3P)\ 5d\ ^2P_{0½} - (^1D)\ 6p\ ^2P^{\circ}_{0½}$
5H*w*	6H	3737. 20	26750. 42	
2H*w*	1*h*	3741. 96	26716. 39	
10	10	3756. 87	26610. 37	$(^3P)\ 5d\ ^2P_{1½} - (^1D)\ 6p\ ^2D^{\circ}_{1½}$
3*h*	5*h*	3762. 05	26573. 73	$(^1D)\ 6s\ ^2D_{1½} - 9^{\circ}_{1½}$
10*	1	3762. 26	26572. 24	
15	15	3763. 37	26564. 41	$(^3P)\ 6s\ ^4P_{1½} - (^3P)\ 6p\ ^4S^{\circ}_{1½}$
3H*d*	3H	3770. 12	26516. 85	
1	1*h*	3775. 49	26479. 13	$(^1D)\ 5d\ ^2D_{2½} - 7^{\circ}_{1½}$
1—	1*h*	3778. 78	26456. 08	$(^3P)\ 6p\ ^4S^{\circ}_{1½} - (^1D)\ 6d\ ^2D_{1½}$
1H		3780. 70	26442. 64	$(^3P)\ 6p\ ^2P^{\circ}_{1½} - (^1D)\ 6d\ ^2D_{2½}$
10*h*	10*h*	3783. 23	26424. 96	$(^1D)\ 5d\ ^2D_{2½} - 5^{\circ}_{1½}$
3	3	3787. 32	26396. 43	$(^3P)\ 5d\ ^4D_{0½} - (^3P)\ 6p\ ^2P^{\circ}_{1½}$
1—	1	3800. 00	26308. 35	
15*h*	20	3800. 99	26301. 49	$(^1D)\ 5d\ ^2D_{2½} - 3^{\circ}_{1½}$
1H	2*h*	3805. 68	26269. 08	
10*h*	15	3807. 29	26257. 97	$(^1D)\ 6s\ ^2D_{1½} - 7^{\circ}_{1½}$
40	40	3811. 05	26232. 07	$(^3P)\ 5d\ ^4D_{2½} - (^3P)\ 6p\ ^4S^{\circ}_{1½}$
1*hw*	1	3815. 16	26203. 81	
2*h*	2	3823. 35	26147. 68	
2*h*	3*h*	3826. 27	26127. 73	$(^3P)\ 6p\ ^4D^{\circ}_{2½} - (^3P)\ 6d\ ^4F_{1½}$
10*h*	10	3829. 77	26103. 85	$(^3P)\ 6p\ ^4P^{\circ}_{2½} - 12_{1½}$
6	6	3848. 58	25976. 27	$(^3P)\ 5d\ ^4P_{0½} - (^1D)\ 6p\ ^2D^{\circ}_{1½}$
50H*l*	40*hl*	3849. 87	25967. 56	$(^3P)\ 6p\ ^4P^{\circ}_{0½} - (^3P)\ 6d\ ^4F_{1½}$
2*h*	1	3852. 40	25950. 51	
20	20	3858. 53	25909. 29	$sp^6\ ^2S_{0½} - (^3P)\ 6p\ ^4D^{\circ}_{1½}$
20	20	3869. 63	25834. 97	$(^3P)\ 5d\ ^2P_{0½} - (^1D)\ 6p\ ^2P^{\circ}_{0½}$
1H	1H	3876. 39	25789. 91	
1H	2H*w*	3883. 67	25741. 57	
20	2	3885. 00	25732. 76	$(^3P)\ 5d\ ^4P_{2½} - (^1D)\ 6p\ ^2D^{\circ}_{2½}$
4H*l*	6H*l*	3885. 45	25729. 78	
1H—	1H*w*	3887. 83	25714. 03	
1—	1—	3901. 92	25621. 19	
1	1	3905. 34	25598. 74	$(^3P)\ 6p\ ^4D^{\circ}_{1½} - (^3P)\ 7s\ ^2P_{1½}$
10	10	3905. 85	25595. 40	$(^3P)\ 5d\ ^4D_{1½} - (^3P)\ 6p\ ^4S^{\circ}_{1½}$

TABLE 1.—*List of* Xe II *lines*—Continued

Intensity		Wave length (air)	Wave number (vac)	Transition
100*hl*	100*hl*	3907. 91	25581. 91	$(^3P)\ 6p\ {}^4D^\circ_{3½} - (^3P)\ 6d\ {}^4F_{3½}$
1*h*	2*h*	3916. 60	25525. 15	$(^3P)\ 6p\ {}^4D^\circ_{5½} - (^3P)\ 6d\ {}^2D_{1½}$
2*h*		3918. 57	25512. 31	$(^3P)\ 6p\ {}^2D^\circ_{1½} - (^1D)\ 7s\ {}^2D_{1½}$
1	1	3920. 18	25501. 84	
1*h*	2*h*	3920. 78	25497. 94	
1	2	3926. 80	25458. 85	$(^1D)\ 5d\ {}^2F_{2½} - (^1S)\ 6p\ {}^2P^\circ_{1½}$
1	1—	3932. 44	25422. 34	
1	2	3933. 22	25417. 29	$(^3P)\ 6s\ {}^2P_{0½} - (^1D)\ 6p\ {}^2P^\circ_{1½}$
2	1—	3937. 66	25388. 63	$(^3P)\ 6p\ {}^4D^\circ_{3½} - (^3P)\ 6d\ {}^4F_{2½}$
15*h*	20	3938. 92	25380. 51	$(^1S)\ 5d\ {}^2D_{1½} - 37^\circ_{2½}$
3	4	3942. 21	25359. 33	$(^3P)\ 5d\ {}^4P_{1½} - (^1D)\ 6p\ {}^2P^\circ_{0½}$
20	20	3943. 57	25350. 58	$(^3P)\ 6s\ {}^4P_{1½} - (^3P)\ 6p\ {}^4D^\circ_{0½}$
5H*l*	5H*l*	3951. 61	25299. 01	$(^3P)\ 6p\ {}^4S^\circ_{1½} - 14_{2½}$
20*hl*	30*hl*	3954. 73	25279. 05	$(^1D)\ 5d\ {}^2F_{2½} - 15^\circ_{2½}$
1*h*	1	3967. 54	25197. 43	
50H*l*	50*hl*	3972. 58	25165. 46	$(^1D)\ 6p\ {}^2F^\circ_{2½} - (^1D)\ 6d\ {}^2F_{2½}$
4	5	3975. 59	25146. 41	$(^3P)\ 5d\ {}^4D_{1½} - (^3P)\ 6p\ {}^2S^\circ_{0½}$
2*h*	2*h*	3978. 98	25124. 99	$(^3P)\ 6p\ {}^2S^\circ_{0½} - (^1D)\ 7s\ {}^2D_{2½}$
2*h*	2*h*	3980. 41	25115. 96	$(^1D)\ 5d\ {}^2F_{3½} - 15^\circ_{3½}$
1	1	3980. 78	25113. 63	
1*h*	1*h*	3981. 21	25110. 92	
60H*l*	60H*l*	3990. 33	25053. 52	$(^3P)\ 6p\ {}^4P^\circ_{0½} - (^3P)\ 6d\ {}^4D_{0½}$
3	4	3996. 05	25017. 66	$(^3P)\ 5d\ {}^2P_{0½} - (^1D)\ 6p\ {}^2D^\circ_{1½}$
1*		3998. 54	25002. 08	
5*h*	5*h*	4000. 55	24989. 52	
1*		4001. 18	24985. 59	
80H*l*	80*hl*	4002. 35	24978. 29	$(^1S)\ 5d\ {}^2D_{1½} - 35^\circ_{2½}$
1H	1H*w*	4008. 46	24940. 21	
2		4013. 91	24906. 29	
	1	4014. 10	24905. 17	
2*h*	2*h*	4016. 56	24889. 92	
2*h*	2*h*	4017. 86	24881. 86	$(^1S)\ 6s\ {}^2S_{0½} - 33^\circ_{1½}$
30	30	4025. 19	24836. 55	$(^3P)\ 5d\ {}^2D_{1½} - (^1D)\ 6p\ {}^2P^\circ_{0½}$
5H*l*	6H*l*	4026. 20	24830. 32	$(^3P)\ 6p\ {}^2P^\circ_{1½} - (^1D)\ 6d\ {}^2D_{1½}$
3*h*	2*h*	4027. 97	24819. 41	
1—		4029. 82	24808. 02	$(^3P)\ 6p\ {}^4D^\circ_{5½} - (^3P)\ 6d\ {}^2P_{0½}$
1	1	4035. 87	24770. 83	$(^3P)\ 5d\ {}^4D_{0½} - (^3P)\ 6p\ {}^4S^\circ_{1½}$
100	50	4037. 29	24762. 12	
200	100	4037. 59	24760. 28	$(^3P)\ 6p\ {}^2S^\circ_{0½} - (^3P)\ 6d\ {}^2D_{1½}$
1—	1	4039. 69	24747. 41	$(^1D)\ 5d\ {}^2F_{2½} - 9^\circ_{1½}$
6H	6H	4044. 64	24717. 12	
8H	8H*l*	4044. 90	24715. 53	
10*h*	10*h*	4051. 27	24676. 67	$(^3P)\ 6p\ {}^4S^\circ_{1½} - (^1D)\ 7s\ {}^2D_{2½}$
	3	4051. 66	24674. 30	
1*h*	2*h*	4053. 46	24663. 34	
200H*l*	200H*l*	4057. 46	24639. 03	$(^3P)\ 6p\ {}^4P^\circ_{3½} - (^3P)\ 6d\ {}^4F_{3½}$
3	1—	4061. 06	24617. 18	$(^3P)\ 6s\ {}^2P_{0½} - (^1D)\ 6p\ {}^2F^\circ_{3½}$
6	6	4062. 12	24610. 76	$(^3P)\ 6p\ {}^4P^\circ_{3½} - 8_{2½}$
	1	4064. 68	24595. 26	
	1H	4064. 94	24593. 69	

TABLE 1.—*List of* Xe II *lines*—Continued

Intensity		Wave length (air)	Wave number (vac)	Transition
1		4065. 10	24592. 72	
2*h*	1—	4066. 90	24581. 84	
6*h*	7*h*	4072. 10	24550. 45	$(^3P)\ 6p\ {}^4D^o_{2\frac{1}{2}} - 12_{1\frac{1}{2}}$
15	15	4073. 50	24542. 01	$(^3P)\ 5d\ {}^4P_{1\frac{1}{2}} - (^1D)\ 6p\ {}^2D^o_{1\frac{1}{2}}$
	1	4078. 84	24509. 88	
1	1	4088. 31	24453. 11	
3*h*	3*h*	4091. 88	24431. 77	$(^1D)\ 5d\ {}^2F_{2\frac{1}{2}} - 7i_{1\frac{1}{2}}$
	1	4092. 78	24426. 40	
1	1	4096. 22	24405. 89	
100*h*	100*h*	4098. 89	24389. 99	$(^3P)\ 6p\ {}^4P^o_{0\frac{1}{2}} - 12_{1\frac{1}{2}}$
20	20	4100. 34	24381. 37	$(^3P)\ 5d\ {}^4D_{1\frac{1}{2}} - (^3P)\ 6p\ {}^4D^o_{0\frac{1}{2}}$
1*h*	2*h*	4100. 97	24377. 62	$(^1D)\ 5d\ {}^2F_{2\frac{1}{2}} - 5i_{1\frac{1}{2}}$
8*hl*	10*hl*	4103. 10	24364. 96	$(^1D)\ 6p\ {}^2P^o_{1\frac{1}{2}} - (^1D)\ 6d\ {}^2F_{2\frac{1}{2}}$
40	40	4104. 95	24353. 98	$(^3P)\ 5d\ {}^2P_{1\frac{1}{2}} - (^1D)\ 6p\ {}^2P^o_{1\frac{1}{2}}$
2	1	4106. 20	24346. 57	
30	30	4110. 41	24321. 63	$(^3P)\ 5d\ {}^4D_{0\frac{1}{2}} - (^3P)\ 6p\ {}^2S^o_{0\frac{1}{2}}$
1	1—	4111. 30	24316. 37	
30H*l*	30*hl*	4112. 14	24311. 40	$(^3P)\ 6p\ {}^4S^o_{1\frac{1}{2}} - (^3P)\ 6d\ {}^2D_{1\frac{1}{2}}$
2	2	4113. 26	24304. 78	$(^1S)\ 6s\ {}^2S_{0\frac{1}{2}} - 31i_{1\frac{1}{2}}$
2	2	4113. 52	24303. 25	$(^3P)\ 5d\ {}^2D_{1\frac{1}{2}} - (^1D)\ 6p\ {}^2D^o_{2\frac{1}{2}}$
1	1	4114. 44	24297. 81	
5*h*	5	4121. 86	24254. 07	$(^1D)\ 5d\ {}^2F_{2\frac{1}{2}} - 3i_{1\frac{1}{2}}$
20	20	4131. 01	24200. 35	$(^3P)\ 5d\ {}^2D_{2\frac{1}{2}} - (^1D)\ 6p\ {}^2D^o_{2\frac{1}{2}}$
3*h*	3*h*	4138. 81	24154. 75	
2*h*	2*h*	4148. 19	24100. 13	$(^3P)\ 6p\ {}^4D^o_{1\frac{1}{2}} - (^3P)\ 6d\ {}^4P_{0\frac{1}{2}}$
1	1—	4152. 74	24073. 72	
2	1	4154. 65	24062. 65	
2*h*	2*h*	4156. 17	24053. 85	
200H*l*	200H*l*	4158. 04	24043. 04	$(^3P)\ 6p\ {}^2S^o_{0\frac{1}{2}} - (^3P)\ 6d\ {}^2P_{0\frac{1}{2}}$
60	60	4162. 16	24019. 24	$(^3P)\ 5d\ {}^2D_{1\frac{1}{2}} - (^1D)\ 6p\ {}^2D^o_{1\frac{1}{2}}$
8H*l*	8H*l*	4170. 99	23968. 39	$(^1D)\ 6p\ {}^2F^o_{3\frac{1}{2}} - (^1D)\ 6d\ {}^2F_{3\frac{1}{2}}$
1000*h*	1000*h*	4180. 10	23916. 16	$(^3P)\ 6p\ {}^4P^o_{1\frac{1}{2}} - (^3P)\ 6d\ {}^4D_{1\frac{1}{2}}$
1*h*	1*h*	4185. 26	23886. 67	
	1*h*	4185. 89	23883. 07	
500*h*	500*h*	4193. 15	23841. 72	
	8	4193. 54	23839. 51	
10H	10H	4197. 81	23815. 26	$(^3P)\ 6p\ {}^2D^o_{2\frac{1}{2}} - 14_{2\frac{1}{2}}$
15H	15H	4201. 25	23795. 76	$(^3P)\ 6p\ {}^2D^o_{1\frac{1}{2}} - (^1D)\ 6d\ {}^2D_{1\frac{1}{2}}$
5	2	4203. 22	23784. 60	$(^3P)\ 7s\ {}^4P_{2\frac{1}{2}} - 39i_{1\frac{1}{2}}$
1	2	4204. 29	23778. 55	
400*h*	300*h*	4208. 48	23754. 88	$(^3P)\ 6p\ {}^4P^o_{1\frac{1}{2}} - (^3P)\ 6d\ {}^4D_{2\frac{1}{2}}$
200*h*	100*h*	4209. 47	23749. 29	$(^3P)\ 6p\ {}^4P^o_{2\frac{1}{2}} - (^3P)\ 6d\ {}^4D_{1\frac{1}{2}}$
400*h*	300*h*	4213. 72	23725. 34	$(^3P)\ 6p\ {}^4D^o_{0\frac{1}{2}} - (^3P)\ 6d\ {}^4P_{1\frac{1}{2}}$
6	6	4214. 69	23719. 88	$(^3P)\ 5d\ {}^4P_{0\frac{1}{2}} - (^1D)\ 6p\ {}^2P^o_{1\frac{1}{2}}$
200	100	4215. 60	23714. 76	$(^3P)\ 6s\ {}^4P_{2\frac{1}{2}} - (^3P)\ 6p\ {}^4D^o_{1\frac{1}{2}}$
1	1	4218. 93	23696. 04	
400*h*	300*h*	4223. 00	23673. 20	$(^3P)\ 6p\ {}^2P^o_{1\frac{1}{2}} - 14_{2\frac{1}{2}}$
500*h*	400*h*	4238. 25	23588. 02	$(^3P)\ 6p\ {}^4P^o_{3\frac{1}{2}} - (^3P)\ 6d\ {}^4D_{2\frac{1}{2}}$; $(^3P)\ 5d\ {}^4P_{2\frac{1}{2}} - (^1D)\ 6p\ {}^2F^o_{3\frac{1}{2}}$
10	10	4243. 88	23556. 73	$(^3P)\ 5d\ {}^4D_{0\frac{1}{2}} - (^3P)\ 6p\ {}^4D^o_{0\frac{1}{2}}$
30	30	4244. 41	23553. 79	$(^3P)\ 5d\ {}^2P_{1\frac{1}{2}} - (^3P)\ 6p\ {}^2F^o_{3\frac{1}{2}}$

TABLE 1.—*List of* Xe II *lines*—Continued

Intensity		Wave length (air)	Wave number (vac)	Transition
500*h*	500*h*	4245. 38	23548. 41	$(^3P)\ 6p\ {}^4P^{\circ}_{2\frac{1}{2}} - (^3P)\ 6d\ {}^4D_{3\frac{1}{2}}$
1	1	4248. 65	23530. 29	
100H*l*	100H*l*	4251. 57	23514. 12	$(^3P)\ 6p\ {}^2P^{\circ}_{0\frac{1}{2}} - (^1D)\ 6d\ {}^2D_{1\frac{1}{2}}$
2	1	4253. 55	23503. 18	
2	1	4255. 96	23489. 87	
1	1—	4260. 68	23463. 85	
30*h*	30*h*	4263. 44	23448. 66	
?	10*h*	4263. 57	23447. 94	$(^1S)\ 6s\ {}^2S_{0\frac{1}{2}} - 25^{\circ}_{1\frac{1}{2}}$
2	1	4267. 86	23424. 38	
1	1*h*	4268. 92	23418. 56	
40	40	4269. 84	23413. 51	$(^3P)\ 6s\ {}^4P_{0\frac{1}{2}} - (^3P)\ 6p\ {}^2P^{\circ}_{0\frac{1}{2}}$
500*h*	500*h*	4296. 40	23268. 78	$(^3P)\ 6p\ {}^4P^{\circ}_{1\frac{1}{2}} - (^3P)\ 7s\ {}^4P^{\circ}_{0\frac{1}{2}}$
2	10	4296. 75	23266. 88	$(^1S)\ 5d\ {}^2D_{1\frac{1}{2}} - 29^{\circ}_{1\frac{1}{2}}$
1*h*	2*h*	4306. 21	23215. 77	$(^1S)\ 5d\ {}^2D_{1\frac{1}{2}} - 25^{\circ}_{1\frac{1}{2}}$
500*h*	500*h*	4310. 51	23192. 61	$(^3P)\ 6p\ {}^2D^{\circ}_{2\frac{1}{2}} - (^1D)\ 7s\ {}^2D_{2\frac{1}{2}}$
1H	1H	4319. 48	23144. 45	
40	40	4321. 82	23131. 92	$(^3P)\ 6s\ {}^4P_{0\frac{1}{2}} - (^3P)\ 6p\ {}^2D^{\circ}_{1\frac{1}{2}}$
1000H*l*	1000H*l*	4330. 52	23085. 45	$(^3P)\ 6p\ {}^4D^{\circ}_{2\frac{1}{2}} - (^3P)\ 6d\ {}^4F_{3\frac{1}{2}}$
10	10	4335. 81	23057. 28	$(^3P)\ 6p\ {}^4D^{\circ}_{2\frac{1}{2}} - 8_{2\frac{1}{2}}$
30H*l*	30H*l*	4337. 07	23050. 58	$(^3P)\ 6p\ {}^2P^{\circ}_{1\frac{1}{2}} - (^1D)\ 7s\ {}^2D_{2\frac{1}{2}}$
6H*l*	8H*l*	4342. 56	23021. 44	$(^3P)\ 6p\ {}^4D^{\circ}_{3\frac{1}{2}} - 10_{2\frac{1}{2}}$
2*h*	3H	4360. 32	22927. 67	
30H	30H	4367. 05	22892. 34	$(^3P)\ 6p\ {}^4D^{\circ}_{3\frac{1}{2}} - (^3P)\ 6d\ {}^4F_{3\frac{1}{2}}$
200H	200H	4369. 20	22881. 08	
2*h*	2*h*	4372. 46	22864. 02	$(^3P)\ 6p\ {}^4D^{\circ}_{3\frac{1}{2}} - 8_{2\frac{1}{2}}$
1*h*	3*hl*	4372. 88	22861. 82	
100H*l*	100H*l*	4373. 78	22857. 12	$(^3P)\ 6p\ {}^4D^{\circ}_{1\frac{1}{2}} - (^3P)\ 6d\ {}^4F_{1\frac{1}{2}}$
10H*l*	10*h*	4379. 44	22827. 58	$(^3P)\ 6p\ {}^2D^{\circ}_{2\frac{1}{2}} - (^3P)\ 6d\ {}^2D_{1\frac{1}{2}}$
60	60	4384. 93	22799. 00	$sp^6\ {}^2S_{0\frac{1}{2}} - (^3P)\ 6p\ {}^4P^{\circ}_{0\frac{1}{2}}$
500H	500H	4393. 20	22756. 08	$(^3P)\ 6p\ {}^4S^{\circ}_{1\frac{1}{2}} - (^3P)\ 6d\ {}^2D_{2\frac{1}{2}}$
500H*l*	500H*l*	4395. 77	22742. 77	
200H*l*	200H*l*	4406. 88	22685. 44	$(^3P)\ 6p\ {}^2P^{\circ}_{1\frac{1}{2}} - (^3P)\ 6d\ {}^2D_{1\frac{1}{2}}$
300	300	4414. 84	22644. 54	$(^1D)\ 6s\ {}^2D_{2\frac{1}{2}} - (^1D)\ 6p\ {}^2D^{\circ}_{2\frac{1}{2}}$
150H*l*	150H*l*	4416. 07	22638. 24	$(^3P)\ 6p\ {}^2D^{\circ}_{1\frac{1}{2}} - 14_{2\frac{1}{2}}$
1*h*	1*h*	4419. 90	22618. 62	
2*h*	2*h*	4427. 52	22579. 69	
50H	50H	4440. 95	22511. 40	$(^3P)\ 6p\ {}^4S^{\circ}_{1\frac{1}{2}} - (^3P)\ 6d\ {}^4P_{1\frac{1}{2}}$
500H*l*	500H	4448. 13	22475. 07	
1H	1H	4451. 32	22458. 96	
1000H*l*	1000H	4462. 19	22404. 25	
	1	4464. 60	22392. 16	$(^3P)\ 5d\ {}^4P_{2\frac{1}{2}} - (^1D)\ 6p\ {}^2F^{\circ}_{2\frac{1}{2}}$
30	30	4470. 90	22360. 61	$(^1D)\ 6s\ {}^2D_{2\frac{1}{2}} - (^1D)\ 6p\ {}^2D^{\circ}_{1\frac{1}{2}}$
4*h*	4*h*	4473. 85	22345. 86	
500H*l*	500*hl*	4480. 86	22310. 90	$(^3P)\ 6p\ {}^4D^{\circ}_{1\frac{1}{2}} - (^3P)\ 6d\ {}^4F_{2\frac{1}{2}}$
20	20	4485. 95	22285. 59	$(^3P)\ 5d\ {}^4P_{1\frac{1}{2}} - (^1D)\ 6p\ {}^2P^{\circ}_{1\frac{1}{2}}$
4H	4H	4488. 60	22272. 43	
5*h*	5*h*	4507. 11	22180. 97	
2*h*	2*h*	4511. 80	22157. 91	
3	3	4519. 69	22119. 23	
100*hl*	100*hl*	4521. 86	22108. 61	$(^1D)\ 6p\ {}^2D^{\circ}_{1\frac{1}{2}} - (^1D)\ 6d\ {}^2F_{2\frac{1}{2}}$

TABLE 1.—*List of* Xe II *lines*—Continued

Intensity		Wave length (air)	Wave number (vac)	Transition
200	200	4524. 21	22097. 13	$(^3P)\ 6s\ ^4P_{0\frac{1}{2}} - (^3P)\ 6p\ ^2P^{\circ}_{1\frac{1}{2}}$
200	200	4532. 49	22056. 76	$(^3P)\ 5d\ ^2D_{2\frac{1}{2}} - (^1D)\ 6p\ ^2F^{\circ}_{3\frac{1}{2}}$
1*h*	1*h*	4535. 09	22044. 12	
80H	80H	4536. 92	22035. 23	$(^3P)\ 6p\ ^4P^{\circ}_{0\frac{1}{2}} - (^3P)\ 6d\ ^4D_{1\frac{1}{2}}$
400*hl*	400*h*	4540. 89	22015. 96	$(^3P)\ 6p\ ^2D^{\circ}_{1\frac{1}{2}} - (^1D)\ 7s\ ^2D_{2\frac{1}{2}}$
400H*l*	400H*l*	4545. 23	21994. 94	$(^3P)\ 6p\ ^4D^{\circ}_{2\frac{1}{2}} - (^3P)\ 6d\ ^4D_{3\frac{1}{2}}$
10H	15*h*	4550. 79	21968. 07	$(^3P)\ 6p\ ^2P^{\circ}_{1\frac{1}{2}} - (^3P)\ 6d\ ^2P_{0\frac{1}{2}}$
200H*l*	200H*l*	4555. 94	21943. 24	$(^3P)\ 6p\ ^4D^{\circ}_{1\frac{1}{2}} - (^3P)\ 6d\ ^4D_{0\frac{1}{2}}$
2H	2H	4563. 00	21909. 29	
4	1—	4569. 12	21879. 94	
30H*d*	30H*w*	4571. 85	21866. 87	
200H	200H	4577. 06	21841. 98	$(^3P)\ 6p\ ^4D^{\circ}_{3\frac{1}{2}} - (^3P)\ 6d\ ^4D_{3\frac{1}{2}}$
80H*l*	80H	4580. 70	21824. 63	$(^1D)\ 6p\ ^2D^{\circ}_{2\frac{1}{2}} - (^1D)\ 6d\ ^2F_{2\frac{1}{2}}$
500H*l*	500*h*	4585. 48	21801. 88	$(^3P)\ 6p\ ^4D^{\circ}_{3\frac{1}{2}} - (^3P)\ 6d\ ^4D_{3\frac{1}{2}}$
1*h*	3	4588. 36	21788. 19	
300H*l*	300*h*	4592. 05	21770. 69	$(^3P)\ 6p\ ^4S^{\circ}_{1\frac{1}{2}} - (^3P)\ 6d\ ^4P_{2\frac{1}{2}}$
6	10	4593. 70	21762. 87	$(^3P)\ 5d\ ^2D_{1\frac{1}{2}} - (^1D)\ 6p\ ^2P^{\circ}_{1\frac{1}{2}}$
1	1	4596. 30	21750. 56	$(^3P)\ 6p\ ^2S^{\circ}_{\frac{1}{2}} - (^3P)\ 7s\ ^2P_{0\frac{1}{2}}$
600*h*	600	4603. 03	21718. 76	$(^3P)\ 6s\ ^4P_{1\frac{1}{2}} - (^3P)\ 6p\ ^4D^{\circ}_{1\frac{1}{2}}$
100*hl*	100*hl*	4615. 06	21662. 14	$(^3P)\ 6p\ ^4P^{\circ}_{1\frac{1}{2}} - 4$
200	200	4615. 50	21660. 08	$(^3P)\ 5d\ ^2D_{2\frac{1}{2}} - (^1D)\ 6p\ ^2P^{\circ}_{1\frac{1}{2}}$
90*hl*	100	4617. 50	21650. 70	$(^3P)\ 6p\ ^2D^{\circ}_{1\frac{1}{2}} - (^3P)\ 6d\ ^2D_{1\frac{1}{2}}$
1	3	4619. 57	21641. 00	
2	2	4620. 11	21638. 47	
50	50	4633. 30	21576. 87	$(^3P)\ 5d\ ^4F_{2\frac{1}{2}} - (^3P)\ 6p\ ^2D^{\circ}_{2\frac{1}{2}}$
2*h*	3*h*	4649. 17	21503. 22	
200	200	4651. 94	21490. 41	$(^3P)\ 6s\ ^2P_{1\frac{1}{2}} - (^3P)\ 6p\ ^2D^{\circ}_{1\frac{1}{2}}$
40	50	4653. 00	21485. 51	$(^3P)\ 5d\ ^4P_{1\frac{1}{2}} - (^1D)\ 6p\ ^2F^{\circ}_{2\frac{1}{2}}$
40H*l*	50*h*	4666. 28	21424. 37	$(^1D)\ 5d\ ^2P_{1\frac{1}{2}} - 33^{\circ}_{1\frac{1}{2}}$
100	100	4668. 49	21414. 23	$(^1D)\ 5d\ ^2D_{1\frac{1}{2}} - (^1D)\ 6p\ ^2P^{\circ}_{0\frac{1}{2}}$
100H*l*	100*hl*	4672. 20	21397. 22	$(^3P)\ 6p\ ^4P^{\circ}_{1\frac{1}{2}} - (^3P)\ 7s\ ^4P_{1\frac{1}{2}}$
40	50	4674. 56	21386. 42	$(^3P)\ 5d\ ^4D_{2\frac{1}{2}} - (^3P)\ 6p\ ^4D^{\circ}_{1\frac{1}{2}}$
200H*l*	200H*l*	4676. 46	21377. 73	
2	10*h*	4676. 75	21376. 41	
2*h*	3*h*	4678. 31	21369. 28	$(^3P)\ 6p\ ^2P^{\circ}_{0\frac{1}{2}} - (^3P)\ 6d\ ^2D_{1\frac{1}{2}}$
3*hl*	5*h*	4679. 45	21364. 08	$(^1D)\ 5d\ ^2P_{0\frac{1}{2}} - 31^{\circ}_{1\frac{1}{2}}$
15*hl*	20*hl*	4693. 34	21300. 85	$(^3P)\ 6p\ ^4S^{\circ}_{1\frac{1}{2}} - (^3P)\ 7s\ ^2P_{0\frac{1}{2}}$
300*hl*	300	4698. 01	21279. 67	$(^3P)\ 6p\ ^4D^{\circ}_{1\frac{1}{2}} - 12_{1\frac{1}{2}}$
3H*l*	6*h*	4699. 62	21272. 38	$(^3P)\ 6p\ ^2D^{\circ}_{2\frac{1}{2}} - (^3P)\ 6d\ ^2D_{2\frac{1}{2}}$
10H*l*	15H*l*	4704. 67	21249. 55	$(^1S)\ 5d\ ^2D_{2\frac{1}{2}} - 19^{\circ}_{1\frac{1}{2}}$
2H	2H*w*	4706. 96	21239. 21	
8*hl*	15*h*	4708. 92	21230. 37	$(^3P)\ 6p\ ^4P^{\circ}_{2\frac{1}{2}} - (^3P)\ 7s\ ^4P_{1\frac{1}{2}}$
40	30	4712. 63	21213. 66	
100	150	4715. 18	21202. 18	$(^3P)\ 6p\ ^2S^{\circ}_{\frac{1}{2}} - (^3P)\ 7s\ ^2P_{1\frac{1}{2}}$
2H*l*	4H*l*	4721. 00	21176. 05	
100*hl*	100*h*	4731. 19	21130. 44	$(^3P)\ 6p\ ^2P^{\circ}_{2\frac{1}{2}} - (^3P)\ 6d\ ^2D_{2\frac{1}{2}}$
15H*l*	20*hl*	4732. 51	21124. 55	$(^1S)\ 5d\ ^2D_{2\frac{1}{2}} - (^1S)\ 6p\ ^2P^{\circ}_{1\frac{1}{2}}$ $(^3P)\ 6p\ ^4P^{\circ}_{1\frac{1}{2}} - 2_{0\frac{1}{2}}$
150	200	4769. 05	20962. 69	$(^3P)\ 5d\ ^2D_{1\frac{1}{2}} - (^1D)\ 6p\ ^2F^{\circ}_{2\frac{1}{2}}$
80*h*	100	4773. 19	20944. 51	$(^1S)\ 5d\ ^2D_{2\frac{1}{2}} - 15^{\circ}_{2\frac{1}{2}}$
5H*l*	20H*l*	4775. 18	20935. 78	$(^1D)\ 6p\ ^2F^{\circ}_{3\frac{1}{2}} - (^1D)\ 7s\ ^2D_{1\frac{1}{2}}$

TABLE 1.—*List of* Xe II *lines*—Continued

Intensity		Wave length (air)	Wave number (vac)	Transition
8H*l*	20H*l*	4775. 76	20933. 24	$(^3P)\ 6p\ ^2D^\circ_{1½} - (^3P)\ 6d\ ^2P_{0½}$
80	100	4779. 18	20918. 26	$sp^6\ ^2S_{0½} - (^3P)\ 6p\ ^4P^\circ_{1½}$
10H*l*	15*h*	4786. 65	20885. 62	$(^3P)\ 6p\ ^2P^\circ_{1½} - (^3P)\ 6d\ ^4P_{1½}$
100	100	4787. 77	20880. 73	$(^1D)\ 5d\ ^2D_{1½} - (^1D)\ 6p\ ^2D^\circ_{2½}$
	3*h*	4790. 20	20870. 14	
	2*h*	4791. 84	20863. 00	
	3*h*	4795. 40	20847. 51	$(^1D)\ 5d\ ^2P_{1½} - 31i^\circ_{1½}$
	10H*l*	4796. 48	20842. 81	}
6H*l*		4796. 53	20842. 60	}
15H*l*	20*hl*	4799. 45	20829. 91	$(^1D)\ 6p\ ^2F^\circ_{2½} - (^1D)\ 6d\ ^2D_{2½}$
1	1—	4802. 10	20818. 42	
3*h*	2*h*	4806. 92	20797. 55	
	60*h*	4817. 14	20753. 42	}
40H*l*		4817. 22	20753. 08	} $(^3P)\ 6p\ ^4S^\circ_{1½} - (^3P)\ 7s\ ^2P_{1½}$
200	200	4818. 02	20749. 63	$(^3P)\ 5d\ ^4D_{1½} - (^3P)\ 6p\ ^4D^\circ_{1½}$
	300	4823. 35	20726. 70	}
300*h*		4823. 41	20726. 45	} $(^3P)\ 6p\ ^4P^\circ_{1½} - (^3P)\ 7s\ ^4P_{2½}$
2H	1	4827. 55	20708. 67	
2H		4830. 11	20697. 70	}
	1	4830. 25	20697. 10	}
2	1	4832. 20	20688. 74	
	3	4834. 65	20678. 26	
1H—	1H	4837. 82	20664. 71	
1		4840. 87	20651. 69	$(^3P)\ 6p\ ^2P^\circ_{0½} - (^3P)\ 6d\ ^2P_{0½}$
2000*h*	3000	4844. 33	20636. 94	$(^3P)\ 6s\ ^4P_{2½} - (^3P)\ 6p\ ^4D^\circ_{3½}$
40	60	4853. 77	20596. 81	$(^1D)\ 5d\ ^2D_{1½} - (^1D)\ 6p\ ^2D^\circ_{1½}$
1	1	4857. 20	20582. 26	
1H	2*h*	4858. 82	20575. 40	
	1000	4862. 45	20560. 04	}
800*hl*		4862. 54	20559. 66	} $(^3P)\ 6p\ ^4P^\circ_{2½} - (^3P)\ 7s\ ^4P_{2½}$
1*h*	2*h*	4868. 87	20532. 93	
500*hl*	500	4876. 50	20500. 80	$(^1D)\ 6s\ ^2D_{2½} - (^1D)\ 6p\ ^4F^\circ_{3½}$
1*d*?	1	4880. 78	20482. 83	
600*h*	600	4883. 53	20471. 29	$(^3P)\ 6s\ ^4P_{0½} - (^3P)\ 6p\ ^4S^\circ_{1½}$
100H	100H	4884. 15	20468. 69	$(^3P)\ 6p\ ^4D^\circ_{0½} - (^3P)\ 6d\ ^4P_{0½}$
4*h*	5*h*	4885. 19	20464. 34	
300*h*	300	4887. 30	20455. 50	$(^3P)\ 6s\ ^2P_{1½} - (^3P)\ 6p\ ^2P^\circ_{1½}$
300*h*	300	4890. 09	20443. 83	$(^3P)\ 6s\ ^4P_{2½} - (^3P)\ 6p\ ^4D^\circ_{2½}$
1	1	4895. 24	20422. 32	
	1	4899. 9	20402. 9	$(^3P)\ 6p\ ^4D^\circ_{3½} - 6_{2½}$
2H	3*h*	4905. 20	20380. 85	
	2	4911. 64	20354. 13	
200	250	4919. 66	20320. 95	$(^3P)\ 6s\ ^2P_{0½} - (^3P)\ 6p\ ^2P^\circ_{0½}$
1*h*	1*h*	4920. 59	20317. 11	
800	1000	4921. 48	20313. 44	$(^3P)\ 6s\ ^2P_{1½} - (^3P)\ 6p\ ^2D^\circ_{2½}$
1*h*	2*h*	4925. 89	20295. 25	
	2	4931. 33	20272. 86	
1	2	4936. 25	20252. 66	
1	2	4941. 10	20232. 78	
1H		4946. 72	20209. 79	$(^3P)\ 6p\ ^4D^\circ_{2½} - 6_{2½}$

TABLE 1.—*List of* Xe II *lines*—Continued

Intensity		Wave length (air)	Wave number (vac)	Transition
1—	1	4947. 70	20205. 79	
	1—	4962. 8	20144. 3	$(^3P)\ 6p\ ^2P^{\circ}_{1\frac{1}{2}} - (^3P)\ 6d\ ^4P_{2\frac{1}{2}}$
4H*l*	8H*l*	4965. 00	20135. 38	$(^1D)\ 6p\ ^2P^{\circ}_{1\frac{1}{2}} - (^1D)\ 7s\ ^2D_{1\frac{1}{2}}$
1*h*	2*h*	4966. 23	20130. 40	
200H*l*	200H*l*	4971. 71	20108. 21	
400*h*	400	4972. 71	20104. 17	$(^1D)\ 6s\ ^2D_{2\frac{1}{2}} - (^1D)\ 6p\ ^2P^{\circ}_{1\frac{1}{2}}$
	1	4974. 41	20097. 30	$(^1S)\ 5d\ ^2D_{2\frac{1}{2}} - 7i_{1\frac{1}{2}}$
2*h*	3*h*	4974. 87	20095. 44	$(^3P)\ 6p\ ^2D^{\circ}_{1\frac{1}{2}} - (^3P)\ 6d\ ^2D_{2\frac{1}{2}}$
2*h*	2*h*	4985. 63	20052. 07	
300*h*	300	4988. 77	20039. 45	$(^3P)\ 6s\ ^2P_{0\frac{1}{2}} - (^3P)\ 6p\ ^2D^{\circ}_{1\frac{1}{2}}$
100H*l*	100H*l*	4991. 17	20029. 81	$(^1D)\ 6p\ ^2P^{\circ}_{1\frac{1}{2}} - (^1D)\ 6d\ ^2D_{2\frac{1}{2}}$
10	20	4993. 03	20022. 35	$(^3P)\ 6s\ ^4P_{0\frac{1}{2}} - (^3P)\ 6p\ ^2S^{\circ}_{0\frac{1}{2}}$
5H*l*	20H*l*	4993. 93	20018. 74	$(^1D)\ 5d\ ^2P_{1\frac{1}{2}} - 27_{2\frac{1}{2}}$
1—	1*h*	4996. 22	20009. 59	
3*h*	10*h*	5001. 01	19990. 40	
50H*l*	100*h*	5012. 83	19943. 26	$(^3P)\ 6p\ ^4D^{\circ}_{1\frac{1}{2}} - 10_{2\frac{1}{2}}$
1	2	5017. 41	19925. 06	
	1	5018. 75	19919. 74	$(^1S)\ 5d\ ^2D_{2\frac{1}{2}} - 3i_{3\frac{1}{2}}$
3H*l*	5*h*	5036. 15	19850. 92	$(^3P)\ 6p\ ^2D^{\circ}_{1\frac{1}{2}} - (^3P)\ 6d\ ^4P_{1\frac{1}{2}}$
2	1*h*	5038. 69	19840. 91	
150*h*	200	5044. 92	19816. 41	$(^1D)\ 6s\ ^2D_{1\frac{1}{2}} - (^1D)\ 6p\ ^2P^{\circ}_{0\frac{1}{2}}$
30*h*	50	5052. 54	19786. 52	$(^3P)\ 6p\ ^4D^{\circ}_{1\frac{1}{2}} - 8_{2\frac{1}{2}}$
3H*l*	4H	5066. 33	19732. 67	
10H*w*	20H*w*	5069. 82	19719. 08	
	1*h*	5073. 8	19703. 6	$(^1D)\ 5d\ ^2S_{0\frac{1}{2}} - 33i_{1\frac{1}{2}}$; $(^3P)\ 6p\ ^2S^{\circ}_{0\frac{1}{2}} - (^3P)\ 6d\ ^4P_{0\frac{1}{2}}$
600*h*	1000	5080. 62	19677. 17	$(^3P)\ 6p\ ^4D^{\circ}_{3\frac{1}{2}} - (^3P)\ 7s\ ^4P_{0\frac{1}{2}}$
30	50	5081. 07	19675. 42	$(^3P)\ 6p\ ^2P^{\circ}_{1\frac{1}{2}} - (^3P)\ 7s\ ^2P_{0\frac{1}{2}}$
	80	5091. 93	19633. 46	$(^1D)\ 6p\ ^2F^{\circ}_{3\frac{1}{2}} - (^1D)\ 6d\ ^2D_{2\frac{1}{2}}$
60H*l*		5092. 02	19633. 12	
5H	10H	5099. 59	19603. 97	
2*h*	5*h*	5108. 58	19569. 47	$(^3P)\ 6p\ ^2P^{\circ}_{0\frac{1}{2}} - (^3P)\ 6d\ ^4P_{1\frac{1}{2}}$
2*h*	5*h*	5117. 76	19534. 37	
200*hl*	300	5122. 42	19516. 60	$(^3P)\ 6p\ ^4P^{\circ}_{0\frac{1}{2}} - (^3P)\ 7s\ ^4P_{1\frac{1}{2}}$
30	100	5125. 70	19504. 11	$(^1D)\ 5d\ ^2D_{2\frac{1}{2}} - (^1D)\ 6p\ ^2D^{\circ}_{2\frac{1}{2}}$
50*h*	100	5178. 82	19304. 06	$(^1D)\ 6s\ ^2D_{2\frac{1}{2}} - (^1D)\ 6p\ ^2F^{\circ}_{2\frac{1}{2}}$
50	80	5184. 48	19282. 98	$(^1D)\ 6s\ ^2D_{1\frac{1}{2}} - (^1D)\ 6p\ ^2D^{\circ}_{2\frac{1}{2}}$
	300	5188. 04	19269. 75	$(^3P)\ 6p\ ^2D^{\circ}_{2\frac{1}{2}} - (^3P)\ 7s\ ^2P_{1\frac{1}{2}}$
200		5188. 11	19269. 49	
300	400	5191. 37	19257. 39	$(^3P)\ 6s\ ^4P_{0\frac{1}{2}} - (^3P)\ 6p\ ^4D^{\circ}_{0\frac{1}{2}}$
80	100	5192. 10	19254. 68	$(^3P)\ 6p\ ^4S^{\circ}_{1\frac{1}{2}} - (^3P)\ 6d\ ^4P_{0\frac{1}{2}}$
5H	20H	5194. 92	19244. 23	$(^3P)\ 6p\ ^4P^{\circ}_{0\frac{1}{2}} - 2_{0\frac{1}{2}}$
	1*h*	5199. 9	19225. 8	$(^3P)\ 6p\ ^4D^{\circ}_{0\frac{1}{2}} - (^3P)\ 6d\ ^4F_{1\frac{1}{2}}$
20	30	5201. 42	19220. 18	$(^1D)\ 5d\ ^2D_{2\frac{1}{2}} - (^1D)\ 6p\ ^2D^{\circ}_{1\frac{1}{2}}$
	10H	5201. 88	19218. 48	$(^1D)\ 6p\ ^2F^{\circ}_{2\frac{1}{2}} - (^1D)\ 6d\ ^2D_{1\frac{1}{2}}$
1*h*	3*h*	5213. 17	19176. 86	
1H	1H	5218. 20	19158. 38	
	50*hl*	5226. 57	19127. 70	$(^3P)\ 6p\ ^2P^{\circ}_{1\frac{1}{2}} - (^3P)\ 7s\ ^2P_{1\frac{1}{2}}$
20*hl*		5226. 62	19127. 51	
?	10*hl*	5226. 90	19126. 49	$(^1D)\ 5d\ ^2S_{0\frac{1}{2}} - 31i_{1\frac{1}{2}}$
1—	1	5240. 9	19075. 4	

TABLE 1.—*List of* Xe II *lines*—Continued

Intensity		Wave length (air)	Wave number (vac)	Transition
20*h*	100	5247. 75	19050. 50	
30	50	5259. 89	19006. 53	(^{3}P) 6*p* ^{4}D$^\circ_{3½}$ — (^{3}P) 7*s* ^{4}P$_{2½}$
200	500	5260. 44	19004. 54	(^{3}P) 6*s* ^{2}P$_{2½}$ — (^{3}P) 6*p* ^{2}P$^\circ_{1½}$
200	500	5261. 95	18999. 09	(^{1}D) 6*s* ^{2}D$_{1½}$ — (^{1}D) 6*p* ^{2}D$^\circ_{1½}$
1	1	5263. 98	18991. 76	
50	100	5268. 31	18976. 15	(^{3}P) 5*d* ^{2}P$_{1½}$ — (^{3}P) 6*p* ^{2}D$^\circ_{1½}$
1*h*	3	5281. 66	18928. 19	
2*h*	20	5282. 46	18925. 32	(^{3}P) 6*p* ^{4}D$^\circ_{1½}$ — (^{3}P) 6*d* ^{4}D$_{1½}$
2*h*	2*h*	5291. 3	18893. 7	
1000	2000	5292. 22	18890. 42	(^{3}P) 6*s* ^{4}P$_{2½}$ — (^{3}P) 6*p* ^{4}P$^\circ_{2½}$
	4	5302. 83	18852. 62	
200	300	5309. 27	18829. 76	(^{3}P) 6*s* ^{2}P$_{1½}$ — (^{3}P) 6*p* ^{4}S$^\circ_{1½}$
800	1000	5313. 87	18813. 46	(^{3}P) 6*p* ^{4}D$^\circ_{3½}$ — (^{3}P) 7*s* ^{4}P$_{2½}$
	3	5319. 83	18792. 38	
1—	1	5320. 44	18790. 23	
	1	5323. 35	18779. 93	
	20	5327. 83	18764. 16	}
3		5327. 90	18763. 93	}
1—	3	5328. 69	18761. 13	
1*h*	1*h*	5338. 38	18727. 08	
	2000	5339. 33	18723. 75	{ (^{3}P) 6*p* ^{4}D$^\circ_{1½}$ — (^{3}P) 6*d* ^{4}D$_{3½}$
1000		5339. 38	18723. 59	{ (^{3}P) 6*s* ^{4}P$_{2½}$ — (^{3}P) 6*p* ^{4}P$^\circ_{1½}$
	3	5350. 03	18686. 30	
1H*l*	2*h*	5357. 9	18658. 9	
1—	1	5359. 41	18653. 60	
1—	2	5360. 73	18649. 00	
	2	5361. 65	18645. 80	
	200	5363. 20	18640. 41	} (^{3}P) 6*p* ^{2}D$^\circ_{1½}$ — (^{3}P) 7*s* ^{2}P$_{0½}$
150		5363. 27	18640. 17	}
100	200	5368. 07	18623. 50	(^{3}P) 5*d* ^{4}P$_{0½}$ — (^{3}P) 6*p* ^{2}P$^\circ_{0½}$
300	500	5372. 39	18608. 53	(^{3}P) 6*s* ^{4}P$_{1½}$ — (^{3}P) 6*p* ^{4}P$^\circ_{0½}$
	1	5383. 17	18571. 27	
1*h*	1	5388. 65	18552. 72	
1—	1	5390. 22	18546. 98	
	1	5392. 78	18538. 17	
1—	2	5393. 90	18534. 32	
1H	2	5397. 47	18522. 06	
1—	1	5402. 90	18503. 45	
	3	5408. 34	18484. 84	
	50H	5415. 36	18460. 87	(^{3}P) 6*p* ^{2}S$^\circ_{0½}$ — (^{3}P) 6*d* ^{4}F$_{1½}$
2*h*	2*h*	5418. 2	18451. 2	
2000	3000	5419. 15	18447. 96	(^{3}P) 6*s* ^{4}P$_{1½}$ — (^{3}P) 6*p* ^{4}D$^\circ_{2½}$
	2*hs*	5428. 07	18417. 65	(^{1}D) 6*p* ^{2}P$^\circ_{1½}$ — (^{1}D) 6*d* ^{2}D$_{1½}$
	3	5430. 06	18410. 90	
400	800	5438. 96	18380. 77	(^{3}P) 6*s* ^{2}P$_{1½}$ — (^{3}P) 6*p* ^{2}S$^\circ_{0½}$
	300	5445. 45	18358. 86	} (^{3}P) 6*p* ^{2}P$^\circ_{0½}$ — (^{3}P) 7*s* ^{2}P$_{0½}$
150		5445. 52	18358. 63	}
100	200	5450. 45	18342. 02	(^{3}P) 5*d* ^{4}P$_{0½}$ — (^{3}P) 6p ^{2}D$^\circ_{1½}$
20	50	5450. 90	18340. 51	(^{1}D) 5*d* ^{2}D$_{1½}$ — (^{1}D) 6*p* ^{2}P$^\circ_{1½}$
300	400	5460. 39	18308. 63	(^{3}P) 5*d* ^{4}D$_{2½}$ — (^{3}P) 6*p* ^{4}D$^\circ_{3½}$

TABLE 1.—*List of* Xe II lines—Continued

Intensity		Wave length (air)	Wave number (vac)	Transition
	50	5469. 54	18278. 01	} (^{3}P) 6*p* ^{4}D$^{\circ}_{1½}$—(^{3}P) 7*s* ^{4}P$_{0½}$
20h		5469. 58	18277. 87	
500	1000	5472. 61	18267. 75	(^{3}P) 5*d* ^{4}D$_{3½}$—(^{3}P) 6*p* ^{4}D$^{\circ}_{3½}$
1*h*	3*h*	5481. 13	18239. 36	
	1	5483. 59	18231. 18	
	2H*w*	5486. 60	18221. 17	
	100H*l*	5494. 86	18193. 78	}
20H*lw*		5495. 07	18193. 09	}
2*h*	20	5507. 46	18152. 16	
	20H*lw*	5509. 20	18146. 43	
1	5	5518. 56	18115. 65	(^{3}P) 5*d* ^{4}D$_{2½}$—(^{3}P) 6*p* ^{4}D$^{\circ}_{2½}$
	1	5520. 00	18110. 92	
	200	5525. 53	18092. 80	} (^{3}P) 6*p* ^{2}D$^{\circ}_{1½}$—(^{3}P) 7*s* ^{2}P$_{1½}$
50		5525. 59	18092. 60	
400	600	5531. 07	18074. 68	(^{3}P) 5*d* ^{4}D$_{3½}$—(^{3}P) 6*p* ^{4}D$^{\circ}_{2½}$
	4H*s*	5551. 50	18008. 16	
3*h*	3*h*	5554. 99	17996. 85	
50	100	5572. 19	17941. 30	
2H	10H	5581. 93	17909. 99	
2H	20H	5583. 5	17905. 0	
2H	100H	5591. 61	17878. 98	(^{1}D) 6*p* ^{2}D$^{\circ}_{1½}$—(^{1}D) 7*s* ^{2}D$_{1½}$
	15H*wl*	5594. 87	17868. 57	
1*h*—	3*h*	5612. 89	17811. 20	(^{3}P) 6*p* ^{2}P$^{\circ}_{0½}$—(^{3}P) 7*s* ^{2}P$_{1½}$
150	300	5616. 67	17799. 21	(^{3}P) 5*d* ^{2}P$_{1½}$—(^{3}P) 6*p* ^{2}D$^{\circ}_{2½}$
1H*l*	10H*l*	5624. 78	17773. 55	(^{1}D) 6*p* ^{2}D$^{\circ}_{1½}$—(^{1}D) 6*d* ^{2}D$_{2½}$
3H	10H*wl*	5633. 24	17746. 86	
1*h*	2H*w*	5650. 53	17692. 56	
150	300	5659. 38	17664. 89	(^{3}P) 5*d* ^{2}P$_{0½}$—(^{3}P) 6*p* ^{2}P$^{\circ}_{0½}$
3*h*	2H	5664. 02	17650. 42	
300	600	5667. 56	17639. 39	(^{3}P) 5*d* ^{4}D$_{1½}$—(^{3}P) 6*p* ^{4}P$^{\circ}_{0½}$
	150	5670. 91	17628. 97	} (^{3}P) 6*p* ^{2}P$^{\circ}_{1½}$—(^{3}P) 6*d* ^{4}P$_{½}$
50		5670. 96	17628. 82	
1	10	5675. 15	17615. 80	(^{3}P) 6*s* ^{2}P$_{1½}$—(^{3}P) 6*p* ^{4}D$^{\circ}_{0½}$
	1	5678. 93	17604. 08	
1*h*	2H*w*	5681. 87	17594. 97	(^{1}D) 6*p* ^{2}D$^{\circ}_{2½}$—(^{1}D) 7*s* ^{2}D$_{1½}$
	2	5682. 63	17592. 62	
2*h*	3*h*	5686. 49	17580. 67	
	2H*s*	5686. 6	17580. 3	
	2	5688. 20	17575. 39	
100	200	5699. 61	17540. 20	(^{1}D) 5*d* ^{2}D$_{1½}$—(^{1}D) 6*p* ^{2}F$^{\circ}_{2½}$
	200	5716. 10	17489. 60	} (^{1}D) 6*p* ^{2}D$^{\circ}_{2½}$—(^{1}D) 6*d* ^{2}D$_{2½}$
100H		5716. 19	17489. 33	
200	500	5726. 91	17456. 59	{ (^{1}D) 5*d* ^{2}F$_{2½}$—(^{1}D) 6*p* ^{2}D$^{\circ}_{2½}$ (^{3}P) 6*p* ^{4}P$^{\circ}_{1½}$—(^{1}D) 5*d* ^{2}S$_{0½}$
	1	5738. 40	17421. 64	
1H*w*	20H	5746. 88	17395. 93	
200	500	5751. 03	17383. 38	(^{3}P) 5*d* ^{2}P$_{0½}$—(^{3}P) 6*p* D$^{\circ}_{1½}$
10	30	5752. 56	17378. 75	(^{3}P) 6*s* ^{2}P$_{0½}$—(^{3}P) 6*p* ^{4}S$^{\circ}_{1½}$
	5	5754. 18	17373. 86	
100	300	5758. 65	17360. 38	(^{1}D) 5*d* ^{2}D$_{2½}$—(^{1}D) 6*p* ^{4}F$^{\circ}_{1½}$
100	300	5776. 39	17307. 06	(^{3}P) 5*d* ^{4}P$_{0½}$—(^{3}P) 6*p* ^{2}P$^{\circ}_{1½}$

TABLE 1.—*List of* Xe II *lines*—Continued

Intensity		Wave length (air)	Wave number (vac)	Transition
1—	2	5780. 83	17293. 77	
	5*hld*	5791. 88	17260. 78	(1D) 6*p* $^2P^{\circ}_{1\frac{1}{2}}$—$14_{2\frac{1}{2}}$
1*hl*		5791. 98	17260. 48	
1—	1H*l*	5797. 76	17243. 27	
1H*w*	1H*w*	5809. 5	17208. 4	(3P) 6*d* $^4F_{2\frac{1}{2}}$—$39^{\circ}_{1\frac{1}{2}}$
50	100	5815. 96	17189. 31	(3P) 5*d* $^4P_{1\frac{1}{2}}$—(3P) 6*p* $^2P^{\circ}_{0\frac{1}{2}}$
1—	2*h*	5821. 57	17172. 75	(1D) 5*d* $^2F_{2\frac{1}{2}}$—(1D) 6*p* $^2D^{\circ}_{1\frac{1}{2}}$
5H*w*	100H*w*	5835. 5	17131. 8	(3P) 6*p* $^4D^{\circ}_{1\frac{1}{2}}$—$6_{2\frac{1}{2}}$
2	6	5846. 69	17098. 97	
1	5H	5855. 47	17073. 33	(1D) 6*p* $^4F^{\circ}_{2\frac{1}{2}}$—(3P) 6*d* $^2D_{1\frac{1}{2}}$
2H	50H	5859. 47	17061. 67	(1D) 6*p* $^2P^{\circ}_{0\frac{1}{2}}$—(1D) 7*s* $^2D_{1\frac{1}{2}}$
1*h*	1*h*	5868. 86	17034. 37	
150	300	5893. 29	16963. 76	(1D) 5*d* $^2D_{2\frac{1}{2}}$—(1D) 6*p* $^2P^{\circ}_{1\frac{1}{2}}$ (1D) 6*p* $^2F^{\circ}_{2\frac{1}{2}}$—$14_{2\frac{1}{2}}$
200	200	5905. 13	16929. 75	(3P) 6*s* $^2P_{0\frac{1}{2}}$—(3P) 6*p* $^2S^{\circ}_{0\frac{1}{2}}$
30*h*	50*h*	5909. 67	16916. 74	(1S) 6*s* $^2S_{0\frac{1}{2}}$—$21^{\circ}_{1\frac{1}{2}}$
5*h*	10	5912. 80	16907. 79	(3P) 5*d* $^4P_{1\frac{1}{2}}$—(3P) 6*p* $^2D^{\circ}_{1\frac{1}{2}}$
50	100	5917. 44	16894. 53	(3P) 6*s* $^4P_{1\frac{1}{2}}$—(3P) 6*p* $^4P^{\circ}_{2\frac{1}{2}}$
1	5H*l*	5921. 50	16882. 95	(3P) 6*p* $^2S^{\circ}_{0\frac{1}{2}}$—$12_{1\frac{1}{2}}$
1H	4H	5934. 55	16845. 82	
300	500	5945. 53	16814. 71	(3P) 5*d* $^4D_{0\frac{1}{2}}$—(3P) 6*p* $^4P^{\circ}_{0\frac{1}{2}}$
50	100	5958. 03	16779. 43	(3P) 5*d* $^4P_{2\frac{1}{2}}$—(3P) 6*p* $^2P^{\circ}_{1\frac{1}{2}}$
1—	2	5964. 52	16761. 17	
200	300	5971. 13	16742. 62	(1D) 6*s* $^2D_{1\frac{1}{2}}$—(1D) 6*p* $^2P^{\circ}_{1\frac{1}{2}}$
1000	2000	5976. 46	16727. 69	(3P) 6*s* $^4P_{1\frac{1}{2}}$—(3P) 6*p* $^4P^{\circ}_{1\frac{1}{2}}$
1	4	5988. 44	16694. 22	
1H	20*h*	5991. 86	16684. 70	(1S) 5*d* $^2D_{1\frac{1}{2}}$—$21^{\circ}_{1\frac{1}{2}}$
	1	5998. 10	16667. 34	
	1	5998. 3	16666. 8	(3P) 5*d* $^2D_{1\frac{1}{2}}$—(3P) 6*p*^{2} $P^{\circ}_{0\frac{1}{2}}$
1—	1	6000. 3	16661. 2	
100	200	6008. 92	16637. 33	(3P) 5*d* $^4P_{2\frac{1}{2}}$—(3P) 6*p* $^2D^{\circ}_{2\frac{1}{2}}$
1	1	6012. 0	16628. 8	
	2	6024. 14	16595. 30	
	2*h*	6024. 58	16594. 08	(3P) 6*p* $^2D^{\circ}_{1\frac{1}{2}}$—(3P) 6*d* $^4P_{0\frac{1}{2}}$
3H		6024. 77	16593. 56	
500	1000	6036. 20	16562. 14	(3P) 5*d* $^4D_{2\frac{1}{2}}$—(3P) 6*p* $^4P^{\circ}_{2\frac{1}{2}}$
	5*h*	6048. 53	16528. 38	(3P) 6*p* $^2D^{\circ}_{2\frac{1}{2}}$—(3P) 6*d* $^4F_{1\frac{1}{2}}$
1000	2000	6051. 15	16521. 22	(3P) 5*d* $^4D_{2\frac{1}{2}}$—(3P) 6*p* $^4P^{\circ}_{2\frac{1}{2}}$
1—	3	6063. 29	16488. 14	
1H—	1	6067. 05	16477. 92	
	1*h*	6069. 33	16471. 73	
	1*h*	6075. 32	16455. 49	
	1	6079. 29	16444. 75	
	1	6081. 36	16439. 15	
1*h*—	5*h*	6083. 21	16434. 15	(3P) 6*p* $^4S^{\circ}_{1\frac{1}{2}}$—$12_{1\frac{1}{2}}$
	2	6085. 38	16428. 29	
	600	6093. 50	16406. 40	(3P) 6*p* $^4D^{\circ}_{1\frac{1}{2}}$—(3P) 7*s* $^4P_{1\frac{1}{2}}$
300		6093. 56	16406. 24	
1000	1500	6097. 59	16395. 39	(3P) 5*d* $^4D_{2\frac{1}{2}}$—(3P) 6*p* $^4P^{\circ}_{1\frac{1}{2}}$
200	400	6101. 43	16385. 07	(3P) 5*d* $^2D_{1\frac{1}{2}}$—(3P) 6*p* $^2D^{\circ}_{1\frac{1}{2}}$
	2	6109. 86	16362. 47	

TABLE 1.—*List of* Xe II *lines*—Continued

Intensity		Wave length (air)	Wave number (vac)	Transition
50	100	6115.08	16348.50	$(^3P)\ 5d\ ^2P_{0\frac{1}{2}} - (^3P)\ 6p\ ^2P^0_{1\frac{1}{2}}$
2	15	6127.44	16315.52	$(^3P)\ 5d\ ^2P_{1\frac{1}{2}} - (^3P)\ 6p\ ^4S^0_{1\frac{1}{2}}$
1*h*	10*h*	6143.40	16273.14	$(^1D)\ 6p\ ^2P^0_{1\frac{1}{2}} - (^3P)\ 6d\ ^2D_{1\frac{1}{2}}$
50	100	6146.45	16265.06	$(^1S)\ 6s\ ^2S_{0\frac{1}{2}} - 19^0_{1\frac{1}{2}}$
1H*w*—	3H	6155.28	16241.73	$(^1D)\ 6p\ ^4F^0_{3\frac{1}{2}} - (^1D)\ 7s\ ^2D_{2\frac{1}{2}}$
	1	6160.72	16227.39	
20	50	6184.57	16164.81	$(^3P)\ 6s\ ^2P_{0\frac{1}{2}} - (^3P)\ 6p\ ^4D^0_{0\frac{1}{2}}$
15	30	6185.03	16163.61	$(^1D)\ 5d\ ^2D_{2\frac{1}{2}} - (^1D)\ 6p\ ^2F^0_{2\frac{1}{2}}$
	3H	6185.79	16161.62	$(^1D)\ 6p\ ^2D^0_{1\frac{1}{2}} - (^1D)\ 6d\ ^2D_{1\frac{1}{2}}$
1H		6185.93	16161.26	
300	500	6194.07	16140.02	$(^1S)\ 6s\ ^2S_{0\frac{1}{2}} - (^1S)\ 6p\ ^2P^0_{1\frac{1}{2}}$
	3	6196.55	16133.56	$(^3P)\ 6p\ ^4D^0_{1\frac{1}{2}} - 2_{0\frac{1}{2}}$
4*h*		6196.63	16133.35	
	1*h*	6203.45	16115.61	$(^1S)\ 6s\ ^2S_{0\frac{1}{2}} - 17^0_{0\frac{1}{2}}$
	50	6206.08	16108.78	
200		6206.16	16108.58	
10H*w*	2H	6234.04	16036.53	$2_{0\frac{1}{2}} - 33^0_{1\frac{1}{2}}$
1*h*	10*h*	6235.40	16033.04	$(^1S)\ 5d\ ^2D_{1\frac{1}{2}} - 19^0_{1\frac{1}{2}}$
1	1	6250.23	15995.00	
1H*l*	1H*l*	6254.0	15985.4	
	2H*l*	6255.32	15981.98	$(^3P)\ 6p\ ^2D^0_{2\frac{1}{2}} - (^3P)\ 6d\ ^4F_{2\frac{1}{2}}$
	1	6264.94	15957.44	
400	500	6270.82	15942.48	$(^1D)\ 6s\ ^2D_{1\frac{1}{2}} - (^1D)\ 6p\ ^2F^0_{2\frac{1}{2}}$
300	400	6277.54	15925.41	$(^3P)\ 5d\ ^4D_{1\frac{1}{2}} - (^3P)\ 6p\ ^4P^0_{2\frac{1}{2}}$
50	100	6284.41	15908.00	$(^1S)\ 5d\ ^2D_{1\frac{1}{2}} - (^1S)\ 6p\ ^2P^0_{1\frac{1}{2}}$
	2	6288.21	15898.39	
	1	6290.15	15893.49	
	10H	6296.39	15877.73	$(^1D)\ 6p\ ^2D^0_{2\frac{1}{2}} - (^1D)\ 6d\ ^2D_{1\frac{1}{2}}$
20	50	6298.31	15872.89	$(^3P)\ 5d\ ^4P_{1\frac{1}{2}} - (^3P)\ 6p\ ^2P^0_{1\frac{1}{2}}$
100	250	6300.86	15866.47	$(^3P)\ 5d\ ^2P_{1\frac{1}{2}} - (^3P)\ 6p\ ^2S^0_{0\frac{1}{2}}$
1*h*	1*h*	6304.09	15858.34	
1*h*	2H	6305.01	15856.03	$(^3P)\ 7s\ ^4P_{2\frac{1}{2}} - 31^0_{1\frac{1}{2}}$
5H*w*	50H*l*	6311.46	15839.82	$(^3P)\ 6p\ ^2P^0_{1\frac{1}{2}} - (^3P)\ 6d\ ^4F_{2\frac{1}{2}}$
	2	6324.94	15806.07	
2H		6325.17	15805.49	
300	400	6343.96	15758.68	$(^3P)\ 5d\ ^4D_{1\frac{1}{2}} - (^3P)\ 6p\ ^4P^0_{1\frac{1}{2}}$
	100*hl*	6353.20	15735.76	$(^3P)\ 6p\ ^4D^0_{1\frac{1}{2}} - (^3P)\ 7s\ ^4P_{2\frac{1}{2}}$
50H*l*		6353.29	15735.53	$(^3P)\ 6p\ ^4P^0_{1\frac{1}{2}} - (^1D)\ 5d\ ^2P_{1\frac{1}{2}}$
500	600	6356.35	15727.96	$(^1S)\ 5d\ ^2D_{1\frac{1}{2}} - 15^0_{2\frac{1}{2}}$
2H	3H	6362.8	15712.0	
100	200	6375.28	15681.25	$(^3P)\ 5d\ ^4P_{0\frac{1}{2}} - (^3P)\ 6p\ ^4S^0_{1\frac{1}{2}}$
60	100	6397.99	15625.60	$(^3P)\ 6s\ ^4P_{0\frac{1}{2}} - (^3P)\ 6p\ ^4D^0_{1\frac{1}{2}}$
20	50	6418.58	15575.47	$(^3P)\ 6p\ ^4P^0_{0\frac{1}{2}} - (^1D)\ 5d\ ^2S_{0\frac{1}{2}}$
	1	6421.47	15568.46	$(^3P)\ 6p\ ^4P^0_{2\frac{1}{2}} - (^1D)\ 5d\ ^2P_{1\frac{1}{2}}$
	2H	6426.73	15555.72	$(^1D)\ 6p\ ^2P^0_{1\frac{1}{2}} - (^3P)\ 6d\ ^2P^0_{0\frac{1}{2}}$
1—	1	6430.15	15547.45	
	1H	6442.3	15518.1	$(^1D)\ 6p\ ^4F^0_{3\frac{1}{2}} - (^3P)\ 6d\ ^2D_{2\frac{1}{2}}$
	10H	6461.48	15472.06	
2H	3H	6479.69	15428.58	$(^1S)\ 6s\ ^2S_{0\frac{1}{2}} - 9^0_{1\frac{1}{2}}$
300*h*	300	6512.83	15350.07	$(^3P)\ 5d\ ^2D_{1\frac{1}{2}} - (^3P)\ 6p\ ^2P^0_{1\frac{1}{2}}$

TABLE 1.—*List of* Xe II *lines*—Continued

Intensity		Wave length (air)	Wave number (vac)	Transition
1H	2H	6515. 48	15343. 83	$(^1S)\ 5d\ ^2D_{1\frac{1}{2}}-11j_{2\frac{1}{2}}$ $(^1D)\ 6p\ ^2P^0_{0\frac{1}{2}}-(^1D)\ 6d\ ^2D_{1\frac{1}{2}}$
200*h*	200	6528. 65	15312. 88	$(^1D)\ 5d\ ^2F_{2\frac{1}{2}}-(^1D)\ 6p\ ^2F^0_{3\frac{1}{2}}$
4	5	6556. 70	15247. 37	$(^3P)\ 5d\ ^4F_{3\frac{1}{2}}-(^3P)\ 6p\ ^4D^0_{1\frac{1}{2}}$ $(^3P)\ 5d\ ^2D_{2\frac{1}{2}}-(^3P)\ 6p\ ^2P^0_{1\frac{1}{2}}$
15	15	6563. 19	15232. 29	$(^3P)\ 5d\ ^4P_{0\frac{1}{2}}-(^3P)\ 6p\ ^2S^0_{0\frac{1}{2}}$
5	8	6569. 13	15218. 52	$(^3P)\ 6p\ ^4P^0_{1\frac{1}{2}}-(^1D)\ 5d\ ^2P_{0\frac{1}{2}}$
30	50	6573. 68	15207. 99	$(^3P)\ 5d\ ^2D_{1\frac{1}{2}}-(^3P)\ 6p\ ^2D^0_{2\frac{1}{2}}$
800	1000	6595. 01	15158. 80	
300	400	6597. 25	15153. 65	$(^3P)\ 5d\ ^4P_{2\frac{1}{2}}-(^3P)\ 6p\ ^4S^0_{1\frac{1}{2}}$
80	100	6598. 84	15150. 00	$(^1D)\ 5d\ ^2F_{3\frac{1}{2}}-(^1D)\ 6p\ ^2F^0_{3\frac{1}{2}}$
4*h*	3	6613. 31	15116. 85	
10H	10*h*	6614. 96	15113. 08	$(^1S)\ 6s\ ^2S_{0\frac{1}{2}}-7j_{1\frac{1}{2}}$
50	40	6618. 40	15105. 23	$(^3P)\ 5d\ ^2D_{2\frac{1}{2}}-(^3P)\ 6p\ ^2D^0_{2\frac{1}{2}}$
200*h*	100	6620. 02	15101. 53	$(^3P)\ 5d\ ^2P_{1\frac{1}{2}}-(^3P)\ 6p\ ^4D^0_{0\frac{1}{2}}$
2	3	6632. 44	15073. 25	
6H*l*	10H*l*	6634. 13	15069. 41	$(^3P)\ 6p\ ^2P^0_{0\frac{1}{2}}-(^3P)\ 6d\ ^4F_{1\frac{1}{2}}$
2*h*	2*h*	6638. 85	15058. 70	$(^1S)\ 6s\ ^2S_{0\frac{1}{2}}-5j_{1\frac{1}{2}}$
1*h*	1*h*	6642. 9	15049. 5	$(^3P)\ 7s\ ^4P_{2\frac{1}{2}}-29j_{1\frac{1}{2}}$
2		6663. 1	15003. 9	$(^1D)\ 6p\ ^2D^0_{1\frac{1}{2}}-14_{2\frac{1}{2}}$
1—	1	6678. 9	14968. 4	
1	2	6691. 22	14940. 84	$(^3P)\ 6p\ ^4S^0_{1\frac{1}{2}}-8_{2\frac{1}{2}}$
400*h*	300	6694. 32	14933. 92	$(^3P)\ 5d\ ^4D_{0\frac{1}{2}}-(^3P)\ 6p\ ^4P^0_{1\frac{1}{2}}$
80	60	6702. 25	14916. 25	$(^1D)\ 5d\ ^2F_{2\frac{1}{2}}-(^1D)\ 6p\ ^2P^0_{1\frac{1}{2}}$
100*h*	150	6788. 71	14726. 28	$(^1D)\ 6s\ ^2D_{2\frac{1}{2}}-(^3P)\ 6p\ ^2D^0_{1\frac{1}{2}}$
80*h*	100	6790. 37	14722. 68	$(^3P)\ 5d\ ^2P_{0\frac{1}{2}}-(^3P)\ 6p\ ^4S^0_{1\frac{1}{2}}$
1000*h*	1000	6805. 74	14689. 43	$(^3P)\ 5d\ ^4F_{3\frac{1}{2}}-(^3P)\ 6p\ ^4D^0_{2\frac{1}{2}}$
10H*w*	10H*w*	6873. 2	14545. 3	
3H*w*	3H	6876. 69	14537. 88	
3H*w*	3H	6890. 41	14508. 93	
100	80	6910. 22	14467. 34	$(^3P)\ 5d\ ^4P_{0\frac{1}{2}}-(^3P)\ 6p\ ^4D^0_{0\frac{1}{2}}$
1000H*w*	800H*w*	6942. 11	14400. 88	
2000	2000	6990. 88	14300. 41	$(^3P)\ 5d\ ^4F_{4\frac{1}{2}}-(^3P)\ 6p\ ^4D^0_{3\frac{1}{2}}$
50	50	7003. 96	14273. 71	$(^3P)\ 5d\ ^2P_{0\frac{1}{2}}-(^3P)\ 6p\ ^2S^0_{0\frac{1}{2}}$
80	50	7017. 06	14247. 06	$(^3P)\ 5d\ ^4P_{1\frac{1}{2}}-(^3P)\ 6p\ ^4S^0_{1\frac{1}{2}}$
3H*w*	3H*w*	7052. 57	14175. 33	
4H*w*	4H*w*	7072. 43	14135. 52	
2H*s*	2H	7075. 0	14130. 4	
200	150	7082. 15	14116. 12	$(^1D)\ 5d\ ^2F_{2\frac{1}{2}}-(^1D)\ 6p\ ^2F^0_{3\frac{1}{2}}$
1H*w*	1*h*	7094. 7	14091. 1	
	5*h*	7100. 8	14079. 0	$(^3P)\ 6p\ ^4S^0_{1\frac{1}{2}}-(^3P)\ 6d\ ^4D_{1\frac{1}{2}}$
10	10	7133. 27	14014. 96	$(^3P)\ 6p\ ^4D^0_{2\frac{1}{2}}-(^1D)\ 5d\ ^2P_{1\frac{1}{2}}$
	2H*w*	7143. 3	13995. 3	
8H*w*		7143. 81	13994. 28	
100H*ws*	50H*ws*	7147. 50	13987. 05	
300*h*	200	7149. 03	13984. 06	$(^3P)\ 6s\ ^2P_{1\frac{1}{2}}-(^3P)\ 6p\ ^4D^0_{1\frac{1}{2}}$
800*h*	500	7164. 83	13953. 23	$(^1D)\ 5d\ ^2F_{3\frac{1}{2}}-(^1D)\ 6p\ ^2F^0_{3\frac{1}{2}}$
20*h*	30	7215. 97	13854. 34	$(^3P)\ 6p\ ^4P^0_{0\frac{1}{2}}-(^1D)\ 5d\ ^2P_{1\frac{1}{2}}$
2*h*	3	7245. 38	13798. 10	$(^3P)\ 5d\ ^4P_{1\frac{1}{2}}-(^3P)\ 6p\ ^2S^0_{0\frac{1}{2}}$
2H	2H	7258. 6	13773. 0	$(^3P)\ 6p\ ^2D^0_{1\frac{1}{2}}-12_{1\frac{1}{2}}$
4H*ws*	2H*w*	7276. 47	13739. 15	
4H*ws*	2H*w*	7279. 75	13732. 96	$(^1D)\ 6p\ ^2D^0_{2\frac{1}{2}}-(^3P)\ 6d\ ^2D_{1\frac{1}{2}}$

TABLE 1.—*List of* Xe II *lines*—Continued

Intensity		Wave length (air)	Wave number (vac)	Transition
100	100	7284. 34	13724. 30	$(^3P)\ 5d\ ^2D_{1½} - (^3P)\ 6p\ ^4S°_{1½}$
200	200	7301. 80	13691. 49	$(^1D)\ 6s\ ^2D_{2½} - (^3P)\ 6p\ ^2P°_{1½}$
300*h*	200	7339. 30	13621. 53	$(^3P)\ 5d\ ^2D_{2½} - (^3P)\ 6p\ ^4S°_{1½}$
30H*w*	20H*w*	7343. 37	13613. 98	$(^3P)\ 6p\ ^2D°_{2½} - 10_{2½}$
30	40	7378. 38	13549. 39	$(^1D)\ 6s\ ^2D_{2½} - (^3P)\ 6p\ ^2D°_{2½}$
4*h*	5*h*	7400. 5	13508. 9	$(^3P)\ 5d\ ^2P_{0½} - (^3P)\ 6p\ ^4D°_{0½}$
4H*w*	6H*w*	7410. 14	13491. 31	$(^3P)\ 6p\ ^2P°_{0½} - 12_{1½}$
50	60	7495. 36	13337. 92	$(^3P)\ 6p\ ^4P°_{0½} - (^1D)\ 5d\ ^2P_{0½}$
3*h*	3*h*	7503. 00	13324. 34	$(^1D)\ 5d\ ^2P_{0½} - 19i_{1½}$
1H		7508. 6	13314. 4	$(^3P)\ 7s\ ^4P_{0½} - 31i_{1½}$
50	50	7530. 70	13275. 32	$(^3P)\ 5d\ ^2D_{1½} - (^3P)\ 6p\ ^2S°_{0½}$
300	300	7548. 45	13244. 11	$(^1D)\ 5d\ ^2D_{1½} - (^3P)\ 6p\ ^2P°_{0½}$
100	80	7618. 57	13122. 22	$(^1S)\ 5d\ ^2D_{2½} - (^1D)\ 6p\ ^2D°_{2½}$
200	200	7670. 66	13033. 10	$(^3P)\ 5d\ ^4P_{1½} - (^3P)\ 6p\ ^4D°_{0½}$
30	50	7712. 42	12962. 54	$(^1D)\ 5d\ ^2D_{1½} - (^3P)\ 6p\ ^2D°_{1½}$
20*h*[3]		7772. 12	12862. 97	
4		7774. 18	12859. 56	
10		7777. 1	12854. 7	
100	60	7787. 04	12838. 32	$(^1S)\ 5d\ ^2D_{2½} - (^1D)\ 6p\ ^2D°_{1½}$
1		7805. 8	12807. 5	$(^1D)\ 5d\ ^2P_{1½} - 19i_{1½}$
10H*w*	15H*w*	7818. 31	12786. 97	
2		7826. 1	12774. 2	
20*h*		7828. 28	12770. 69	
3		7862. 7	12714. 8	$(^1D)\ 6p\ ^2P°_{1½} - (^3P)\ 7s\ ^2P_{1½}$
20		7882. 71	12682. 51	$(^1D)\ 5d\ ^2P_{1½} - (^1S)\ 6p\ ^2P°_{1½}$
50*h*		7889. 4	12671. 8	
5H*s*		7897. 7	12658. 4	$(^1D)\ 5d\ ^2P_{1½} - 17i_{0½}$
10H*w*	6H*w*	7920. 48	12622. 03	
100		7942. 54	12586. 97	
2		7970. 0	12543. 6	
20*h*		7974. 76	12536. 12	
3H*w*		7976. 4	12533. 5	$(^3P)\ 6s\ ^2P_{0½} - (^3P)\ 6p\ ^4D°_{0½}$
100H*w*		7981. 1	12526. 2	
40	60	7987. 99	12515. 36	$(^3P)\ 6s\ ^4P_{0½} - (^3P)\ 6p\ ^4P°_{0½}$
5H	5H	7991. 5	12509. 9	$(^3P)\ 6p\ ^4P°_{1½} - (^1S)\ 5d\ ^2D_{1½}$
100H		7992. 34	12508. 54	
3H*w*		7996. 5	12502. 0	$(^3P)\ 6p\ ^4D°_{0½} - 2_{0½}$
10*hs*		8001. 95	12493. 52	
2		8005. 8	12487. 5	$(^1D)\ 5d\ ^2P_{0½} - 9i_{1½}$
300*h*		8008. 45	12483. 38	
50*hs*		8014. 26	12474. 33	
5		8020. 07	12465. 30	$(^3P)\ 6p\ ^4D°_{1½} - (^1D)\ 5d\ ^2S_{0½}$
50*h*		8023. 85	12459. 42	
1H*w*		8028. 0	12453. 0	$(^3P)\ 6p\ ^2P°_{1½} - (^3P)\ 6d\ ^4D_{1½}$
100*h*		8031. 64	12447. 34	
20*h*		8035. 40	12441. 51	
100*h*		8038. 26	12437. 09	
20*h*		8047. 28	12423. 15	
50		8070. 97	12386. 68	
50*hs*		8080. 31	12372. 36	

[3] Beginning at this point and going in the direction of longer wave lengths, the effect of inductance has not been investigated fully. Possibly a few of the infrared lines belong to Xe III.

TABLE 1.—*List of* Xe II *lines*—Continued

Intensity		Wave length (air)	Wave number (vac)	Transition
10*h*		8095. 13	12349. 71	
12*h*		8098. 55	12344. 50	
50*h*		8115. 94	12318. 05	
30		8120. 16	12311. 65	
20		8131. 40	12294. 63	
30*h*		8136. 83	12286. 42	(^{3}P) 6*p* ^{4}S°$_{1½}$ — 6$_{2½}$
5H		8142. 13	12278. 43	}
	5H	8142. 6	12277. 7	}
3H*w*	5H*w*	8144. 8	12274. 4	(^{3}P) 6*p* ^{2}S°$_{0½}$ — 4
100	150*h*	8151. 80	12263. 86	
10*h*		8167. 55	12240. 21	
10*h*		8186. 9	12211. 2	
1		8194. 9	12199. 4	
2*h*		8213. 50	12171. 73	
20	30	8214. 85	12169. 74	(^{3}P) 5*d* ^{4}F$_{2½}$ — (^{3}P) 6*p* ^{4}D°$_{3½}$
4		8245. 37	12124. 69	
2*h*		8251. 30	12115. 98	
20		8256. 40	12108. 49	
5		8260. 81	12102. 02	
30*h*		8262. 73	12099. 22	
15*h*		8282. 85	12069. 82	
15*h*	20*h*	8285. 70	12065. 67	(^{1}D) 6*s* ^{2}D$_{2½}$ — (^{3}P) 6*p* ^{4}S°$_{1½}$
100*h*		8297. 55	12048. 44	
	10H*w*	8316. 2	12021. 4	
40H*w*		8317. 10	12020. 12	
30H*w*	40H*w*	8329. 44	12002. 31	
100		8347. 24	11976. 72	(^{3}P) 5*d* ^{4}F$_{2½}$ — (^{3}P) 6*p* ^{4}D°$_{2½}$
3		8351. 3	11970. 9	(^{1}D) 5*d* ^{2}P$_{1½}$ — 9°$_{1½}$
30*h*		8366. 4	11949. 3	
	2H*w*	8372. 2	11941. 0	
5*h*		8378. 3	11932. 3	(^{1}D) 6*p* ^{2}D°$_{2½}$ — (^{3}P) 6*d* ^{4}P$_{1½}$
2		8446. 6	11835. 8	
1—		8467. 8	11806. 2	(^{3}P) 6*p* ^{2}P°$_{1½}$ — (^{3}P) 7*s* ^{4}P$_{0½}$
5*h*	8*h*	8482. 64	11785. 55	(^{1}D) 5*d* ^{2}D$_{1½}$ — (^{3}P) 6*p* ^{2}D°$_{2½}$
2*h*		8500. 96	11760. 15	
50H*w*	50H*w*	8515. 19	11740. 50	
1*h*		8565. 1	11672. 1	
2*h*		8566. 7	11669. 9	
1		8584. 0	11646. 4	(^{1}D) 6*s* ^{2}D$_{1½}$ — (^{3}P) 6*p* ^{2}P°$_{0½}$
50H*w*		8604. 23	11619. 00	
25*h*		8628. 94	11585. 73	(^{1}D) 5*d* ^{2}D$_{2½}$ — (^{3}P) 6*p* ^{2}D°$_{1½}$
2H*w*		8636. 4	11575. 7	
3H		8655. 72	11549. 89	
1*h*		8704. 3	11485. 4	
50*h*		8716. 19	11469. 76	(^{3}P) 5*d* ^{2}P$_{1½}$ — (^{3}P) 6*p* ^{4}D°$_{1½}$
7H		8752. 14	11422. 64	
6H		8760. 14	11412. 21	
4H*w*		8785. 88	11378. 77	
2*h*		8796. 92	11364. 50	(^{1}D) 6*s* ^{2}D$_{1½}$ — (^{3}P) 6*p* ^{2}D°$_{1½}$
30		8804. 61	11354. 57	

TABLE 1.—*List of* Xe II *lines*—Continued

Intensity	Wave length (air)	Wave number (vac)	Transition
3H	8839. 9	11309. 2	
5H	8855. 74	11289. 02	
2H	8869. 40	11271. 63	
2H	8881. 48	11256. 30	
5H	8902. 66	11229. 52	
2H	9068. 0	11024. 8	
1	9106. 24	10978. 47	$(^1S)\ 5d\ ^2D_{2\frac{1}{2}} - (^1D)\ 6p\ ^2F^0_{3\frac{1}{2}}$
5H	9136. 6	10942. 0	
2*h*	9193. 8	10873. 9	$(^3P)\ 6s\ ^2P_{1\frac{1}{2}} - (^3P)\ 6p\ ^4P^0_{0\frac{1}{2}}$
7*h*	9226. 39	10835. 51	$(^3P)\ 5d\ ^4P_{0\frac{1}{2}} - (^3P)\ 6p\ ^4D^0_{1\frac{1}{2}}$
2*h*	9238. 59	10821. 19	
2*h*	9244. 15	10814. 69	
1*h*	9259. 60	10796. 64	
10*h*	9265. 67	10789. 57	$(^3P)\ 6p\ ^4D^0_{2\frac{1}{2}} - (^1S)\ 5d\ ^2D_{1\frac{1}{2}}$
5H	9288. 4	10763. 2	$(^1D)\ 5d\ ^2S_{0\frac{1}{2}} - 13^0_{0\frac{1}{2}}$
2H	9298. 7	10751. 2	
1*h*	9304. 77	10744. 23	$(^3P)\ 6p\ ^4D^0_{1\frac{1}{2}} - (^1D)\ 5d\ ^2P_{1\frac{1}{2}}$
4*h*	9331. 67	10713. 26	$(^3P)\ 6s\ ^2P_{1\frac{1}{2}} - (^3P)\ 6p\ ^4D^0_{2\frac{1}{2}}$
15*h*	9400. 59	10634. 72	$(^3P)\ 6s\ ^4P_{0\frac{1}{2}} - (^3P)\ 6p\ ^4P^0_{1\frac{1}{2}}$
1	9407. 57	10626. 82	
1	9447. 6	10581. 8	$(^1S)\ 5d\ ^2D_{2\frac{1}{2}} - (^1D)\ 6p\ ^2P^0_{1\frac{1}{2}}$
10H	9464. 3	10563. 1	
3*h*	9475. 23	10550. 94	$(^1D)\ 5d\ ^2D_{2\frac{1}{2}} - (^3P)\ 6p\ ^2P^0_{1\frac{1}{2}}$
2*h*	9577. 70	10438. 06	
50*h*	9591. 35	10423. 19	$(^3P)\ 5d\ ^4F_{2\frac{1}{2}} - (^3P)\ 6p\ ^4P^0_{2\frac{1}{2}}$
7*h*	9604. 50	10408. 93	$(^1D)\ 5d\ ^2D_{2\frac{1}{2}} - (^3P)\ 6p\ ^2D^0_{2\frac{1}{2}}$
4*h*	9615. 71	10396. 80	
3H	9630. 95	10380. 35	
4H	9641. 6	10368. 9	
50*hl*	9698. 68	10307. 86	$(^3P)\ 5d\ ^4P_{2\frac{1}{2}} - (^3P)\ 6p\ ^4D^0_{1\frac{1}{2}}$
2H	9706. 2	10299. 9	
3H	9734. 0	10270. 5	
1*h*	9744. 8	10259. 1	$(^1D)\ 5d\ ^2P_{0\frac{1}{2}} - 1^0_{1\frac{1}{2}}$
1*h*	9774. 8	10227. 6	$(^3P)\ 6p\ ^4D^0_{1\frac{1}{2}} - (^1D)\ 5d\ ^2P_{0\frac{1}{2}}$
2H	9810. 28	10190. 6	
2*h*	9820. 90	10179. 58	
2*h*	9837. 8	10162. 1	
6H	9865. 56	10133. 50	
1H	9895. 8	10102. 5	
2H	9908. 9	10089. 2	
1*h*	9983. 4	10013. 9	
2H	9990. 9	10006. 4	
1*h*	10054. 2	9943. 3	
1H	10095. 7	9902. 5	
1	10206. 9	9794. 6	
3*h*	10220. 8	9751. 3	

Impurity lines due to traces of other noble gases have been found on some spectrograms, particularly in cases where refilled tubes were used as sources. It is believed that these impurity lines have all been removed, along with such lines of Xe I as appear in condensed

discharges. The only other impurity lines which might plausibly remain are band lines caused by traces of moisture or by organic compounds. These would be expected to be very faint, since tubes after some hours of use "clean up" and give a remarkably pure noble-gas spectrum.

5. PRECISION OF WAVE-LENGTH MEASUREMENTS

The wave lengths are given in table 1 to six figures, or hundredths of an angstrom unit, one less being retained for a few lines observed only once or showing poor agreement between observations. The wave numbers are given to seven figures, or hundredths of a reciprocal centimeter, for wave numbers smaller than 31,600 cm^{-1}, and to six figures for greater wave numbers. At this point in the wave-number scale, or correspondingly at 3160 A in the wave length scale, an error of 0.01 A affects the wave number by 0.1 cm^{-1}. The seventh place has no significance for wave numbers associated with six-place wave lengths shorter than 3160 A. The question of retention of significant figures in the wave number is not of great importance since it is a derived and not a measured quantity. The precision of data can be determined best in a classified spectrum by application of the combination principle. This has been done for a part of the classified lines of Xe II. A list was prepared of the wave numbers of lines represented by transitions between low levels, leaving out only those not observed with gratings. This list contained 228 entries, including all the intense, sharp classified lines. The differences between observed and calculated wave numbers were recorded, and, adjacent to these, the derived differences between observed and calculated wave lengths. The combination principle is regarded as an exact physical law. Hence, these differences may be regarded as representing errors of observation, assuming that the most satisfactory adjustment of the relative values of the levels has been obtained. Of the 228 lines, 146 showed a wave-number error less than 0.05 cm^{-1} and the average for the group was 0.054 cm^{-1}. Similarly, 134 showed a wave-length error less than 0.01 A, with a group average, 0.012 A. This study indicates that in the case of the sharp lines, the measurements are precise enough to permit retention of seven figures in the final values of wave lengths, which is hardly necessary unless difficulty is encountered in making an unambiguous classification of the lines. Xe II contains a preponderance of lines which are hazy or unsymmetrical. Obviously, these cannot be measured with a precision comparable with that of the group just discussed. It is believed, however, that on account of the large number of observations represented in the final compilation, the wave lengths are known with sufficient precision to permit finding any observable regularities.

6. SPECTRA OF XENON IN THE EXTREME ULTRAVIOLET

The xenon spark spectra in the extreme ultraviolet have been observed by Boyce, who used the Carnegie Institution vacuum spectrograph located at the Massachusetts Institute of Technology. These data, which are much superior, both in extent and precision, to the earlier description of Abbink and Dorgelo [6], have been made available for use in this analysis. The progress of the work has been materially aided by Boyce's generous cooperation. A selected portion of these

extreme-ultraviolet data already published [7] contains 128 classified Xe III lines and 20 classified Xe II lines which could be identified with certainty when the paper appeared. The place of the extreme-ultraviolet data in the array of classified lines will be pointed out in the following discussion of the analysis of the spectrum.

III. ANALYSIS OF XE II

1. THEORETICAL TERMS

The singly ionized xenon atom, in common with singly ionized atoms of the other noble atmospheric gases, is characterized by an outer electronic structure the same as that of neutral atoms of the halogen elements or of doubly ionized alkali metals. It is isoelectronic with neutral iodine and doubly ionized cesium. The Hund [8] theory predicts for Xe II, the spectrum characteristic of Xe^+, an array of levels corresponding in number and assignment of inner quantum numbers to those belonging to the spectra of the elements mentioned. Such levels may be regarded as fine-structure components of multiple spectral terms for atoms or ions characterized by the *ls*-coupling scheme, and the use of the generally adopted spectral notation, if strictly interpreted, presupposes that such a scheme is operative, at least to such an extent that the multiplets are clearly recognizable. When the coupling is of the *jj* type the multiplet relationships have disappeared completely and the usual notation is no longer valid. For a given electron configuration the same number of levels occur as in other coupling schemes with an identical set of j values.

Cases of pure *jj* coupling are unknown. Instances of intermediate coupling are fairly common. All noble-gas spectra depart considerably from *ls* coupling. Their first spectra are still described by the special notation used by Paschen for Ne I [9], although many levels can be designated unambiguously by the later quantum notation. There is a progressive approach toward *jj* coupling as one goes down through the column of rare gases and, as expected, xenon shows the characteristics of such coupling more than the others. Conspicuous features of Xe II are: Nonconformity to multiplet interval rules, overlapping of terms both from the same and from different configurations, abundance of intersystem and interlimit transitions, and frequent occurrence of levels of indistinguishable characteristics as to j value and combining properties, indicating strong configuration interactions. In spite of the difficulties of interpretation, it has seemed advantageous to retain the customary notation [10] for designating levels because of its simplicity and because it facilitates comparison with analogous spectra, particularly Kr II. The symbols have been used, therefore, with the reservations based on the considerations just given.

The normal electron configuration of Xe^+, $5s^2\ 5p^5$, gives rise to an inverted doublet, $^2P^o_{1½,\ ½}$, the lowest term of Xe II. The two levels of this term are the convergence limits of the various series in Xe I.[1] The importance of this term in the analysis of rare-gas spectra has been discussed in detail [3]. Except for the next lowest term ^2S, from $5s5p^6$, all of the remaining terms are associated with the electron group $5s^2\ 5p^4$ of the doubly charged atom. The configuration $5s^2\ 5p^4$ gives rise to ^3P, ^1D, and ^1S terms in the third spectrum, Xe III [4].

[1] Only first members of Xe I series converging to $^2P_{½}$ are known. Second members of these series would be expected to lie higher than the convergence limit $^2P_{1½}$ and would acquire negative values.

These terms are the convergence limits for three families of terms in the second spectrum, Xe II. These Xe II terms are derived from the addition of *ns*, *np*, *nd*, probably *nf*, and possibly *ng* electrons to the $5s^2\ 5p^4$ configuration of the doubly charged atom. The terms which may be theoretically expected to account for the second spectrum of a rare gas are shown for the specific case of Xe II in table 2, where the term correlation with electron configuration and convergence limits is illustrated. Because of the presence of three families of terms corresponding to the three convergence limits, the second spectra of rare gases are fairly complex. With Geissler-tube sources there is, however, very little development of series. Of the theoretically predicted terms listed in table 2 only those caused by the interaction of a valence electron of *s*, *p*, or *d* type have been identified as certain. There is some question about the identification of *f*-type terms. None from *g* electrons have been found. Because a large number of lines, for the most part relatively faint and hazy, remain unclassified, it may be inferred that many of these *f*- and *g*-type terms are developed but with an insufficient number of combinations to be detected by regularities. Such lines may also arise from combinations of second- or third-series members, or it is barely possible that some other configuration, such as $sp^5\ np$, may be responsible for undetected terms, although terms from the latter configuration have not yet been found in spectra originating in singly ionized noble-gas atoms.

TABLE 2.—*Electron configurations and spectral terms of* Xe II

Electron configuration			
$5s^2\ 5p^5$	$^2P^\circ$		
$5s\ 5p^6$	^2S		
	Term limit $5s^2\ 5p^4\ ^3P$	*Term limit* $5s^2\ 5p^4\ ^1D$	*Term limit* $5s^2\ 5p^4\ ^1S$
$5s^2\ 5p^4\ 6s$	$^2P\ ^4P$	^2D	^2S
$5s^2\ 5p^4\ 6p$	$^2S^\circ\ ^2P^\circ\ ^2D^\circ\ ^4S^\circ\ ^4P^\circ\ ^4D^\circ$	$^2P^\circ\ ^2D^\circ\ ^2F^\circ$	$^2P^\circ$
$5s^2\ 5p^4\ 5d$	$^2P\ ^2D\ ^2F\ ^4P\ ^4D\ ^4F$	$^2S\ ^2P\ ^2D\ ^2F\ ^2G$	^2D
$5s^2\ 5p^4\ 7s$	$^2P\ ^4P$	^2D	^2S
$5s^2\ 5p^4\ 7p$	$^2S^\circ\ ^2P^\circ\ ^2D^\circ\ ^4S^\circ\ ^4P^\circ\ ^4D^\circ$	$^2P^\circ\ ^2D^\circ\ ^2F^\circ$	$^2P^\circ$
$5s^2\ 5p^4\ 6d$	$^2P\ ^2D\ ^2F\ ^4P\ ^4D\ ^4F$	$^2S\ ^2P\ ^2D\ ^2F\ ^2G$	^2D
$5s^2\ 5p^4\ 6f$	$^2D^\circ\ ^2F^\circ\ ^2G^\circ\ ^4D^\circ\ ^4F^\circ\ ^4G^\circ$	$^2P^\circ\ ^2D^\circ\ ^2F^\circ\ ^2G^\circ\ ^2H^\circ$	$^2F^\circ$
$5s^2\ 5p^4\ 6g$	$^2F\ ^2G\ ^2H\ ^4F\ ^4G\ ^4H$	$^2D\ ^2F\ ^2G\ ^2H\ ^2I$	^2G

2. TABLE OF TERMS

A total of 103 levels have been found in Xe II, which are reported in this publication. A considerable number of possible levels have not been retained because of an insufficient number of combinations, regularities requiring too large a tolerance, or conflicts with existing classifications. There remain a few ambiguous classifications, generally of hazy lines, for which the possibility of duplicity is reasonable. Complete quantum designations are given for 75 levels. *j* values are assigned to the remaining 28 levels, and each is designated by a number even or odd according to the parity of the level and in the order of their magnitude. All the known terms and unclassified

levels are assembled in table 3. These are grouped according to electron configuration, and the series-forming terms are correlated with the appropriate limits. The levels are arranged in order of magnitude, beginning with the lowest, so far as the arrangement is not in conflict with the grouping scheme.

TABLE 3.—Xe II *terms*

Electron configuration			
$5s^2\ 5p^5$		$^2P^{\circ}_{1½}$ 171068.4 $^2P^{\circ}_{½}$ 160531.1	
$5s\ 5p^6$		$^2S_{0½}$ 80194.57	
	Term limit $5s^2\ 5p^4\ ^3P$	*Term limit* $5s^2\ 5p^4\ ^1D$	*Term limit* $5s^2\ 5p^4\ ^1S$
$5s^2\ 5p^4\ 6s$	$^4P_{2½}$ 78000.00 $^4P_{1½}$ 76004.06 $^4P_{0½}$ 69910.89 $^2P_{1½}$ 68269.34 $^2P_{0½}$ 66818.34	$^2D_{2½}$ 61505.25 $^2D_{1½}$ 58143.70	$^2S_{0½}$ 46998.31
$5s^2\ 5p^4\ 6p$	$^4D^{\circ}_{3½}$ 57363.07 $^4D^{\circ}_{2½}$ 57556.11 $^4D^{\circ}_{1½}$ 54285.29 $^4D^{\circ}_{½}$ 50653.53 $^4P^{\circ}_{2½}$ 59109.56 $^4P^{\circ}_{1½}$ 59276.32 $^4P^{\circ}_{0½}$ 57395.55 $^4S^{\circ}_{1½}$ 49439.60 $^2D^{\circ}_{2½}$ 47955.90 $^2D^{\circ}_{1½}$ 46778.90 $^2P^{\circ}_{1½}$ 47813.79 $^2P^{\circ}_{0½}$ 46497.38 $^2S^{\circ}_{0½}$ 49888.58	$^4F^{\circ}_{3½}$ 41004.37 $^4F^{\circ}_{2½}$ 42201.21 $^2D^{\circ}_{2½}$ 38860.72 $^2D^{\circ}_{1½}$ 39144.64 $^2P^{\circ}_{1½}$ 41401.83 $^2P^{\circ}_{0½}$ 38327.31	$^2P^{\circ}_{1½}$ 30858.18 $^2P^{\circ}_{0½}$
$5s^2\ 5p^4\ 5d$	$^4F_{4½}$ 71663.50 $^4F_{3½}$ 72245.54 $^4F_{2½}$ 69532.75 $^4F_{1½}$ $^4D_{3½}$ 75030.80 $^4D_{2½}$ 75671.72 $^4D_{1½}$ 75034.96 $^4D_{0½}$ 74210.26 $^4P_{2½}$ 64593.23 $^4P_{1½}$ 63686.65 $^4P_{0½}$ 65120.86 $^2F_{3½}$ $^2F_{2½}$ $^2D_{2½}$ 63061.15 $^2D_{1½}$ 63163.90 $^2P_{1½}$ 65755.07 $^2P_{0½}$ 64162.29	$^2G_{4½}$ $^2G_{3½}$ $^2F_{3½}$ 56154.44 $^2F_{2½}$ 56317.32 $^2D_{2½}$ 58364.82 $^2D_{1½}$ 59741.47 $^2P_{1½}$ 43541.0 $^2P_{0½}$ 44057.7 $^2S_{0½}$ 41819.9	$^2D_{2½}$ 51982.90 $^2D_{1½}$ 46766.22
$5s^2\ 5p^4\ 7s$	$^4P_{2½}$ 38549.7 $^4P_{1½}$ 37879.2 $^4P_{0½}$ 36007.5 $^2P_{1½}$ 28686.2 $^2P_{0½}$ 28138.4	$^2D_{2½}$ 24763.0 $^2D_{1½}$ 21266.0	$^2S_{0½}$
$5s^2\ 5p^4\ 6d$	$^4F_{4½}$ $^4F_{3½}$ 34470.7 $^4F_{2½}$ 31974.3 $^4F_{1½}$ 31428.1 $^4D_{3½}$ 35561.2 $^4D_{2½}$ 35521.4 $^4D_{1½}$ 35360.2 $^4D_{0½}$ 32342.0 $^4P_{2½}$ 27669.0 $^4P_{1½}$ 26928.2 $^4P_{0½}$ 30185.0 $^2F_{3½}$ $^2F_{2½}$ $^2D_{2½}$ 26683.4 $^2D_{1½}$ 25128.3 $^2P_{1½}$ $^2P_{0½}$ 25845.7	$^2G_{4½}$ $^2G_{3½}$ $^2F_{3½}$ $^2F_{2½}$ 17036.1 $^2D_{2½}$ 21371.1 $^2D_{1½}$ 22983.2 $^2P_{1½}$ $^2P_{0½}$ $^2S_{0½}$	$^2D_{2½}$ $^2D_{1½}$

TABLE 3.—Xe II *terms*—Continued

Unclassified even levels

$2_{01/2}$	38151.5	$10_{21/2}$	34341.9
$4_{01/2}$ or $1_{3/2}$	37614.2	$12_{11/2}$	33005.6
$6_{21/2}$	37153.3	$14_{21/2}$	24140.6
$8_{21/2}$	34498.8		

Unclassified odd levels

$1[1/2]_{1/2}$	33798.9	$23[1/2]_{1/2}$	27598.6
$3[3/2]_{1/2}$	32063.0	$25[1/2]_{1/2}$	23550.4
$5[1/2]_{1/2}$	31939.56	$27[3/2]_{1/2}$	23523.8
$7[1/2]_{1/2}$	31885.48	$29[1/2]_{1/2}$	23499.8
$9[1/2]_{1/2}$	31569.77	$31[1/2]_{1/2}$	22693.5
$11[3/2]_{1/2}$	31422.3	$33[1/2]_{1/2}$	22116.0
$13[3/2]_{1/2}$	31056.9	$35[3/2]_{1/2}$	21787.4
$15[3/2]_{1/2}$	31038.29	$37[1/2]_{1/2}$	21385.7
$17[3/2]_{1/2}$	30882.75	$39[1/2]_{1/2}$	14765.5
$19[1/2]_{1/2}$	30733.28	$41[1/2]_{1/2}$	13846.3
$21[1/2]_{1/2}$	30081.4		

3. LOW LEVELS OF Xe II

The lines of Xe II vary greatly in appearance. The range of intensities represented by numbers from 1 to 3,000 is enormous. Some of the lines are sharp and symmetrical and not affected, except possibly in intensity, by changes in the electrical circuit. The majority are broad and hazy in varying degrees. Usually, but not always, the effect of inductance is to sharpen a line. In some cases the line position is slightly changed with insertion of inductance. In such instances two entries are shown in table 1.

The sharp lines are invariably classified as transitions between levels of first excited states, specifically transitions from the levels arising from the interaction of the $6p$ electron with $5s^2\,5p^4$ to levels due to $6s$ or $5d$. The precision with which the combination principle is satisfied for these transitions leaves no question as to the reality of these levels, although the meaning of the symbolic designations should not be overemphasized owing to the properties of this spectrum mentioned in the discussion of the origin of the terms. Only one very intense sharp line, located at 6595.01 A, remains unclassified. Reference to table 3 will show that nearly all levels of first excited states have been found. The identifications have been based mainly on intensities of combinations and comparison with analogous spectra, particularly Kr II.[3] For instance, we expect the combinations of the $6s$ levels to be somewhat more intense than those of $5d$ levels. The distinction between doublets and quartets has to be based partly on intensity considerations, but this is not very clear-cut because of the high intensity of intersystem combinations. Hund's rule for complex spectra[4] is obeyed in regard to relative elevation of quartets and doublets from a given configuration, the former being lower in every case but one. The second part of the rule, namely, that among terms of the same multiplicity from a given configuration those of greatest l value are lowest, is not obeyed at all.

With the single exception of the level designated $5d\,^4F_{2\frac{1}{2}}$, all even levels of j value $2\frac{1}{2}$ or less combine with the low doublet, $5s^2\,5p^5\,^2P°$. The lines caused by these transitions occur in Boyce's extreme-ultraviolet data. In some instances these levels have been confirmed by searching through the extreme-ultraviolet data for the doublet difference.

[4] Linienspectren [8, p. 124].

Grouping of the experimental terms into families according to the respective convergence limits, the low terms of Xe III, has been facilitated by the analysis of the third spectrum of xenon [4]. The relative values of the low terms of Xe III are indicated as follows:

$^3P_2$	0
$^3P_1$	9795
$^3P_0$	8131
$^1D_2$	17100
$^1S_0$	37398

Although a knowledge of the positions of the series limits indicates at what elevation levels of the various families should appear in the term scheme, it is not a certain criterion owing to the prevalence of interfamily transitions. The grouping of the low odd levels is fairly certain. These all arise from one configuration, $5s^2\,5p^4\,6p$, the theoretically predicted quantum numbers are found, and the levels fall into fairly compact groups separated by intervals which can be reasonably predicted from the positions of the convergence limits.

The $6p$ levels present some problems, however, owing to the similarity of combining properties of levels of like j values. It has been explained that such ambiguities are attributable to configuration interactions and inherent in spectra of this character. The level at 57556.11 was chosen for $6p\ ^4D^\circ_{2\frac{1}{2}}$ rather than 59109.56 because of the combinations with $5d\ ^4F$. $^4S^\circ$ was selected because of strong quartet combinations and because the choice placed it highest among the quartets of the odd group converging to (^3P). The level at 49888.58 is assigned to $^2S^\circ$ and is lower than $^4S^\circ$. This assignment is the result of the single change which was made in the term scheme after study of the Zeeman effects. The group of six odd levels converging to ^1D, which are of reasonably certain origin, are arranged in almost the same order as the analogous group in Kr II. The level at 30858.18 is found among a large group of odd levels but is assigned to $(^1S)\ ^2P^\circ_{1\frac{1}{2}}$ because its combinations are much more intense than those of any of its neighbors.

The level at 80194.57, for which the assignment $5s\,5p^6\,^2S$ has been retained from the earlier paper [2], is of interest because the classification was regarded as questionable by Fitzgerald and Sawyer [11] in a paper on Cs III and Ba IV, which are isoelectronic with Xe II. They predicted this ^2S term by the irregular doublet law at 102,700 cm^{-1} above the lowest state, bringing it very close to 68269.34 assigned to $6s\ ^2P_{1\frac{1}{2}}$. The latter term certainly has a j value of $1\frac{1}{2}$, leaving the only alternative choice for ^2S, 69910.89 assigned to $6s\ ^4P_{1\frac{1}{2}}$. For a term arising from a single s electron coupled with a completed shell of p electrons the g value is exactly 2 for both ls and jj couplings. Zeeman-effect data indicate a g value of 2 for 80194.57 within the limits of precision of the measurements and confirm the original assignment for ^2S.

4. HIGH LEVELS OF Xe II

About half of the high even levels combine with the low doublet giving extreme-ultraviolet lines in Boyce's data. Assignments have been made for most of these levels as second-series members from the configurations $5s^2\,5p^4\,7s$ and $5s^2\,5p^4\,6d$. The possibility of g-type levels among this group has been mentioned. The configuration $5s^2\,5p^4\,6g$ would lead to many more levels of larger j value than have been found. The less probable hypothesis of terms from $5s\,5p^5\,6p$ has been mentioned also.

Twenty-one high odd levels have been found. In Kr II the analogous group was interpreted as *f*-type levels, second-series members from the interaction of *p* electrons being the alternative explanation. It is not felt that there is sufficient evidence in the experimental data to justify more than the assignment of *j* values of such levels in Xe II. If they are second-series members of *p* type, the series constants differ considerably from those associated with the series of even terms, for when an attempt is made to correlate second-series members with the first, the second-series members seem to be somewhat low if the scale of absolute term values is at all correct.

5. ABSOLUTE VALUES OF TERMS

The absolute values of the terms are based on the $^4P_{2\frac{1}{2}}$ series from the *s*-electron configuration. The estimate is retained from the earlier publication [2]. There is no important evidence to justify a revision of the calculation which gave an ionization potential of 21.1 volts for Xe II.

In conclusion, the author acknowledges his indebtedness to those whose assistance and cooperation have furthered the progress of this investigation; to Wm. F. Meggers, who has collaborated in the experimental work, measurement of spectrograms, and reduction of data; to T. L. deBruin of the Laboratory "Physica," in Amsterdam, for his unpublished Zeeman effects; and to J. C. Boyce, of the Massachusetts Institute of Technology, for use of his unpublished extreme-ultraviolet data and for helpful discussion during the progress of the work.

V. REFERENCES

[1] Wm. F. Meggers, T. L. deBruin, and C. J. Humphreys, BS J. Research **3**, 731–763 (1929) RP115.
[2] C. J. Humphreys, T. L. deBruin, and W. F. Meggers, BS J. Research **6**, 287–293 (1931) RP275.
[3] T. L. deBruin, C. J. Humphreys, and Wm. F. Meggers, BS J. Research **11**, 409–440 (1933) RP599.
[4] C. J. Humphreys, J. Research NBS **16**, 639–648 (1936) RP898.
[5] L. Bloch, E. Bloch, and G. Déjardin, Ann. Physik **10**, 461 (1924).
[6] J. H. Abbink and H. B. Dorgelo, Z. Physik **47**, 221 (1928).
[7] J. C. Boyce, Phys. Rev. **49**, 730–732 (1936).
[8] F. Hund, Linienspektren und periodisches System der Elemente (Julius Springer, Berlin, 1927).
[9] F. Paschen, Ann. Physik **60**, 405–453 (1919).
[10] See, *Report on notation for atomic spectra*, Phys. Rev. **33**, 900 (1929).
[11] Sister M. Ambrosia Fitzgerald and R. A. Sawyer, Phys. Rev. **46**, 576–580 (1934).

WASHINGTON, July 22, 1938.

U. S. DEPARTMENT OF COMMERCE NATIONAL BUREAU OF STANDARDS

RESEARCH PAPER RP1165

Part of Journal of Research of the National Bureau of Standards, Volume 22, January 1939

SOLUBILITY OF LEAD SULFATE IN SOLUTIONS OF SULFURIC ACID, DETERMINED BY DITHIZONE WITH A PHOTRONIC CELL

By D. Norman Craig and George W. Vinal

ABSTRACT

New determinations of the solubility of lead sulfate in sulfuric acid solutions have been made, using diphenylthiocarbazone, commonly called dithizone, as the reagent. This provides a very sensitive method for small quantities of lead. The equivalence point was detected by a simple arrangement of a photronic cell and color filter. The range of concentrations of acid extended from 0.1 to 50 percent H_2SO_4. Determinations of the lead could be made with an average error not exceeding 0.7 microgram (μg). Determinations were made at 25° and 0° C, employing solutions, some of which were brought to saturation equilibrium from undersaturation and others from supersaturation. Important maxima and minima in the solubility curves which had not been reported previously were found. Tables are given for the solubility of the salt at 25° and 0° C. Comparison is made of the effect of H_2SO_4 on the solubility of lead and mercurous sulfates. The trend of the curves for these is strikingly similar, although the latter is more than 80 times as soluble.

CONTENTS

	Page
I. Introduction	55
II. Experimental procedure	57
1. Materials	57
2. Saturation of solutions	57
3. Description of the method	58
4. Details of the determinations	59
5. Test of the method	60
6. Determination of sulfuric acid	63
III. Experimental results	64
IV. Solubility of lead sulfate at regular intervals of sulfuric acid concentration	65
V. Discussion of results	66
VI. Comparison with the results of others	69
VII. References	70

I. INTRODUCTION

Lead sulfate, which plays an important part in chemical reactions of the lead storage battery, is formed in accordance with Faraday's law during discharge. Considerable amounts may exist in the active material of the plates, but the amounts which are dissolved in the sulfuric acid electrolyte are extremely small under equilibrium conditions. Only a few previous papers have reported solubility measurements of lead sulfate in sulfuric acid solutions of concentrations comparable with those used in batteries. It seemed desirable, therefore, that some further investigation should be made of this subject, especially as sensitive determinations can now be made by methods not previously used in this problem.

In 1929 Fischer [1] [1] introduced a sensitive reagent for small quantities of lead which has found interesting applications in widely diverse fields. Diphenylthiocarbazone, or dithizone as it is commonly called, has the formula

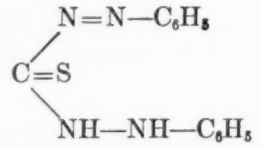

according to Fischer [2]. We have made no study of this reagent, except to find means of using it in our problem of measuring the solubility of lead sulfate.

Dissolved in chloroform, dithizone imparts a noticeable green tint to the solution, provided the solution is not too concentrated. The lead-dithizone complex, however, has a bright cherry-red color. Spectrophotometric studies of these solutions have been reported previously in the technical literature. A discussion of the spectral transmission and its applications to the quantitative determination of lead may be found in a paper by Clifford and Wichmann [3].

In some of our earlier experiments, spectrophotometric measurements of a few solutions were made with the cooperation of members of the Spectrophotometry Section. As a result of these experiments we have developed a simpler and quicker method, employing a photronic cell with light source and color filter as a means of detecting the equivalence point. This method was tested many times by making determinations on solutions to which one observer added known amounts of lead, while the determinations were made by another observer who did not know these amounts until the experiments were completed. The accuracy attained was considered ample for the purpose and we feel confident that this method, which involves the use of simple and readily obtainable apparatus, fulfilled our needs.

Dithizone is known to react with metals other than lead. The precautions taken to avoid interference by other metals are discussed on page 58. These precautions, together with the spectroscopic analysis of the lead salt and the redistillation of water and acid, make it highly improbable that the results were affected by other metals. Confirmation of this is found in the analysis of solutions of known lead content.

Comparisons of the results of our measurements with those of others who employed different methods for the determination of lead are given in a later section of this paper.

The range of acid concentrations covered by the present work is from 0.08 to 50 percent. Some of the solutions were brought to saturation equilibrium with respect to lead sulfate from an undersaturated state and others from a supersaturated state. Determinations were made at two temperatures, 25° and 0° C.

In the course of the work a well-defined maximum of solubility was found for solutions of approximately 10 percent or molar concentration of acid. This is similar to the solubility of mercurous sulfate in sulfuric acid solutions. Although the mercurous sulfate is more than 80 times as soluble as the lead sulfate in solutions of corresponding

[1] Numbers in brackets indicate the literature references given at the end of this paper.

strength, the similarity of curves for lead and mercurous sulfates is remarkable. The ratio of the two salts holds constant when the molarity of the acid concentrations varies from 0.0025 to 2.5 molar. This is discussed in the paper, and reference is made to the solubility data for calcium and silver sulfates as found in the technical literature.

II. EXPERIMENTAL PROCEDURE

1. MATERIALS

The lead sulfate was part of a sample prepared from lead nitrate which had been twice recrystallized. In converting the lead nitrate to lead sulfate, redistilled sulfuric acid was used. It was added slowly to the hot lead nitrate solution which was stirred continuously. The lead sulfate was repeatedly digested on the steam bath in solutions of redistilled sulfuric acid. A sample of the final product was tested spectroscopically for the presence of impurities by the Spectroscopy Section of this Bureau. Only faint traces of iron and magnesium were reported.

The sulfuric acid conformed to the requirements recommended by a committee of the American Chemical Society for reagent grade acid [4]. As a further precaution this was distilled and the middle fractions only used in this work.

The water was all redistilled. At the time it was made its conductivity was 1×10^{-7} or below. This was considerably better, therefore, than ordinary distilled water. It was prepared from time to time as required.

The principal reagent used in this work was diphenylthiocarbazone commonly called by the shorter name, "dithizone." It was obtained from the Eastman Kodak Co. All other reagents including nitric acid, ammonium hydroxide, potassium cyanide, and chloroform were of reagent grade and these were used in exactly the same quantities in the known and unknown solutions during the analysis.

The standard lead solution was prepared from high-grade lead as a nitrate solution, containing 100 μg of lead per milliliter of solution.

2. SATURATION OF SOLUTIONS

The saturation of the solutions was accomplished by agitating them mechanically with Pyrex-glass stirrers in 500-ml Pyrex flasks, containing a liberal excess of lead sulfate. At 25° C the temperature was controlled thermostatically to ±0.02° C in a water bath. At 0° C the temperature was controlled by a mixture of ice and water in large Dewar flasks. The experimental results at both temperatures include values obtained by approaching the saturation equilibrium from a condition of incomplete saturation and from supersaturation. For the latter, solutions previously saturated at a higher temperature were employed.

After agitating the solutions for 3 days at 25° C and 6 days at 0° C, the stirrers were removed and the flasks were allowed to stand at their respective temperatures 10 to 24 hours before removing the samples. The samples of the supernatant solutions were carefully removed by suction through fritted-glass filters. Five samples of 25 ml were drawn from each flask and the first four samples were discarded. Analysis was made of the fifth sample which was placed in a silica

dish for evaporation to dryness. After each time the funnels were used they were cleaned by passing $6N$ HNO_3 through them in the reverse direction and this was followed by repeated washings with distilled water. They were kept in closed vessels when not in use.

3. DESCRIPTION OF THE METHOD

The usefulness of dithizone for determining small quantities of lead depends upon the reaction of lead with dithizone, which is accompanied by a change in color from the original green of dithizone in chloroform to the cherry red of the lead-dithizone complex. The reaction is conveniently carried out in a two-phase liquid system, one phase being an aqueous solution of fixed pH, greater than 7, and the second phase an organic liquid immiscible with water, such as chloroform or carbon tetrachloride, which readily dissolves the lead-dithizone complex. Free dithizone is soluble also in aqueous ammonia solutions, producing a yellow color. The distribution of dithizone between chloroform and ammonia solutions depends upon the pH of the aqueous phase. The distribution of lead in the two phases is dependent not only on the pH of the aqueous phase, but also on the concentration of the dithizone.

Dithizone is known to react with many metal ions forming various colored complexes, each of which has its own characteristic color. Several authors [5] have reported that the number of metals whose ions react with the dithizone may be greatly reduced by the addition of potassium cyanide to the aqueous solution. As a precaution, which may not have been necessary, we used potassium cyanide in analyzing all of our solutions. There still remain thallium, bismuth, and stannous tin which may interfere notwithstanding the presence of potassium cyanide. However, any errors which might have been caused by these were doubtless inappreciable, because the report of spectroscopic test of the lead sulfate stated specifically that the spectrum was examined for sensitive lines of these and about 50 other elements, but only faint traces of iron and magnesium were found. Dithizone is not sensitive to magnesium and the amount of iron present was too small to be significant. This conclusion is further justified by analyses of known solutions reported later in this paper. We believe, therefore, the analyses were not affected by interfering elements. It is not the purpose of this paper to discuss equilibria involved in the use of dithizone, but rather to report the use of dithizone for determining small amounts of lead with relatively simple apparatus.

The procedure which we have followed was the result of preliminary experiments which showed that known amounts of lead could be accurately measured. The apparatus consisted of a light source (21 cp 12–16 v lamp with collimator), a red filter of selenium glass, a photronic cell, and a sensitive microammeter for measuring the electric current delivered by the photronic cell. Current for the lamp was supplied by a storage battery through soldered connections. Errors which might have arisen from drift in the intensity of the light source or in the response of the photronic cell were avoided by the procedure outlined on page 61. This arrangement affords a very sensitive method of correlating color changes of the solutions with the lead content.

4. DETAILS OF THE DETERMINATIONS

The 25-ml portions of sulfuric acid solutions saturated with lead sulfate were evaporated to dryness in silica dishes on an air bath over a carefully regulated bunsen flame. Care was taken to avoid contamination of the samples at all times. After evaporation had been completed 0.4 ml of concentrated HNO_3 were added to the lead sulfate residue in the silica dish. The dish was then slowly tipped and rotated until the acid wet all parts of the inner surface. Ten ml of water were then added and the process repeated while the surface was rubbed with a policeman which was reserved for this purpose. The solution was then transferred to a Pyrex separatory funnel, cleaned immediately before use, and reserved for this purpose.[2]

The process of rinsing the silica dish was then repeated twice, using 0.3 ml of concentrated acid and 10 ml of water. After rubbing all parts of the inner surface of the silica dish with the policeman, both rinsings were in turn added to the solution in the separatory funnel. Three successive portions of water, 2 ml each, were added to the dish and the policeman used as before. Each of these solutions in turn was transferred to the Pyrex separatory funnel. The separatory funnel then contained the lead sulfate residue in 36 ml of water and 1 ml of HNO_3.

Thirty-six ml of water and 1 ml of concentrated HNO_3 were then placed in a second separatory funnel using the same pipettes as in the previous case. To each of the solutions in the separatory funnels 3 ml of concentrated NH_4OH followed by 0.5 ml of KCN solution (10 g in 50 ml H_2O) were added. The two solutions in their respective separatory funnels were at this point identical in volume and composition except for the amount of lead sulfate in the first separatory funnel. This solution will hereafter be designated as the unknown solution. The other solution to which a measured amount of lead was to be added will be designated as the known solution.

Measured portions of a solution of dithizone in chloroform were added to the unknown solution. The addition of each portion was followed by shaking, and this process was repeated until the additions of the dithizone were sufficient to cause a visual change in color of the chloroform solution from cherry red to a purplish red, which indicated that a slight excess of dithizone had been added. The concentration of dithizone in the chloroform being known, an approximate calculation of the lead in the unknown solution could be made. A volume of standard lead nitrate solution containing nearly an equivalent amount of lead was added immediately to the known solution in the other separatory funnel, using a 1-ml pipette graduated to hundredths. The same number of equal portions of dithizone in chloroform were then added to the known solution. After each portion was added, the solution was shaken. At this point the two solutions contain exactly the same amount of dithizone, chloroform, approximately the same amount of lead, and both should have a purplish-red color.

The colored chloroform solution was then delivered into a cylindri-

[2] The process of cleaning the separatory funnels is important. Each was partially filled with dilute ammonia and a chloroform solution of dithizone. The funnels were then shaken repeatedly and examined between each shaking for change in color of the dithizone. If this experiment is tried on soft glass containing lead the effect of the lead in the glass may be detected. When the Pyrex funnels were satisfactorily cleaned they were drained and used without further rinsing.

cal glass cell with flat bottom. This was placed over the photronic cell and the reading of the microammeter recorded for comparison with readings of the meter immediately before and after. The ratio of the reading when the cell was present to the mean of the two readings without the cell was then calculated. The chloroform solution was then returned to the separatory funnel. The same process was repeated with the other chloroform solution using the same glass cell. It was evident from the readings of the meter which solution contained less lead. To this solution a small portion of the standard lead nitrate solution was added. Both separatory funnels were shaken simultaneously and measurements with the photronic cell repeated. This process was continued until there was definitely more lead in this solution than in the other solution. The observations were correlated with the amounts of lead and the equivalence points with respect to lead determined graphically.

5. TEST OF THE METHOD

The following examples serve a double purpose in illustrating the method and in showing the accuracy which may be attained in analyzing solutions which are designated as "test solutions." Actually, the amounts of lead in the test solutions were known to one of us, but the analyses were made by the other who did not know the amounts until after the experiments were completed.

The tests of the method were first made on solutions of lead nitrate, which did not require evaporation of the solutions. An example is given in detail below. Other tests were made on sulfuric acid solutions to which lead was added as lead nitrate. These were evaporated in silica vessels exactly as was done in the case of the unknown solutions which were saturated with lead sulfate. Tests of the method were made repeatedly, but three experiments are sufficient to illustrate (1) the method of making the determinations and (2) the reliability of determinations of lead initially present in sulfuric acid solutions which necessitated evaporation to dryness.

Experiment 1. Determination of lead in a test solution containing 70.3 μg of lead, no sulfuric acid and without evaporation of solutions.—A preliminary calculation, made after the visual color change, indicated that the lead exceeded 55 μg. Consequently, this amount was added to the comparison, or "known solution," before using the photronic cell. The first determination with the photronic cell showed this amount to be too small, as was expected. The next amount of lead, 11.8 μg, was still not enough and 11.3 μg more were added. The measurements with the photronic cell at this point showed that the total amount of lead in the known solution exceeded that in the test solution. The equivalence point having been passed, all the data needed to calculate the final result were available. The details of procedure are given below, followed by the calculations in table 1.

Procedure	Solution	
	Known	Test
Lead added, micrograms	54.9	[a] (70.3)
Readings with photronic cell, microamperes:		
a. Initial readings without solution	27.96	27.95
b. Solutions present	16.20	20.26
c. Final reading without solution	28.13	28.03
d. Mean, readings without solution	28.04	27.99
Transmission ratios b/d	0.578	0.724
Lead added to known solution, micrograms	11.8	
Readings with photronic cell, microamperes:		
e. Initial readings without solution	28.03	28.14
f. Solutions present	19.56	20.57
g. Final readings without solution	28.28	28.24
h. Mean, readings without solution	28.15	28.19
Transmission ratios f/h	0.695	0.730
Lead added to known solution, micrograms	11.3	
Readings with photronic cell, microamperes:		
i. Initial readings without solution	28.04	28.08
j. Solutions present	23.86	20.58
k. Final readings without solution	28.08	28.14
l. Mean, readings without solution	28.06	28.11
Transmission ratios j/l	0.850	0.732

[a] This amount was unknown to the analyst.

Considering the transmission ratios, we have the results in table 1.

TABLE 1.—*Determination of lead added to a test solution containing no sulfuric acid*

[Evaporation to dryness not required]

	Known solution		Test solution		Ratio of transmissions
	Total lead	Transmission	Total lead	Transmission	
	μg		μg		
Initial condition	0		70.3		
Comparison 1	54.9	0.578	70.3	0.724	1.25 [a]
Comparison 2	66.7	.695	70.3	.730	1.05 [a]
Comparison 3	78.0	.850	70.3	.732	0.86 [a]
Lead by analysis, experiment 1, figure 1			69.8		1.00 [a]
Difference			−0.5		

The transmission ratios in the last column of table 1 were plotted (fig. 1) against the amounts of lead in the known solution. The relationship is evidently linear within a limited range. The equivalence point is shown by the intersection at a ratio of unity. The amount of lead corresponding to this unit ratio is 69.8 μg, which agrees with the amount in the test solution to within 0.5 μg, or 0.7 percent. It is possible to go back and forth over the equivalence point.

Similar tests, described below, were made on known amounts of lead in strong and also in dilute solutions of sulfuric acid which were carried through the evaporation process. By numerous checks of this kind we satisfied ourselves that the method can be used with

sufficient accuracy to determine the solubility of lead sulfate in sulfuric acid solutions of varying concentration.

Experiments 2 and 3. Determination of lead in test solutions of 50 percent and 2 percent H_2SO_4, respectively, which were evaporated to dryness.—These experiments followed in a general way the details of the preceding experiment after the evaporation of the sulfuric acid had been completed and the lead sulfate residues transferred to the separatory funnels. Details of these experiments are, therefore, omitted, but the results are given in table 2 and figure 1.

TABLE 2.—*Determination of lead added to test solutions containing sulfuric acid*

[Evaporation to dryness required]

	Total lead in known solution	Test solution		Ratio of transmissions
		H_2SO_4	Total lead	
	μg	*Percent*	*μg*	
Initial condition	0	50	44.5	
Comparison 1	40.4	0	44.5	1.04
Comparison 2	46.8	0	44.5	0.96
Comparison 3	[1] 46.8	0	[1] 52.3	1.06
Lead by analysis, experiment 2, figure 1			44.0	1.00
Difference			−0.5	
Initial condition	0	2	40.3	
Comparison 1	41.2	0	40.3	0.99
Comparison 2	41.2	0	40.3	1.00
Comparison 3	49.8	0	40.3	0.89
Comparison 4	49.8	0	40.3	0.89
Lead by analysis, experiment 3, figure 1			41.2	1.00
Difference			+0.9	

[1] 7.8 *μg* of lead were added to the test solution to carry the comparison back through the equivalence point. This is equivalent to subtracting this amount from the lead in the known solution, while the amount in the test solution is regarded for purposes of computation as remaining unchanged.

Figure 1 shows that the relation between the ratios of transmission and the lead in the known solution is linear as in the case of the first experiment. The determinations of experiments 2 and 3 were made, using portions of the same solution of dithizone and the parallelism of the plotted result is significant. The plot of the results of experiment 2 is of interest because the solution was carried back through the equivalence point by adding lead to the test solution. This can be done provided enough dithizone is present in each funnel. The results of all comparisons fall on the same straight line. The small figures indicate the numerical order of the comparisons. Although it is difficult to distinguish more than two points on the line, for experiment 3 there are actually four comparisons, as shown in table 2.

The small changes in repeated determinations of the transmission of the test solution, as shown in table 1, always progress in the same direction. This has been observed repeatedly. These changes are probably not accidental variations, but indicate a slow oxidation of the dithizone. We believe that this explanation is more probable than that given by Clifford and Wichmann [3, page 140] who studied the equilibrium conditions and concluded that lead is continuously

drawn from the organic phase merely by prolonged shaking of the solutions. This and other points relating to the pH of the solutions deserve further consideration and test in establishing a method for determining lead. They did not, however, seem to justify further time and effort in the present work as our problem was primarily to determine the solubility of lead sulfate. The results of tests on solutions to which known amounts of lead were added showed that our method was amply accurate for the purpose.

Any error that arises from oxidation of the dithizone was minimized in our experiments by taking the successive ratios of transmis-

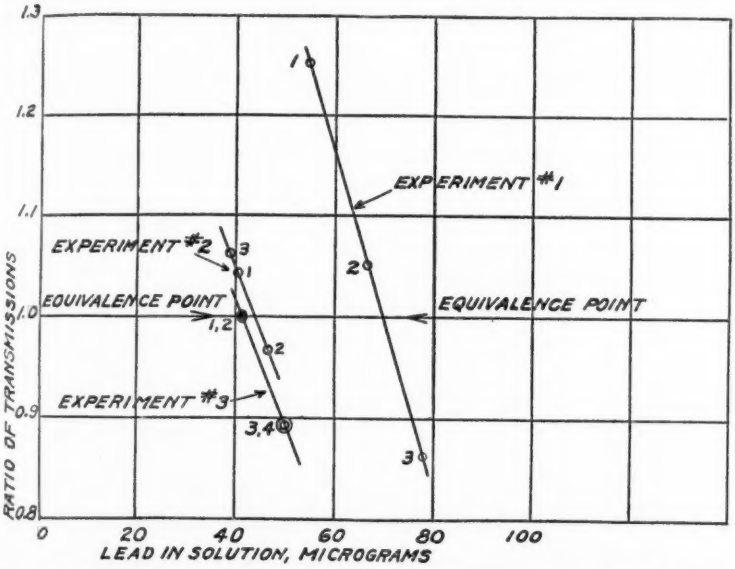

FIGURE 1.—*Relation of transmission ratios to the amounts of lead in solution.*

sion. Likewise, any error which would result from an unknown distribution of the lead between the aqueous and organic phases is nullified by the comparison of known and unknown solutions carried through exactly the same processes.

The desirability, however, of extending the work to study the use of green filters or both red and green filters is recognized. For some lead concentrations one may be better than the other. If both are used, two different curves could be obtained, and the equivalence point calculated from one should check the determination from the other.

We made two determinations of the pH of the aqueous phase, using a glass electrode, and obtained the value 9.4, which is within the range recommended by Clifford and Wichmann.

6. DETERMINATION OF SULFURIC ACID

The method for determining H_2SO_4 in the solutions was by densities at 25°, as described in detail in our paper entitled Chemical Reactions in the Lead Storage Battery [6], except in the more dilute solutions. In these the acid concentration was determined by titration.

III. EXPERIMENTAL RESULTS

The amount of lead in 25 ml of each solution, saturated at 25° C, was determined and the experimental data are given in table 3 as observed values, together with the acid concentration of the respective solutions expressed as the percentage of H_2SO_4. Columns 3, 5, and 6 of this table need not be considered now. They relate to smoothed curves, shown in figure 2, which are discussed on page 65. Corresponding data are given in table 4 for determinations made at 0° C. The direction from which saturation equilibrium was approached is indicated in these tables by *D* ("down" points) if approached from a supersaturated condition and by *U* ("up" points) if approached from an unsaturated condition.

TABLE 3.—*Experimental data at 25° C and comparison with smoothed curve, figure 2*

H_2SO_4	Weight, Pb in 25 ml		Direction	Difference	Difference
	Observed	From curve			
Percent	*μg*	*μg*		*μg*	*Percent*
0.086	89.7	88.3	*D*	+1.4	+1.6
.118	82.5	82.9	*U*	−0.4	−0.5
.647	80.0	80.0	*U*	0	0
1.57	89.2	89.0	*U*	+.2	+.2
2.28	93.7	93.5	*D*	+.2	+.2
2.60	94.3	95.3	*U*	−1.0	−1.0
5.31	106.2	106.2	*U*	0	0
9.65	114.0	114.0	*U*	0	0
10.09	115.5	115.4	*U*	+.1	+.1
11.80	112.7	113.1	*D*	−.4	−.4
19.87	90.0	89.5	*U*	+.5	+.6
21.58	79.4	80.7	*D*	−1.3	−1.7
21.93	78.2	79.0	*U*	−0.8	−1.0
24.90	68.2	67.0	*U*	+1.2	+1.8
31.87	42.0	42.0	*U*	0	0
32.51	38.5	39.7	*U*	−1.2	−3.0
33.31	39.1	38.0	*D*	+1.1	+2.9
45.48	20.1	20.7	*D*	−0.6	−2.9
48.58	19.5	19.1	*U*	+.4	+2.1
Average of all determinations				±0.6	±1.0

TABLE 4.—*Experimental data at 0° C and comparison with smoothed curve, figure 2*

H_2SO_4	Weight, Pb in 25 ml		Direction	Difference	Difference
	Observed	From curve			
Percent	*μg*	*μg*		*μg*	*Percent*
0.053	45.8	47.1	*D*	−1.3	−2.8
.065	45.7	44.5	*U*	+1.2	+2.7
.280	35.2	35.4	*D*	−0.2	−.6
.462	35.0	35.1	*U*	−.1	−.3
1.13	36.3	36.0	*D*	+.3	+.8
4.70	40.2	41.5	*U*	−1.3	−3.1
7.46	48.3	46.7	*D*	+1.6	+3.4
8.93	46.2	48.5	*U*	+2.3	+4.7
10.09	49.4	49.0	*D*	+0.4	+.8
17.49	41.1	41.8	*U*	−.7	−1.7
19.87	38.7	38.5	*D*	+.2	+.5
37.58	8.2	11.3	*D*	−3.1	−27.4
38.95	11.6	10.2	*U*	+1.4	+13.7
Average of all determinations				±1.1	±4.8
Average, 0- to 20-percent acid				±.0.9	±2.0

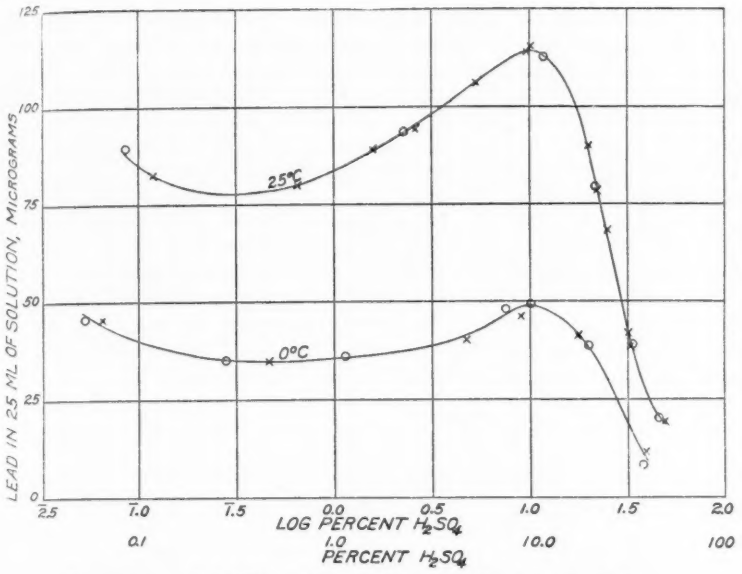

FIGURE 2.—*Solubility of lead sulfate in sulfuric acid solutions.*

Circles represent equilibrium values approached from supersaturated solutions and crosses from undersaturated solutions.

IV. SOLUBILITY OF LEAD SULFATE AT REGULAR INTERVALS OF SULFURIC ACID CONCENTRATION

Since the experimental determinations reported in tables 3 and 4 were made at acid concentrations which have no simple relation to each other, all of the data were plotted and the solubility read from the curves at regular intervals. To avoid errors which might result from drawing a single curve, three separate plots on large scales were made, using the percentage of the acid concentrations, the square root of the percentage, and the logarithm of the percentage as abscissas. The average solubilities were then calculated from the readings made of these three plots, except below 1 percent, where the rectangular plot was not serviceable.

The average solubilities were plotted against the logarithms of the respective concentrations to obtain the curves shown in figure 2. The individual points which were plotted for the purpose of drawing the curves are not shown in the figure, but the actual experimental determinations are plotted to show their deviations from the smoothed curve. These deviations afford a means of estimating the priecision of individual determinations. For each point the deviataon in micrograms from the smoothed curve of figure 2 has been read and tabulated in tables 3 and 4. The average deviations are less than 1μg in the case of the determinations at 25° C and slightly more than 1μg for the determinations at 0° C. The average percentage deviations are about 1 percent at the higher temperature, but at the lower temperature, they are, as might be expected, considerably more. This is because the total amount of lead sulfate in solutions at 0° C is very small. If we consider only the solutions of less than 20 percent

H_2SO_4 the average deviation is 2 percent. Above this concentration of acid the amount of lead in the 25-ml samples was about 10μg and an error of only 1μg appears as a percentage error of 10 percent. It is probably better, therefore, to consider the accuracy of the work from the standpoint of the actual weight of the lead which is in question. The precision is of the order of 1μg in the more difficult determinations at 0° C. It might appear that the percentage error could have been reduced by increasing the size of the sample. This, however, would have required changes in the procedure introducing other difficulties and consequently we thought it better to proceed in the same manner as for the solutions for which 25-ml samples were adequate.

Having obtained the most probable curves to represent the experimental data, the solubility of $PbSO_4$ in milligrams per liter was then calculated at regular intervals of the acid concentration. These results are given in table 5 for both 25° and 0° C.

TABLE 5.—*Solubility of lead sulfate in solutions of sulfuric acid*

H_2SO_4	Weight, $PbSO_4$ in a liter		H_2SO_4	Weight, $PbSO_4$ in a liter	
	t=25° C	t=0° C		t=25° C	t=0° C
Percent	*mg*	*mg*	*Percent*	*mg*	*mg*
0.1	4.99	2.37	6.0	6.33	2.58
.2	4.61	2.13	7.0	6.47	2.69
.3	4.55	2.07	8.0	6.57	2.79
.4	4.57	2.05	9.0	6.64	2.84
.5	4.60	2.06	10.0	6.68	2.86
.6	4.65	2.06	15.0	6.28	2.63
.7	4.71	2.07	20.0	5.18	2.21
.8	4.77	2.07	25.0	3.87	1.76
.9	4.84	2.08	30.0	2.82	1.27
1.0	4.91	2.10	35.0	2.02	0.84
2.0	5.37	2.18	40.0	1.52	.53
3.0	5.70	2.27	45.0	1.23	----------
4.0	5.95	2.36	50.0	1.08	----------
5.0	6.15	2.46			

V. DISCUSSION OF RESULTS

The data given in table 5 and in figure 2 show definite maxima and minima for the solubility. Each curve for a specified temperature shows that three different solutions with the same lead content are possible. At each temperature the curve passes through a maximum at about 10 percent acid and a minimum at about 0.3 percent acid.

It is interesting to compare these results with those published by us [7] 2 years ago for mercurous sulfate in corresponding concentrations of sulfuric acid. In order to compare the solubility curves of lead sulfate and mercurous sulfate and to show the remarkable similarity in their characteristics, we have computed the lead sulfate results to the same basis of acid concentration as was used in the former paper. In figure 3 the results for both salts are plotted, but it should be noted that mercurous sulfate is given as the ordinate instead of mercury as in the earlier paper. The similarity of the curves is at once apparent.

If correction is made in the case of the mercurous sulfate for the total molar concentration in the dilute solutions, since mercurous sulfate is sufficiently soluble to affect the properties of the solution, the dotted portion of the upper curve is obtained.

We may now compare the solubility of mercurous sulfate and lead sulfate in solutions of corresponding strength. The results are given in table 6. The ratio of mercurous sulfate at 28° C to lead sulfate at 25° C is surprisingly constant over a very wide range of acid concen-

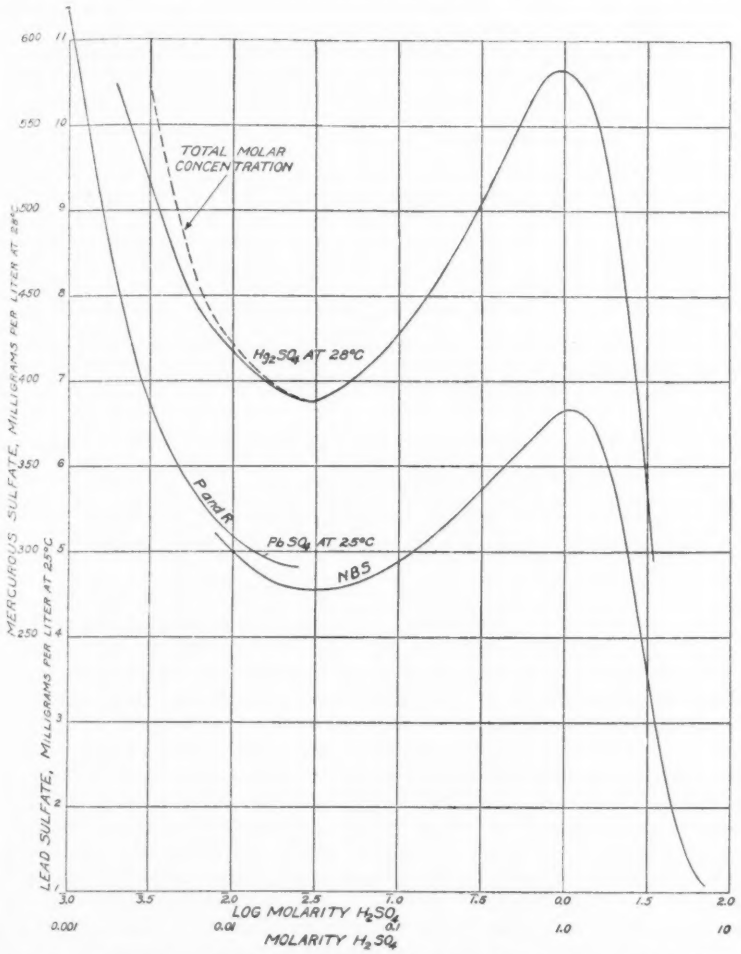

FIGURE 3.—*Comparison of solubility curves of lead and mercurous sulfates in solutions of sulfuric acid.*

The curve marked "*P* and *R*" represents data of Purdum and Rutherford [8] calculated to 25° C. The dotted portion of the Hg_2SO_4 curve represents the total concentration of H_2SO_4 plus Hg_2SO_4.

trations. From 3.5 molar to 0.0025 molar, more than a 1000:1 change in the acid concentration, the ratio of solubilities is nearly constant. The average deviation of a single comparison from the mean value, 88, is about 2. This is comparable with the experimental error estimated for the two series of measurements. Above 2 molar acid the ratios differ slightly more, but it should be noted that in such cases the

amounts of lead and mercurous sulfate are relatively small and percentage errors naturally become larger.[3]

TABLE 6.—*Comparison of the solubilities of lead and mercurous sulfates*

Molar concentration of acid plus salt[a]	Lead sulfate per liter at 25° C	Mercurous sulfate per liter at 28° C	Ratio: $\frac{Hg_2SO_4}{PbSO_4}$	Molar concentration of acid plus salt[a]	Lead sulfate per liter at 25° C	Mercurous sulfate per liter at 28° C	Ratio: $\frac{Hg_2SO_4}{PbSO_4}$
	mg	*mg*			*mg*	*mg*	
0.002	7.3	615	84[b]	0.60	6.27	559	89
.005	5.9	490	83[b]	.80	6.51	579	89
.010	4.99	419	84	1.00	6.67	583	87
.025	4.58	390	85	1.50	6.47	560	87
.04	4.57	393	86	2.00	5.81	507	87
.06	4.65	405	87	2.50	4.80	439	91
.08	4.77	418	88	3.00	3.87	364	94
.10	4.89	426	87	3.50	3.07	295	96
.20	5.36	470	88				
.40	5.91	524	89		Average		88

[a] The concentration of the solution has been corrected for the dissolved salt only in the case of mercurous sulfate (see fig. 2) when the acid concentration was below 0.03 molar. No correction is necessary for higher concentrations nor for the lead sulfate in any concentration given in the table.
[b] Lead sulfate data of Purdum and Rutherford [8] calculated to 25° C. NBS data, remainder of table.

The first decrease in solubility of the salts at the left in figure 3 is undoubtedly the "common ion effect." The effect of sulfuric acid in repressing the solubility of lead sulfate is very pronounced in dilute solutions. The solubility of the salt in water as determined by others is approximately 10 times that found by us in 0.03 molar acid. We gave a hypothesis for the rise to the second maximum in the case of the mercurous salt and we believe that the same explanation holds true in the case of the lead salt. The correspondence of the curves for these two salts suggests strongly that the solubility of the salts is governed by the ionic equilibrium of the sulfuric acid existing at any particular concentration. In sulfuric acid solutions both sulfate and bisulfate ions are present.

The solubilities of both calcium [9] and silver [10] sulfates attain a maximum in the general region of molar concentration of sulfuric acid according to data in the technical literature. In the case of calcium sulfate the maximum appears to be at about 0.76 molar acid and for silver sulfate at about 1.2 molar acid. Both calcium and silver sulfates are more soluble than either the mercurous sulfate or lead sulfate. Neither calcium sulfate nor silver sulfate shows an initial decrease which might be expected to result from the common ion effect. At least the data in references quoted above fail to show it. The reason for not finding an initial decrease in solubility of these salts is evident if the data are plotted against total molar concentrations, as we have done in the case of mercurous sulfate, figure 3. The lowest total concentrations are in the region of or above that at which we observed the minimum solubility of lead and mercurous sulfates.

[3] A comparison might be made on the basis of corresponding ionic strength of the solutions. Such a comparison, however, would differ little from that given in table 6 and would affect principally the comparison of solubilities in the two most dilute solutions shown in the table. Further comparisons of still more dilute solutions cannot be made because of hydrolysis of the mercurous sulfate.

VI. COMPARISON WITH THE RESULTS OF OTHERS

Various determinations of the solubility of lead sulfate in water and in solutions of sulfuric acid have appeared in the technical literature. Several of these are mentioned in Dolezalek's book [11] and in the papers by Purdum and Rutherford [8], by Crockford and Brawley [12], and Huybrechts and Ramelot [13]. Data are given also by Seidell [14] and by Mellor [15]. We have made use of the data of Purdum and Rutherford in table 6 to supply values in the range of low acid concentrations which our work does not cover. Their determinations overlap ours in the region of 0.1 to 0.25 percent sulfuric acid. A comparison of their results with ours is given in table 7. Since their results were given at 20° C, we have converted them to 25° C by applying linear corrections based on our observations at 0 and 25° C. Such a procedure cannot be justified for large temperature differences. The comparison of our results with those of Purdum and Rutherford, which were obtained by an entirely different method, then shows very close agreement.

TABLE 7.—*Comparison of results with those of Purdum and Rutherford*

Concentration H_2SO_4		Lead sulfate per liter		Difference
Equivalent per liter	Percent	Purdum and Rutherford, calculated to 25° C	NBS, observed at 25° C	
		mg	*mg*	*mg*
0.02	0.098	5.2	5.0	0.2
.05	.245	4.8	4.6	.2

Comparison of our results with those of Crockford and Brawley is difficult because the actual determinations made by them are not reported in their paper, and the number of their determinations is not known. Their data, which were evidently read from a smoothed curve, fail to show any indication of a maximum solubility, which we observed in molar acid. Although they estimate their results to be accurate to 0.2 part per million of solution in this range, there is a large discrepancy between their results and ours, which are threefold greater than theirs at this point. We feel very confident that this maximum exists. We found it at both 25° and 0° C. It is entirely analogous to the results for mercurous sulfate, and the accuracy of our individual determinations, as shown by table 3, is amply sufficient to establish it. At the higher concentrations of acid reported in this paper better agreement with their data was found.

Huybrechts and Ramelot made determinations of the solubility of lead sulfate in sulfuric acid solutions up to 10 percent. In general, our values at 25° C are in good agreement with theirs and almost uniformly lie between their values at 18° and 30° C.

VII. REFERENCES

[1] H. Fischer, Z. anorg. Chem. **42,** 1025 (1929).
[2] H. Fischer, Z. anorg. Chem. **47,** 685 (1934).
[3] P. A. Clifford and H. J. Wichmann, J. Assn. Official Agr. Chem. **19,** 130 (1936).
[4] Ind. Eng. Chem. **17,** 756 (1925).
[5] See [1 and 2], also [3, p. 131].
[6] G. W. Vinal and D. N. Craig, J. Research NBS **14,** 456 (1935) RP778.
[7] D. N. Craig, G. W. Vinal, and F. E. Vinal, J. Research NBS **17,** 709 (1936) RP939.
[8] Purdum and Rutherford, J. Am. Chem. Soc. **55,** 3221 (1933).
[9] F. K. Cameron and J. F. Breazeale, J. Phys. Chem. **7,** 574 (1903).
[10] G. Åkerlöf and H. C. Thomas, J. Am. Chem. Soc. **56,** 597 (1934).
[11] F. Dolezalek, Theory of the Lead Accumulator, p. 144 (1904).
[12] H. D. Crockford and D. J. Brawley, J. Am. Chem. Soc. **56,** 2600 (1934).
[13] M. Huybrechts and H. Ramelot, Bul. soc. chim. Belg. **36,** 239 (1927).
[14] A. Seidell, Solubilities of Inorganic and Organic Compounds.
[15] J. W. Mellor, Comprehensive treatise on inorganic and theoretical chemistry **7,** 803 (1927).

WASHINGTON, August 8, 1938.

U. S. Department of Commerce National Bureau of Standards

RESEARCH PAPER RP1166

Part of Journal of Research of the National Bureau of Standards, Volume 22, January 1939

PERMEABILITY OF NEOPRENE TO GASES

By Theron P. Sager and Max Sucher

ABSTRACT

The specific permeability of Neoprene to hydrogen, helium, and carbon dioxide at 25° C is shown to be about one-fifth to one-sixth that of rubber. Permeability is inversely proportional to the thickness of film. The increase in the rate of permeation of hydrogen with temperature is shown to be exponential since, when log permeability is plotted against reciprocal of absolute temperature, straight lines are obtained. Various factors regarding the behavior of coated fabrics are discussed. Moderate amounts of the usual compounding ingredients do not appreciably affect the rate of permeation. The use of highly volatile solvents in spreading cements tends to produce pinholes. Toluol or its equivalent appears to be the most satisfactory solvent.

CONTENTS

	Page
I. Introduction	71
II. Materials and methods	72
III. Permeability of unsupported films	72
1. Effect of thickness	72
2. Relative permeability to gases	73
3. Effect of temperature	73
IV. Permeability of coated fabrics	76
1. Effect of weight of coating	76
2. Effect of composition of coatings	77
3. Effect of solvents employed in cements	79

I. INTRODUCTION

The properties most generally associated with Neoprene are its rubber-like character and its resistance to the deteriorative action of mineral oils. To this combination of properties it owes its principal commercial applications. A less generally known characteristic is the relatively low permeability of this material to gases. The most suggestive utilization of this property is in the construction of various forms of gas containers for use in lighter-than-air craft, particularly in view of the fact that the material may be readily applied to cloth as a continuous film having elastic extensibility. The work represented by this report was undertaken as a result of the interest which the Bureau of Aeronautics of the United States Navy Department maintains in all materials which offer promise of application in this field.

Since rubber is the material which has been employed to the greatest extent for gas containers, it is used as the basis for comparison in the present study. Aside from its practical application, the behavior of Neoprene toward gases is of interest because of the relation of its chemical composition to that of other dienes which possess elasticity. The substance used as the base for Neoprene compounds is polymerized chloroprene (2-chloro-1, 3-butadiene). The chemical composition of chloroprene, $CH_2=CCl-CH=CH_2$ differs from that of other conjugated dienes, whose polymers are characterized by elastic extensibility, in that 40 percent of its molecule consists of chlorine.

II. MATERIALS AND METHODS

The Neoprene employed throughout this work was that designated by the manufacturer as type *E*. The compounding materials were all of the type and quality recommended for use with Neoprene. The compounds were prepared in the customary manner, the Neoprene being masticated on a differential-speed mill, the compounding ingredients being added on the mill. The rubber compounds were similarly prepared. In the preparation of cements the thinly sheeted materials were dissolved in toluol which was kept in continuous agitation. The cements were filtered through cloth and stored in tinned containers.

The coated fabrics were prepared by applying a plurality of thin coats to a balloon cloth by means of a small spreading machine equipped with a doctor blade. The cloth was a closely woven cotton fabric weighing 2.05 oz/yd [2], and having a thread count of 120 in both warp and filling directions. The unsupported films were prepared in the same manner except that the base was uncoated Cellophane from which the films, after being cured, could be readily stripped.[1]

Curing in all cases was effected in dry heat. For Neoprene the conditions were a 1-hr rise to 257° F (125° C) followed by 2 hr at 257° to 266° F (125° to 130° C).

Permeability was determined by means of a gas interferometer of the Rayleigh type. The apparatus and conditions of test have been previously described.[2] Except where otherwise noted, all determinations were made under the following standard conditions: The film or fabric is maintained at a temperature of 25° C, with air at atmospheric pressure (760 mm of mercury) on one side of the specimen and the gas whose rate of permeation is being measured at an excess pressure of 30 mm of water on the other side. Permeability is expressed as liters per square meter per 24 hr determined under these standard conditions. The permeabilities in metric units may be converted to their corresponding values in cubic feet per square yard per 24 hr by multiplying the former by the factor 0.0295. Specific permeabilities are expressed as milliliters per square centimeter per centimeter thickness per minute.

III. PERMEABILITY OF UNSUPPORTED FILMS

1. EFFECT OF THICKNESS

In the preparation of unsupported films the following compound was employed:

Compounding ingredient	*Parts by weight*
Neoprene *E*	100
Magnesium oxide	10
Rosin	5
Carbon black (*P–33*)	5
Phenyl-β-naphthylamine (Neozone *D*)	2
Zinc oxide	10

The permeabilities to hydrogen, helium, and carbon dioxide obtained with different thicknesses of films are presented in table 1. The close agreement of the specific permeabilities, calculated from the permeabilities of films of various thickness, indicates that the rate of

[1] T. P. Sager, Ind. Eng. Chem., Anal. Ed. **9**, 156 (1937).
[2] J. D. Edwards and S. F. Pickering, BS Tech. Pap. **11** (1918) T113; BS Sci. Pap. **16**, 327–362 (1920) S337.

TABLE 1.—*Permeabilities of unsupported films of Neoprene*

Thickness of film *cm*	Permeability at 25° C and 1 atm Liters/m²/24 hr			Specific permeability at 25° C and 1 atm ml/cm²/cm/min×10⁺⁶		
	Hydrogen	Helium	Carbon dioxide	Hydrogen	Helium	Carbon dioxide
0.010	6.3	4.1	12.1	4.3	2.8	8.4
.010	6.0	3.7	11.6	4.1	2.5	8.0
.016	3.7	2.5		4.1	2.7	
.017	3.9	2.7	8.3	4.5	3.1	9.7
.022	2.7			4.1		
.029	2.1			4.2		
.035	1.8	1.1	3.6	4.3	2.6	8.7
.039	1.6			4.3		
.068	0.9	0.6	2.0	4.2	2.8	9.4
Average				4.2	2.7	8.8

permeation is inversely proportional to the thickness. This is shown in figure 1, in which is presented the relationship of the gas impedance (reciprocal of permeability) to the thickness of film.

2. RELATIVE PERMEABILITY TO GASES

The average value of the ratio of helium permeability to hydrogen permeability of Neoprene, calculated from the values in table 1, is 0.65, which is the same as the corresponding value for rubber given in the literature. The average of the ratios for carbon dioxide to hydrogen is 2.0, which is somewhat lower than the corresponding values for rubber, which are reported as ranging from 2.46 to 2.91.

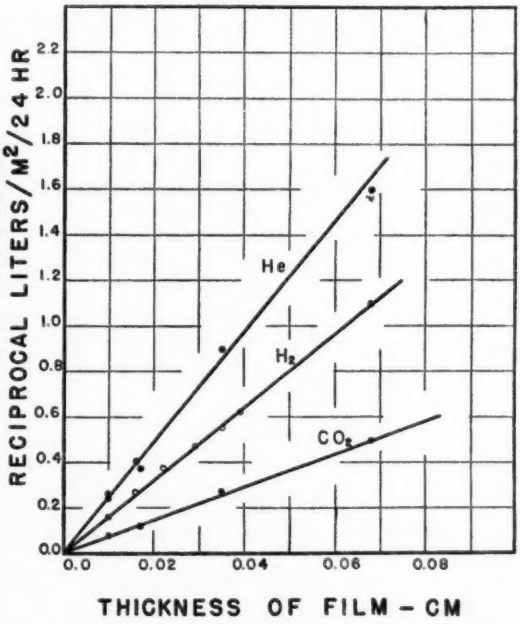

FIGURE 1.—*Relation of Thickness of Neoprene Films to Gas Impedance.*

Values for the specific permeability of rubber to hydrogen, given in the literature, range from about 20×10^{-6} to 27×10^{-6} ml/cm²/min for 1 cm thickness. According to these values, it is apparent that the specific permeability of this Neoprene compound is about one-fifth to one-sixth that of rubber.

3. EFFECT OF TEMPERATURE

For the determination of the effect of temperature on the permeability of Neoprene to hydrogen, the thickness of films chosen was such that convenient values for permeability could be obtained

throughout a range of temperatures. For comparison, the permeability of a film of rubber was also measured under the same conditions. The essential data concerning the rubber compound are as follows:

Compounding ingredient	*Parts by weight*
Smoked sheet rubber	100
Sulfur	4
Zinc oxide	5
Zinc stearate	1
Mercaptobenzothiazole (Captax)	1
Phenyl-β-naphthylamine (Neozone D)	1

Cure: Thirty minutes at 288° F.

The values obtained at the various temperatures are given in table 2, and the relations between permeability and temperature are shown in figure 2. In figure 3 are plotted the logarithms of the permeabilities against the reciprocals of the absolute temperatures. The fact that the points fall fairly closely on straight lines indicates, as has been shown in the case of rubber,[3] and in the case of regenerated cellulose and cellulose derivatives,[4] that the increase in permeability with temperature is exponential. The dependence of permeability upon temperature is expressed by means of the equation $Q_m = Ae^{-E/RT}$, in which Q_m is the permeability at the temperature T in moles per square centimeters per second at 1 cm thickness. A is a constant having the same dimensions as Q_m, which bears a relation to the spatial requirements of the reacting molecules. E is the activation energy expressed in calories per mole. R and T are the gas constant and absolute temperature, respectively. When values obtained from figure 3 were employed in this equation the values for E and A which resulted are shown in table 3.

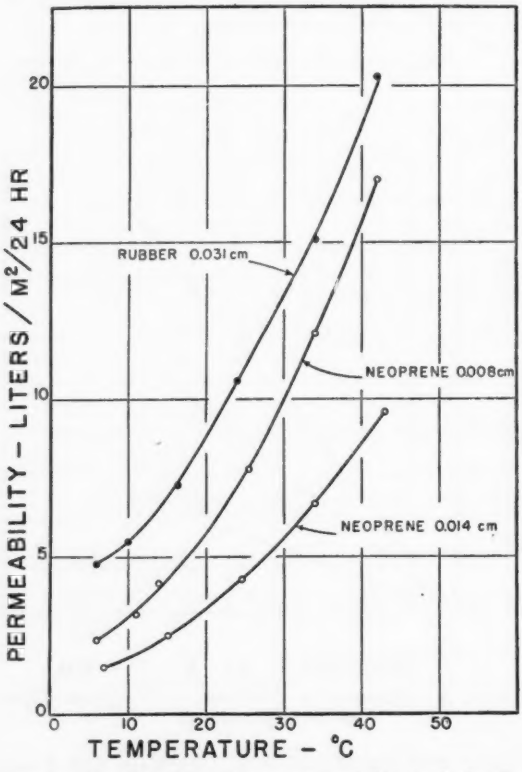

FIGURE 2.—*Relation between permeability to hydrogen and temperature.*

[3] R. M. Barrer, Nature 140, 106 (1937).
[4] J. H. De Boer and J. D. Fast, Rec. trav. chim. 57, 317 (1938).

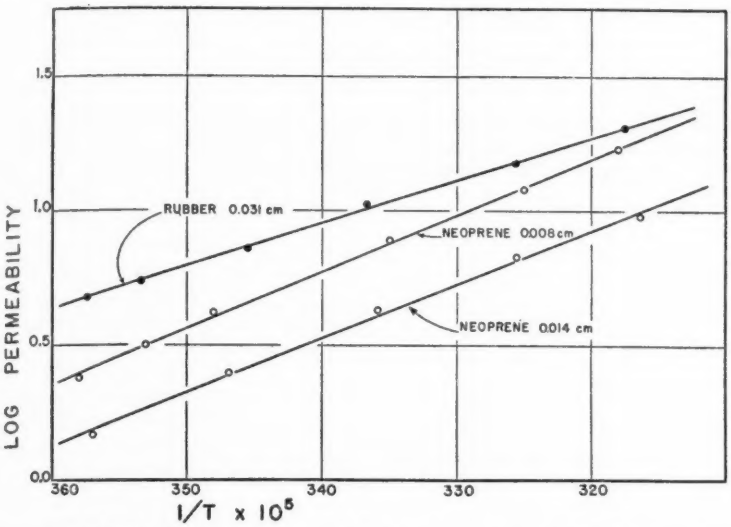

FIGURE 3.—*Relation between log permeability and reciprocal of absolute temperature.*

TABLE 2.—*Variation of permeability with temperature*

Temperature of test	Permeability to hydrogen
Neoprene 0.008 cm thickness	
°C	*Liters/m²/24 hr at 1 atm at t °C*
6.0	2.4
11.0	3.2
14.0	4.2
25.5	7.8
34.0	12.1
42.0	17.0
Neoprene 0.014 cm thickness	
7.0	1.5
15.2	2.5
24.7	4.3
34.0	6.7
43.0	9.6
Rubber 0.031 cm thickness	
6.0	4.8
10.0	5.5
16.4	7.3
24.0	10.6
34.0	15.1
42.0	20.3

TABLE 3.—*Values for E and A, in the equation* $Q_m = A_o^{-E/RT}$, *for hydrogen*

Material	Thickness	*E*	*A*
	cm	*cal/mole*	*Moles/cm³ sec for 1 cm thickness*
Neoprene	0.014	9,376	$22.2 \times 10^{-}$
Do	.008	9,422	24.2
Rubber	.031	6,998	2.2

IV. PERMEABILITY OF COATED FABRICS

1. EFFECT OF WEIGHT OF COATING

In figure 4 are shown the permeabilities obtained with cloth, coated with various weights of the same Neoprene compound that was employed in the preparation of the unsupported films. Values obtained with cloth coated with similar weights of rubber are shown for comparison. The rubber compound was the same as that employed in the determination of the effect of temperature on permeability.

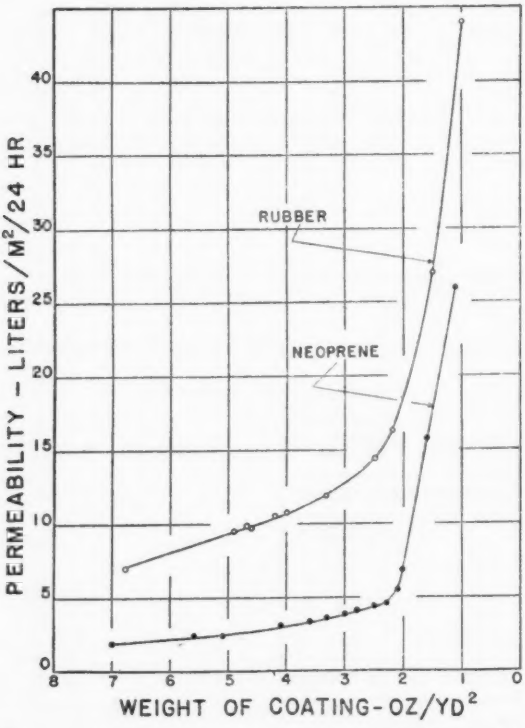

FIGURE 4.—*Comparison of the permeabilities to hydrogen obtained with fabrics coated with various amounts of rubber and Neoprene.*

From the standpoint of airship fabric construction the permeabilities obtained with weights of coating in the neighborhood of 2 oz/yd² are of particular interest. It is apparent that within this range the greatest impedance for a unit weight of coating is obtained. Below about 2 oz/yd² of coating the permeability changes somewhat more rapidly in the case of Neoprene than of rubber. The specific gravity of the rubber compound is approximately 1.0, while that of the Neoprene compound is between 1.3 and 1.4. The covering power of the latter is consequently less than that of rubber and it becomes increasingly more difficult to obtain a continuous film on the cloth. It is this difference in specific gravities which accounts for the difference between the specific permeabilities and the permeabilities on a weight basis of the two materials. Based on the latter, the permeability of Neoprene is about one-third to one-fourth that of rubber.

In figure 5 a comparison is shown between the permeabilities of Neoprene-coated fabrics and those of unsupported films of the same weights per unit area as the weights of coatings on the fabrics. The difference in permeabilities illustrates a well-known fact that the cloth makes a definite contribution to the gas impedance of a coated fabric. It has been noted that this ratio between the permeabilities of coated fabrics and unsupported films is nearly constant for both Neoprene and rubber within the range shown in figure 5. The effect of the cloth on the permeability doubtless becomes more involved

TABLE 4.—*Characteristics of multiple-ply fabrics*

Construction (order of layers in cross section)	Type of fabric		
	Ballonet	Airtight envelope	Gastight envelope
	O^2/yd^2	O^2/yd^2	O^2/yd^2
Aluminum-pigmented Neoprene		0.7	0.7
Neoprene	0.5	1.0	1.0
Cloth	2.05	2.05	2.05
Neoprene	3.5	1.6	1.6
Cloth	2.05	[a]2.05	[a]2.05
Neoprene	0.5	1.6	3.6
Cloth		2.05	2.05
Neoprene		0.5	0.5
Permeability to hydrogen (liters/m^2/24 hr)	3.8	2.8	1.6

[a] Fabric laid on bias.

when the fabrics are constructed of two or more plies. Typical constructions of such fabrics, employing Neoprene as coatings, and the permeabilities obtained are shown in table 4.

2. EFFECT OF COMPOSITION OF COATINGS

As with rubber, the physical properties of Neoprene compounds vary considerably with the nature and proportions of the compounding ingredients. In table 5 are shown the permeabilities to hydrogen obtained with a number of compounds which were applied to cloth. It was not feasible to attempt to produce fabrics all having the same weight of coating, but since for a given compound the product of the weight of coating and the permeability is nearly constant within the range of weights represented, it was considered permissible, in order to secure a uniform comparison, to express the permeabilities relative to a single weight of coating. A comparison of the permeabilities calculated to a weight of coating of 3.5 oz/yd^2 is shown in figure 6.

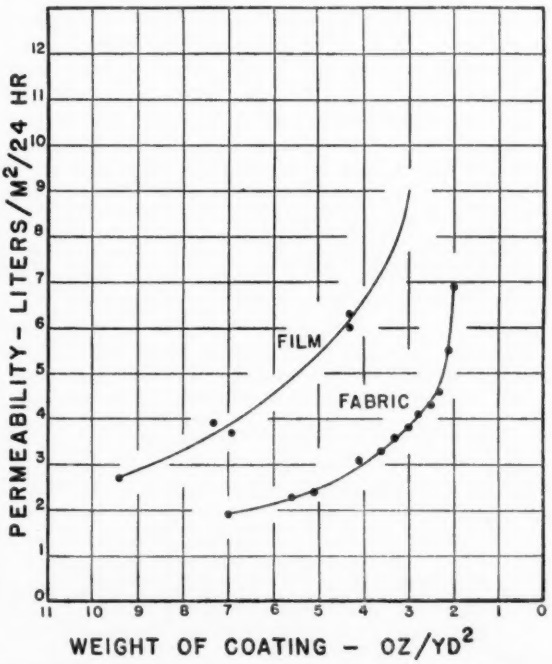

FIGURE 5.—*Comparison of the permeabilities to hydrogen obtained with unsupported film and fabric coated with the same weight of film.*

The compounds comprise two groups. Group 1 includes the conventional compounding materials which are added to secure satisfactory cure, increased flexibility, and similar characteristics. Group 2 contains, in addition, substances which are not usually associated with Neoprene.

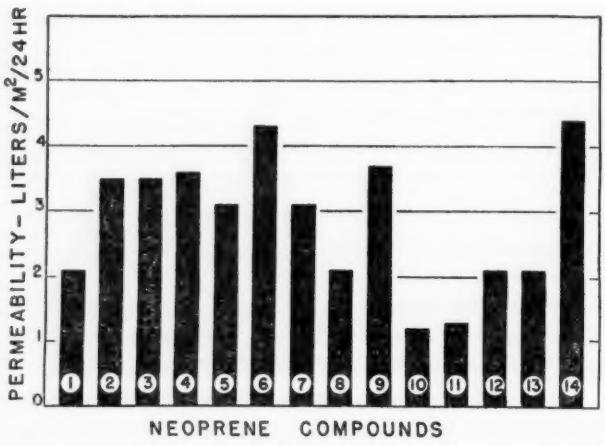

FIGURE 6.—*Comparison of the permeabilities obtained with the compounds given in table 5 calculated to a uniform weight of coating of 3.5 oz/yd².*

TABLE 5.—*Effect of composition of Neoprene compounds upon permeabilities of coated fabrics*

Ingredients	Compound (parts by weight)													
	1	2	3	4	5	6	7	8	9	10	11	12	13	14
GROUP 1														
Neoprene *E*	100	100	100	100	100	100	100	100	100	100	100	100	100	100
Magnesium oxide	----	10	10	10	10	10	10	10	10	10	10	10	10	10
Phenyl-β-naphthylamine (Neozone D)	2	2	2	2	2	2	2	2	2	2	2	2	2	2
Zinc oxide	----	10	10	10	10	10	10	10	10	10	10	10	10	10
Carbon black (*P-35*)	----	5	5	5	5	30	5	5	5	5	5	5	5	5
Sulfur	----	----	1	1	----	----	----	----	----	----	----	----	----	----
Wood rosin	----	----	----	10	----	5	5	5	5	5	5	----	5	5
Pine tar	----	----	----	----	10	----	----	----	----	----	----	----	----	----
Cottonseed oil	----	----	----	----	5	10	----	----	10	----	5	----	----	----
Cumar (*P-25*)	----	----	----	----	5	10	----	----	10	----	10	----	----	----
GROUP 2														
Paraffin wax (55° C mp)	----	----	----	----	----	----	5	20	----	----	----	----	----	----
Spermaceti	----	----	----	----	----	----	----	----	----	40	40	----	----	----
Chlorinated naphthalene resin (Arochlor)	----	----	----	----	----	----	----	----	----	----	----	40	----	----
Soft-brown factice	----	----	----	----	----	----	----	----	40	----	----	----	----	----
Aluminum powder	----	----	----	----	----	----	----	----	----	----	----	----	40	80
Weight of coating (oz/yd²)	3.1	3.6	3.5	3.8	3.1	4.0	3.1	3.4	3.4	3.6	3.3	2.7	3.2	3.2
Permeability (liters/m²/24 hr)	2.4	3.4	3.5	3.4	3.5	3.8	3.6	2.2	3.9	1.2	1.4	2.8	2.3	4.9

The behavior of the compounds in the first group indicates that the inclusion of moderate amounts of the orthodox compounding ingredients does not appreciably affect the rate of permeation. This is in agreement with general experience in the behavior of rubber compounds. Of the compounds in the second group the behavior of that containing spermaceti is noteworthy. It should be stated, however, that the relative permeabilities obtained with various compounds are not always reliable indications of their usefulness. Factors connected with the manufacture, and the subsequent ability to withstand hand-

ling and exposure, of aircraft fabrics determine their utility to fully as great an extent as their rate of permeation. The behavior of the compounds containing aluminum powder is of interest since the presence of this pigment is of value because of its high reflecting power and opacity. The results obtained with paraffin illustrate the difficulty of employing a compounding material inherently incompatible with Neoprene. Paraffin wax itself is highly impermeable to hydrogen. Balloon cloth impregnated with about 2.4 oz/yd² of paraffin wax is permeable to hydrogen to the extent of only 0.5 liter/m²/24 hr. Its use for aircraft fabrics is limited, for obvious reasons, to its supplementary employment on material such as rubberized fabric. An example of the treatment of a Neoprene-coated fabric in this manner is then of interest. The fabric coated with compound 9 in table 4 was coated on one surface with 0.4 oz/yd² of paraffin wax (55° mp). The permeability to hydrogen of the fabric was reduced from 3.5 to 1.0 liters/m/24 hr.

3. EFFECT OF SOLVENTS EMPLOYED IN CEMENTS

Early in the experimental preparation of Neoprene-coated fabrics the formation of pinholes was a matter of considerable concern. Under the conditions of preparation the presence of these did not appear to be related to the nature of the compound nor to the number of coats applied. Furthermore, their persistence was not appreciably affected by the thickness of film built up on the fabric. The method of coating the fabrics was similar to that employed commercially except that the cements contained a higher percentage of solvent. The cement was applied to the cloth, which was under moderate tension, in several successive coats. A source of heat, in the form of heating coils, located beneath the fabric hastened the evaporation of the solvent. It was considered advisable to compare films deposited from several different solvents which were suitable for Neoprene and economically within reason. Fabrics were coated with these cements under conditions of forced evaporation and at room temperature. The coated fabrics were examined, both before and after curing, over a light bank, for the presence of pinholes. No changes, so far as the presence of pinholes was concerned, occurred as the result of the curing. Excessive pinhole formation, as noted by visual inspection, corresponds to the high permeabilities in table 6.

TABLE 6.—*Effect of solvents in cements on pinhole formation*

Solvent	Evaporation at 140° F (60° C)		Evaporation at 78° F (25.5° C)	
	Weight of coating	Permeability to hydrogen	Weight of coating	Permeability to hydrogen
	oz/yd²	Liters/m²/24 hr	oz/yd²	Liters/m²/24 hr
Carbon tetrachloride	3.1	>50	3.2	>50
Benzol	3.5	23	3.1	4.5
Toluol	3.6	3.1	2.8	4.6
Xylol	2.7	4.6		

Too rapid evaporation of the solvent may not always be the only cause of pinholes, but in extreme cases it would appear to be the most obvious contributing factor. Toluol or its equivalent is the most satisfactory solvent used.

WASHINGTON, September 23, 1938.

115782—39——6

U. S. DEPARTMENT OF COMMERCE NATIONAL BUREAU OF STANDARDS

RESEARCH PAPER RP1167

Part of Journal of Research of the National Bureau of Standards, Volume 22, January 1939

APPLICATION OF GRAPHS OF MAXIMUM USABLE FREQUENCY TO COMMUNICATION PROBLEMS

By Newbern Smith, Samuel S. Kirby, and Theodore R. Gilliland

ABSTRACT

The maximum usable frequency for any distance is the highest frequency which can be effectively used for radio sky-wave transmission over the given distance. Graphs for the maximum usable frequencies for the latitude of Washington are being published monthly. These graphs are useful in determining the best frequency for communication over a given path at a given time. The general rule is given for determining this optimum frequency: Use the highest available frequency that will not skip. This is more important in the daytime than at night, on account of absorption. The diurnal and seasonal variations recur regularly and the variations with the sunspot cycle may be estimated for a reasonable time in advance, and therefore estimations of future maximum usable frequencies may be made. The methods of applying these graphs to communication problems are discussed.

CONTENTS

		Page
I.	Introduction	81
II.	Relation of vertical- to oblique-incidence transmission	82
III.	Maximum-usable-frequency factors	83
IV.	Maximum-usable-frequency curves	84
V.	Choice of optimum frequency for communication	86
VI.	Examples of use of curves	87
VII.	Experimental check of theory	91
VIII.	Conclusions	92

I. INTRODUCTION

Since June 1937 the National Bureau of Standards has broadcast each Wednesday, from its station WWV, values of the critical frequencies and virtual heights of the principal ionosphere layers, together with the maximum frequencies which could be used for radio sky-wave communication over various distances.[1] Graphs [2] showing the maximum usable frequencies for various distances and times of day, for average conditions during the month have been published and are being published currently. These values of maximum usable frequency are derived from the regular vertical-incidence ionosphere measurements made by the Bureau at Washington, also published currently (see footnote 2). They are representative of conditions at other places on the earth not too widely differing in latitude from that of Washington.

[1] The Weekly Radio Broadcasts of the National Bureau of Standards on the Ionosphere and Radio-Transmission Conditions, National Bureau of Standards Letter Circular LC499 (May 15, 1937).

[2] T. R. Gilliland; S. S. Kirby, N. Smith, and S. E. Reymer, *Characteristics of the ionosphere and their application to radio transmission*, J. Research NBS **18**, 645 (1937) RP1001; Proc. Inst. Radio Engrs. **25**, 823 (1937). *Maximum usable frequencies for radio sky-wave transmission, 1933 to 1937*, J. Research NBS **20**, 627 (1938) RP1096; Proc. Inst. Radio Engrs. **26**, 1347 (1938). *Characteristics of the ionosphere at Washington, D. C.*, series of monthly reports beginning in the September 1937 issue of the Proc. Inst. Radio Engrs.

The method of deriving maximum usable frequencies from vertical-incidence ionosphere measurements has been described elsewhere.[3] It is the purpose of this paper to give a brief discussion of the significance of maximum usable frequencies in communication problems and of the methods of using them.

II. RELATION OF VERTICAL- TO OBLIQUE-INCIDENCE TRANSMISSION

When a radio wave is sent obliquely up into an ionized region, as in transmission over a distance, the ionized medium is able to return waves of frequencies considerably higher than the vertical-incidence

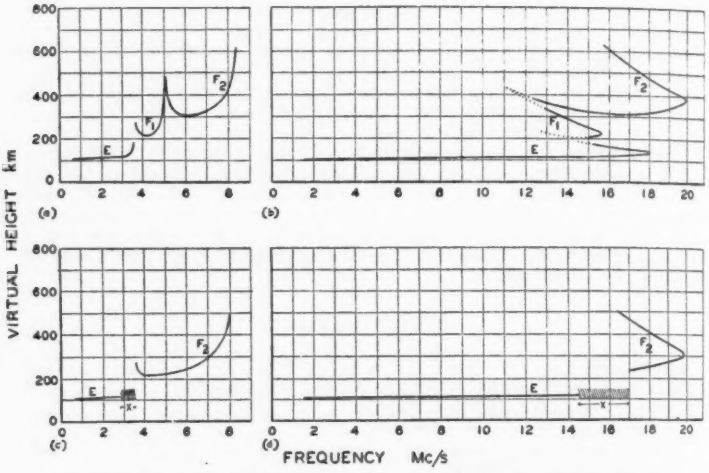

FIGURE 1.—*Vertical and oblique-incidence transmission.*

Curves of virtual height of ionosphere layers against frequency. Curves *a* and *c* are idealized vertical-incidence curves, and curves *b* and *d* are theoretical oblique-incidence curves derived from them for transmission over an 1,800-km path. The dotted portions of the curves show where transmission via a given layer is shielded by reflection from a lower layer. *X* represents a band of frequencies completely absorbed.

penetration frequency. In general, a region of given ionic density returns waves of frequencies which are higher, the greater the angle of incidence upon the layer. Thus, so far as the curvature of the earth permits, higher frequencies can be reflected, the greater the distance of transmission and the lower the height of reflection.

Figure 1 gives typical curves of virtual height against frequency, for vertical incidence, and for oblique incidence (single-hop transmission over a distance of 1,800 km). In general, the virtual heights vary similarly with frequency in both vertical- and oblique-incidence cases, but the oblique-incidence curves turn back at the maximum usable frequency for each layer instead of merely curling up as they do at vertical incidence. Because of this, transmission at the maximum usable frequency of a layer is relatively unabsorbed through penetration of the layer, whereas vertical-incidence transmissions near a

[3] N. Smith, *The extension of normal-incidence ionosphere measurements to oblique-incidence radio transmission*, J. Research NBS **19**, 89 (1937) RP1013; *Application of vertical-incidence ionosphere measurements to oblique-incidence radio transmission*, J. Research NBS **20**, 683 (1938) RP1100; *The relation of radio sky-wave transmission to ionosphere measurements*, Proc. Inst. Radio Engrs. (Publication pending.)

critical frequency are usually highly absorbed.[4] Because of its lower height, the E-layer may often have a greater maximum usable frequency than the F_1 or F_2 layer, although its critical frequency is usually lower.

III. MAXIMUM-USABLE-FREQUENCY FACTORS

It is possible to describe some of the relations between vertical- and oblique-incidence ionosphere transmission in terms of factors by which one may multiply the vertical-incidence critical frequencies to

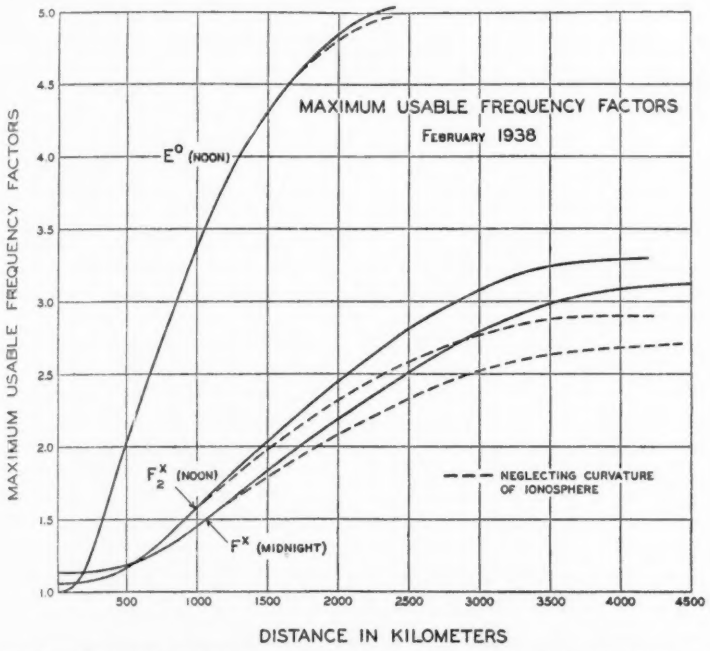

FIGURE 2.—*Factors by which vertical-incidence critical frequencies (ordinary ray or "o"-component) may be multiplied in order to obtain maximum usable frequencies for transmission via the indicated layers, for February 1938.*

Dashed curves are similar factors computed neglecting the curvature of the ionosphere.

get the maximum usable frequencies. It is usually most convenient to refer the factors to the critical frequency for the ordinary ray, or "*o*"-component, even though for *F*-layer transmission the "*x*"-component has the higher maximum usable frequency. Figure 2 shows curves of typical factors by which one may multiply $f^o{}_E$, $f^o{}_{F_1}$, and $f^o{}_{F_2}$ to get the maximum usable frequency by E^o-, $F^x{}_1$-, and $F^x{}_2$-layer transmission, respectively.[5] These factors were calculated for noon and midnight conditions at Washington in February 1938.

These curves indicate the order of magnitude of the values to be expected for these factors. The *E*-layer factors remain essentially the same throughout the year. The midnight *F*-layer factors are

[4] S. S. Kirby, L. V. Berkner, and D. M. Stuart, *Studies of the ionosphere and their application to radio transmission*, BS J. Research **12**, 15 (1934) RP632; Proc. Inst. Radio Engrs. **22**, 481 (1934).

[5] The notation is conventional. Capital letters refer to layers, *f* means vertical-incidence critical frequency and *o* and *x* refer to the wave components.

essentially the same throughout the year, but the noon F_2-layer factors are much less in summer than in winter, because of greater virtual heights in the summer. The F-layer factors are not unity at zero distance, because f^x, is about 800 kc/s higher than f^o, at Washington. The slow increase of the factors with distance at the shorter distances is due to the slow increase of sec ϕ with ϕ for small values of ϕ. The curvature of the earth causes a slowing down of the rate of increase at the greater distances, so that the factors at these distances are not as great as if the earth were flat. The curvature of the ionosphere itself, however, partly compensates for this effect. To demonstrate this, the dashed curves in figure 2 were computed for a flat ionosphere.

IV. MAXIMUM-USABLE-FREQUENCY CURVES

The maximum-usable-frequency data consist of the values of three variables: Distance, frequency, and time of day. These may be

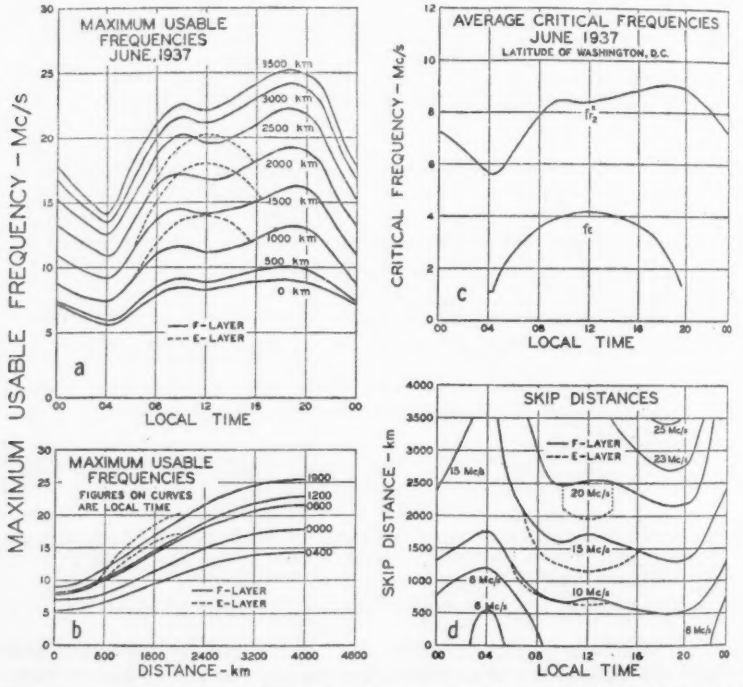

FIGURE 3.—*Methods of plotting maximum-usable-frequency data, June 1937*

The critical-frequency curves, for vertical incidence, are also given to show their close resemblance to the maximum-usable-frequency-time curves, and to suggest the possibility of obtaining the one directly from the other.

plotted usefully in three ways, as shown in figure 3 for average conditions in June 1937:

1. Maximum usable frequency against time of day for various distances (curves *a*);
2. Skip distance against time of day for various frequencies (curves *d*);
3. Maximum usable frequency against distance for various times of day (curves *b*).

Curves *c* show the average critical frequencies at vertical incidence for various times of day during June 1937. The similarity of these curves to those in (*a*) permits the use of approximate factors to obtain maximum-usable-frequency curves from the average vertical-incidence curves for a given month.

Of these three ways of plotting the data, that using the curves of maximum usable frequency against distance is perhaps the least useful, since neither the maximum usable frequencies nor the skip distances vary monotonically with time of day. This type of curve is of interest chiefly where the data are limited, for example, where the maximum-usable-frequency data are available for but one or two definite times, such as noon and midnight. It indicates merely the maximum usable frequencies and the skip distances to be expected for conditions similar to those for which the curves are plotted. For example, where the curve is given for noon, the values may be used as typical for as many hours as those during which the ionosphere conditions resemble noon conditions.

The curves of maximum usable frequency against time of day are the ones published monthly in the Proceedings of the Institute of Radio Engineers by the National Bureau of Standards, and contain the available data most concisely and completely, and in a form which can be readily used. This type of curve is particularly adapted to the service of fixed radio stations, where the distance of transmission is fixed and certain frequencies are available, and it is desired to determine the optimum hours to use certain frequencies or the optimum frequencies to use during certain hours.

The skip distance-time curves present the same data as those given in the maximum-usable-frequency–time curves, but in a form not as well adapted to easy interpolation. This type of curve is particularly adapted to a mobile radio service, where the distance varies continuously, and it is desired to determine the optimum frequency to use in communication with a mobile unit at a given time. This of course applies to distances great enough to necessitate sky-wave communication.

The maximum-usable-frequency curves represent only the first step in the solution of the problem, which is the choice of suitable frequencies for a communication service. The next step consists in determining the maximum usable frequency for a given time and over a specific transmission path.

The geographical part of the ionosphere which controls long-distance high-frequency radio transmission is that part traversed by the wave in passing from the transmitter to the receiver. In the case of single-hop transmission, this part is half-way between the transmitter and the receiver. For places not differing greatly in latitude, ionosphere conditions are essentially the same at the same local time. For places differing greatly in latitude, ionosphere data for the several latitudes should be used if available.

On days when the ionosphere is undisturbed the maximum usable frequency at a given hour may be considered to vary but little (usually not over $\pm 15\%$) from the average for the month. On days of ionosphere storms (disturbances of the ionosphere of the type associated with magnetic storms),[6] however, variations are often greater than 50 percent from the average.

[6] S. S. Kirby, T. R. Gilliland, E. B. Judson, and N. Smith, *The ionosphere, sunspots, and magnetic storms*, Phys. Rev. **48**, 849 (1935).
S. S. Kirby, T. R. Gilliland, N. Smith, and S. E. Reymer, *The ionosphere, solar eclipse, and magnetic storm*, Phys. Rev. **50**, 258 (1936).

The maximum theoretically possible distance range for single-hop transmission, corresponding to zero angle of departure above the horizontal, is about 2,400 km for *E*-layer transmission, and about 3,500 to 4,500 km for F_2-layer transmission, depending on the virtual height of the layer. Practically, it is usually impossible to realize high-frequency communication at this zero angle of departure over land because of absorption at the ground. Observations of transmissions within the continental United States have indicated that angles of departure less than about 3½° do not result in satisfactory communication. If 3½° be assumed as the minimum practical angle of departure over land, the maximum distance for single-hop transmission is about 1,700 km for *E*- and 3,000 to 3,500 km for F_2-layer transmission. Single-hop transmission may often be possible at greater distances, while at the same time multihop transmission may be more efficient.

In determining the maximum usable frequencies for a given time and transmission path, it is necessary to ascertain the number of hops and the type of transmission to be expected over the path, and the local time at the midpoint of each hop. The length of each hop depends on the virtual height at the midpoint; the higher the layer is, the longer the hop. The height, in turn, depends on the frequency; the closer this is to the maximum usable frequency, the greater the virtual height. Table 1 gives approximately the heights in kilometers which may be used in estimating the number and length of hops for frequencies at, 20 percent below, or 40 percent below the maximum usable frequency (abbreviated muf). Since the maximum usable frequency is a function of the length of hop, it is necessary to carry out the calculation by a method of approximation. The existence of paths of different lengths for multihop transmission by the same layer may be important, for one of the hops may involve reflection near the maximum usable frequency, and another hop may involve reflection considerably below it.

TABLE 1.—*Virtual heights to be used in estimating the number and length of hops for transmission via different layers*

Layer	Frequencies		
	at muf	20% below muf	40% below muf
	km	*km*	*km*
Night F	420	350	310
Summer day F_2	450	380	.....
Summer day F_1	220	200	.....
Winter day F_2	350	300	250
E	130	115	110

V. CHOICE OF OPTIMUM FREQUENCY FOR COMMUNICATION

The process has been outlined for determining the maximum usable frequency for the given path and time, but it yet remains to select the optimum frequency for communication from the available frequency spectrum below the maximum usable frequency. We may state a simple rule for this, that is, *choose the highest available frequency that will not skip, allowing for variations in critical frequency.* The varia-

tions of critical frequencies and maximum usable frequencies below the monthly average for a given hour are usually less than 15 percent on the quiet days; therefore we should ordinarily choose a frequency at least 15 percent below the average maximum usable frequency to avoid the danger of skipping. As the frequency is lowered, the absorption of the waves is increased, especially in the daytime. As the absorption increases, the efficiency of the transmission decreases, until conditions may be reached where enormous power is necessary.

In general, however, fair efficiency of communication may be provided in the daytime by frequencies somewhat greater than half the maximum usable frequencies, and at night by frequencies down to somewhat less than half the maximum usable frequencies. Definite limits cannot be set because: (1) there is no sharp dividing line between frequencies at which absorption is high and those at which it is low, and (2) there are large irregular variations of absorption with time over both short and long periods.

At frequencies near the maximum usable frequencies there is relatively little difference between night and day absorption. As the frequency is lowered, however, the daytime absorption increases relatively much more rapidly.

VI. EXAMPLES OF USE OF CURVES

A few examples of the use of the graphs will now be given. First, let us take an example of the use of the skip-distance-time graphs in a mobile radio service. Figure 4 shows a hypothetical airplane trip

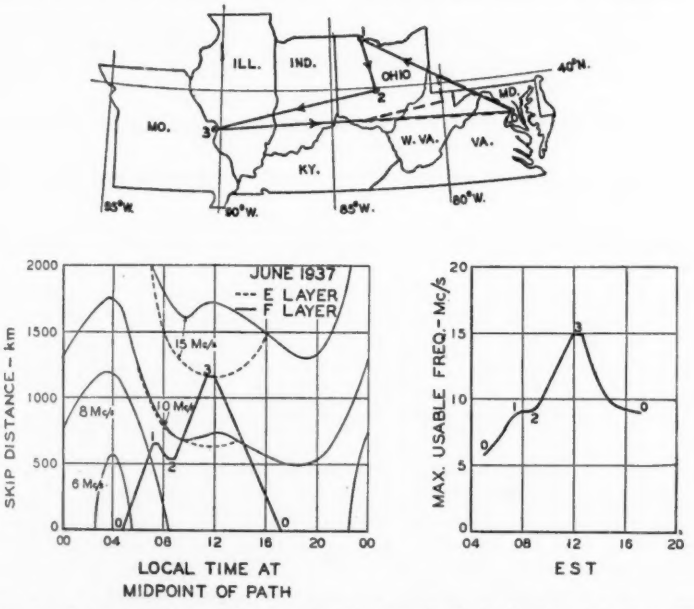

FIGURE 4.—*Determination of frequencies for hypothetical airplane trip from Washington, D. C. (0), to Toledo, Ohio (1), to Columbus, Ohio (2), to St Louis, Mo. (3), and back to Washington.*

Lower left curve is a plot of the midpoint of the path from Washington to the airplane against local time at this midpoint. Curve at lower right is maximum usable frequency for this trip against time at Washington.

in June 1937. The plane is supposed to leave Washington at 0500 EST, flying at 150 miles per hour, and fly to Toledo, Ohio, remaining there 20 minutes; thence to Columbus, Ohio, remaining there 30 minutes; thence to St. Louis, Mo., remaining there 45 minutes, and thence back to Washington at 1720 EST. The heavy dashed line on the map shows the course of the midpoint of the distance from Washington to the plane. This is the place where a radio wave must be reflected from the ionosphere for communication between

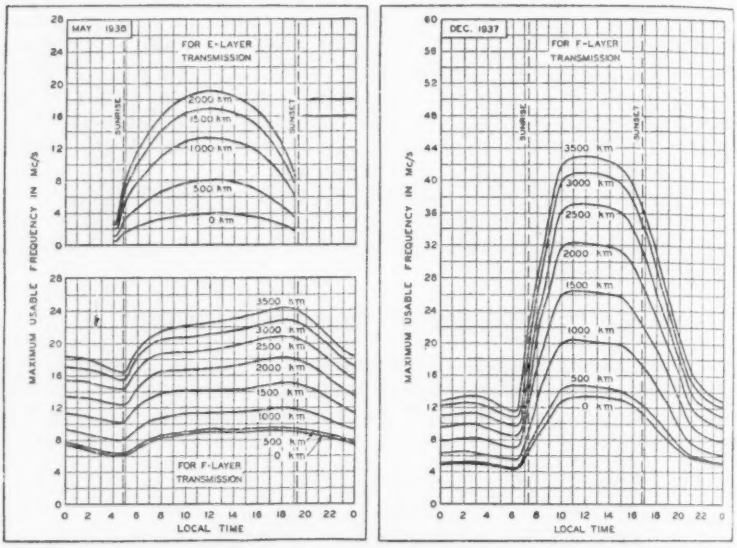

FIGURE 5.—*Maximum-usable-frequency–time curves obtained at Washington for December 1937 and May 1938.*

No *E*-layer curves are given for December 1937, because the maximum usable frequencies for *E*-layer were far below those for *F*-layer transmission.

the plane and Washington. It is the place for which transmission calculations must be made.

To find the maximum usable frequency at any time during the flight, we plot the distance of the plane against the local time at the midpoint of the path. This curve is then placed on the skip-distance-time graphs, as shown at the lower left of the figure, and the maximum usable frequency can be read off for any part of the flight. The lower right-hand graph shows the maximum usable frequencies thus obtained.

Choice of frequencies may then be made in accordance with the rule previously stated, that is, use the highest available frequency that will not skip, in order to avoid absorption. A factor of at least 15 percent should be allowed for variation of the ionosphere from the average conditions for the month. If we allow a factor of 15 percent, and there are available frequencies of, say, 2,500, 5,000, 10,000, and 14,000 kc/s, then: 5,000 kc/s should be used from 0500 to 1000 EST and from 1400 to 1720 EST; 10,000 kc/s should be used from 1000 to 1400 EST; 2,500 kc/s is too low for daytime use and would be highly absorbed; and 14,000 kc/s is too near the maximum usable frequency and might skip.

As an example of the use of the maximum-usable-frequency–time curves in a fixed service, let us take the cases of single-hop transmission from Washington to Chicago, Ill., a distance of 1,000 km, and of two-hop transmission from Washington to San Francisco, Calif., a distance of 4,000 km. Figure 5 shows maximum-usable-frequency–time curves for December 1937 and May 1938, representative of winter and summer conditions at Washington at the present phase of the sunspot cycle. In the winter there are no *E*-layer curves given, for

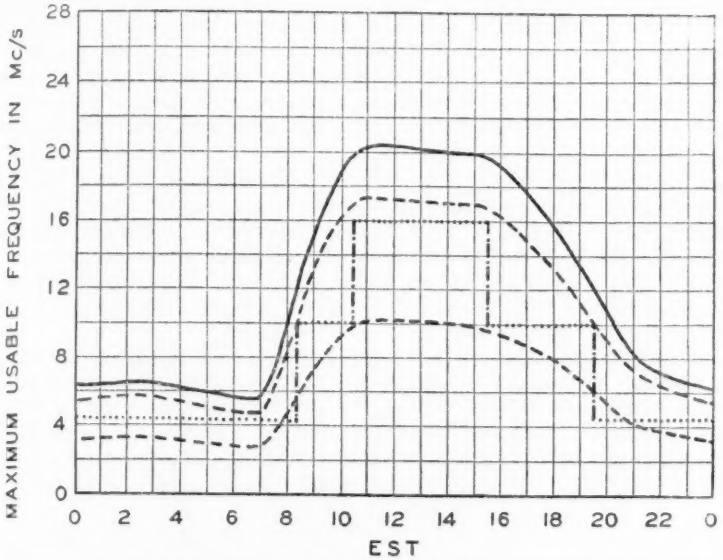

FIGURE 6.—*Graph showing method of determining frequencies to be used over a 1,000-km path in December 1937.*

Dotted lines show frequencies to be used and vertical dot-dashed lines show times for changing frequency.

then the F_2 layer determines the maximum usable frequency in the daytime. In the summer, however, the *E*-layer is the determining factor at some distances.

For single-hop transmission to Chicago the local time at the reflection point is about 22 minutes earlier than at Washington. Washington time is 8 minutes earlier than Eastern Standard Time. The maximum-usable-frequency curve, which reads local time at the midpoint of the path, must be displaced about 30 minutes to the right on the coordinate paper so that the time will be Eastern Standard Time. We shall allow a 15 percent minimum factor of safety to avoid skipping, and avoid as much as possible a case where the frequency employed is 50 percent or more below the maximum usable frequency.

A suggested method for determining the frequencies to be used is as follows. The maximum-usable-frequency curve for 1,000 km should be replotted and displaced as outlined above so that the time is Eastern Standard Time. The resulting curve is shown in figure 6, for December 1937. Two auxiliary curves are drawn on the same graph, one 15 percent below and the other 50 percent below the maximum-usable-frequency curve. These are the dashed curves in figure 6. The frequencies chosen should then lie between these two

auxiliary curves and should be chosen so as to involve as few changes of frequency as possible during the day. The dotted lines show one possible set of frequencies which might be used over this path during this month. These frequencies are: About 4.5 Mc/s from 1930 to 0830 EST; about 10 Mc/s from 0830 to 1030 EST; about 16 Mc/s from 1030 to 1530 EST; and about 10 Mc/s from 1530 to 1930 EST. The vertical dot-dashed lines show the times at which frequency should be changed.

A similar procedure applied to the curves for May 1938, yields the following suggested set of frequencies: About 6.5 Mc/s from 2300 to 0700 EST, and about 9 Mc/s from 0700 to 2300 EST. During the middle of the day, in May 1938, transmission would be by both E and F_2 layers.

Transmission from Washington to San Francisco cannot take place efficiently by one hop, except for a high F layer (such as may be encountered during an ionosphere storm). We must then investigate transmission conditions by two-hop F_2-layer transmission, and one-hop E plus one-hop F_2-layer transmission. For two-hop F_2-layer transmission the local times at the reflection points are about 45 minutes, and 2 hours 15 minutes earlier than at Washington. For the first hop, then, the curves must be shifted to the right by about 53 minutes, and for the second by about 2 hours 23 minutes, in order for the time to read Eastern Standard Time.

Let us consider the case for December 1937. If we again try as much as possible to confine the frequency used between 50 and 85 percent of the maximum usable frequency, the recommended frequencies for each hop are, in terms of local time at the midpoint of the hop, about 6 Mc/s from 2000 to 0730 local time; about 13 Mc/s from 0730 to 0930 local time; about 27 Mc/s from 0930 to 1530 local time; and about 13 Mc/s from 1530 to 2000 local time.

The Eastern Standard Times during which these frequencies may be used over the eastern and western hop, separately, would then be (a) for eastern hop: 6 Mc/s from 2053 to 0823 EST; 13 Mc/s from 0823 to 1023 EST; 27 Mc/s from 1023 to 1623 EST; and 13 Mc/s from 1623 to 2053 EST; and (b) for western hop: 6 Mc/s from 2223 to 0953 EST; 13 Mc/s from 0953 to 1153 EST; 27 Mc/s from 1153 to 1753 EST; and 13 Mc/s from 1753 to 2223 EST.

The maximum usable frequency for the entire path is the lower of the maximum usable frequencies over the two hops. If we combine the results for the two hops, then the recommended frequencies are: About 6 Mc/s from 2053 to 0953 EST; about 13 Mc/s from 0953 to 1153 EST; about 27 Mc/s from 1153 to 1623 EST; and about 13 Mc/s from 1623 to 2053 EST.

At certain times of day the absorption over one of the hops can be avoided only by the use of a frequency greater than the maximum usable frequency over the other hop. These times are thus particularly unfavorable for consistent communication over this path. This condition will be most likely to occur between about 0823 and 1153 EST (absorption being greater on the eastern hop) and between about 1623 and 2223 (absorption being greater on the western hop).

The other possible path, by one-hop E plus one-hop F-layer transmission, must be considered during the daytime. By the geometry of the path the length of the E hop would be about 1,200 km, and the maximum usable frequency would be far below that for F-layer transmission over the same path. The calculation for two-hop F-layer transmission will give the best frequencies to use.

The calculation for two-hop *E*-layer transmission may be made in the same manner for May 1938. For one-hop *E* plus one-hop *F*-layer transmission the length of the *E* hop could be only about 800 km, so the two-hop *F*-layer transmission would be the preferred one here also.

One other point should be noted. If the local time at the transmitter is on the up- or downgoing parts of the maximum-usable-frequency curve for a given distance, then a different frequency should be used for transmitting over that distance eastward from the transmitter than over the same distance westward from the same transmitter. This does not mean that different frequencies should be used in transmitting in opposite directions over the same path. Except in unusual cases, transmission is essentially the same in the two directions over the same path.

VII. EXPERIMENTAL CHECK OF THEORY

Figure 7 shows an example of the type of experimental confirmation of the maximum-usable-frequency theory that has been obtained. The upper part of the figure is a continuous record by the National

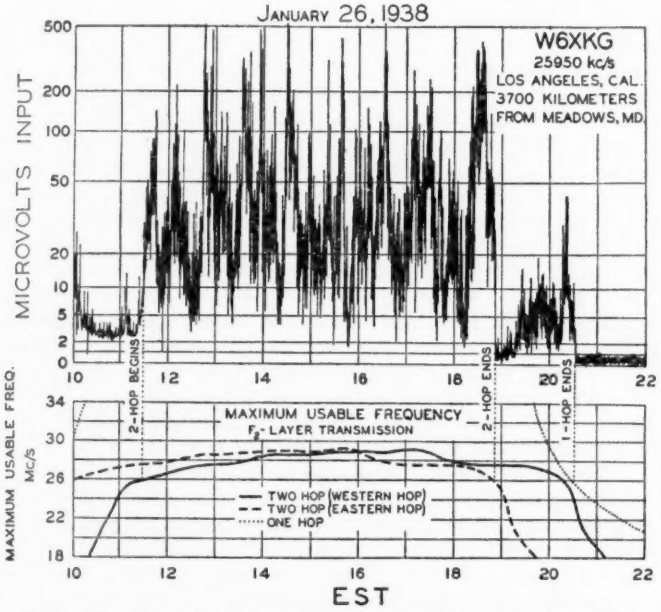

FIGURE 7.—*Field-intensity record of transmission from W6XKG.*

Below are given the maximum-usable-frequency curves computed from ionosphere data taken at Washington on the same day. The major changes in transmission coincide with the times when the maximum usable frequency passes through 26 Mc/s. (The intensity around 1100 EST is really nearly zero; the discrepancy is due to a drift in the zero of the recorder).

Bureau of Standards of the field intensity of W6XKG, Los Angeles, Calif., on 25,950 kc/s, at a distance of 3,700 km. In the lower part are shown graphs of the calculated maximum usable frequency over this distance, for both one- and two-hop transmission. This distance is slightly beyond the maximum distance for good one-hop transmission during the winter day, on the basis of the 3½° angle of depar-

ture. The changes between one- and two-hop transmission are well marked, and the ratio of signal strength is well over 100:1. This difference is due partly to the increased absorption over the flatter trajectory and partly to the unfavorable angle of departure. It should be noted how the times of beginning and ending of two-hop transmission agree with the times the calculated maximum usable frequency passed through about 26 Mc/s at the western and eastern hops, respectively. The two-hop transmission began as soon as the western hop permitted and ended when the eastern hop failed.

After the failure of two-hop transmission, the station still came in by one hop. As the evening progressed the intensity increased, owing to the departure of the daytime absorption and the rise in the height of the layer, with a consequent more favorable angle of departure. The failure of single-hop transmission also is seen to agree with the fall of the calculated maximum usable frequency through 26 Mc/s.

The National Bureau of Standards has checked its calculation of maximum usable frequencies against many records such as this, and it is believed that, for the ionosphere conditions on which they are based, the error is inappreciable for practical purposes. They are assumed to be good, however, only for latitudes nearly that of Washington. Both ionosphere data at other places and observations on transmissions over long paths indicate that there is some latitude difference in ionosphere conditions. When one considers a path such as from Europe to Washington, it is not to be expected that extrapolation would yield results consistent in all details. It has been found, however, that the Washington observations give a fair indication of conditions over even such a path. For more precise results, maximum usable frequencies over such paths should be based on ionosphere observations at latitudes closer to those at which reflections occur.

VIII. CONCLUSIONS

Approximate values of the factors by which the critical frequencies can be multiplied to obtain the maximum usable frequencies may be tabulated for various seasons and times of day. Thus maximum usable frequencies may be obtained from vertical-incidence critical frequencies, and vice versa. These factors probably do not vary greatly with latitude, at least outside the polar regions. The use of these factors may well extend quite appreciably the geographical range of our ionosphere knowledge.

To summarize, the following may serve as a guide in choosing best frequencies for a given path.

1. The smallest number of hops, consistent with the absorption and a favorable angle of departure, is best.
2. The highest frequency, up to within a variation factor (usually about 15%) of the maximum usable frequency, is best.
3. The lower the frequency the greater the absorption and the less the efficiency of transmission.

And finally, the use of the maximum-usable-frequency factors, in conjunction with our present knowledge of ionosphere conditions, suggests the possibility of estimating usable frequencies months and perhaps even years in advance, in accordance with the variations of season and of the sunspot cycle.

WASHINGTON, August 22, 1938.

U. S. Department of Commerce National Bureau of Standards

RESEARCH PAPER RP1168

Part of Journal of Research of the National Bureau of Standards, Volume 22, January 1939

NOTE ON THE SPECTRAL REFLECTIVITY OF RHODIUM

By W. W. Coblentz and R. Stair

ABSTRACT

The spectral reflectivity of rhodium in the ultraviolet and in the visible spectrum is described. The samples examined consisted of mirrors of rhodium deposited electrolytically on plate glass and upon a highly polished surface of copper. The reflectivity of rhodium decreases rapidly with wave length, to a low value in the ultraviolet. In the visible spectrum the reflectivity is somewhat higher than for chromium, and hence rhodium is more efficient as a reflecting surface.

Because of the relatively high reflecting power of rhodium for visible radiation and its resistance to tarnish, electroplated surfaces of this metal have in recent years come into commercial use in plating jewelry and as mirrors for searchlights, headlights, etc.

The object of this note is to supply the demand for information on the spectral reflectivity, particularly in the ultraviolet, of recent productions of highly polished surfaces of rhodium, prepared on a commercial scale, by electrolytic deposition on polished glass, copper, or other suitable material.

To complete the description of the reflectivity of rhodium from the extreme ultraviolet into the far infrared, reference is made to a previous paper [1] [1] on the infrared reflecting power of a highly polished surface on an ingot of rhodium prepared by von Wartenberg [2]. It was found that the reflecting power increases rapidly from about 77 percent in the yellow (579 mμ) to 92 percent at 2,500 mμ (curve 3, fig. 1), beyond which point the reflectivity increases gradually to about 94 percent at 9,000 mμ [1]. The reflectivity (77 percent) in the visible spectrum is in good agreement with the measurements on the best sample of the herein described electroplated deposits. The much lower ultraviolet reflectivity values obtained in 1930 on another ingot of rhodium [6] are to be ascribed to the condition of the surface of that sample, which contained blowholes and was not so highly polished.

It is to be noted that the reflectivity in the ultraviolet is easily affected by the method of preparation of the mirror (cathode sputtering, etc.) and by the kind of polishing material used. The present contribution therefore reveals the performance that may be expected of present-day commercially prepared rhodium mirrors.

The apparatus used in making the herein described spectral-reflectivity measurements in the ultraviolet, visible, and near infrared spectrum consisted of a quartz-fluorite achromatic lens spectrometer [5] and a vacuum thermopile. The source of radiation was a vertical quartz-mercury-vapor (Uviarc) lamp. By means of a quartz-fluorite lens an image of the luminous column of mercury vapor was

[1] Numbers in brackets indicate the literature references at the end of this paper.

focused upon the entrance slit of the spectroradiometer, and the spectral intensities were measured, after reflection from (a) the hypotenuse face of a right-angled quartz prism and (b) after reflection from the mirror (in this case, rhodium) under investigation. During the latter measurement a thick quartz plate was placed before the spectrometer slit to compensate for the reflection losses at the surfaces and the change in optical path when the rays pass through the quartz

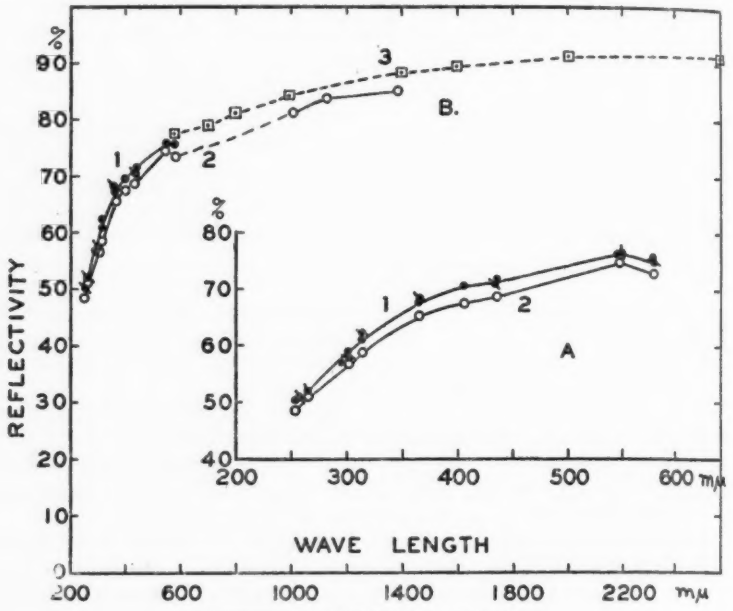

FIGURE 1.—*Reflectivity of rhodium*

Curve 1, electrolytic deposit on glass; curve 2, electrolytic deposit on polished copper; and curve 3, mirror surface, polished on an ingot of rhodium.

prism [3, 4]. In this manner the reflectivity data are obtained without making any corrections.

Two of the mirrors of rhodium included in this report were prepared by electrolytic deposition on plate glass. Whether the first conducting coating on the glass was copper or silver was not disclosed by the manufacturer (name not disclosed). These samples, which were submitted by the Electrical Testing Laboratories, were entirely opaque, except for a few small-sized holes. As shown in figure 1, curve 1, there is no appreciable difference in their ultraviolet spectral reflectivity.

Several mirrors were available in which the rhodium was deposited electrolytically upon a thick, flat plate of optically polished copper. They were made by the Bart Laboratories, Inc., Belleville, N. J. The sample (size about 5 by 5 cm) selected for measurement was deposited from a solution taken from a large tank used in the factory for plating large mirrors.

Although the rhodium mirror that was deposited electrolytically on copper appeared to have a finer surface, as shown in figure 1, curve 2, the spectral reflectivity is a few percent lower than that of the samples deposited on glass.

In both kinds of mirrors (deposited on glass and on metal) the spectral reflectivity of rhodium decreases rapidly with wave length in the ultraviolet and is so much lower than that of chromium and aluminum that it is not a promising source of material for mirrors for reflecting ultraviolet radiation [4]. Because of its high reflecting power in the visible and near infrared, as shown in figure 1, rhodium is more suitable than chromium (previously described [4]), as a material for reflectors of visible radiation.

Repeated measurements on these mirrors showed a slightly lower reflectivity at 579 mμ than at 547 mμ (see fig. 1), followed by a much higher reflectivity beyond 1014 mμ in the infrared. Apparently, there is a slight flattening of the reflectivity curve in the region of 600 to 700 mμ, similar to the low reflectivity observed in chromium [4]; but confined to a much narrower spectral band, as observed in tungsten [3], which has a narrow minimum of reflection at about 800 mμ.

In conclusion, it is to be emphasized that in the present state of development, electroplated mirrors of rhodium are found to differ appreciably from sample to sample in the total amount of light reflected. However, there appears to be a similarity in the general trend of their spectral reflectivity. The possibility of electroplating or evaporating rhodium on astronomical mirrors is foreshadowed.

---

[1] W. W. Coblentz, Bul. BS. **7,** 197 (1911) S152.
[2] Von Wartenberg, Verhandel. Phys. Ges. **12,** 121 (1910).
[3] W. W. Coblentz and W. B. Emerson, BS Sci. Pap. **14,** 307 (1918) S308.
[4] W. W. Coblentz and R. Stair, BS J. Research **2,** 343 (1929) RP39.
[5] W. W. Coblentz, R. Stair, and J. M. Hogue, BS J. Research **7,** 738 (1931) RP370.
[6] W. W. Coblentz and R. Stair, BS J. Research **4,** 189 (1930) RP141.

WASHINGTON, September 20, 1938.

115782—39——7

U. S. Department of Commerce National Bureau of Standards

RESEARCH PAPER RP1169

Part of Journal of Research of the National Bureau of Standards, Volume 22, January 1939

AN IMPROVED RADIO METEOROGRAPH ON THE OLLAND PRINCIPLE

By L. F. Curtiss, A. V. Astin, L. L. Stockmann, and B. W. Brown

ABSTRACT

A description is given of the construction and tests of a radio telemeter of high precision built according to the Olland principle, in which all indicating arms rotate on a common axis. Combined with a 5-meter radio transmitter of push-pull type, this telemeter provides a radio meteorograph which has been tested under actual working conditions and found to be reliable and accurate in its indications. Since it gives relatively strong signals with a good stability in frequency, it is easy to operate and very little retuning during an observation is required. Special attention has been given to the thermal insulation of the compartment containing batteries and transmitter so that no failures due to drop in battery temperature have been observed even at altitudes above 60,000 feet. The cost of manufacture compares very favorably with that of other models recently developed in this country.

CONTENTS

	Page
I. Introduction	97
II. Radio telemeter	98

I. INTRODUCTION

In September 1935 the authors described [1] the results of their preliminary investigation into the possibilities of developing a practical system for observation of temperature, pressure, and relative humidity at high altitudes by means of radio-equipped sounding balloons. As there reported, the radio problems involved are very simple, and by using the Olland principle, which requires the transmitter to be in operation for a very small fraction of the observation period, relatively strong signals of 5-meters wave length can be obtained at all attainable altitudes and for distances of a hundred miles or more.

Attention has since been turned to the development of a radio telemeter which would be accurate in its indications and convenient to attach to a sounding balloon. In this period many models have been tested both in the laboratory and in the air. The chief problems encountered were those of: (1) Reliable keying contacts; (2) consistent indicating system for the sensitive elements; (3) adequate ventilation for the sensitive elements; (4) stable antenna position during flight; (5) maintenance of battery temperatures; and (6) dependable and uniform operation of the driving mechanism. The model here described has shown in repeated tests that these problems have been solved to the extent that they no longer interfere with reliable and accurate operation of the instrument.

[1] L. F. Curtiss and A. V. Astin, J. Aeron. Sci. 3, 35 (1935).

II. RADIO TELEMETER

The preliminary experiments were made with clock-driven equipment. These trials served a very useful purpose in testing the range and stability of the radio signals, but it soon became evident that escapement errors introduced by the clock movement seriously limited the accuracy. Furthermore, even slight decreases in temperature frequently caused the clockwork to stop, especially if the pressure on the contact arms carried by the motor was sufficient always to give dependable signals. Tests were therefore made of small direct-current motors,[2] which convinced us that they would provide a more satisfactory driving mechanism. Slow changes in speed could be corrected for automatically [3] in reading the record. Through cooperation of manufacturers small electric motors were made available. These weighed less than 50 grams and required about 5 milliamperes at 1.5 volts for their operation. Tests of their speed fluctuations revealed that the slow variations present could be kept to less than a few percent. In addition, these motors rarely stop in flight since they operate without lubricants and have about 100 times the power of a spring-driven clock of the same weight.

To protect the batteries and transmitter from excessive reductions in temperature, a thermally insulated inclosure is required. Likewise, the motor and electrical contacts for keying the transmitter should be protected from icing and other unfavorable conditions. We have found that a box with cellular walls made up of several layers of corrugated paper is best for this purpose. This inclosure is built up of several layers of corrugated paper glued together. The thermal insulation secured in this way is far superior to that provided by balsa-wood containers. This is shown by the following values which give the interior temperatures at approximately 5-minute intervals after surrounding the outside of the thermal inclosure with dry ice, −78° C. An inclosure with ¼-inch balsa-wood walls will drop to dry-ice temperature in about 12 minutes under the same conditions.

Time	Inside temperature
	°C
1:17	28
1:22	25
1:30	6
1:35	2
1:40	−6
1:45	−7
1:55	−10
2:00	−13

It should be pointed out that Cellophane inclosures of the type described previously [4] are in every way superior for maintaining the temperature of the battery inclosure at a high level in comparison with the external temperatures at the higher altitudes when the sun is above the horizon. For this reason Cellophane inclosures are still used by the authors [5] for cosmic-ray balloon equipment, which is

[2] L. F. Curtiss and A. V. Astin, Rev. Sci. Instr. **7**, 358 (1936).
[3] The authors are indebted to D. M. Little and A. H. Mears of the U. S. Weather Bureau for a simple device for this purpose.
[4] L. F. Curtiss and A. V. Astin, J. Aeron. Sci. **3**, 35 (1935).
[5] L. F. Curtiss, A. V. Astin, et al., Phys. Rev. **53**, 23 (1938).

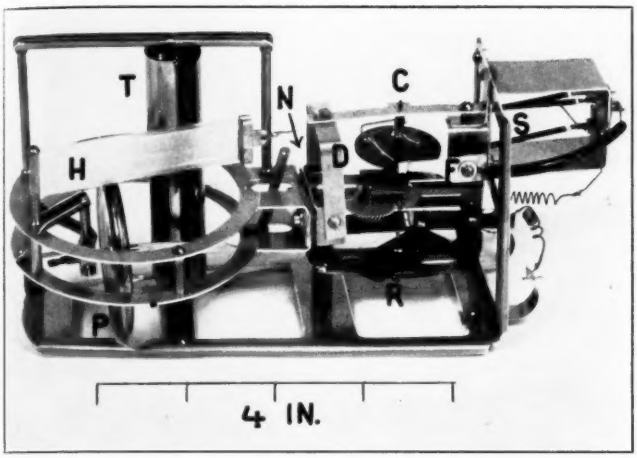

FIGURE 1.—*Olland type radio telemeter driven by electric motor.*

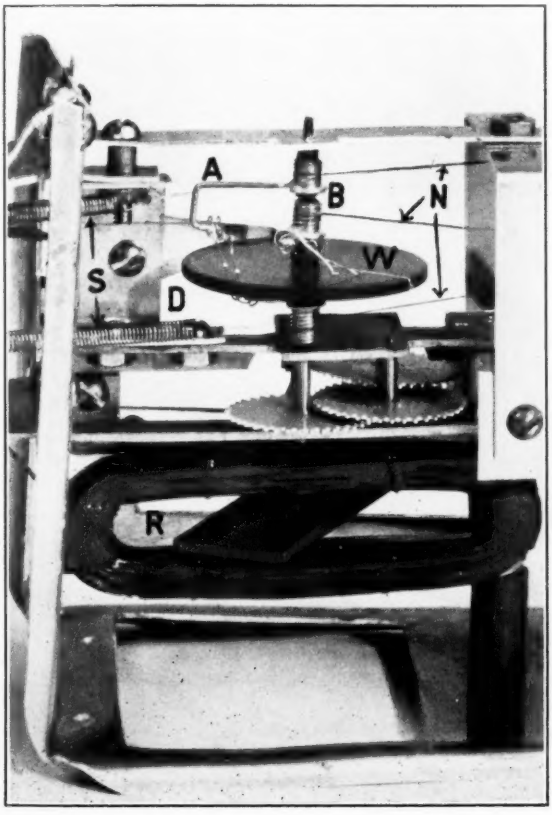

FIGURE 2.—*Detailed view of contact system of Olland type telemeter.*

FIGURE 3.—*Sample of actual tape record from telemeter, showing one Olland cycle.*

FIGURE 4.—*Assembled radio meteorograph ready for release.*

released almost exclusively when the sun is above the horizon. However, the majority of radio-meteorographic observations are made by the Weather Bureau at night, and therefore the corrugated-paper inclosure was adopted to reduce heat loss as much as possible. In this way satisfactory results have been obtained without the use of auxiliary means of heating the interior.

With such an arrangement it becomes necessary to design the telemeter so that the sensitive elements can be outside the thermal inclosure and the motor and contacts inside. Our method for accomplishing this can be explained by reference to figures 1 and 2, which are two views of the telemeter. The electric motor, of which *R* is the rotor, is mounted in a light aluminum frame used to support also the pressure, temperature, and humidity elements, *P*, *T*, and *H*. The contact system, *C*, shown in more detail in figure 2, is mounted directly on the output spindle of the motor, which turns at a speed of 4 revolutions per minute, giving four complete sets of measurements per minute. The contact system consists of a Bakelite disk, *D*, rigidly attached to the output spindle and turning with it. Imbedded radially in this disk is the platinum wire, *W*, which is in electrical contact at one end with the motor spindle. The exposed side of this wire, which is bent around and similarly imbedded in the lower surface of the disk, *D*, is polished down even with the surface of the disk. This permits electrical contact with the indicating arms without disturbing their angular position. These indicating arms, as shown at *A*, figure 2, are fastened to brass sleeves, *B*, threaded on the outside and provided with Bakelite bushings inside. Each of these arms is tipped with a double prong of fine platinum-iridium wire. The Bakelite bushings, lubricated with dry graphite, fit smoothly on the output spindle of the motor. The threaded brass sleeves are connected with their respective indicating elements by the fine Nichrome wires, *N*, each one of which passes from the free end of a sensitive element around a separate threaded sleeve, *B*, and is attached to a tension spring, *S*, anchored through an insulator to the right-hand side of the frame in figure 1. In this way linear displacements of the sensitive elements are transformed into angular displacements of the indicating arms of the contact system so that backlash is reduced and the number of moving parts is kept at a minimum. Since the spindle on which the indicating arms are pivoted is in constant rotation, and as there is some vibration in addition from the motor, no difficulty has been encountered in securing a reliably responsive action from the contact arms.

Since the electric motor has considerable power, the limit to the pressure of the tips of the indicating arms on the Bakelite disk is determined by the indicating systems. This pressure must not be so great as to cause dragging of the contact arms. By use of the platinum-iridium tips mentioned above, it has been found easy to obtain reliable electric contacts with moderate pressures. To insure the stability of the indicating systems relatively powerful elements have been used. The bimetallic spiral, *T*, (fig. 1) and the pressure diaphragm, *P*, have been designed to give strong positive action under all conditions. For the humidity element, *H*, goldbeaters skin has been used, which can be readily cut to a size of sufficient strength and has been found to be several times as responsive as human hair. Its response to changing conditions of humidity has also been found to be

more definite. The diameter of the threaded boss sleeves, *B*, has been chosen with relation to the linear travel of the sensitive elements to give about 1½ turns of the indicating arms for the required ranges of temperature and pressure. The humidity arm is limited to ½ turn, which has been found quite satisfactory.

The electrical circuit for keying the transmitter consists of the insulated anchor springs, *S*, and Nichrome wire cables which are in electrical contact with the brass sleeves, *B*, and therefore also with the indicating arms, *A*. The platinum-iridium tips of these arms contact the wire, *W*, which is grounded to the motor frames. Thus the keying leads are attached, one to the remote ends of the anchor springs in parallel and the other to the frame. An additional contact at *F* is fixed and connected to the insulated ends of the anchor springs. This provides the reference signal to mark off the separate Olland cycles on the record.

The double prong of platinum-iridium mounted at the tip of each indicating arm by means of which electrical contact is made with wire, *W*, has a spacing which is different for each of the three arms. Thus a different double contact is made for the indication for each element which can be identified at once on the record. This is of great value both in calibration and in observations, particularly where, as in the present case, the indicating arms cover more than one Olland cycle. A further convenience in calibration, where each element is calibrated separately, is that the other two may be disconnected so as to give no signal. A typical record for 1 cycle is shown in figure 3, which shows a strip of actual record. The characteristic spacings of the three doublets, *P*, *T*, and *H*, are easily observed. Signals, *RR*, are made by the fixed contact marking the beginning and end of an Olland cycle. Stylograph tape is used for recording in a tape chronograph driven by a synchronous motor operated from alternating-current mains.

The framework supporting the sensitive elements is circular so that it may support a cylindrical solar shield of paper covered on both sides with aluminum foil. In the model shown, the distance between the circular frame and the motor spindle has been made as short as convenient. However, this distance may be increased if desired. This might be necessary under some conditions to protect the sensitive elements more effectually from the radiation from the warmer inclosure containing the batteries and transmitter.

The complete radio meteorograph, consisting of telemeter, transmitter, batteries, and antenna, is assembled as shown in figure 4. The small cylinder at the right is the solar shield inclosing the sensitive elements. The other cylindrical container is the thermal inclosure for transmitter motor and batteries. The frame of the telemeter forms a rigid connecting link between the thermal inclosure and the solar shield. The antenna is brought out of the top of the thermal inclosure, permitting it to be stretched straight up along the supporting cord. A top view with cover removed is shown in figure 5, where the sensitive elements *P*, *T*, and *H* are labeled. Inside the thermal inclosure may be seen the oscillator, *O*, of the transmitter and one 45-volt *B* battery, *V*. Figure 6 is a bottom view, where the other 45-volt battery, *V*, and the filament battery, *G*, may be seen.

An advantage of this general arrangement in which the telemeter is treated as a unit is that the telemeter may be used with any trans-

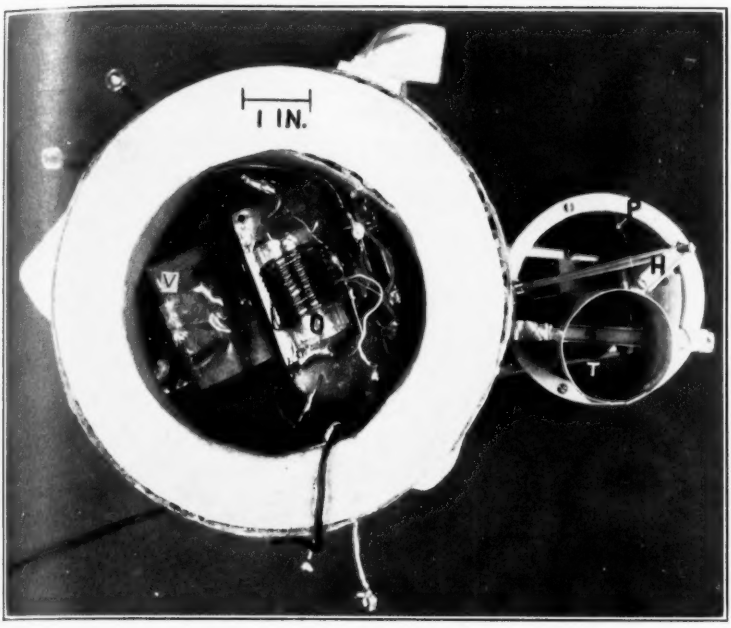

FIGURE 5.—*Interior of radio meteorograph viewed from top.*
Outer solar shield has been removed.

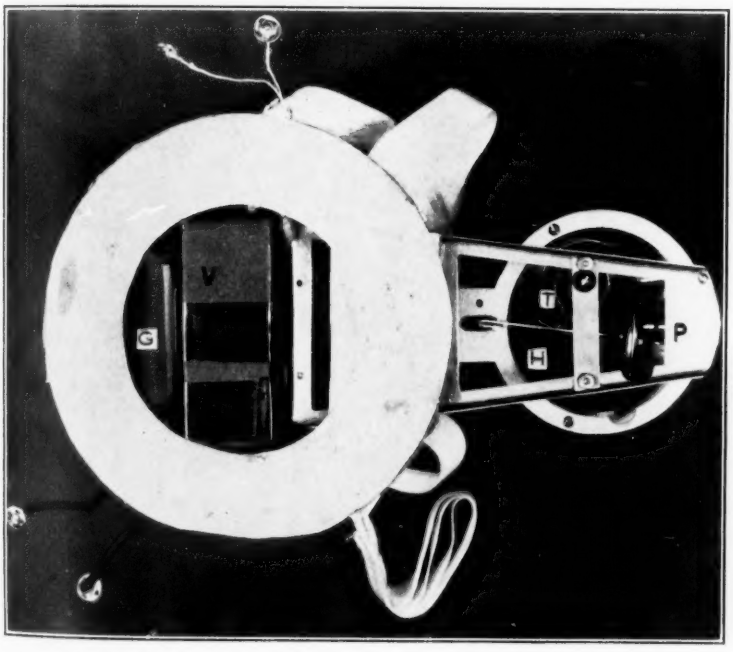

FIGURE 6.—*Interior of radio meteorograph viewed from below.*

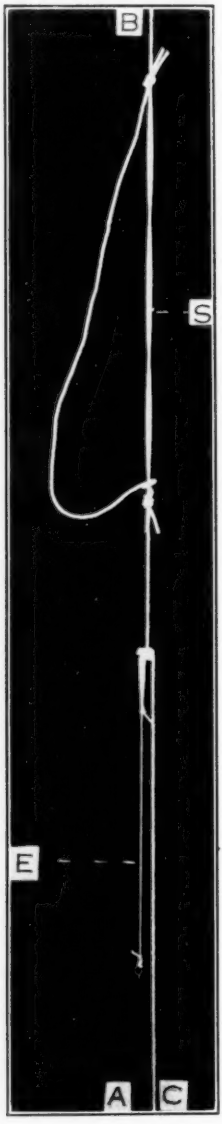

FIGURE 7.—*Arrangement for suspending radio meteorograph from balloon to maintain straight, vertical antenna.*

mitter desired. Furthermore, since they are calibrated independently of the transmitter, a number of calibrated telemeters may be held in reserve ready for use. In those cases where reconditioned instruments are used after recovery from flight, the telemeter may be separated readily from the remainder of the instrument and repaired and recalibrated as a separate unit. Since in the repair of the telemeter and of the transmitter two different types of operations are involved, this is a convenience.

Special attention has been given to the position of the voltage-fed antenna. It has been found desirable to maintain this antenna in a taut vertical position and to prevent excessive swinging of the instruments below in order to preserve strong signals with reasonable stability in frequency. The suspension system shown in figure 7 has been found satisfactory and does not require the antenna to take the full weight of the instrument. *A* in figure 7 is the antenna and *C* the load cord, both of which are attached to the instrument some distance below the section shown. *E* is an elastic cord which holds the antenna stretched and limits the pull upon it. *S* is a heavy-elastic shock cord by which the whole weight is suspended, which reduces considerably the tendency of the antenna to swing. The cord at *B* is attached to the balloon or parachute.

The radio meteorograph has been subjected to numerous laboratory tests. These show that the telemeter is capable of measuring temperatures to $\pm 0.5^\circ$ C. The response of the humidity element is rapid and exceeds in magnitude by several times that of human hair. The time lag is too great to give very accurate readings with ascensional rates usually used. However, the changes in humidity are very clearly revealed and an accuracy of ± 5 percent can be obtained under favorable conditions. In a discussion of the precision of the instrument, it should be noted that the demand for accuracy of the pressure element is much greater than that required of the temperature element. It is desirable in many cases to know the pressure to within 1 millibar, if possible, whereas a knowledge of the temperature to the nearest degree is usually adequate. This represents an accuracy of about 0.1 percent of the total pressure range and only 1 percent of the total temperature range. Therefore, in precision tests we have paid most attention to the pressure indications.

The best illustration of the actual precision of which the indicating mechanism used in this radio meteorograph is capable is provided by the authors' experience with a radio barograph constructed in the same way as the radio meteorograph but without temperature or humidity elements. Approximately 50 of these instruments have been sent aloft and about 30 have been returned intact. These returned instruments were recalibrated and the data compared with the original curves. We have found that about 50 percent of the original calibration points reproduce to within ± 1 millibar and that not more than 10 percent were off by as much as ± 3 millibars. An actual example of this reproducibility of results is shown in the curve in figure 8, which shows the original calibration curve of a barograph and the check points determined after the recovery from an ascension to 92,000 feet. None of the check points depart by more than 1 millibar from the original curve.

To test the effectiveness of the solar shield and thermal insulation of the battery box several test flights have been made with models assembled as described above. Weakened signals of varying frequency due to drop in battery temperatures as well as slowing of the motor would be expected in the absence of sufficient protection for the battery compartment. In all flights strong signals of frequency constant to ±60 kilocycles (0.001%) were received both on the ascent and also on the descent where the rate of fall was sufficiently slow. In some of the flights the slot cut in the battery box to admit the telemeter was left open. This resulted in a slowing of the motor

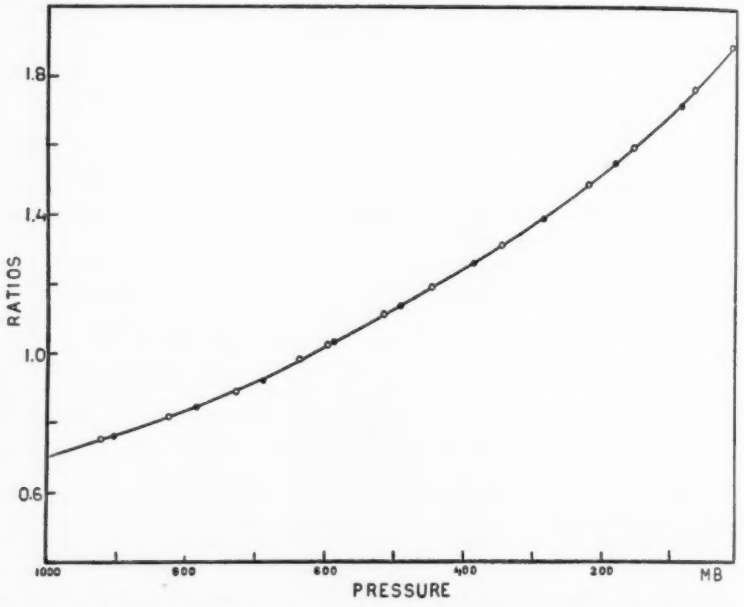

FIGURE 8.—*Calibration of curve of pressure element with redetermined points to show accuracy and reproducibility.*

Solid circles, original calibration; and open circles, recalibration. Maximum deviation, 1 millibar.

at the higher altitudes. When this opening was properly closed very little change in motor speed was observed.

The question of accuracy under actual working conditions is difficult to deal with in the absence of a standard for comparison. The best we can offer is a comparison of one of our records made on July 20, 1938 at 5:37 a. m. with one made for the Weather Bureau by the Navy, using a Navy type of instrument [5] released at a point about 8 miles away at 6:00 a. m. This record is shown in figure 9 plotted on an adiabatic chart. There is a consistent difference throughout in the temperatures, ours being above. At the present time we have no adequate explanation for this discrepancy. It is possible that the calibration of one or both instruments used in the above comparisons

[5] H. Diamond, W. S. Hinman, Jr., and F. W. Dunmore, Bul. Am. Meteor. Soc. **18**, 73 (1937).

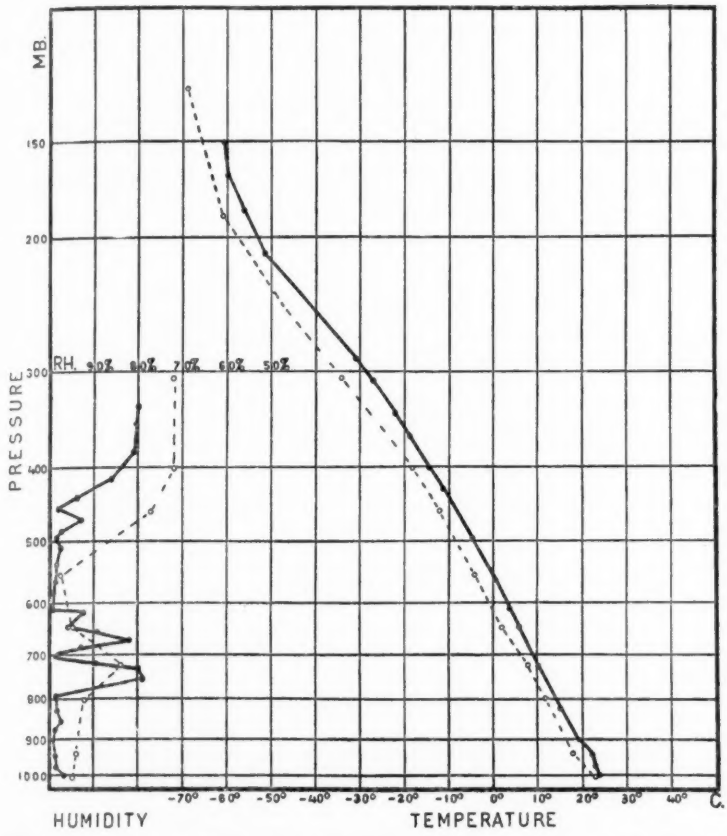

FIGURE 9.—*Records of Navy type instrument (dotted lines) plotted on same chart with data (solid lines) obtained by authors' instrument.*

Instruments released about the same time at points 8 miles apart.

was in error. The general agreement in trends is very satisfactory and indicates that these methods can be used reliably to obtain upper-air data.

We acknowledge the aid of the United States Weather Bureau in providing means for the construction and test of the telemeter and for suggestions regarding improvements and modifications.

WASHINGTON, September 28, 1938.

U. S. DEPARTMENT OF COMMERCE NATIONAL BUREAU OF STANDARDS

RESEARCH PAPER RP1170

Part of Journal of Research of the National Bureau of Standards, Volume 22, January 1939

X-RAY DIFFRACTION PATTERNS OF CRYSTALLINE SOL RUBBER PREPARED FROM ETHEREAL SOLUTION

By George L. Clark,[1] Siegfried T. Gross,[2] and W. Harold Smith

ABSTRACT

Included in an earlier publication on the X-ray diffraction patterns of sol, gel, and total rubber, obtained from stretched and from frozen specimens, was a pattern of discrete gel rubber crystals which had been formed in an ethereal solution at temperatures between −40° and −50° C. Attempts to obtain a pattern of sol crystals, formed similarly in ethereal solution, failed, in spite of the fact that an examination of them in polarized light indicated a crystalline structure.

By using more of the crystalline sol rubber, and a shorter distance from specimen to film in the X-ray technique, a pattern has been obtained, the measurements of which agree with those reported for the crystals mentioned in the previous paper.

CONTENTS

	Page
I. Introduction	105
II. Preparation of the specimens	106
III. X-ray measurements	106

I. INTRODUCTION

In a previous publication [3] there was reproduced an X-ray diffraction pattern of crystals obtained from a solution, cooled to temperatures between −40° and −50° C, of an ether-gel fraction of rubber from *Hevea brasiliensis*. Measurements of three strong interferences indicated that the crystals were similar to those of stretched gel rubber and of frozen sol, gel, and total rubber. Although many attempts were made at that time, unsatisfactory diffraction patterns were obtained with crystalline ether-sol rubber. The interferences were faint and not suitable for accurate measurement and analysis. Since the crystalline material is bulky and some specimens are more compact than others, it seemed possible that the average number of cell diameters was too small to permit sharp definition, and that more material was required for the examination by X-rays. However, it is not certain that lack of definition was caused by insufficient crystalline rubber. The possibility that parts of the long-chain molecules become crystalline and that parts remain amorphous is not excluded, and might be its cause. Additional work with crystalline sol rubber, using a slightly different experimental procedure and more material than in earlier experiments, finally resulted in a satisfactory pattern.

[1] Professor, University of Illinois.
[2] Special Research Appointee, University of Illinois.
[3] George L. Clark, Enno Wolthuis, and W. Harold Smith, J. Research NBS **19**, 479 (1937) RP1039.

II. PREPARATION OF THE SPECIMENS

The crystalline sol rubber, prepared as has been previously described,[4] was collected by filtration in a paper thimble having a smooth inner surface free from detachable fibers. During filtration, a cold current from solid carbon dioxide was impinged upon the opening of the thimble. To remove amorphous rubber, the crystalline material was thoroughly washed with successive portions of ethyl ether, which were chilled to temperatures below −35° C to avoid dissolving the crystals. The ether was finally displaced by 95-percent ethyl alcohol which had been previously cooled to −10° C, and the thimble was transferred to a glass container filled with cold alcohol. The container, packed in solid carbon dioxide, was shipped to the University of Illinois for examination by X-rays.

III. X-RAY MEASUREMENTS

For the present investigation the collimating tube of the low-temperature cylindrical camera of Wolthuis [5] was lengthened, and, as a result, patterns could be made at a distance of approximately 2.6 cm. The exact distance from the specimen to the film was determined by calibration with sodium chloride. The specimen holder was cooled by the exhaust from solid carbon dioxide.

Typical X-ray patterns which have been obtained are shown in figure 1(a, b, and c). They represent successive attempts to procure well-defined interferences. A double halo is present in figure 1(a). This pattern was produced by unfiltered $K\alpha$ radiation from copper, and it is entirely different from that of gel rubber and of unstretched total rubber. The spacings corresponding to the two rings differ completely from the one fundamental halo which is characteristic of unstretched total rubber. The pattern could be interpreted as that of a liquid crystal rather than of a three-dimensional solid. The melting of some of the crystals during the transfer of the sample to the cooled camera could be assigned as its origin, even though the opaque crystalline rubber, stable below approximately 0° C, had not become noticeably transparent, as is usual when the crystals melt completely. The pattern with the double halo was obtained with three samples of the same lot of crystalline sol rubber, and at first was thought to have a special significance. However, there had been evidence of faint but definite interferences in other samples, and observations of crystalline rubber between crossed nicol prisms indicated that the pattern of a truly crystalline material should be obtained.

[4] W. Harold Smith, Charles Proffer Saylor, and Henry J. Wing, BS J. Research **10**, 479 (1933) RP544.
[5] See footnote 3.

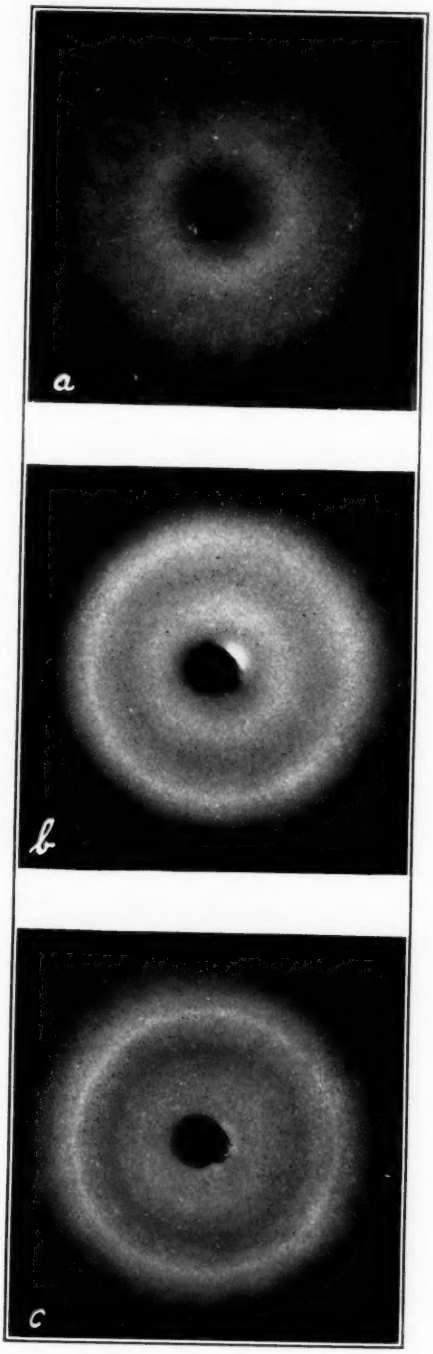

FIGURE 1.—*X-ray patterns shown in figures (a, b, and c) represent successive attempts to obtain well-defined interferences with crystalline sol rubber, produced from ethereal solutions.*

The double halo in figure 1 (*a*) is different from that of gel rubber and of unstretched total rubber. The latter produces one fundamental halo. In figure 1 (*b*) the double halo is partially resolved, and in figure 1 (*c*) the resolution is sufficient to permit measurements of the interferences.

UNIV. OF MICH.

TABLE 1.—*X-ray diffraction results*

R	*θ*	*d*
Crystallized sol rubber—Distance from specimen to film, 2.57 cm		
cm	*Degrees*	*A*
0.65	7°6′	6.21
.82	8°51′	5.00
1.01	10°44′	4.14
1.14	11°57′	3.71
Crystallized gel rubber—Distance from specimen to film, 10.32 cm		
2.62	7° 7.5′	6.19
3.31	8°53.5′	4.97
4.04	10°41.5′	4.14
"Frozen" sol rubber—Distance from specimen to film, 10.32 cm		
2.63	7°9′	6.18
3.32	8°55′	4.96
3.61	9°38′	4.15
4.59	11°59′	3.70

Patterns shown in figure 1(a and b) were obtained with unfiltered $K\alpha$ radiation from copper during an exposure of 3 hours. In figure 1(b) partial resolution of the double halo has taken place, and in figure 1(c) it has proceeded to definite interferences, which were measured. The results in table 1 were obtained with four lines, and for comparison, interplanar distances of similar lines from crystallized gel rubber and from "frozen" rubber are reproduced. Frozen gel and frozen total rubber gave similar values which are not included. In the table, d is the distance between the set of planes making an angle θ with the incident beam, and R is the radius of the diffraction ring as measured on a flat film.

L. G. Polhamus, Bureau of Plant Industry, Department of Agriculture, supplied the Hevea latex used in this work, and his kindness is acknowledged.

WASHINGTON, October 20, 1938.

U. S. DEPARTMENT OF COMMERCE NATIONAL BUREAU OF STANDARDS

RESEARCH PAPER RP1171

Part of Journal of Research of the National Bureau of Standards, Volume 22, January 1939

ENGINEERING SIGNIFICANCE OF NATIONAL BUREAU OF STANDARDS SOIL-CORROSION DATA

By Kirk H. Logan

ABSTRACT

Approximately 33,000 specimens of various pipe materials have been buried by the National Bureau of Standards in representative soils throughout the United States for the purpose of determining the effects of soils on pipe lines. Early in the investigation it was learned that the rate of penetration of pits on ferrous metals was not constant and that the maximum pit depth on a large specimen was greater than that on a small specimen of the same material. Because of these effects, the results of the tests of small specimens do not show directly what will happen on a pipe line.

The results of soil-corrosion tests should be expressed in terms of three factors. One of these factors represents the inherent corrosiveness of the soil or the pit depth on a unit area for a unit period of exposure. The second factor represents the effect of time on the rate of penetration. The third factor gives the relation of the area from which the maximum pit is measured to the depth of that pit.

Empirical equations which take account of these factors have been suggested, and the constants have been determined for two such equations with respect to 47 of the National Bureau of Standards test sites. This paper presents some of the equations and shows the effect of applying them to the estimation of the condition of a 30-year-old, 8-in. line 1,000 ft. long having a wall thickness of 0.322 in.

A comparison of the computed pit depths with field experience has been attempted for a few soils. It is shown that although no close correlation between the data and experience should be expected, since experiences in the same soil may differ, the data indicate in a general way the corrosiveness of the soils tested.

CONTENTS

		Page
I.	Introduction	109
II.	Relation between the area from which the deepest pit is measured and its depth	111
III.	Effect of the duration of the exposure on the depth of the deepest pit	114
IV.	Extrapolation of soil-corrosion data	116
V.	Comparison of test data with field experience	121
VI.	Summary	123
VII.	References	125

I. INTRODUCTION

The National Bureau of Standards investigation of the effects of soils on metals began in 1922 with the burial of approximately 7,000 specimens of the commonly used pipe materials in 46 representative soils. Additional specimens have been added from time to time, until the total in 1938 has reached approximately 33,000, of which about two-thirds have been removed for examination.

The original specimens were for the most part samples of ferrous pipes supplied from stock by their manufacturers. The specimens were 6 in. long and 1½, 3, or 6 in. in nominal diameter. Grease, rust, and loose mill scale were removed. The cut ends were covered with

a heavy coating of asphalt. The specimens were buried at depths corresponding to the prevailing depths of pipe lines in the localities where the test sites were located. Care was taken to avoid sites subject to stray electric currents.

The rates of penetration of the specimens 6 in. in length, as given in most of the reports [1] [1] are based on the averages of two deepest pits, one on each of two 1½-in. specimens or on the average of a proportionally larger number of pits for larger specimens. This is roughly equivalent to taking the unit of area from which to select the deepest pit as 0.2 ft.^{2} In Research Paper 883 [1] estimated maximum pit depths on ferrous specimens of several sizes and materials are also given. These are based on 12 observations.

With few exceptions the ferrous and nonferrous specimens buried in 1932 and 1937 were 1½-in. pipes approximately 12 in. long or plates having the equivalent area. The reported pit depths are the averages of the deepest pits on each of two specimens and represent areas of approximately 0.4 ft.^{2} In a recent paper [2] by the author and his associates, the area used for computations is 0.4 ft.^{2} The reason for specifying the methods used for reporting the pit-depth data in the papers referred are shown in section II of this paper.

The National Bureau of Standards data on soil corrosion may be employed in the determination of the effects of certain properties or characteristics of soils on corrosion or in the study of the effects of various elements on the resistance of alloys to soil corrosion. For these purposes the methods heretofore used are reasonably satisfactory for presenting data on wrought ferrous materials. Frequently, however, it is desired to estimate the life of a pipe under specified soil conditions or to compare competitive pipe materials. For these purposes it is necessary to take into account certain factors in underground corrosion which until recently, have not been expressed quantitatively.

In this paper the original data on pit depths have been adjusted in accordance with two empirical equations derived largely from pipeline experience for the purpose of showing more clearly the significance of the soil-corrosion data with respect to the corrosion of pipe lines.

The relation between the experimental data and the corrosion of pipes in the vicinities of the test sites is also discussed.

Soils differ greatly in corrosiveness, and their corrosivity is affected by many soil properties. Table 1 shows the maximum and minimum values of certain data on soils at National Bureau of Standards test sites. The range of values for all soils in this country is considerably greater. Widely different soils frequently are to be found within a few hundred feet of each other, and corrosive soils are to be found in most parts of the United States.

Since soil characteristics differ greatly and corrosive soils are widely distributed, it is obvious that no average value for the corrosiveness of soils and no allowance or factor of safety based on average soil conditions should be used in the design of a pipe line to be installed under specific soil conditions. It is necessary in each case to consider the corrosiveness of the soils which the pipe line will encounter if proper account of soil corrosion is to be taken. Any other procedure

[1] Numbers in brackets indicate the literature references at the end of this paper.

must result in waste on parts of the line and inadequate protection for other parts.

TABLE 1.—*Maximum and minimum values of certain properties of the soils at the National Bureau of Standards test sites* [1]

Property	Unit	Maximum value	Minimum value
Electrical resistivity	Ohm-centimeters	54,400	32
Moisture equivalent	Percent	75.5	2.3
Air-pore space	do	40.6	1.1
Apparent specific gravity	do	2.08	1.41
Volume shrinkage	do	42.7	0
Total acidity	Milligram equivalent per 100 grams of soil	297.0	0
pH		10.2	2.6
Annual precipitation	Inches [2]	61.6	2
Mean air temperature	°F [2]	71.8	39
Composition of water extract:			
Na+K as Na	Milligram equivalent per 100 grams of soil	45.1	[3] 0
Ca	do	19.24	0
Mg	do	9.45	0
CO_3	do	4.6	0
HCO_3	do	2.1	0
Cl	do	43.3	0
SO_4	do	46.5	0

[1] Determinations by I. A. Denison, R. B. Hobbs, and I. C. Frost.
[2] Data furnished by U. S. Weather Bureau.
[3] Zero values are estimated from the specific resistance of the soil.

II. RELATION BETWEEN THE AREA FROM WHICH THE DEEPEST PIT IS MEASURED AND ITS DEPTH

Early in the course of the soil-corrosion investigation it was observed that there was a tendency for the specimens which were 3 in. in diameter to contain deeper pits than specimens of similar materials 1½ in. in diameter. This is illustrated in table 2, which permits a comparison of the maximum pit depths on areas of 66 and 126 in.^{2} of pipe surfaces for two metals exposed for approximately 12 years to 38 soils. Since the specimens differed in diameter, as well as in area, it is possible that the difference in pit depths is affected by differences in curvature of the specimens. However, according to Shepard, [3] the greater curvature of the smaller specimens should tend to concentrate the corrosion and consequently intensify the pitting on the smaller area.

The apparent effect of area seems to be different for different soils and to be slightly different for the two materials. Data, as well as theoretical considerations, indicate that the pit-depth-area relation is influenced by soil characteristics, although just what the characteristics are has not been determined. Sufficient data are not available to determine whether or not the relation is the same for all ferrous materials, but data on pitting factors suggest that the corrosion of wrought iron is somewhat more uniform and that of pit-cast iron somewhat less uniform than that of steel. The difference, however, if any exists, is not great.

The observed values of maximum pit depths are shown in table 3 as a function of the area inspected. In this table are tabulated depths of the deepest pits on each of a number of 20-ft lengths of pipe and also the averages for the depths of the deepest pits on each foot of the corresponding lengths. The data were obtained from measurements made on a 12-in. oil line in Miller clay. The data for individual lengths of pipe rather than the averages for all the lengths are given in order

that the reader may realize how much pit depths may vary in a single type of soil. It will be noted that the deepest pit on 48 lengths of pipe, 950 ft, was 306 mils, the average for depths of the deepest pit on each length of pipe, 208 mils, and the average of the deepest pits on each foot of pipe, 126 mils.

TABLE 2.—*Effect of area inspected on the observed maximum pit depths on National Bureau of Standards specimens*

[Pit depth in mils.]

Soil ↓ / Area→	Depth of maximum pit				Soil ↓ / Area→	Depth of maximum pit			
	Bessemer steel		Wrought iron			Bessemer steel		Wrought iron	
	66 in.²	126 in.²	66 in.²	126 in.²		66 in.²	126 in.²	66 in.²	126 in.²
1	119	101	81	83	27	73	83	52	59
3	71	72	90	96	30	61	69	52	56
4	85	84	88	93	31	36	45	31	46
5	49	55	52	46	32	48	70	47	67
6	19	40	22	38	33	92	103	108	111
7	46	65	43	48	34	42	60	42	66
8	77	119	103	84	35	28	90	42	59
9	36	50	46	47	36	54	47	49	50
10	43	60	54	52	37	79	99	73	82
12	57	72	58	91	38	37	52	44	29
15	58	85	61	83	39	53	113	58	74
16	61	69	67	60	40	73	83	71	70
17	42	47	40	42	41	87	80	127	89
18	44	50	48	43	42	131	97	95	98
19	78	61	71	79	43	108	90	80	173
20	78	56	52	51	44	63	99	58	73
22	71	71	66	60	45	113	137	106	92
24	25	31	25	29	46	75	136	72	80
26	48	39	47	45	47	30	29	59	38
Average for 38 soils						63	74	63	68

TABLE 3.—*Relation between area inspected and the observed depth of the maximum pit*

Pipe section number	Maximum pit depth on each length [a]	Average pit depth for 1-ft lengths	Pipe section number	Maximum pit depth on each length [a]	Average pit depth for 1-ft lengths
	Mils	*Mils*		*Mils*	*Mils*
1	176	90.8	25	287	180.0
2	126	58.6	26	185	101.2
3	183	125.0	27	122	63.7
4	205	126.2	28	290	154.7
5	208	136.7	29	258	126.3
6	202	116.7	30	160	94.5
7	227	122.0	31	125	67.9
8	174	138.3	32	258	144.4
9	207	144.3	33	233	138.5
10	217	105.3	34	190	115.9
11	137	79.6	35	188	115.8
12	257	159.3	36	207	127.4
13	306 [b]	169.7	37	253	154.6
14	202	149.9	38	253	130.6
15	216	158.6	39	154	94.9
16	187	139.8	40	251	97.6
17	179	91.3	41	274	133.7
18	195	127.9	42	185	121.1
19	200	140.3	43	192	138.0
20	195	143.2	44	164	95.5
21	206	127.7	45	195	123.4
22	245	147.9	46	195	141.0
23	247	152.4	47	237	142.8
24	240	161.1	48	212	138.2
Average				208	126

[a] Approximately 20 ft of 12-in. pipe, area 67 ft².

[b] Deepest pit on 950 ft of pipe.

The relation between the average of the depths of the deepest pits on unit areas and the size of that unit is illustrated in figure 1. The data for this figure are measurements of the deepest pit on each 20-ft. length of 15 miles of a 10-in. pipe line traversing a sandy-loam soil. From these data it was possible to determine the maximum pit depth on areas corresponding to any number of lengths of pipe up to the length of the line.

The lengths of the vertical lines crossing the curve represent four times the standard error of the average of the maximum pit depths. The numbers on the line show the number of observations upon which the average was based. If the pit-depth–area relation were determined for a line traversing more than one soil, the data would obviously be affected by the variety of soils traversed.

Scott [4], after an extensive examination of the Bureau's soil-corrosion data and of the measurements of pits on areas up to 10,000 ft ^{2}

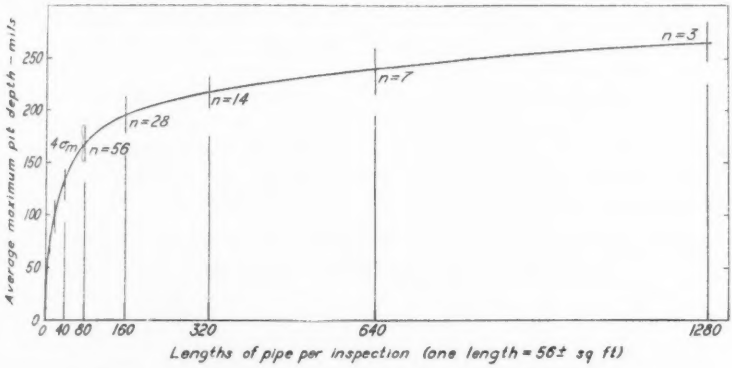

FIGURE 1.—*Relation of maximum pit depth to area inspected.*

on oil and gas lines, found that the relation between the maximum pit depth and the area from which it was selected could be represented approximately by the equation $P=b\,A^a$, in which P is the maximum pit depth associated with an area A, and a and b are constants which differ for different conditions.

From an unpublished study of data from eight National Bureau of Standards test sites and from seven sets of pipe-line data, Ewing found that on the average, the equation $P=P_1\,(C \log A+1)$, in which P is the maximum pit depth associated with an area A, P_1 the maximum pit depth on a unit area, and C is a constant varying with conditions, fitted the data better than did Scott's equation.

The fact that buried metal does not corrode uniformly can be accounted for by assuming that conditions over the surface of the metal are not uniform. This condition may be the result of lack of uniformity in the metal, differences in the soil in contact with the metal at different points, or differences in aeration resulting from the way the soil was placed over the surface of the metal. An explanation of the pit-depth–area phenomenon applicable only to small isolated specimens differing in area, is as follows: If a difference of potential exists between two areas on the surface of a specimen, the current which flows between these areas when the circuit is completed through an electrolyte is influenced by the area of the cathode, because of its

effect on the resistance of the circuit and because of its effect on polarization. The longer the specimen the larger will be the possible area of the cathode. However, there are few data which show definitely what the area of the cathode associated with a single pit is.

If the explanations that have been given fully account for the pit-depth–area relation, it might be expected that when maximum pit depths on a number of specimens having large areas are averaged, some area would be found such that larger areas would not contain deeper pits.

Figure 1 suggests that such may not be the case, since the maximum pit appears to increase in depth with increase in the area chosen for the unit of inspection up to 15 miles of pipe or up to an area of approximately 72,000 ft.[2]

It seems possible that the apparent relation between pit depth and area arises, in part at least, from the use of the maximum pit depth as the criterion for corrosivity. The probability that a deeper pit will develop on a larger area than on a small area must be some function of the relative sizes of the areas and must always be greater than 50 percent.

It seems likely, therefore, that the pit-depth–area relation may be, in part at least, a probability relation, but that it is modified to some extent by certain factors related to soil characteristics. However the relationship may be regarded, it must be taken into account if soil-corrosion data are to be correctly interpreted.

III. EFFECT OF THE DURATION OF THE EXPOSURE ON THE DEPTH OF THE DEEPEST PIT

For many soils the depth of the deepest pit is not proportional to the period of the exposure of the metal to the soil. This is illustrated by figure 2. A number of empirical equations have been offered to express the relation of pit depth to the duration of the exposure. Fetherstonhaugh [5] suggested the equation $D=A\sqrt[3]{T}$, in which D is the depth of the pit at any time, T, and A is the pit depth for unit time of exposure. Putnam [6] proposed the equation $P=KT^{0.61}$, which differs from Fetherstonhaugh's equation only in the value of the exponent of T. These equations indicate that the change in pit depths with time follows a similar course in all soils. That such is not the case is indicated by figure 2, which shows that after the first few years the increase in the pit depths is roughly proportional to the increase in the period of exposure and that the slopes of the pit-depth–time curves differ greatly for different soils.

Brennan [7], from a study of pipe-line data, decided that the relation of pit depth to time could be represented by the equation $y=(A+BZ)\log(x/h+1)$, where y is the depth of the pit at a time x, Z is the Corfield soil-corrosivity index [8], and A, B, and h are constants to be derived from a study of test data.

Scott [9], after analyzing the National Bureau of Standards data, decided that the relation of pit depth to time could be represented approximately by the equation $P=UT/(B+T)$, in which P is the pit depth at time T, and U and B are constants which characterize the soil.

Ewing found that the occurrence of leaks on pipe lines was consistent with the equation $P=kT^n$, in which k and n are constants depending on soil characteristics. Denison [2] found that this equa-

tion was also applicable to the Bureau's data. This equation differs from those of Fetherstonhaugh and Putnam in that it does not require that all pit-depth–time curves shall have the same general shape. This equation has been used in several papers prepared by members of the staff of the National Bureau of Standards and by some others, and it is used in this paper.

Values of the constants k and n have been determined for the soils at the National Bureau of Standards test sites, where the accumulated data justify an attempt to fix their values. The value of k has been associated with the fundamental corrosivity of the soil, whereas n seems to be related to the aeration of the soil. The degree of aeration

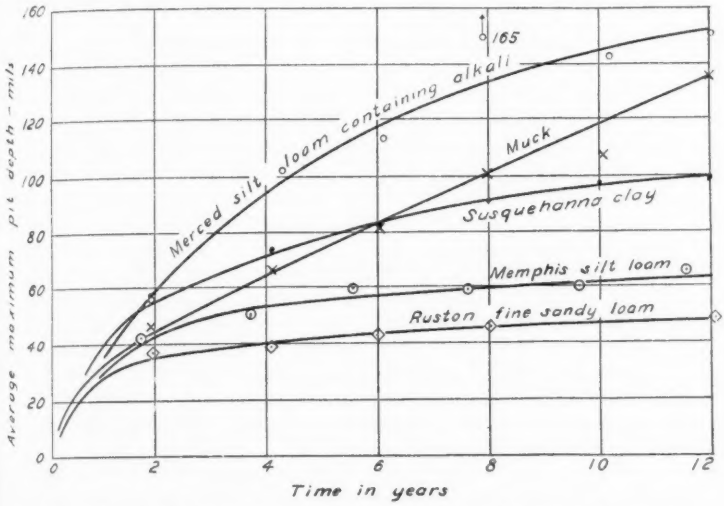

FIGURE 2.—*Relation of maximum depth of pits to duration of exposure.*

of a soil largely determines the effectiveness of the corrosion products in protecting the metal against continued corrosion. Based on the relation of aeration to corrosion, values of n to be used in the absence of data from which they can be determined directly have been assigned [2] to classes of soils according to their aeration.

A great deal of stress has been placed on the fact that the rate of corrosion decreases with the period of exposure. For most soils the relation between pit depths and the age of the pipe buried therein can be represented approximately by some curved line. However for many soils the bending of the curves is very slight after the first few years of exposure and the equation for a straight line, $P=a+bx$, will approximate the shape of the curve beyond the first few years of exposure almost as well as a more complicated equation, because, at best, the data on pit depths are not precise.

The assumption that maximum pit depths are proportional to the period of exposure of the pipe leads to estimates of pipe life that are much too low when the estimates are based on pit depths on pipes that have been exposed to well-aerated soils for only a few years. However, when the exposures to these soils are long or when the pipes are exposed to very poorly aerated soils, the errors resulting from the above assumption may be no larger than the allowances

which must be made because of the lack of precision in the original observations. Since a large part of the severely corrosive soils are poorly aerated, too much reliance should not be placed on the possibility of a decline in the rate of corrosion.

All of the equations which have been given are empirical and approximately represent the relations between pit depth and time or area. The dispersions of soil-corrosion data are such that no simple equation could fit all of the data exactly. For any one set of data one of the equations may fit better than the other equations, but none of the equations fits all the data better than all other equations.

IV. EXTRAPOLATION OF SOIL-CORROSION DATA

Any of the equations for the relation between pit depth and time may be combined with any of the equations representing the relation between pit depth and area. The choice of which equations should be combined depends somewhat on the ease with which the resulting equation can be applied to the data at hand and on the precision desired for the calculations. While the use of different equations will yield different results, in many cases the standard errors of the differences resulting from the application of different equations to a set of data indicate that the differences in the results may not be significant. When the extrapolations by means of different equations are small, the differences in the results are often not very important. When the extrapolations are large, the standard errors of the results are large, and large apparent differences are therefore to be expected. The equations should be regarded as means for roughly estimating the corrosivity of soils and for this purpose are very useful. In every case the standard error of the estimate should be computed in order to give an indication of its reliability.

For the purposes of this paper, Ewing's pit-depth–time equation has been combined with Scott's and with Ewing's pit-depth-area equations. This gives the following equations, respectively, $P=kT^nA^a$ and $P=kT^n$ $(C \log A+1)$, in which P is the pit depth on an area, A, at any time, T, and C, a, k, and n are constants derived from an analysis of the data on pit depths. Table 4 gives the values of these constants for 47 soils. By means of the equations given above, the average depth of the deepest pits on 1,000 linear ft of 8-in. pipe exposed 30 years were calculated. By rearrangement of the equations it was possible to calculate the average length of pipe associated with a puncture in 30 years and the time required for an average of one puncture of the pipe wall per 1,000 ft of pipe. These values are also shown in table 4. Since the data for pure open-hearth iron, wrought iron, Bessemer steel, open-hearth steel, and open-hearth steel containing 0.2 percent of copper were not definitely different, they were averaged for the calculation of the constants in table 4. The data for cast iron were more erratic and were not used on this account.

The values of $k_{5.3}$, column 5, are the averages of maximum pit depth on specimens having areas of 0.4 ft.^{2} Their exposure was 5.3 years. The values of $k_{5.3}$ range between 21 and 107 mils. The values of the area factor, a, column 3, range from 0.08 to 0.32. The values of the time factor, n, column 7, range between 0 and 0.92.

TABLE 4.—*Calculated data on pit depths and leaks on a pipe line*

TABLE 4.—*Calculated data on pit depths and leaks on a pipe line*

[Length of unit section 1,000 feet, diameter of pipe 8.625 inches, thickness of pipe wall 322 mils]

Soil		Constants								Scott's pit-depth–area equation				Ewing's pit-depth–area equation			
No.	Type	a	σ_a	$k_{5.3}$	$\sigma_{k_{5.3}}$	n	σ_n	C_A	σ_{C_A}	Deepest pit in 30 years	Standard error	Length of pipe per puncture in 30 years	Time for puncture per 1,000 feet of pipe	Deepest pit in 30 years	Standard error	Length of pipe per puncture in 30 years	Time for puncture per 1,000 feet of pipe
1	2	3	4	5	6	7	8	9	10	11	12	13	14	15	16	17	18
										Mils	*Mils*	*Feet*	*Years*	*Mils*	*Mils*	*Feet*	*Years*
1	Allis silt loam	0.146	0.021	58.5	2.7	0.49	0.06	0.417	0.069	475	103	6.2×10	13	351	53	3.1×10^{3}	25
2	Bell clay	.131	.030	45.4	2.2	.34	.08	.370	.099	254	76	6.1×10^{3}	60	195	42	1.6×10^{7}	130
3	Cecil clay loam	.144	.024	68.8	2.3	.17	.05	.413	.082	320	73	1.0×10^{3}	31	235	36	1.9×10^{6}	190
4	Chester loam	.160	.020	51.6	6.4	.59	.17	.459	.068	572	208	6.3×10	11	390	130	9.1×10	22
5	Dublin clay adobe	.144	.030	37.0	3.0	.47	.13	.407	.106	290	102	2.0×10^{3}	37	211	61	1.8×10^{5}	74
6	Everett gravelly sandy loam	.144	.028	21.7	1.1	0	.05	.409	.092	75	20	2.4×10^{7}	∞	55	9	∞	∞
7	Fairmount silt loam	.116	.009	31.1	2.0	.46	.07	.309	.026	188	30	1.0×10^{5}	97	149	22	1.3×10^{11}	160
8	Fargo clay loam	.133	.009	64.4	0.9	.32	.07	.365	.032	353	51	4.9×10^{2}	22	266	35	2.4×10^{4}	55
9	Genesee silt loam	.172	.028	44.0	5.4	.16	.15	.511	.107	257	97	3.7×10^{3}	120	169	54	1.4×10^{9}	170
10	Gloucester sandy loam	.184	.027	37.2	3.2	.42	.13	.553	.099	378	127	4.2×10^{2}	20	237	64	1.0×10^{6}	62
11	Hagerstown loam	.140	.021	62.9	2.7	.32	.06	.396	.071	367	78	3.9×10^{3}	20	272	42	1.4×10^{4}	51
12	Hanford fine sandy loam	.140	.031	51.2	14.0	.13	.73	.398	.109	215	284	1.7×10^{4}	670	159	208	2.4×10^{9}	6,500
13	Hanford very fine sandy loam	.193	.015	63.7	7.8	.18	.20	.573	.055	465	181	1.6×10^{2}	4	275	100	8.8×10^{3}	74
14	Hempstead silt loam	.158	.033	85.5	4.5	.48	.07	.472	.123	770	241	4.0	5	545	116	4.0	10
15	Houston black clay	.100	.015	51.4	3.6	.32	.11	.265	.044	212	155	6.4×10^{4}	110	178	39	1.2×10^{9}	190
16	Kalmia fine sandy loam	.118	.017	66.0	3.7	.32	.13	.320	.053	319	88	1.0×10^{3}	31	252	63	7.8×10^{4}	64
17	Keyport loam	.125	.038	33.1	1.9	.19	.07	.360	.123	136	48	1.0×10^{6}	2,900	108	26	8.7×10^{15}	9,400
18	Knox silt loam	.111	.018	46.0	5.8	.18	.12	.301	.053	164	47	4.4×10^{5}	1,300	134	35	8.2×10^{12}	4,000
19	Lindley clay loam	.103	.010	51.9	1.6	.34	.04	.270	.026	226	28	2.8×10^{4}	83	188	17	2.0×10^{8}	140
20	Mahoning silt loam	.188	.038	34.7	3.0	.43	.10	.584	.131	371	120	4.7×10^{2}	22	234	58	1.2×10^{5}	63
21	Marshall silt loam	.129	.012	55.7	3.1	.60	.07	.351	.033	480	81	4.5×10	15	364	52	1.7×10^{3}	24
22	Memphis silt loam	.082	.009	57.7	1.1	.21	.03	.212	.024	169	16	2.7×10^{6}	650	149	11	6.9×10^{12}	1,200
23	Merced silt loam	.139	.044	107.3	2.9	.51	.04	.391	.140	863	334	0.8	4	640	144	0.7	8
24	Merrimac gravelly sandy loam	.172	.035	22.7	1.6	.11	.09	.515	.128	121	42	2.9×10^{8}	2.1×10^{8}	80	19	1.1×10^{30}	8.8×10^{6}
25	Miami clay loam	.088	.008	40.8	2.0	.29	.06	.227	.026	144	19	9.2×10^{6}	480	125	16	7.7×10^{15}	780

TABLE 4.—*Calculated data on pit depths and leaks on a pipe line*—Continued

No.	Soil Type	Constants								Scott's pit-depth-area equation				Ewing's pit-depth-area equation			
		a	σ_a	$k_{5.3}$	$\sigma_{k_{5.3}}$	n	σ_n	C_A	σ_{C_A}	Deepest pit in 30 years	Standard error	Length of pipe per puncture in 30 years	Time for puncture per 1,000 feet of pipe	Deepest pit in 30 years	Standard error	Length of pipe per puncture in 30 years	Time for puncture per 1,000 feet of pipe
1	2	3	4	5	6	7	8	9	10	11	12	13	14	15	16	17	18
										Mils	*Mils*	*Feet*	*Years*	*Mils*	*Mils*	*Feet*	*Years*
26	Miami silt loam	.120	.028	45.7	7.1	.41	.22	.336	.091	262	125	5.5×10^3	49	211	93	3.6×10^6	85
27	Miller clay	.170	.037	38.1	1.6	.65	.08	.511	.130	511	179	3.2×10	15	343	76	4.4×10^2	27
28	Montezuma clay adobe	.106	.005	86.0	13.2	.92	.22	.277	.041	1,059	437	0.01	8	865	362	0.02	10
29	Muck	.178	.043	92.0	2.0	.60	.03	.538	.152	1,211	455	0.6	5	783	154	.50	7
30	Muscatine silt loam	.123	.033	32.1	7.0	.53	.26	.351	.112	233	139	1.3×10^4	55	187	100	6×10^7	84
31	Norfolk sand	.172	.027	40.4	2.0	0	.08	.508	.095	179	49	3.0×10^4	∞	117	22	9.1×10^{13}	∞
32	Ontario loam	.165	.039	44.8	2.6	.33	.07	.502	.138	330	120	8.6×10^2	28	229	51	2.2×10^5	84
33	Peat	.168	.028	56.4	7.1	.74	.16	.500	.109	868	338	2.7	8	585	197	2.6	13
34	Penn silt loam	.157	.012	41.0	5.4	.54	.18	.447	.042	406	144	2.3×10^2	19	280	96	7.9×10^2	39
35	Ramona loam	.318	.067	26.5	1.3	.25	.08	1.227	.321	638	381	1.2×10^2	2	229	60	7.3×10^4	120
36	Ruston sandy loam	.097	.014	45.4	0.9	.14	.03	.255	.041	134	20	8.6×10^6	1.5×10^4	114	11	1.2×10^{17}	5.2×10^4
37	St. Johns fine sand	.191	.017	65.4	3.7	.27	.09	.570	.063	544	121	6.4×10	4	328	60	7.8×10^2	28
38	Sassafras gravelly sandy loam	.153	.028	27.5	0.4	.23	.02	.443	.095	154	38	1.2×10^5	750	109	15	5.6×10^{14}	3.3×10^3
39	Sassafras silt loam	.150	.015	47.4	2.4	.51	.07	.424	.051	419	78	1.7×10^2	18	297	45	3.2×10^3	35
40	Sharkey clay	.144	.019	60.9	3.9	.50	.10	.405	.064	503	124	4.5×10	12	365	76	1.8×10^2	23
41	Summit silt loam	.095	.018	54.8	3.9	.39	.20	.252	.055	245	95	1.7×10^4	61	210	78	1.3×10^7	90
42	Susquehanna clay	.098	.009	84.7	0.4	.30	.006	.256	.026	332	26	7.3×10^2	27	279	14	1.5×10^4	48
43	Tidal marsh	.195	.023	83.2	4.0	.47	.06	.590	.081	1,013	274	2.8	3	605	90	2.8	17
44	Wabash silt loam	.148	.038	58.5	0.4	.30	.009	.440	.140	353	116	5.3×10^2	22	260	52	2.6×10^4	60
45	Unidentified alkali soil	.142	.025	54.3	6.8	.78	.16	.406	.084	716	260	3.6	11	530	174	3.6	16
46	Unidentified sandy loam	.186	.011	79.3	4.4	.18	.08	.545	.040	540	96	6.2×10	2	331	52	7.1×10^2	26
47	Unidentified silt loam	.237	.030	20.7	1.4	.30	.09	.762	.120	270	84	2.1×10^3	54	134	28	1.2×10^{10}	550

Attention is called to the values of k, a, and n in order that the reader may realize how greatly soils differ, and also to the standard errors of these values so that he can see the erratic nature of soil corrosion, even under conditions that are somewhat less diverse than those frequently encountered by pipe lines.

In columns 11 and 15 of table 4 are shown the computed averages of the maximum pit depth to be expected on a group of 8-in. pipes 1,000 ft long and 30 years old. The standard errors in columns 12 and 16 are a measure of the variations that may be expected from the listed pit depths. The standard errors (σ_p) for the pit depths derived by Scott's equation are computed by means of the equation

$$\left(\frac{\sigma_p}{P}\right)^2=(2.3\sigma_a \log A)^2+(2.3\sigma_n \log T)^2+\left(\frac{\sigma_k}{k}\right)^2$$

The standard errors for the pit depths derived by Ewing's equation were calculated from the equation

$$\frac{\sigma_p}{P}=\left(\frac{\sigma_c \log A}{C \log A+1}\right)^2+(2.3\sigma_n \log T)^2+\left(\frac{\sigma_k}{k}\right)^2$$

In these equations σ is the standard error of the quantity indicated by the subscript. The other letters have the same significance as in the other equations. In table 4 the unit of area is 0.4 ft^2 and the unit of time is 5.3 years. The large values of the standard errors of P show that columns 11 and 15 indicate only the order of magnitude of the pit depths to be expected under the assumed conditions.

Columns 13 and 17 show the computed average length per puncture for a 30-year-old 8-in. pipe line having a wall thickness of 0.322 in. Columns 14 and 18 show the estimated time required for the development of an average of 1 leak per 1,000 ft on 8-in. pipes having a wall thickness of 0.322 in. It can be shown that if the extrapolation of the pit-depth data is large with respect to either the area exposed or the period of exposure, the standard error of the estimate is correspondingly large. Since many of the computed lengths and times are very long, their standard errors are very great, and consequently they indicate only that the corresponding soils are not very corrosive.

Figure 3, which is plotted from data in table 4, shows graphically the estimated maximum depth of pit on 1,000 ft of 30-year-old 8-in. pipe and the standard errors of the estimates. The standard errors of the predictions are such that in most cases the values predicted by one equation fall within the average predicted by the other plus or minus once or twice its standard error. For smaller extrapolations the results obtained by the two equations would of course differ less.

Although the data in table 4 must be recognized as rough approximations, they are of use to those interested in selecting the proper thickness for a pipe wall or in determining whether a protective coating should be applied.

The relative depth of pits on pipes in different soils varies with the area of the exposed material and with the period of exposure. Column 5 shows the pit depths on 0.4 ft.^{2} after 5.3 years of exposure. If the data in this column are compared with those in columns 14 and 18, it will be seen that although after 5 years' exposure the specimens in Cecil clay loam, soil 3, were pitted more deeply than those in Chester loam, soil 4, a pipe in the first-named soil would last much longer than one in the other soil.

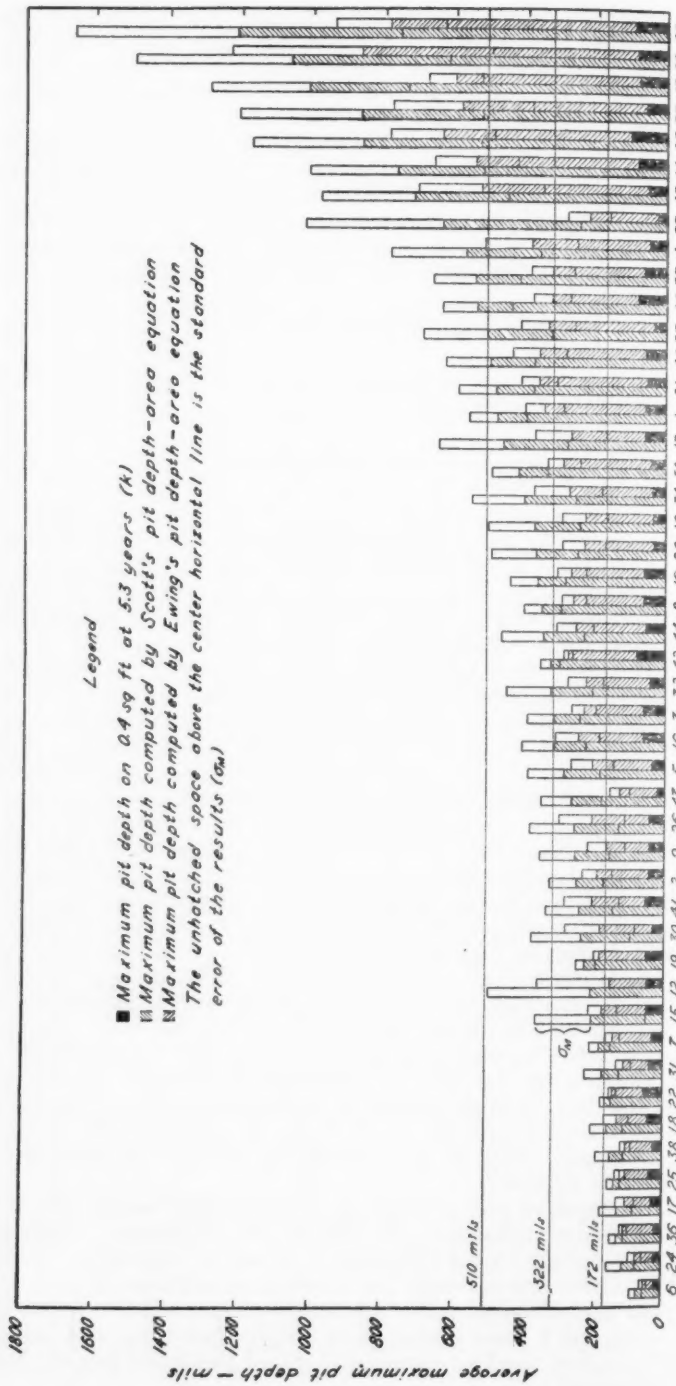
Legend
Maximum pit depth on 0.4 sq ft at 5.3 years (k)
Maximum pit depth computed by Scott's pit depth-area equation
Maximum pit depth computed by Ewing's pit depth-area equation
The unhatched space above the center horizontal line is the standard error of the results (σ_w)
Average maximum pit depth — mils
Number of test site
510 mils
322 mils
172 mils
σ_w
0
200
400
600
800
1000
1200
1400
1600
1800
6 24 36 17 25 38 18 22 31 7 15 12 19 30 41 2 9 26 47 5 16 3 32 42 44 8 16 20 10 34 39 13 1 21 40 27 46 37 4 35 45 14 23 33 43 28 29

FIGURE 3.—*Estimated maximum pit depth on 1,000 feet of 30-year-old 8-inch pipe.*

One hundred seventy-two mils has been suggested as the permissible thickness for 8-in. water-supply pipe for pressures up to 250 lb/in.[2] An examination of column 11 indicates that within 30 years such an unprotected pipe would average at least 1 puncture per 1,000 ft in 38 of the 47 soils. According to column 15, punctures on the same length would occur in 34 of the 47 soils. A good protective coating would of course reduce the number of punctures. Since supply lines frequently are readily accessible, the cost of repairing them may not be great and it is quite possible that the cost of repairs would be less than the cost of a protective coating or of thicker pipe. The table therefore does not indicate that light-weight pipe should not be used. Column 15 indicates that standard-weight steel pipe (0.322 in.) would develop a leak in 14 soils and class *B* cast-iron pipe (0.51 in.) in 7 soils under the same conditions.

It has already been said that probably Ewing's pit-depth–area equation represents available data somewhat better than Scott's. Table 4 shows that Ewing's equation results in the prediction of shallower pits, fewer leaks and longer pipe life.

V. COMPARISON OF TEST DATA WITH FIELD EXPERIENCE

Much has been said about the value of experience in estimating the corrosivity of soils. It is difficult, however, to express experience in sufficiently definite terms to make the information usable in the way that the results of tests are used, because the conditions under which the data of experience are obtained are often poorly defined, and because observations of identical conditions are usually not numerous enough to permit an estimate of the standard error or reproducibility of the experience. When experiences are analyzed it is often difficult to determine their exact significance or their applicability to some new condition. Experiences are frequently contradictory and they may be the results of some unrecognized conditions. They should therefore be examined carefully if they are to be applied to new construction.

Since the National Bureau of Standards soil-corrosion tests were conducted with the cooperation of operators of pipe lines who furnished the test sites and local labor, it might be assumed that a comparison of the Bureau's data with the field experience of the cooperators would furnish a key to the application of the results of the tests to pipe-line corrosion. When such a comparison is attempted a number of difficulties are encountered. Although there are pipes in the vicinities of most of the test sites, their extent in the soils of the test sites can be determined only by extensive soil surveys. Most of the pipe lines originally carried some kind of a protective coating. In many cases this coating was very thin and imperfect, although in some instances the coatings were quite heavy. In certain cases the lines have been reconditioned and the kind of coating changed from time to time. Most pipe lines carry currents which tend to protect certain portions of the line at the expense of other portions. Pipe networks in cities are frequently affected by stray currents from street railways, which modify the corrosive effects of the soils. The interconnection of one variety of pipe material to another, such as the connection of copper, brass, lead, or galvanized steel to cast iron, wrought iron, or steel mains, introduces additional galvanic corrosion. The passage of a line through two different soils sets up a galvanic current. The pipe

which lies in the same type of soil as the test specimens may be buried deeper or shallower, and thus lie in a soil horizon that is quite different in texture, aeration, acidity, or resistivity from that of the specimens. The interconnection of a new pipe with an old one sets up a condition which may accelerate the corrosion of the newer line. Two pipes of the same material in the same street or right-of-way may corrode at different rates. In many cases records of the pipe lines are incomplete. In other cases the owners are reluctant to disclose their experiences because of possible effects on the valuation of their lines or the rates they may be allowed to charge for amortization as common carriers. For these reasons and others, no general comparison of the test data with the conditions of pipe lines has been attempted. However, a few comparisons will be made where conditions are especially favorable for such comparisons, although in no case are the conditions affecting the pipe line identical with those affecting the test specimens, and it is impossible to evaluate the effect of the differences accurately.

Soil 1. Allis silt loam.—Severe corrosion of service pipes in this soil has been reported, but definite data are not available. Ewing's equations indicate an average of 1 leak per 1,000 ft. of 8-in. steel pipe in 25 years.

Soil 8. Fargo clay loam.—This soil is similar to much of that in the city of Winnipeg, where severe corrosion of cast-iron water mains has been reported. Originally, the corrosion was attributed to stray-current electrolysis, but the extent of the corrosion attributable to stray currents has not been established. Ewing's equations indicate that in this soil an 8-in. steel pipe should develop in 30 years an average maximum pit depth of 266 mils on a 1,000-ft. length.

Soil 9. Genesee silt loam.—A 6-in. steel line paralleling the test site was renewed because of corrosion after 14 years. Ewing's equations indicate that this soil is not corrosive.

Soil 15. Houston black clay.—Severe corrosion of cast iron and steel has been reported in this soil. Table 4 indicates that this soil is not very corrosive.

Soil 23.—Leaks developed on an 8-in. steel line in this soil within 5 years. Table 4 shows this soil to be very corrosive.

Soil 27. Miller clay.—Frequent leaks developed on a 12-in. line in this soil in about 9 years. The data in table 3 are from observations on such a line in Miller clay somewhat better drained than that in which the specimens were buried. Ewing's equations indicate that an 8-in. steel pipe should average 1 leak per 1,000 ft in 27 years.

Soil 28. Montezuma clay adobe.—This is said to be a very corrosive soil, but no specific data have been obtained. Table 4 shows this to be one of the most corrosive soils tested.

Soil 29. Muck.—Water mains in the vicinity of the test site corrode rapidly. The corrosion was attributed to electrolysis at one time, but the cause of the corrosion has not been definitely determined. Table 4 shows this to be one of the most corrosive soils tested.

Soil 32. Ontario loam.—The test site lies within a few feet of a 38-in. steel water main having a ⅝-in wall. Within 2,000 ft of the test site this line developed 25 leaks in 42 years. The line was protected by a japan varnish baked on. The length of the pipe in this soil at this location is 7,480 ft, in which length there were 50 leaks, or an average of 1 leak for 150 ft in 42 years. According to Scott's pit-depth-area equation, the National Bureau of Standards data indicate there

should have been an average of 1 leak in 5,349 ft of pipe. The formula of Ewing would indicate that the length per leak should be greater. The Bureau's data show that in this case the soil is much less corrosive than experience proved it to be. However, this steel main is paralleled by a 36-in. wrought-iron main having a ⅜-in. wall which has developed no leaks in this soil in 61 years. The difference in the two experiences is greater than the difference between the test data and experience.

The difference in the performance of the two pipe lines may be explained in several ways. The materials used were different as were the protective coatings. It has been shown, [10] in certain cases at least, that when a new pipe is connected to an old one the latter is protected at the expense of the former. As for the difference between the results calculated from the tests and the leak records of the two pipe lines, it is obviously impossible for the experimental results to agree with both experiences. Most of the leaks on the steel line occurred on the top three-fifths of the pipe. This is rather unusual, as most cases of severe corrosion occur on the bottom of the line. The severe corrosion of the steel line may be the result of a difference in soil conditions at the top and the bottom of the pipe or because the coating on the top of the pipe was injured by the backfill. The record of these pipe lines illustrates very well how conditions not duplicated in a test may alter the results when the material tested is used in a practical way.

Soil 35. Ramona loam.—The specimens at this site are laid adjacent to a 6-in. cast-iron gas main which has carried gas for 29 years without developing a leak in the city block containing the specimens. This block also contains five services, one of which served without a leak for more than 25 years. Another service developed a leak in 9 years. Using Scott's pit-depth–area relation, the average of the maximum pit depths for 500 ft. of 6-in. cast iron is 468 mils for a period of 29 years. This indicates that the cast-iron pipe in this soil, the wall thickness of which is 430 mils, should have developed, on the average, one puncture per block at the time the information was obtained. However, the comparison of the field and experimental data is of doubtful value because the extent of the pipe in Ramona loam has not been determined, because the pitting factor for cast iron being greater than for steel the value for "*a*" should be less, and because cast iron may be punctured by corrosion and still carry low-pressure gas without leaking.

Although a review of these comparisons of test data with field experience indicates no very close relation between the two, usually the soils which the test has shown to be corrosive are shown by experience also to be corrosive. Corrosion is affected by so many factors that it can scarcely be expected that any test could completely duplicate the conditions which buried metals encounter in service. Knowledge of service conditions is in most cases so incomplete that it would be difficult to use an equation that took account of all significant field conditions even if such an equation could be developed.

VI. SUMMARY

The corrosion of pipe lines depends on a number of factors which make it impossible to fully report underground-corrosion phenomena in the terms commonly used for the reporting of corrosion data. For

this reason the data presented in previously published reports on the National Bureau of Standards soil-corrosion investigation do not give readers a clear and adequate idea of the corrosiveness of soils with respect to pipe lines. This is especially important with respect to maximum pit depths.

The maximum pit depth observed on any area will, on the average, be less than the maximum pit depth on a larger area exposed to the same conditions.

Pits usually change in depth more slowly as they become older, but this change, as well as the pit depth, differs greatly for different soils. It is therefore necessary to accompany rates of penetration by data on the effects of area and time if the pit depths are to be used for an estimation of the life of pipe. Such estimates should be based on data for the particular soil conditions associated with the pipe rather than on rates of penetration for average soil conditions.

The relative depths of pits on two materials or on the same material exposed to two soils may differ for different periods of exposure or for different exposed areas.

A number of empirical equations have been developed by investigators for the purpose of expressing the relations of area and time to maximum pit depths. All of these equations represent some observations on pipe lines approximately, but no one equation fits every set of pipe-line data better than any other equation.

The most generally applicable equation for the relation of pit depths to time and area of exposure is $P_2=P_1(C \log A+1)T^n$, in which P_2 is the average of the deepest pits on a number of specimens having areas A, and T is the age of the specimens. P_1 is the pit depth on a unit area exposed for a unit time and C and n are constants which depend on soil characteristics. This and another equation have been applied to the data from the soil-corrosion investigation, and the maximum pit depths for 1,000 ft of 8-in. pipe have been computed for a time of 30 years. The results give a better indication of the corrosiveness of the soils investigated than can be obtained directly from an examination of the data on the test specimens.

Some of the soils which produced relatively high initial rates of corrosion are shown to be less destructive to pipe lines than others with lower initial rates of corrosion. On the whole, more of the 47 soils tested are shown to be seriously corrosive than were thought to be corrosive by some who examined the results of the investigation in their original form. From this it follows that unprotected lightweight pipe is suitable for use in fewer soils and protection to pipe is more generally needed.

The standard errors of the computed values are quite large and the results must be considered as only roughly approximating the behavior to be expected of a pipe line under practical conditions.

To test the reliability of the adjusted data, comparisons have been made between these data and the corrosion of pipe lines near some of the test sites. In view of the fact that two pipe lines in the same locality do not always corrode alike, a close agreement between the calculated and observed behavior of a pipe is not to be expected. Comparisons between experience and predictions of corrosion based on experiments are frequently unsatisfactory because the pipe lines may be subjected to influences not represented in the experiment. In

general, however, the observed correspondence is sufficiently good to warrant the conclusion that if local conditions are properly taken into account, the results of the soil-corrosion investigation properly adjusted for the effects of area and time constitute the best available basis for decisions as to the proper wall thickness and the necessity for protection of a proposed pipe line.

Much valuable assistance in the calculation and checking of the data has been received from R. B. Darnielle and W. H. Johnson and M. Romanoff. I. A. Denison and S. P. Ewing have made helpful suggestions as to the treatment and interpretation of the data.

VII. REFERENCES

[1] K. H. Logan and V. A. Grodsky, *Soil-corrosion studies, 1930. Rates of corrosion and pitting of bare ferrous specimens.* BS J. Research **7,** 1 (1931) RP 329.
K. H. Logan and R. H. Taylor, *Soil-corrosion studies, 1932. Rates of loss of weight and pitting of ferrous and nonferrous specimens and metallic coatings,* BS J. Research **12,** 119 (1934) RP 638.
K. H. Logan, *Soil-corrosion studies, 1934. Rates of loss of weight and pitting of ferrous specimens.* J. Research NBS **16,** 431 (1936) RP 883.
[2] Symposium on Corrosion Testing Procedures, Am. Soc. Testing Materials, p. 95 (1937).
[3] E. R. Shepard, *Some factors involved in soil corrosion.* Ind. Eng. Chem. **26,** 723 (1934).
[4] G. N. Scott, *Adjustment of soil corrosion pit depth measurements for size of sample,* Proc. Am. Petroleum Inst. **14,** pt. 4, 204 (1934).
[5] E. P. Fetherstonhaugh, *Discussion of underground corrosion,* Proc. Am. Soc. Civil Engrs. **101,** 828 (1936).
[6] J. F. Putnam, *Soil corrosion,* Proc. Am. Petroleum Inst. **16,** pt. 4, 66 (1935).
[7] J. F. Brennan, *A mathematical theory of corrosion,* Gas Age Record **75,** 359 (1935).
[8] G. Corfield, *Running a soil survey on a large distribution system,* Western Gas **6,** No. 3, 25 (1930).
[9] G. N. Scott, *A preliminary study of the rate of pitting of iron pipe in soils,* Proc. Am. Petroleum Inst. **14,** pt. 4, 212, 1934.
[10] K. H. Logan, Walter Rogers, and J. F. Putnam, *Pipe Line Currents,* Am. Petroleum Inst. Prod. Bul. 204. p. 116 (1930).

Washington, September 20, 1938.

○